Geochemistry, petrography, geochronology, and radiogenic isotopes of the weakly mineralized intrusions in Thunder Bay North Igneous Complex

Khalid Yahia

Lakehead
UNIVERSITY

Department of Geology

A thesis submitted in partial fulfillment of the requirements
for the Degree Master of Science

December 2023

ABSTRACT

The Thunder Bay North Igneous Complex (TBNIC) is located approximately 50 km northeast of Thunder Bay, Ontario, Canada. It comprises two Cu–Ni–PGE-mineralized mafic–ultramafic intrusions, the Escape and Current Intrusions, and five smaller mafic–ultramafic intrusions whose mineralization potential has yet to be fully assessed, namely the Lone Island Lake, Greenwich, Southeast Anomaly (SEA), and 025 intrusions, and the East–West Connector (EWC). The five gabbroic to peridotitic intrusions are the focus of this study. They are characterized by high magnetic anomalies and crosscut the Archean granitoids and metasedimentary rocks of the Quetico Subprovince. U-Pb dating yielded an age of 1107.6 ± 0.9 Ma for the Escape intrusion, which is the oldest date among TBN intrusions, and an age of 1105 ± 0.9 Ma for the Greenwich intrusion.

Field observations and drill core logging of the five intrusions indicates that they are gabbroic to peridotitic in composition with approximately 6-9% sulfides. The sulphides are dominantly pyrite, with lesser amounts of chalcopyrite and pyrrhotite. Petrographic analysis of the five intrusions show them to comprise gabbronorite with lesser leuco-gabbro, gabbro, and websterites for the Lone Island intrusion, gabbronorite to websterite and lherzolite for 025, gabbro to websterite for SEA, and highly altered gabbro in the EWC and Greenwich intrusions.

The five intrusions are characterized by negative Nb, Zr, Hf, Ti, Y and Sc anomalies, and contain high incompatible element contents, enriched light rare-earth elements (LREE) with La/Sm_n = 2-3.7, flat to fractionated heavy REE (HREE) with Gd/Yb_n = 1-6, and Th/Nb_n = 0.09-0.11. The five intrusions also have moderate to strong negative Nb anomalies with Nb/Nb* ranging between 0.90 and 0.05. Generally, the five intrusions show slightly positive Eu anomalies with Eu/Eu*range between 0.53 and 1.14, which is consistent with the elevated plagioclase content of the five intrusions.

Based on major and trace element chemistry, three sample populations were identified. Population A includes Lone Island, EWC, and SEA intrusions, and population B includes part of the 025 intrusion (025-

1) and part of the Greenwich intrusion (Greenwich-1). Populations A and B are OIB-like magmas with enriched LREE and steep patterns on primitive mantle-normalized diagrams. They are similar to the Eva Kitto, Jackfish, Seagull, and McIntyre intrusions and relatively close to the Thunder intrusions from the MCR. Population C includes Greenwich-2 and 25-2. This population is less enriched in LREE and has a flatter pattern on primitive mantle-normalized diagrams, and they are similar to Nipigon Sills, Inspiration, Crystal Lake, Coubran Lake and Tamarack intrusions.

Sm–Nd and Rb–Sr isotopes were utilized to assess the role of crustal contamination in the formation of the five intrusions. The intrusions are characterized by generally negative $\varepsilon_{Nd(T)}$ values of -7.4 to +0.14 and Sr_i of 0.70309 to 0.70587. The most negative $\varepsilon_{Nd(T)}$ values of -7.20 and -7.49 were recorded in samples from the most LREE enriched portions of the Greenwich, whereas the +0.14 value is a hybrid grey (altered grey gabbro) sample from the 025 intrusion. Two country rock samples (an Archean metasedimentary rock and a granitoid) have $\varepsilon_{Nd(1.1\ Ga)}$ values of -20.50 and -20.19, Sr_i values of 0.7636 and 0.7057, and Th/Nb_n of 2.33 and 1.50 respectively. The negative $\varepsilon_{Nd(T)}$ values for the intrusions and the country rocks, along with their elevated bulk-rock Th/Nb_n ratios, and negative Nb anomalies suggest that the intrusions were contaminated by older crustal material. Three possible sources of contamination were identified, one with less negative $\varepsilon_{Nd(T)}$ and lower Sr_i that affected Lone Island, SEA, EWC, Greenwich-1, and 025-1. Secondly, one with higher Sr_i and more negative $\varepsilon_{Nd(T)}$ that affected Greenwich-2. The third type of contamination affected 025-2, and is characterized by a lesser LREE enrichment and lower degree of crustal contamination and it affected 025-2.

The three types of magmas from TBNIC that have been characterized in this study are all plume derived magmas, were generated from distinct melt sources and went through different types and degrees of crustal contamination.

Acknowledgments

I would like to deeply thank Dr. Peter Hollings for his continued support, guidance, and overall insights throughout this research project. I am also grateful to Dr. Shannon Zurevinski for her help and support. I am extremely thankful to my research team Dr. Mathew Brzozowski and Connor Caglioti, MSc for their unlimited assistance during sampling and for their thoughtful discussions and environment. I would also like to thank Abraham Drost, MSc, Allan MacTavish, MSc, Dr. Geoff Heggie, Andrey Zagoskin, MSc and Ethan Beardy from Clean Air Metals Inc. for their finance, support, and open doors, and to all of their staff who made this project possible. I would also like to thank all of my colleagues, professors, and Lakehead University staff for everything. Finally, I can not forget to thank my family and friends for their encouragement and unconditional backup.

Table of Contents

List of Figures

List of Tables

1 Introduction

1.1 Location and accessibility

The Thunder Bay North Igneous Complex (TBNIC) is located approximately 50 km northeast of Thunder Bay, Ontario, Canada (Fig. 1.1). The TBNIC consists of two Cu-Ni PGE mineralized intrusions, namely the Escape Intrusion and the Current Intrusion, and a number of other smaller intrusions. This study focuses on five of the poorly understood intrusions that are situated within the TBN property.

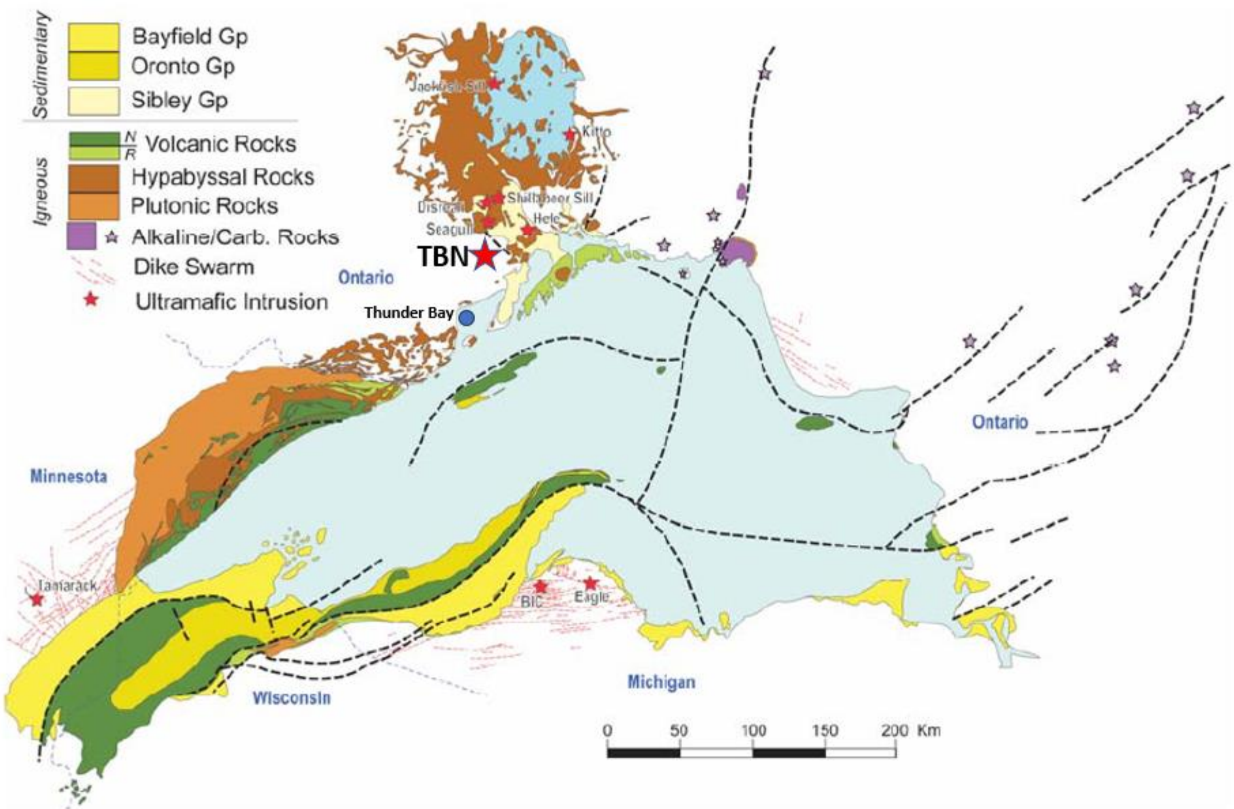

Fig 1.1 Map showing the location of the study area and the other Ni-Cu PGE deposits in the region (From Nicholson et al., 2013).

The five intrusions that are the focus of this study are the Lone Island Intrusion (LI), Greenwich Intrusion (GI), Southeast Anomaly Intrusion (SEA), 025 Intrusion, East-west Connector (EWC). The LIL, SEA, and EWC are located close to each other, whereas the Greenwich and 025 intrusions are located 5 km from Current Lake Intrusion and about 4 km from each other (Fig. 2.4).

1.2 Ni-Cu PGE Overview

Mafic-ultramafic-hosted base and precious-metal deposits are considered the most economically significant sources of Ni, Cu, and PGE (Holwell & Macdonald, 2010). Magmatic sulfide deposits can be generally divided into two main groups; those that are valued for their Ni and Cu contents which generally contain 20-90% sulfide, and those that are valued for their platinum group element (PGE) contents and contain 0.5-5% sulfide (Naldrett, 2011).

Mafic-ultramafic bodies are emplaced in four environments 1) the continental or ocean floor synvolcanic activities during the Archean, 2) continental rift environments, 3) cratonic environments, or active orogenic belts (Naldrett, 1997). Bodies related to rifted plate margins are divided into those associated with continental crust and those with no association with continental crust (Naldrett, 1997). The mafic-ultramafic bodies of the MCR are an example of an association with continental crust (Naldrett, 1997).

Naldrett (2011) proposed seven stages for magmatic sulfide deposits 1) creation of the source (mafic-ultramafic magma resulting from mantle melting), 2) development of the source (ascent of magma from the mantle to the crust), 3) fertilization of the source (interaction of magma with crust), 4) delivery (further ascent of mantle derived magma + immiscible sulfides to the upper crust), 5) growth (concentration of sulfides during magma emplacement), 6) nourishment (enrichment of sulfides by interaction with flowing magmas), and full maturity (cooling and crystallization of the host rock and related sulfides).

If the primary sulfur content of the magma is sufficient, or if sulfur is added to the system, droplets dispersed throughout the magma may form a separate sulfide liquid (Eckstrand & Hulbert, 2007). Many researchers have proposed that PGE are principally concentrated by magmatic sulfides (e.g., Barnes et al., 1985 and Naldrett, 2011).

Magmatic Ni-Cu PGE sulfide deposits form by the segregation and concentration of droplets of liquid sulfide from mafic or ultramafic magmas followed by concentration in small volumes of rock with the chalcophile elements that preferentially partition into sulfide magmas (Naldrett, 2011). The greater density of the sulfide droplets allows them to sink towards the base of the magma to form sulfide concentrations, which cool and crystalize to form ore deposits (Eckstrand & Hulbert, 2007). If sulfide immiscibility and segregation at the base of the magma chamber occurred earlier than crystallization of the silicates, the sulfide droplets form massive and semi-massive ores, whereas if sulfide segregation and silicate crystallization occurred at the same time, they settle down together forming disseminated sulfides (Song et al., 2011). Most of the disseminated deposits occur within the size of a droplet (>1mm diameter), which can easily be entrained in vertically ascending magma (Barnes et al., 2016). This confirms the importance of high flow rates in dynamic conduit related Ni-Cu-PGE related systems (Barnes et al., 2016). Segregation of immiscible sulfide melt from silicate magma is controlled by magma mixing, rapid cooling, differentiation, and contamination (Maier et al., 1998). The S saturation of a magma may be triggered by the addition of externally derived S to the magma (devolatilization), partial melting or bulk assimilation of sulfide of the country rocks. An increase in oxygen fugacity of magma by contamination can also lead to S saturation, because it would promote the precipitation of magnetite and chromite, which would lower the FeO content of the magma reducing the sulfur carrying capacity of the magma (Houghton et al., 1974; Buchanan and Nolan, 1979; Maier, 2005).

Magmatic PGE ore deposition is favoured by prolonged high-volume flow over a horizontal floor in the base of a channelized sill, tube or blade-dyke (Barnes et al., 2016). Ni-Cu-PGE deposits are hosted in sheet-like intrusions (e.g., large portion of Duluth complex), reefs in small tholeiitic bodies (e.g., Sonju Lake intrusion), and smaller conduit deposits (Ripley et al., 2015). The composition of sheet-style deposits differ from conduit related deposits, as sheet-like intrusions typically have lower Ni and Cu grades compared to conduit style of deposits (Ripley et al., 2015). Conduit related Ni-Cu-PGE deposits form in near-vertical and horizontal portions of conduit systems (Ripley & Li, 2011). Sulfide accumulation by gravitational settling in the horizontal portions of magma conduits is one of the processes that can generate PGE mineralization, as at the Voisey's Bay and Eagle deposits (Ripley and Li, 2011). Changes to the conduit morphology can lead to changes in the physical and chemical properties of the magma, which can cause concentration, capture, and containment of sulfides (Evans-Lamswood, 2000). These changes might include width variation, obstructions, or changes in the orientation of the conduit (Evans-Lamswood, 2000). These changes affect velocity and flow rate of the magma, which can change both the sulfur concentration in the magma and magma's interaction time with the wall-rock, inducing sulfide immiscibility (Evans-Lamswood, 2000).

1.3 Thesis Scope and objectives

The objective of this study was to characterize the five intrusions (LI, EWC, 025, SEA, and GI) using whole rock geochemistry, thin-section analysis, radiogenic isotope data (Rb-Sr and Sm-Nd) and U-Pb geochronology to investigate the genetic relationships between the five intrusions and their potential to host orthomagmatic Ni-Cu-PGE mineralization. This study also compared the five intrusions to other mineralized intrusions situated on the north shore of Lake Superior and world class Cu-Ni-PGE deposits.

2 Regional Geology

2.1 Archean Superior Province

The Superior Province is the nucleus of the Canadian Shield (Goodwin, 1968; Percival, 2012), and it is the largest Archean craton covering an area of approximately 1.4 x 106km^2 (Fig. 2.1; Percival, 2012). It consists of a variety of rock types and records the formation and modification of both continental and oceanic crust in a range of tectonic environments between 4.30-2.57 Ga (Percival, 2012). The Superior Province is surrounded by Proterozoic orogenic belts; the Grenville Province to the southeast, the Churchill Province to the east, north and west and the Southern Province to the south (Card and Ciesielski, 1986).

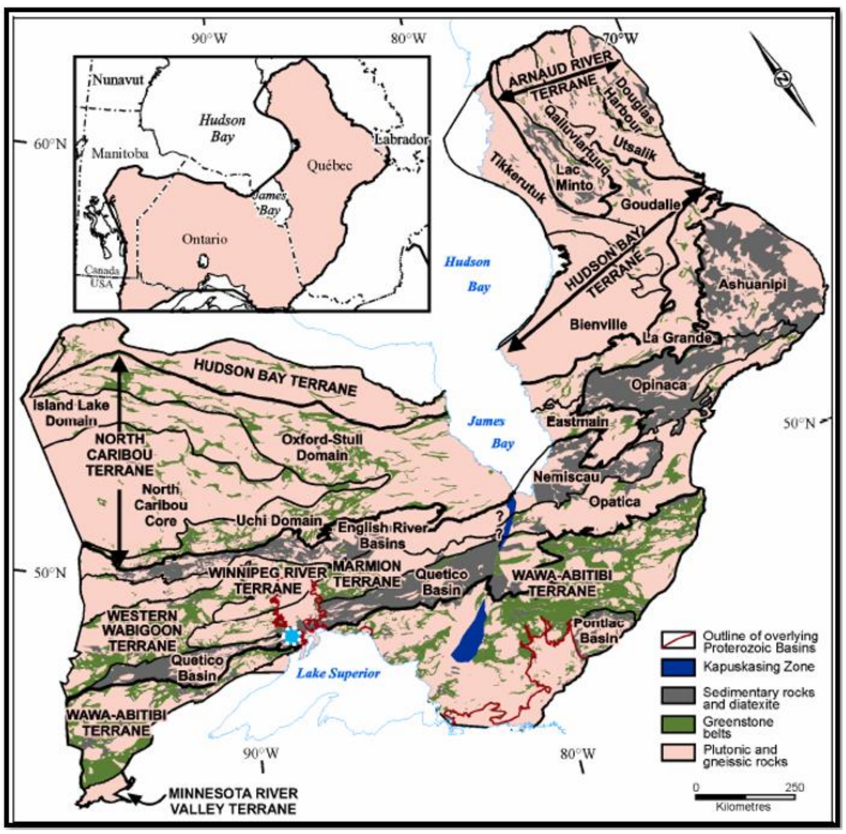

Fig 2.1. Map of the Archean Superior Province (from Stott, 2010). The blue circle indicates the location of the Thunder Bay Igneous Complex within the Quetico Subprovince.

Based on lithology, structure, metamorphic grade, and geophysical patterns Card and Ciesielski (1986) proposed four main subprovince types in the Superior Province (Fig. 2.1): 1) volcano-plutonic subprovinces (greenstone belts); 2) metasedimentary subprovinces (dominated by greywacke and their magmatic derivatives); 3) plutonic subprovinces (mainly granitoid intrusions); 4) high grade gneissic subprovinces (e.g., the Pikwitonei subprovince).

2.1.1 Wawa-Abitibi Terrane

Many researchers accept the correlation between the Wawa and Abitibi terranes across the transverse Kapuskasing uplift structure (Percival, 2006). The Wawa subprovince represents the western part of the Wawa-Abitibi terrane and comprises greenstone belts and granitic plutons that bound the Quetico Basin (Williams et al., 1991). The Abitibi subprovince covers the eastern part of the Wawa-Abitibi terrane (Stott et al., 2010). The volcanic activity in the Wawa Subprovince started around 2.745 Ga (Percival, 2006). The central zone of the Abitibi terrane is mainly plutonic rocks, whereas the northern Abitibi region is mostly comprised of 2.735-2.720 Ga volcanic assemblages (Ludden et al., 1986; Chown et al., 1992; Legault et al., 2002; Percival, 2006).

2.1.2 Quetico Basin

The Quetico Basin consists of Neoarchean metasedimentary rocks, and is located between the Abitibi-Wawa terrane to the south and the Western Wabigoon, Winnipeg River to the north (Fig. 2.1; Wang et al., 2020). Zircons in the Quetico metasedimentary rocks range in age from 2698 ± 3 Ma to 3009 ± 4 Ma (Davis et al., 1990). The basin consists of marginal metagraywacke that grades into axial migmatite and granitic plutons (Percival and Williams, 1989). Granitoids represent the dominant plutonic rocks within the Quetico Basin (Percival and Williams, 1989). Seven plutonic suites have been categorized in the Quetico Basin : 1) early mafic-ultramafic intrusions, 2) tonalite and diorite (2688-2687 Ma, 3) nepheline syenite, 4) syenites (2680 ± 1 Ma), 5) granitic rocks (2670-2653 Ma), 6) diorite granodiorite-syenite sanukitoids (2670 Ma), and 7) a diorite-monzodiorite-syenite sanukitoid suite (Wang et al., 2020).

2.2 Proterozoic sedimentary rocks

2.2.1 Paleoproterozoic sedimentary rocks

Paleoproterozoic sedimentary rocks in the northern Lake Superior region overlie Archean metasedimentary rocks, metavolcanic rocks, and granites. The Gunflint and Rove Formations of the Animikie Group consist of Paleoproterozoic chemical and siliciclastic sedimentary rocks (Poulton et al., 2004). The Gunflint Formation consists of conglomerate, black shale/slates, iron rich carbonate, chert, and jasper and hematite-magnetite greenstones (Pufahl, 1996; Metsaranta, 2006). Zircons from reworked volcanoclastic beds in the Gunflint Formation yielded an age of 1878.3 ± 1.3 Ma (Fralick et al., 2002). The Rove Formation consist of black shale, sandstone, and siltstone (Metsaranta, 2006). The Rove Formation conformably overlies the Gunflint Formation, and zircons from a tuffaceous material in the base of Rove yielded an age of 1840 Ma (Poulton et al., 2004). The sedimentary rocks of the ca. 2 Ga Animikie Group contain disseminated pyrite with high $\delta^{34}S$ values (Winter & Knauth, 1992). The Animikie Group is overlain by the Mesoproterozoic Sibley Group.

2.2.2 Mesoproterozoic sedimentary rocks

The Sibley Group comprises Mesoproterozoic sedimentary rocks (Rogala et al., 2007). The Sibley Group contains five Formations, from base to top these are the Pass Lake, Rossport, Kama Hill, Outan Island and Nipigon Bay Formations (Rogala et al., 2007). The average sulfate $\delta^{34}S$ content of the Sibley Group ranges from +15 ‰ to +20 ‰ (Metsaranta, 2006). A Rb/Sr whole rock isochron yielded an age of 1339 ± 33 Ma (Franklin 1978b; Franklin et al., 1980). The Sibley Group is intruded by mafic sills (e.g., Inspiration diabase and Nipigon sills) and is overlain by mafic volcanic rocks and associated clastic sedimentary rocks of the Osler Group (Davis and Sutcliffe, 1985; Metsaranta, 2006).

2-3 Midcontinent Rift and related magmatism

The 1.1 Ga Midcontinent Rift (MCR) is a large, arcuate anorogenic structure located in the central portion of North America (Ojakangas et al., 2001). The MCR has greatly affected and disturbed the lithospheric and tectonic structure of the region, and has consequently shaped the present-day tectonics, structure, and mineral resources (Hinze & Chandler, 2020). Cannon & Hinze (1992) proposed that the MCR formed due to the arrival of a mantle plume near the base of the lithosphere at ca. 1115 Ma.

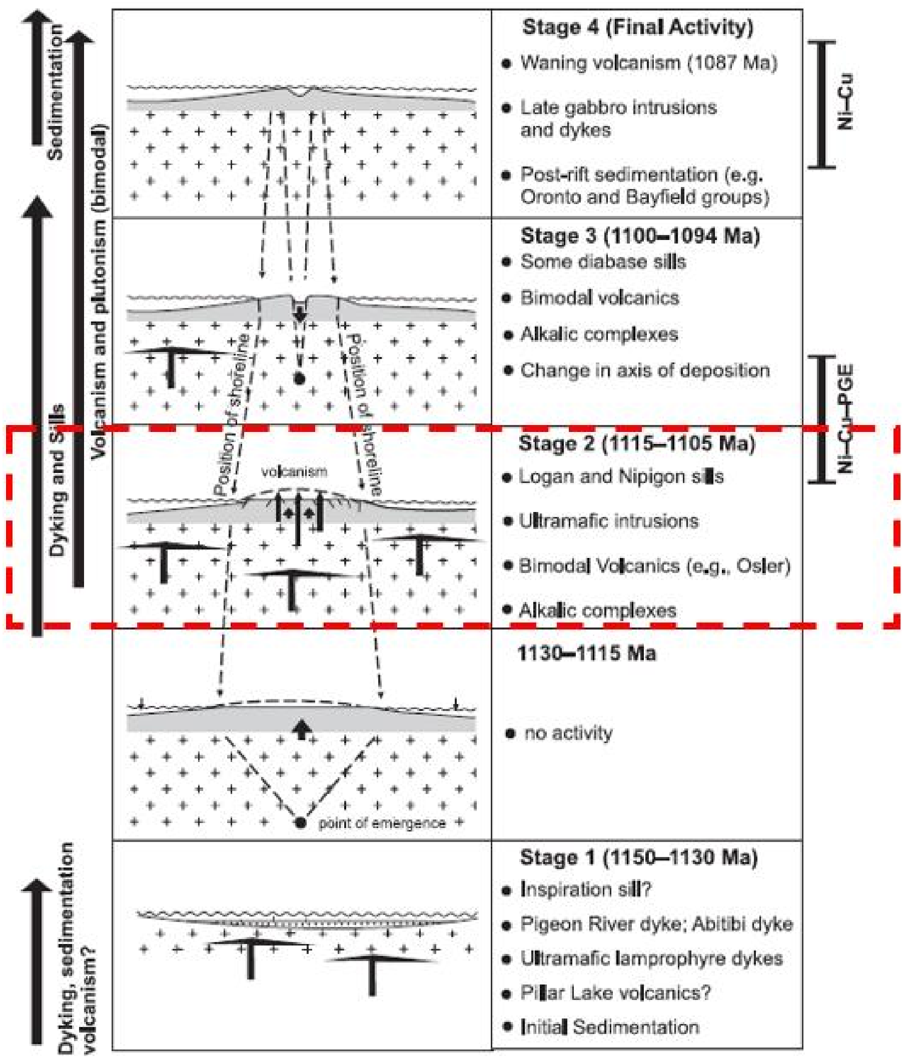

Fig 2.2. Schematic diagram showing the various magmatic stages of the MCR (from Heaman et al., 2007). The red rectangle highlights the stage during which the fives intrusions of this interest to this study formed.

Heaman et al. (2007) divided the MCR into four main stages (Fig. 2.2). Stage 1 occurred between 1150–1130 Ma and it comprises ultramafic lamprophyres, tholeiitic basalts, and associated feeder dykes (e.g., the Abitibi dyke swarm). Stage 2 occurred between 1115–1105 Ma and comprises ultramafic intrusions (e.g., Seagull, Hele, and Kitto), basaltic sills and flows, rhyolite flows, and alkaline magmatism. Stage 3 occurred between 1100–1094 Ma and includes gabbroic intrusions (e.g., the 1099.6 ± 1.2 Ma Crystal Lake intrusion and 1094.7 ± 3.1 Ma Moss Lake intrusion). Stage 4, the youngest magmatic stage of the MCR formation, includes the Michipicoten Island porphyry in Ontario, with an age of ca. 1087.2 ± 1.6 Ma, and is considered a period of waning volcanism (Fig. 2.2).

Miller et al. (2013) discussed the evolution history of the MCR and proposed five magmatic stages. The Initiation Stage (1115-1110 Ma) represented by the Thunder Bay-Lake Nipigon ultramafic to mafic intrusions and a buried intrusion in Michigan (Cannon and Nicholson, 2021; Miller et al., 2013). The Initiation Stage rocks show reverse polarity and have geochemical characteristics of picritic lavas in the lower portions of the Mamainse Point, PowderMill, North Shore, and Osler volcanic sequences (Miller et al., 2013). The Early Stage (1110-1106 Ma) includes reverse polarity lavas and ultramafic to felsic intrusions (Miller et al., 2013). The reverse polarity volcanic roots of the Early Stage have Mg# > 50 and evidence of crustal contamination is suggested by $\varepsilon Nd < -2$ and Th/Yb >1 (Miller et al., 2013). The Hiatus Stage (1105-1101 Ma) represents a period of cessation of mafic magmatism and intermittent felsic magmatism (Miller et al., 2013). The Main Stage (1101-1094 Ma) is represented by normal polarity volcanic and intrusive rocks ranging from primitive basalts to rhyolites with a little evidence of contamination based on $\varepsilon Nd = +2$ to -2 and Th/Yb < 1 (Miller et al., 2013). Late Stage (1049-1086 Ma) represents a period of deposition of immature detrital sediments and intermittent volcanic activity (Miller et al., 2013). The Late stage eruptions are dominated by intermediate to felsic magmas (Miller et al., 2013).

All stratified sedimentary and volcanic rocks associated with the MCR were considered to be part of the Keweenawan Supergroup (Morey and Green, 1982). Miller et al. (2002) suggested that all the intrusions associated with the MCR should be considered part of Midcontinent Rift Intrusive Supersuite comprises i) large subvolcanic intrusive complexes (e.g., Duluth Complex), ii) isolated alkali and carbonatitic intrusions (e.g., Coldwell complex), iii) mafic dyke and sill swarms (e.g., Nipigon and Logan suites), and iv) mafic-ultramafic chonoliths (e.g., Eagle, Seagull, Tamarack, Sunday Lake, and the intrusions of the TBN).

2.3.1 Ultramafic Intrusions in the Lake Nipigon Area

There are six main ultramafic intrusions associated with the MCR between Lake Superior and Lake Nipigon, namely the Disraeli, Seagull, Hele, Kitto, Jackfish, and Shillabeer intrusions (Heaman et al., 2007). These ultramafic intrusions typically consist of a pyroxene peridotite core with cumulate textures (Heaman et al., 2007). Geochemically, the six intrusions are mostly similar with uniform rare-earth element (REE) and high field-strength element (HFSE) ratios for the ultramafic intrusions (e.g., Gd/Yb 2.3-5.2 and La/Yb 4-30), which are higher than the Nipigon diabase sills (Hollings, 2007). The ultramafic intrusions have REE and HFSE ratios that are comparable to ocean-island basalts (Hollings, 2007).

The 1112.8 ± 1.4 Ma Seagull Intrusion consists of a lower 650m ultramafic section and an upper mafic section crosscut Quetico metasedimentary rocks, Sibley Group metasedimentary rocks and granite to pegmatites (Fig. 2.3; Heggie, 2005). The ultramafic section is texturally largely cumulate olivine and poikilitic clinopyroxene with lithologies consisting of dunites, peridotites and pyroxenites (Heggie, 2005). The 1117. 5 ± 3.7 Ma Kitto Intrusion is located on the east side of Lake Nipigon (Fig. 2.3; Heaman et al., 2007). It largely consists of lherzolite and olivine websterite with cumulate to poikilitic texture, in addition to pyroxenite and gabbros (Laarman, 2007). The Kitto Intrusion formed by two magmatic pulses in the southern part of the intrusion and a peridotitic and a pyroxene-porphyritic melanogabbroic pulse in the central and the northern part of the intrusion (Laarman, 2007). The process of assimilation of external sulphur from the basement lithologies likely caused sulfur saturation in the Kitto intrusion (Laarman, 2007). The Disraeli Intrusion is located south of Lake Nipigon and was emplaced into the Sibley group and underlying Archean rocks (Fig. 2.3; Hart & MacDonald, 2007). The 1109.9 ± 1.4 Ma Disraeli Intrusion mainly consists of fine-to medium-grained gabbro to olivine gabbro, clinopyroxenite, and wehrlite (Heaman, 2007). The 1106.6 ± 1.5 Ma Hele intrusion has an elliptical shape and has been interpreted to have been emplaced as a sill within the Kama Hill Formation of the Sibley Group (Fig. 2.3; Flank, 2011; Cundari, 2013). The Shillabeer sill is located in the southeast corner of Lake Nipigon and consists of a pyroxene peridotite core with cumulative textures and olivine gabbro irregular outer rims (Fig. 2.3; Heaman, 2007).

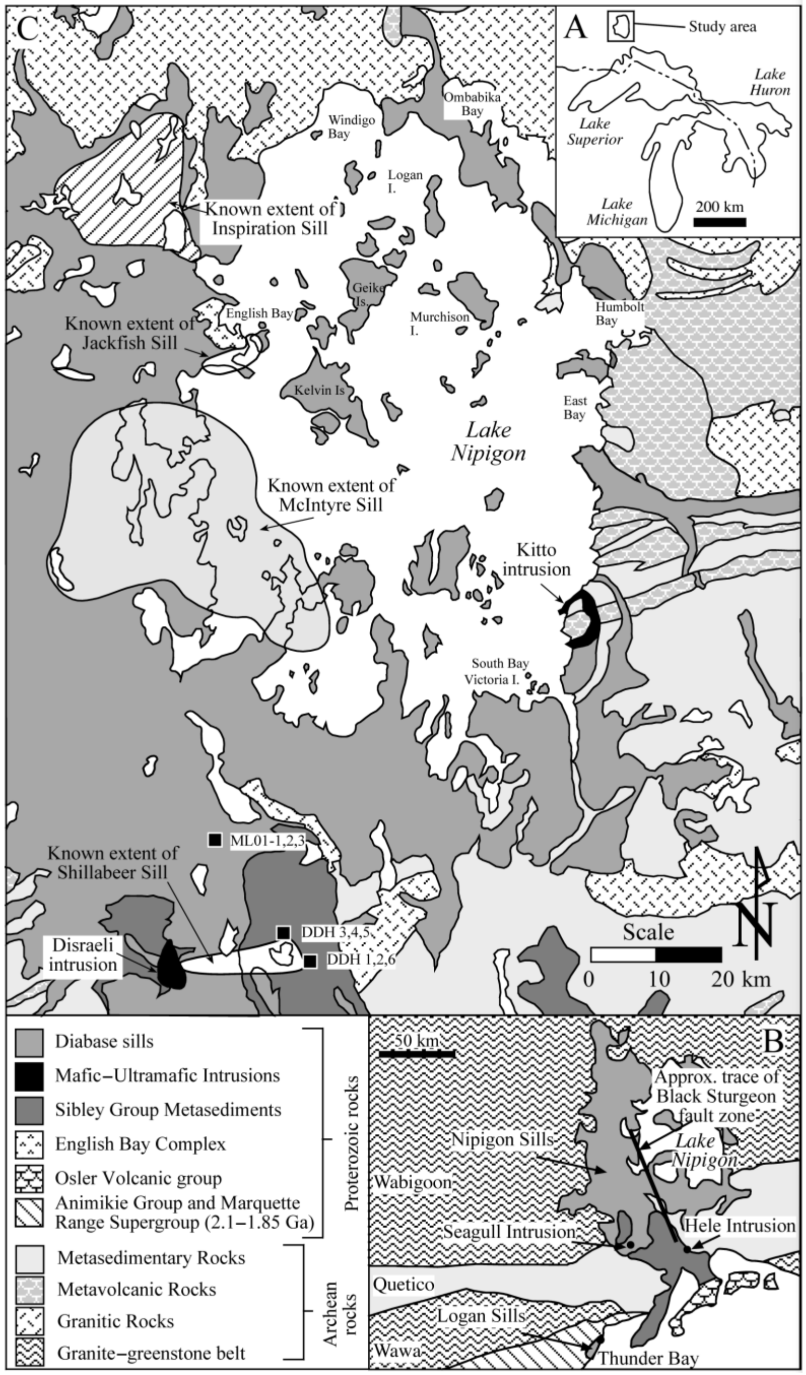

Fig 2.3. Maps A, B, and C showing the location of Seagull, Kitto, Disraeli and Hele intrusions and the Shillabeer sill beside the other MCR related mafic and ultramafic intrusions and the surrounding geology. The maps A,B and C are from Hollings et at., (2007b), Sutcliffe (1986) and MacDonald (2007).

The 1108 ± 1.0 Ma Thunder intrusion is a Cu-PGE mineralized intrusion, located on the outskirts of Thunder Bay, and it comprises a lower mafic to ultramafic basal unit and an upper gabbroic unit. The Thunder intrusion is associated with the initial stages of the MCR (Trevisan, 2015). It represents an ocean island basalt magma with evidence of contamination, such as the Th content and the Nb anomaly, in addition to εNd_T values of (-0.7) and (+1.0) and $^{87}Sr/^{86}Sr_i$ ratios that range from 0.70288 to 0.70611, which has been indicated to be the result of shallow level crustal contamination (Trevisan, 2015).

2.3.2 Mafic and mafic-ultramafic sills

2.3.2.1 Logan and Nipigon sills

The 1115-1106 Ma mafic-ultramafic sills extend west toward Lake Nipigon and to the south of Thunder Bay (Hollings et al., 2007b). The medium- to coarse-grained dominantly diabase sills should properly be named gabbronorite to gabbro, however the term diabase is used with the sills that crosscut the other MCR related rocks to differentiate these sills from the other MCR related older intrusions (Heaman, 2007). The diabase to gabbro sills include Logan sills, Nipigon Embayment, McIntyre sills, Inspiration sills, and the Shillabeer sill (Heaman, 2007). All of these diabase rocks show Subophitic to ophitic texture (Heaman, 2007).

2.3.2.2 Thunder Bay North Igenous Complex and surrounding intrusions

The Thunder Bay North Igneous Complex (TBNIC) and the other surrounding mafic-ultramafic intrusions all formed during the 1.1 Ga MCR (Fig. 2.4). According to Heggie and MacTavish (2015) the TBNIC intrusions were emplaced during the early stages of MCR development (1115-1106 Ma). The mafic and ultramafic intrusions were emplaced into the Archean granitoids and metasedimentary rocks of the Quetico Subprovince (Thomas et al., 2009). The Current, Escape, and Lone Island North and South intrusions seem to be connected by the diffuse East-West Complex (Clark, 2020). Most of the presently identified Ni-Cu-

PGE mineralization is hosted by the Current and Escape intrusions that comprise two of five Mesoproterozoic Keweenawan conduits along the failed MCR margin (Clark, 2020).

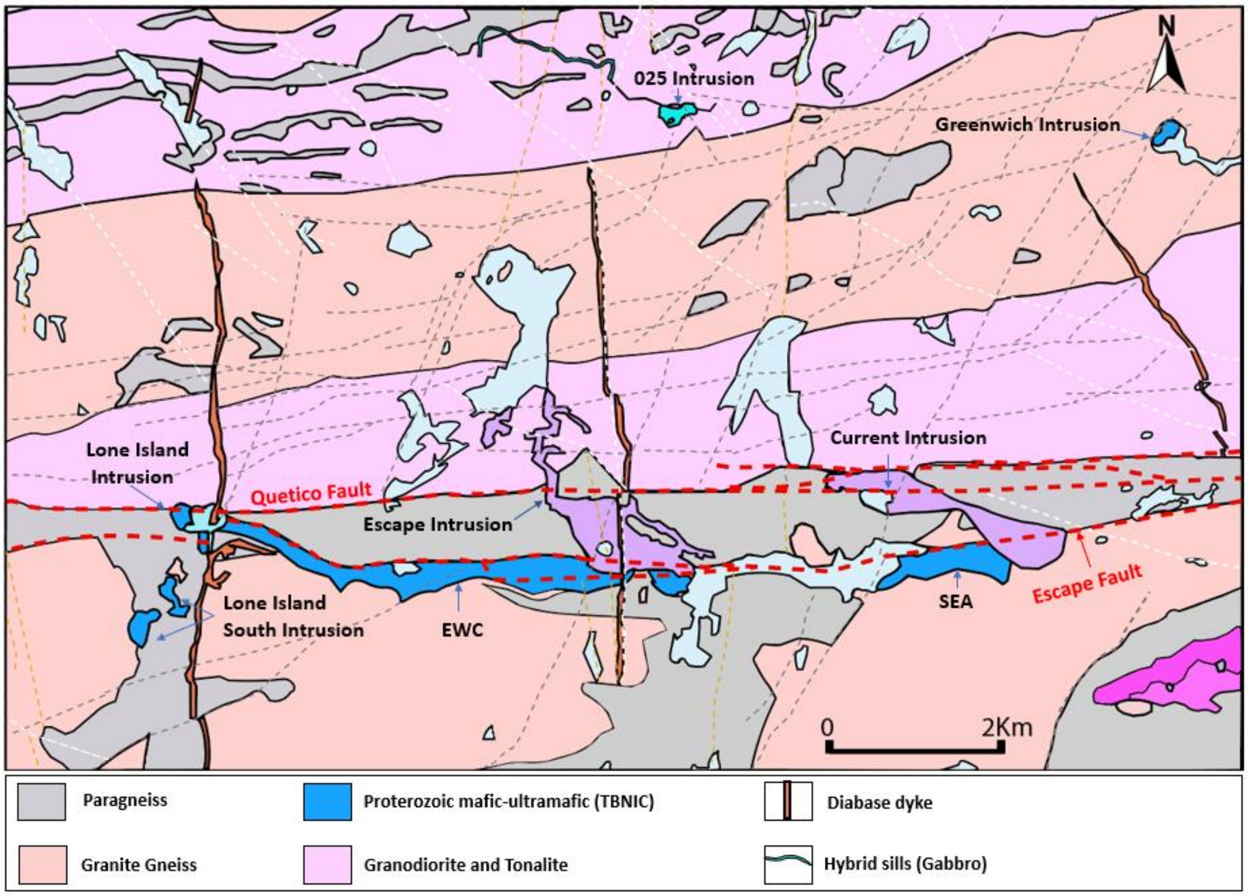

Fig 2.4. A geologic map of the study area showing the locations of the TBNIC, other surrounding intrusions, and the older Archean granitoids and metasedimentary rocks of Quetico Subprovince. The main faults in the area are illustrated by red dashed lines, and the intrusions comprising the TBN highlighted by yellow (modified from Clean Air Metals, 2021).

Based on diamond drilling and magnetic interpretation, TBNIC consists of a sequence of small to medium sized intrusions, thin dykes, sills, and mineralized chonoliths stretching across an area of 18km by 5km (Fig. 2.4; Heggie and MacTavish, 2015). A repeated pattern of intrusions is seen in the TBN magmatic system, which is separated into two levels based on presumed age and petrogenic relationships (Heggie and MacTavish, 2015). Level 1 (L1): consist of the SEA, Escape Lake (EL), and Lone Island Lake Intrusion (LIL) occurring along on E-W trend (Fig. 2.4). These intrusions are defined by their magnetic anomalies and circular shape, ranging in size from 1 to 2km (diameter) and a thickness of 700m. Drilling results suggest a morphology similar to a lopolith (Heggie and MacTavish, 2015). Exploration results show no magma linkage between L1 intrusions (SEA, EL, and LIL), but some similar lithogeochemical sequences were observed between the SEA and the top portion of lithogeochemical sequence of the LIL. Level 2 (L2): includes the Current chonolith (Beaver Lake, Bridge zone, and Current Lake areas) to the N-NW of the SEA Intrusion, and the Escape chonolith (Fig. 2.4, Heggie and MacTavish, 2015). L2 intrusions are classified as chonoliths which are irregularly shaped igneous bodies that do not fall under any of the main categories of the plutonic structures, and they emanate from L1 (Heggie and MacTavish, 2015).

2.3.2.1 Current Intrusion

The Current Intrusion (CI) is a mafic-ultramafic intrusion that hosts PGE Cu-Ni mineralization (Thomas et al., 2009). The CI lies a long the regional structural orientation of the Quetico and Escape faults (Fig. 2.4). Bleeker (2020) obtained a U-Pb age of 1106 ± 1.6 Ma for the CI. Based on aeromagnetic surveys, the CI represents a 6 km long chonolith-shaped intrusion, which is emplaced in the granitoids and metasedimentary rocks of the Quetico Basin (Chaffee, 2015). The main lithologies of CI comprise feldspathic peridotite, lherzolite, and olivine melagabbro (Goodgame, 2010; Thomas et al., 2009). The core of the CI consists of feldspathic dunite with 50-70% olivine (altered to serpentine), 10-25% plagioclase, 4-12% clinopyroxene and orthopyroxene, and 5% magnetite (Chaffee, 2015). The olivine melagabbro to feldspathic core hosts the sulphide mineralization that comprise a few percent to locally greater than 25% of pyrrhotite, chalcopyrite, pentlandite, pyrite, cubanite, and violarite that are interstitial to the silicate gangue (Clark, 2020). According to Chaffee (2015), a portion of the CI is a texturally and mineralogically distinct zone of heterogenous, highly altered, inclusion-bearing, mafic-intermediate intrusive rocks around the edges of the main mineralized body. The rocks have been termed Hybrids and have been subdivided into the Red Hybrid and Grey Hybrid. Chaffee (2015) demonstrated that the Red Hybrid is a fine-to medium-grained, variably-textured subophitic gabbro-quartz ferrodiorite that is highly altered and hematized with local poor mineralization. The Grey Hybrid represents fine-to medium-grained, subophitic quartz bearing gabbro to melagabbro that has been moderately to intensively altered (Chaffee, 2015).

2.3.2.2 Escape Intrusion

The Escape Intrusion is a shallow, south to southeast plunging intrusion (Fig. 2.5) that is more complex than the Current intrusion with significant morphological changes from south to north (Clark, 2020). North of the Quetico Fault, a portion of the Escape Intrusion is a tall hourglass-shaped tube, suggesting presence of two merged conduits with olivine melagabbro to peridotite rocks (Clark, 2020). South of the Quetico Fault, a change in shape is observed from a multi-level tube to a tabular body with a fluted top and base (Clark, 2020).

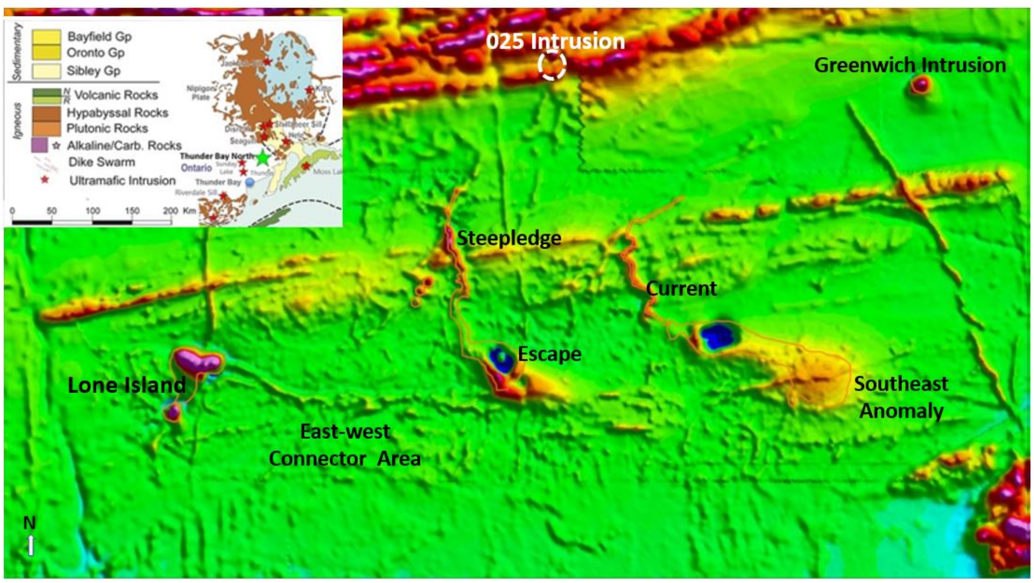

Fig 2.5. A total magnetic intensity map of the TBN. Escape Intrusion, CLI, Southeast Anomaly (SEA), Lone Island Lake (LIL), East-west Connector Area (EWC), Greenwich Intrusion, and 025 intrusion (from Heggie and MacTavish, 2015).

According to D'Angelo, (2016), the lithology of the lower part of the Escape Intrusion is similar to that of the Current Intrusion comprising a magmatically foliated olivine gabbro in contact with peridotite and with olivine pyroxenite in the lower portion. The upper portion of the Escape intrusion has local variations in texture with local rhythmic layering of gabbro and olivine gabbro (D'Angelo, 2016).

2.3.2.3 Lone Island Intrusion

Heggie (2010) described the Lone Island intrusion (LI) as a 1 km circular magnetic anomaly to the west of the EWC (Fig. 2.5). It consists of the Lone Island south (LIS) and Lone Island Lake intrusions (Heggie, 2010). Based on geophysical data and twelve drillholes, the PGE Cu-Ni mineralized Lone Island intrusion is a flat lying gabbroic intrusion (Heggie, 2010). Metsaranta and Kamo (2021) dated a sample from the LI using U-Pb, and it yielded an age of 1106.3 ± 2.1 Ma. Two magmatic fractionation cycles were identified within the LI Intrusion (Cycle-1 and Cycle-2; Heggie, 2010). Cycle-1 (C1) is a fine-to medium-grained and homogenous gabbro intrusion with lateral variation in thickness (Heggie, 2010). Heggie (2010) described the contact between the LI and the overlying Archean rocks as a sharp and diffuse contact containing xenoliths with a thermal metamorphism of the metasedimentary rocks that reaches to amphibolite grade and about 12 m of hematitic alteration (Fig. 2.6).

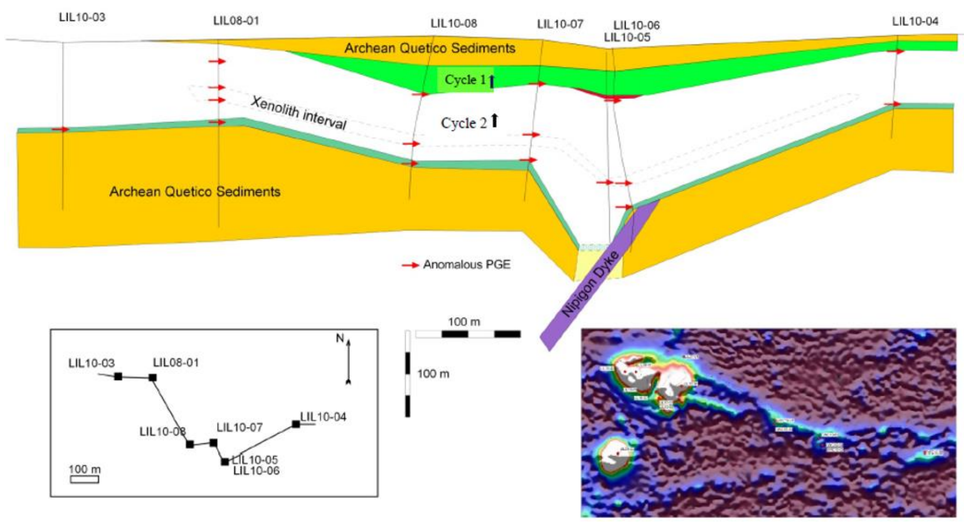

Fig 2.6. A Longitudinal cross-section of LI depicting the location and the relationship of the two fractional cycles of LI (C1 and C2), yellow Archean Quetico sediments, purple Nipigon dyke, and thin hybrid in red with the two black arrows showing the upward direction of fractionation in both C1 and C2 (from Heggie, 2010).

Cycle-2 (C2) is located at base of the intrusion (Fig. 2.6) and exhibits greater lateral variations in thickness compared to C1 (Heggie, 2010). At the thickest portion of the LI intrusion, hybrid-like lithologies were identified in the upper part of the C2 cycle (Heggie, 2010). Based on the presence of xenoliths, pyroxene phenocrysts, and contrasting geochemistry that intersects with the observed fractional sequence, Heggie (2010) suggested that the complexity of C2 is a result of it being contaminated.

2.3.2.4 East-West Connector

The East–West Connector (EWC) exhibits a linear, low magnetic anomaly extending east–west and connecting the Current, Escape, and Lone Island intrusions (Fig. 2.5). Based on eight drill holes, the EWC is a thin mafic intrusion (<5m) with well-defined chill margins associated with the Quetico Fault system (Heggie, 2010). The EWC intrusion is enriched in light REE (LREE) relative to the medium REE (MREE), and MREE relative to the heavy REE (HREE; Heggie, 2010). Negative Hf and Nb anomalies are observed in some of the EWC samples but not in all of them (Heggie, 2010). Negative Nb values are associated with assimilation of continental crust (Dupuy and Dostal, 1984; Heggie, 2010), suggesting that the EWC magmas were variably contaminated by crustal material (Heggie, 2010).

2.3.2.5 Southeast Anomaly Intrusion

The Southeast Anomaly Intrusion (SEA) is part of the Current intrusion, it consists of mostly fine-to medium-grained, dark grey to green lithologies ranging from peridotite in the lower portions of the body to olivine gabbro, ferrogabbro, and quartz gabbro in the upper portions of the body (Scoates and Heggie, 2011). These lithologies were interpreted to be a single complete fractionation sequence from peridotite to quartz gabbro (Scoates and Heggie, 2011). Based on airborne magnetic interpretation, the SEA exhibits a large circular magnetic high trending E-W, following a linear structural feature along the south margin of TBN, which also controls the emplacement of the LI and EWC intrusions (Fig. 2.5; Heggie and Hughes, 2011).

2.3.2.6 025 Intrusion

The 025 intrusion is located 3 km north of Current Lake (Fig. 2.5; Heggie and MacTavish, 2015). According to Heggie and MacTavish (2015) the 025 Intrusion represents the only intrusion that has a surface exposure of olivine cumulate among all the intrusions of Thunder Bay North project area. It is also the only mineralized intrusions with no direct association with the Quetico Fault zone (Heggie and MacTavish, 215). The multi-outcrop exposure mostly consists of fine-grained peridotite that is similar to the boulders and drill core of Current Lake Intrusion (Heggie and MacTavish, 2015). A single drill hole targeted the center of the 025, which intersected low-grade mineralization that comprised of 1% disseminated sulphides (Heggie and MacTavish, 2015).

2.3.2.7 Greenwich Intrusion (GI)

The Greenwich Intrusion is a mafic intrusion, which crosscuts migmatites and metasedimentary rocks of the Quetico subprovince and is crosscut by granitic intrusions (Setterfield and Gilman, 2009). Fourteen drill holes depict a strongly to moderately altered mafic intrusion.

2.4 Mineralization of the TBN

Most of the Pt-Pd-Cu-Ni mineralization in TBN is located within Current and Escape intrusions, although some mineralization has been observed within the LIL and the 025 intrusions (Clark, 2020). Mineralization in the 025 consists of 1% finely disseminated pyrrhotite and chalcopyrite hosted in fine- grained peridotite (Clark, 2020). Based on the low abundance of sulfides within an interval in 025 intrusion that contained up to 0.617g/t Pd, 0.533 g/t Pt, 2130 ppm Cu and 2110 ppm Ni. Clark (2020) proposed that the tenor of the sulfides was relatively high. The mineralization in the Lone Island South (LIS) Intrusion is localized in fine disseminated pyrrhotite and chalcopyrite (Clark, 2020). Basal mineralization in the Lone Island intrusion varies from disseminated mineralization to sulfide blebs with various grades (Heggie, 2010). Some anomalous Pt + Pd values from the SEA are associated with contaminated intervals (Heggie, 2010). The SEA intrusion is relatively deep with a separate and distinct mineralization (Clark, 2020). The mineralization of the SEA is hosted in at least one channelized conduit with disseminated sulphide mineralization ranging from a few precent up to about 25% (Clark, 2020). Resource estimates depict a total of 14.0 million Tonnes of indicated resource (8.2 million Tonnes in Current deposit ,and 5.8 million Tonnes in Escape deposit) with an average of 1.2 million ounces of platinum and palladium (Clean Air Metals, 2023). The mineralization in the Current and Escape intrusions is hosted within magmatic conduits of melanocratic gabbro and peridotites (Clark, 2020).

2.6 Exploration History

Exploration in the area started in 1949 with the uranium discoveries at the Christianson showing on the Greenwich Lake property 5km east of Current Lake. In 1976 Rio Tinto Exploration Ltd. acquired the area and continued working on the Christianson showing and added more ground followed by mapping and drilling (Clark, 2020). Airborne and magnetic and electromagnetic surveys were completed in the area by the Ontario Geological Survey in 1991 that covered 20% of the southern project area (Clark, 2020). In the time between 1993 to 2000 rock chip sampling, prospecting, petrographic and geochemistry works was focused on the Greenwich area and ground magnetic survey was performed in the vicinity of Current Lake (Clark, 2020). Mineralized ultramafic peridotite boulders were discovered along the western side of the shoreline of Current Lake by Graham and Wilson in 2001 (Clark, 2020). From 2001 to 2002 the Current Lake property was optioned by Pacific Northwest Capital Corporation who completed ground magnetic and electromagnetic surveys in 2001 (Clark, 2020). Magma Metals completed intensive drilling and geophysical surveys on the property, and between 2006 to 2012 801 holes were drilled on the Current Intrusion (Clark, 2020). SRK Consulting reported the first mineral resource estimation on behalf of Magma Metals in 2009 followed by a mineral resource calculation by AMEC Americas in 2010 (Clark, 2020). More exploration work was done on the Escape intrusion in 2016 by Rio Tinto Exploration Canada (RTEC, Clark, 2020). In 2019 Benton Resources Inc. (BEX) entered a three year option agreement with RTEC for Escape and Escape North properties and paid C$3 million out of C$6 million (Clark, 2020). In 2020 Clean Air Metals (CAM) optioned BEX, followed by C$3 M payment to RTEC between 2020-2021, which has given CAM 100% ownership of Escape and Escape north properties (Clark, 2020). In 2012 Magma Metals was taken over by Panoramic Resources Ltd. (Clark, 2020). At the current time of writing, the Thunder Bay North project is 100% owned by Clean Air Metals.

3 Analytical methods

Introduction

Core logging and fieldwork took place in the summer of 2021, resulting in the collection of 110 samples from 29 drill holes and seven outcrops. The drill core samples were collected from holes that were selectively re-logged (n = 25; focusing on the mafic–ultramafic samples portions) or fully re-logged (n = 3). The seven surface samples were collected from seven different outcrops of the 025 intrusion. 105 samples were prepared into polished thin sections for the petrographic analysis, 94 samples were utilized for whole-rock analysis, 20 samples were utilized for isotope analysis (17 samples from the five intrusions of this study and three samples from the Escape intrusion), and six samples were submitted for U-Pb zircon geochronological dating.

3.1 Petrography

One hundred five polished thin sections were prepared at the lapidary facility at Lakehead University. Samples were cut, polished, and prepared for reflected and transmitted light microscopic work. Photomicrographs of the polished thin sections were taken with an Olympus BX51 microscope equipped with an Olympus DP70 camera. All 105 samples with their full description are in the Appendix A. Representative polished thin sections were selected from the five intrusions and described in the results chapter.

3.2 Whole-rock geochemistry

Ninety-four samples were submitted to ALS Geochemistry – Thunder Bay, Ontario for whole-rock geochemical analysis, where all sample preparation was done. All samples were weighed, crushed to 70% <2mm using package-CRU-31, spilt using a riffle splitter (package-SPL-21), and pulverized to 250g 85% <75 um. After the 94 samples were prepared, they were sent to ALS lab in Vancouver for chemical analysis. Multiple analytical packages offered by ALS were utilized to obtain the range of elements required for full lithogeochemical examination (Table 3.1). The OA-GRA05 method was used to determine loss on ignition by thermal decomposition furnace. A total of 1 g of each sample were weighed, placed in an oven at 1000°C for one hour, cooled, and then weighed again. The precent loss on ignition was calculated from the difference in weight before and after ignition. Total carbon and sulfur were obtained using LECO infrared spectroscopy.

Major elements were analyzed using fusion decomposition with inductively coupled plasma atomic emission spectroscopy method (ICP-AES). A prepared sample (0.1g) was added to lithium tetraborate flux ($LiBO_2/Li_2B_4O_7$), mixed well, and fused in a furnace at 1025°C. The resulting melt was then cooled and dissolved in an acid mixture containing nitric, hydrochloric, and hydrofluoric acids. This solution was then analyzed by ICP-AES, and the major element results were corrected for spectral inter-element interferences.

Trace elements were analyzed using the inductively coupled plasma mass spectroscopy (ICP–MS). Lithium borate fusion was used to determine 29 trace-elements (Table. 3.1). These elements were analyzed by ICP–MS after the samples were processed by lithium borate fusion and strong acid dissolution. Precious metals and metalloids were also analyzed using ICP-MS. Base metals were determined by four-acid digestion and ICP-AES. All the whole rock geochemistry raw results for the tested 94 samples are presented in Appendix B. All concentrations of elements in this study were recalculated based on 100% volatile free values (anhydrous).

Table 3.1 shows the eight various analytical packages utilized to get a full lithogeochemical examination.

ALS Code	Description	Instrument	Element analyzed
MEICP06	**Whole Rock** (Package-ICP-AES)	**ICP-AES**	Major oxides
C-IR07	**Total Carbon** (IR spectroscopy)	**LECO**	C
S-IR08	**Total Sulfur** (IR spectroscopy)	**LECO**	S
ME-MS81	**Lithium Borate Fusion** ICP-MS	**ICP-MS**	Ba, Ce, Cr, Cs, Dy, Er, Ga, Gd, Ge, Hf, Ho, La, Lu, Nb, Nd, Pr, Rb, Sm, Sn, Ta, Tb, Th, Tm, U, W, V, Y, Yb, and Zr
ME-MS42	Up to 34 **trace elements**	**ICP-MS**	As, Bi, Hg, Re, Sb, Se, Te, and Tl.
OA-GRA05	**Loss on ignition** at 1000°C	**WST-SEQ**	Loss on ignition of hydrous content
ME-4ACD81	**Base Metals** by 4-acid diq.	**ICP-AES**	Ag, Cu, Ni, Mo, Pb, Co, Zn, Zn, Cd, Sc, Zn, Li, and U.

3.3 Isotope analysis

Samples were prepared in a clean laboratory at the Isotope Geochronology and Geochemistry Research Centre (IGGRC) at Carleton University. Rock powders were doped with a ^{148}Nd-^{149}Sm mixed spike before being dissolved in a mixture of concentrated HF and HNO_3. After the sample solutions were dried, the residues were sequentially dissolved in 7 M HNO_3 and in 6 M HCl, and finally dried again. The sample residues were then dissolved in 1.5 mL of 2.5 M HCl and loaded onto 14 mL Bio-Rad borosilicate glass chromatography columns containing 3.0 mL of Bio-Rad AG50W-X8 cation exchange resin. Columns were washed with 16 mL of 2.5 M HCl before Sr was eluted in 7 mL of 2.5 M HCl. The columns were then washed with 3.5 mL of 6 M HCl before the rare earth elements (REE) were eluted using 9 mL of 6 M HCl. The REE fractions were dissolved in 0.26 M HCl and were loaded onto 2 mL of prepacked Ln resin columns (Eichrom Technologies, LLC, USA).

Neodymium was eluted using 0.26 M HCl, followed by Sm elution using 0.5 M HCl. The Sr fractions were purified further to remove Rb and other impurities using columns containing 100 microliters of Sr-Spec resin (Eichrom Technologies, LLC, USA). The Sr fractions were loaded onto the columns and washed in 1.6 ml of 7M HNO_3. Strontium was eluted in 1.6 ml of distilled water.

Strontium and Nd isotope ratios were measured at IGGRC using a Thermo-Finnigan Neptune MC-ICP-MS. Sr and Nd isotopic ratios were normalized against $^{86}Sr/^{88}Sr = 0.1194$ and $^{146}Nd/^{144}Nd = 0.7219$, respectively. $^{143}Nd/^{144}Nd$ ratios were corrected for the offsets using neodymium isotope reference (bracketing JNdi-1) average values against an average JNdi-1 value of 0.512100 determined using a Thermo-Finnigan Triton thermal ionization mass spectrometer at IGGRC. The average values of bracketing standard reference materials (NBS987 for Sr and JNdi-1 for Nd) for a period of six months covering this analytical session are $^{87}Sr/^{86}Sr = 0.710238 \pm 0.000023$ (2SD, n = 28) and $^{143}Nd/^{144}Nd = 0.512094 \pm 0.000012$ (2SD, n = 38). The total procedure blanks are <250 pg and <50 pg for Sr and Nd, respectively. Appendix C exhibits all the isotope raw data with their detection limits.

3.4 Geochronological dating

Samples for U-Pb geochronology were fully processed in the Jack Satterly Geochronology Laboratory at the University of Toronto. Rocks were crushed using a conventional jaw crusher followed by a disk mill. Initial separation of heavy minerals was carried out by passing the heavy concentrate over a shaking, riffled water (Wilfley) table multiple times. Further processing employed density separations with methylene iodide and magnetic separations, with a Frantz isodynamic separator. Final sample selection was achieved by hand picking in alcohol under a binocular microscope, choosing the freshest, least cracked, core- and inclusion-free grains of zircon.

The samples were processed via chemical abrasion pretreatment (CA, modified slightly after Mattinson, 2005) followed by isotope dilution thermal ionization mass spectrometry (CA-ID-TIMS). Zircon grains that underwent CA treatment were annealed in quartz crucibles at 900°C for 48 hours. This removes much, although not all, of the radiation damage induced by the decay of U and Th contained in the mineral, rendering the least altered zircon more inert to chemical attack. The annealed grains were subsequently leached in approximately 0.10 ml of concentrated hydrofluoric (HF) acid for several hours in teflon vessels at 195°C. The altered parts of the crystals, which contain isotopically disturbed Pb, dissolve more rapidly than the annealed, unaltered crystal domains for low to moderate levels of radiation damage. The degree of dissolution is variable, depending on the uranium concentration of the grains and the consequent degree of radiation damage. Chemical abrasion has the advantage of penetrative removal of alteration domains where Pb-loss has occurred, and generally improves concordance.

Weights of mineral fractions chosen for ID-TIMS analysis were estimated from scaled digital photomicrographs, using the density of zircon. Estimated weights should be accurate to about ±20%. This affects only U and Pb concentrations, not age information, which depends only on isotope ratio measurements. Samples were washed briefly in 7 N HNO_3 prior to dissolution. A mixed ^{205}Pb-^{235}U isotopic spike was added to the dissolution capsules during sample loading, and zircon grains were dissolved using concentrated HF in Teflon bombs at 195°C for four days, then dried and re-dissolved in 3N HCl overnight. U and Pb were isolated using 50 microliter anion exchange columns using HCl elutions, dried down, and then loaded onto outgassed rhenium filaments with silica gel (Gerstenberger and Haase, 1997).

Pb and UO_2 were analyzed on a VG354 mass spectrometer using a Daly collector in pulse counting mode. The mass discrimination correction for this detector was constant at 0.07%/AMU. Thermal mass discrimination corrections are 0.10%/AMU for Pb and U. Dead time of the Daly system was 16 ns for Pb during the analytical period, monitored using the SRM982 Pb standard.

Mass spectrometric data were reduced using in-house software (UtilAge program) coded by D. Davis. Corrections for initial ^{230}Th disequilibrium in zircon were applied to the ^{206}Pb/^{238}U ages, assuming a Th/U ratio in the magma of 4.2. All common Pb was assigned to procedural blank. Initial Pb from geological sources above 1 picogram was corrected using the Pb evolution model of Stacey and Kramers (1975). Plotting of Concordia curves and averaging of age results were carried out using the Isoplot 3.71 Add-In for MS Excel (Ludwig, 2009). In the U-Pb data plots, the curve for Concordia is shown as a ‘band’, incorporating uncertainties in the ^{235}U and ^{238}U decay constants. Ages calculated are generally based on weighted averages of ^{207}Pb/^{206}Pb ages (ratios) or regressions using a modified version of the York (1969) algorithm, in which points are weighted proportional to the inverse of the square of the assigned errors, incorporating error correlations (see Ludwig, 2009); in cases involving secondary Pb loss chords, lower and upper concordia intercept ages are provided, but do not incorporate uncertainties in the U decay constants. Probabilities of fit would be expected to be 50% on average for random data with correctly chosen analytical errors. All age errors and error ellipses are given at the 2 sigma or 95% level of confidence. Appendix D shows all the geochronological raw data with detection limits.

4 Results

4.1 Field observations

The 025 and Lone Island are the only intrusions that crop out within the study area, but only the outcrops of the 025 were found in this study. Seven outcrops from the 025 intrusion were visited, all of which comprise peridotitic to gabbroic rock. The 025 intrusion crosscuts the Archean granitoids and metasedimentary rocks of the Quetico Subprovince in all the visited locations (Fig. 4.1).

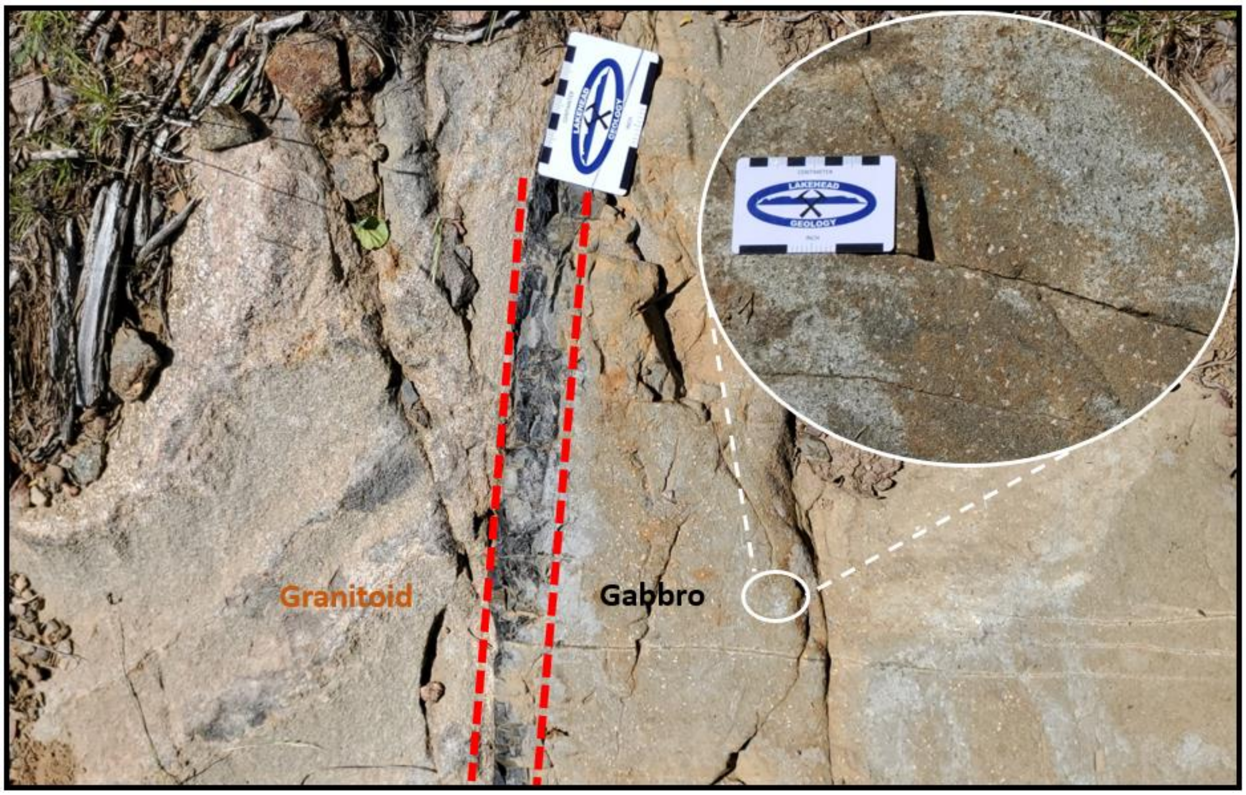

Fig 4.1. Photograph showing the contact between the 025 mafic intrusion and the Archean granitoid country rocks, with a visible chilled margin. The inset photograph in the upper right corner (white circle) highlights porphyritic texture in some of the gabbroic rocks of the 025.

The lithology of the 025 outcrops ranged between gabbro to peridotite. The gabbroic rocks were the most abundant composition, comprised of fine-to medium-grained, grey-colored gabbro (locally named hybrid grey). The hybrid grey gabbro is variably altered with about 35-45% plagioclase, 10-25% pyroxene, 5% magnetite, intruded into paragneiss country rocks, it has a similar mineralogy and texture to the hybrid grey gabbro identified in drill core of other mafic–ultramafic intrusions in the TBNIC. In one of the outcrops, a contact between gabbro and the granitoid country rocks was observed; this contact is marked by a chilled margin (4–5 cm wide, Fig. 4.1). In the center of the outcrop, the gabbro comprises a fine-grained groundmass of pyroxene with medium-grained plagioclase phenocrysts. Most of the hybrid grey gabbro in the drill core of the 025 is medium-to coarse-grained. Some of the hybrid grey gabbro is darker in color with dominant pyroxene and lesser plagioclase, for example sample CAM-021-KY-062 from this outcrop is moderately altered (weakly serpentinized) and fine-grained, comprises greenish grey dominant pyroxene with some plagioclase crystals (Fig. 4.2).

Fig 4.2. Photograph of fine-grained hybrid grey gabbro, with some visible pyroxene and plagioclase crystals (sample CAM-2021-KY-062). The inset photograph shows a close-up view of the hybrid grey with a dominant pyroxene and lesser plagioclase crystals.

The upper surface of the hybrid grey gabbro of the 025 intrusion comprises fine-grained, greyish black pyroxene and plagioclase crystals, and exhibits polygonal jointing (Fig. 4.3). Three main sets of joints were observed in the top of the fine-grained hybrid grey gabbro of the 025 intrusion (Fig. 4.3).

Fig 4.3. Photograph showing the polygonal jointing observed in the top of the fine-grained hybrid grey gabbro of the 025 intrusion.

Most of the surface outcrops of the 025 comprised peridotite, including those outcrops in the center of the intrusion where the first and third holes were drilled (115TB001 and 115TB003). An outcrop of fine-grained, dark greenish–black peridotite was noted about 500 m from drill hole 115TB001 (Fig. 4.4); this peridotite is strongly altered, comprising fine-to very fine-grained crystals of olivine and some pyroxene (Sample CAM-021-KY-066).

Fig 4.4. Photograph of a strongly a fine-grained peridotite of the 025 intrusion with hardly identified pyroxene and olivine with some plagioclase and rare carbonates.

4.2 Petrography

A total of 105 polished thin sections were analyzed, described, and used to characterize the five intrusions. The number of samples utilized in the petrographic analysis of this study is more than those used in whole rock analysis (94 samples), because some mafic and ultramafic sections in the drill core were too small or broken to intervals that were not sampleable. A complete description of the 105 polished thin sections is provided in Appendix B.

4.2.1 Lone Island intrusion

The main lithology of the Lone Island intrusion is gabbronorite, with lesser orthopyroxene gabbro, and websterite, the latter of being located at the base of the intrusion. The gabbro to gabbronorite mostly exhibit a poikilitic texture, with coarse- to medium-grained clinopyroxene (Cpx), orthopyroxene (Opx), and magnetite with exsolution lamellae of ilmenite altered to hematite and enclosed by coarse-grained plagioclase and clinopyroxene oikocrysts (Fig. 4.5a and b).

The orthopyroxene gabbro samples consist of coarse-to medium-grained plagioclase (30-50%), clinopyroxene (10-20%), orthopyroxene (2-8%), and hornblende (1-3%). Rare olivine occurs in the shallow portion of the Lone Island and continues to 154/175 m depth (Fig. 4.5b). The dominant gabbronorite is mostly medium-grained poikilitic to weakly subophitic plagioclase with 35-65% plagioclase, 10-35% clinopyroxene, 3-30% orthopyroxene and sometimes has 1-3% hornblende and/or rare olivine, it starts appearing at 154 to 175 m depth and deeper (Fig. 4.5a). Samples from the Lone Island South and Lone Island Lake portions of the intrusion exhibit no major differences in mineralogy, texture, and alteration intensity. All drill holes show an upward increase in intensity of alteration, starting from weak until it reaches the highest at the contact with country rocks, where strong to pervasive hematization is present. Some samples from the country rocks were collected and analyzed, including felsic to intermediate rocks (granite and tonalite) and a metasedimentary rock (schist), which contains pyrite and chalcopyrite veins

(Fig. 4.5d). The ultramafic rocks from the base of the Lone Island was not sampled due to incomplete drill core sections at the time of sampling.

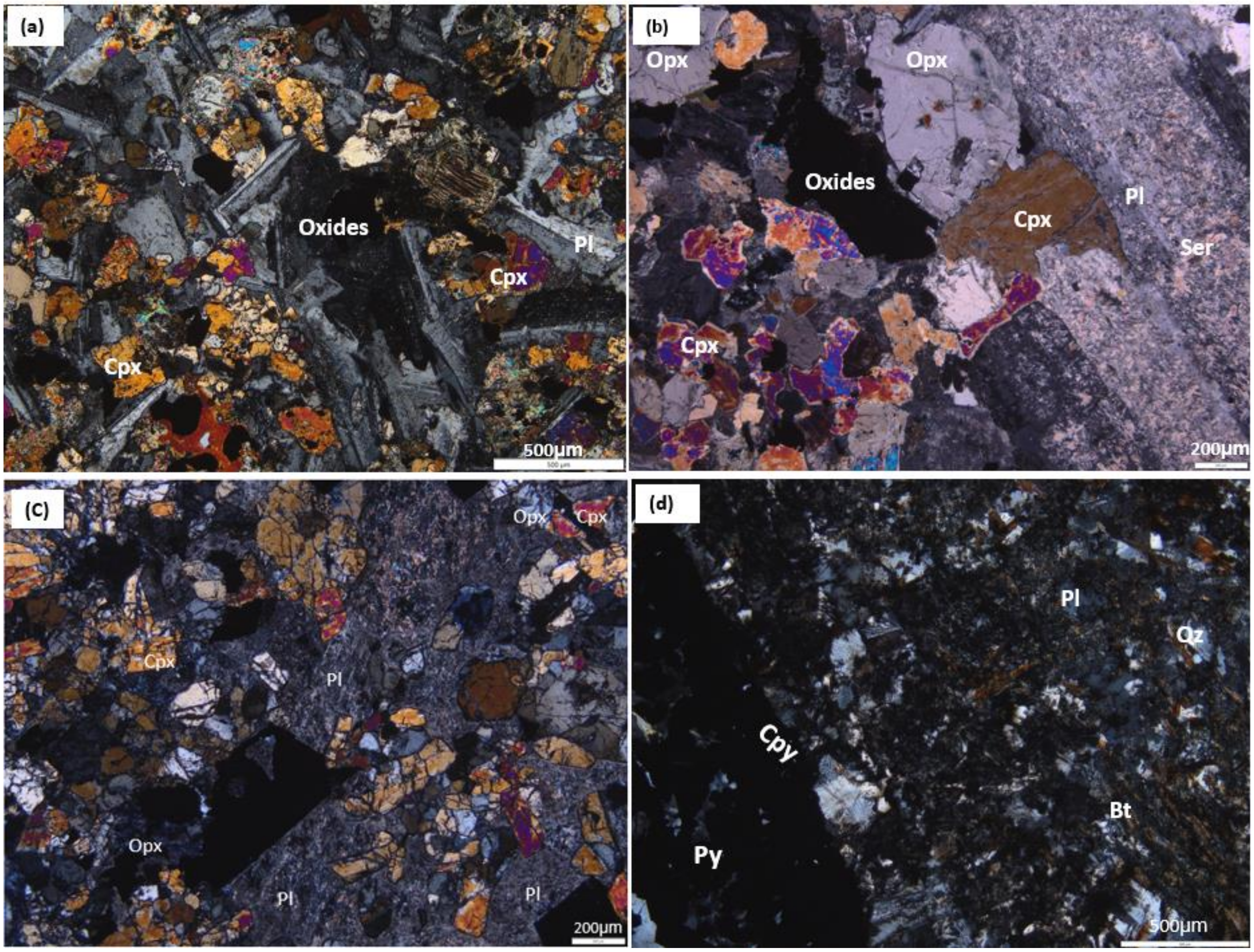

Fig 4.5. Photomicrographs (a) depicting the dominant poikilitic to weakly subophitic gabbronorite in Lone Island beside anhedral oxides (sample: CAM-021-KY-052, depth: 133.4m, drill hole: LIL10-05), (b) showing a gabbro from Lone Island with strongly sericitized pl and Cpx and Opx (sample: CAM-021-KY-001, depth: 18.75m, drill hole: LIL08-01), (c) exhibits a medium-fine-grained orthopyroxene gabbros of Lone Island (sample: CAM-021-KY-011, depth: 62.87m, drill hole: LIL08-02), (d) showing a transmitted light photomicrograph of a country rock sample (schist) with py and Cpy in veins (sample: CAM-021-KY-013, depth: 66.9m, drill hole: LIL08-02). Cpx: clinopyroxene, Opx: orthopyroxene, Pl: plagioclase, Py: pyrite, and Cpy: chalcopyrite.

More than 70% of the opaque minerals in Lone Island comprise fine- to medium-grained, subhedral to euhedral primary magnetite, with ilmenite oxy-exsolution altering to secondary hematite (Fig. 4.6b). Pyrite, chalcopyrite, and pyrrhotite are present in Lone Island, but they are not abundant (Fig. 4.6a). Pyrrhotite can coexist with or be altered to pyrite (Fig. 4.6a). All the mafic samples of the Lone Island intrusion contain fine-grained blebs of chalcopyrite that are sometimes intergrown or included in pyrrhotite, pyrite, ilmenite, or magnetite crystals. Pentlandite is also present as exsolution lamellae or intergrown with pyrrhotite crystals.

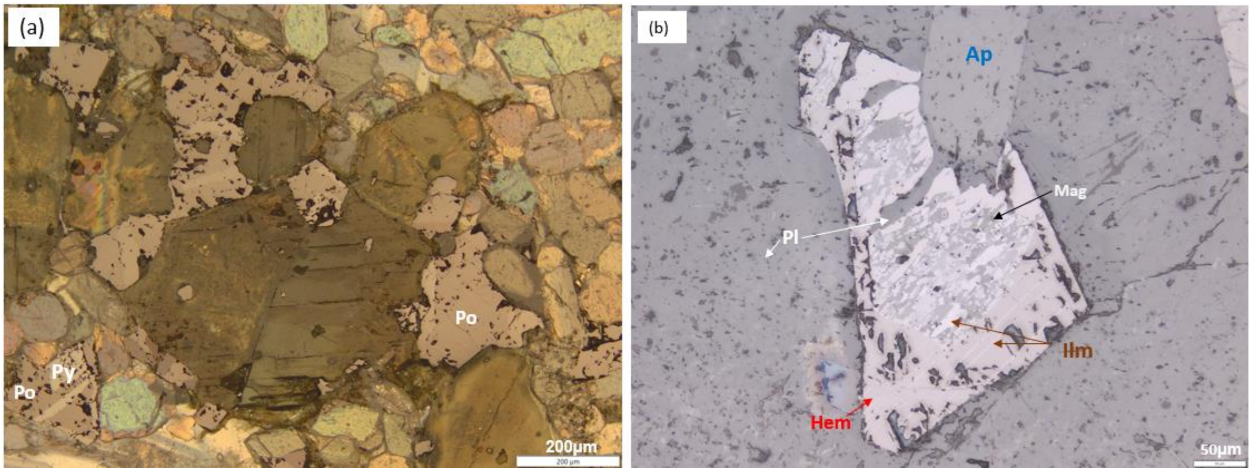

Fig 4.6. Reflected light photomicrographs from LI showing (a) a Po and altered to pyrite and very fine-grained rare chalcopyrite aggregate (sample: CAM-021-KY-053), and (b) primary subhedral magnetite, with ilmenite oxy-exsolution lamellae, being replaced by hematite (sample: CAM-021-KY-001). Mag: magnetite, Il: ilmenite, Hem: hematite, Pl: plagioclase, Ap: apatite, Cpy: chalcopyrite and Py: pyrite.

4.2.2 025 Intrusion

Surface outcrop and drill core samples of the 025 intrusion range in lithology from gabbronorite to websterite and lherzolite. The gabbronorite rocks are generally medium-to coarse-grained, exhibit poikilitic and sometimes poikilitic and subophitic textures with 10-50% plagioclase (higher in surface samples), 9-40% clinopyroxene, 5-33% orthopyroxene,1-30% sericite, 1-20% serpentine, in addition to 1-10% primary biotite and hornblende in some samples (Fig. 4.7a–d). The gabbronorite rocks have 1-15% fine-to medium-grained magnetite with rare ilmenite exsolution, moderately to strongly altered to hematite with 1-2% pyrrhotite and less than 1% very-fine to fine disseminated blebs of chalcopyrite present in all of the samples. Websterite is the second most common lithology in the 025 intrusion after gabbronorite, it comprises medium-grained 0-10% plagioclase, 15-45% clinopyroxene, 5-40% orthopyroxene, 1-10% biotite, 0-10% hornblende. Alteration minerals in websterite include 3-15% weak to moderate sericite replacing clinopyroxene, orthopyroxene and plagioclase, 4-20% weak to moderate serpentine and 0-3% iddingsite (Fig. 4.8a and b). CAM-021-KY-095 is the only ultramafic sample from the

025 that was characterized as lherzolite, it is moderately serpentinized (12% serpentine) with coarse-grained poikilitic clinopyroxene (60%) and 10% orthopyroxene with 6% biotite and 3% plagioclase (Fig. 4.8c and d).

Based on grain size and degree of alteration, the O25 can be subdivided into two main lithological groups. The first group (I) is distinguished by coarse-to medium-grain sizes, with oikocrysts of plagioclase surrounding chadacrysts of clinopyroxene, orthopyroxene, olivine, oxides, and sulphides. This group is very strongly to pervasively altered, with plagioclase altered to sericite, and olivine ± pyroxene altered to serpentine (Fig. 4.7a and b). The second group (II) is characterized by a medium-to fine-grain size, subophitic plagioclase, and weak to moderate sericitization and serpentinization (Fig. 4.7c and d).

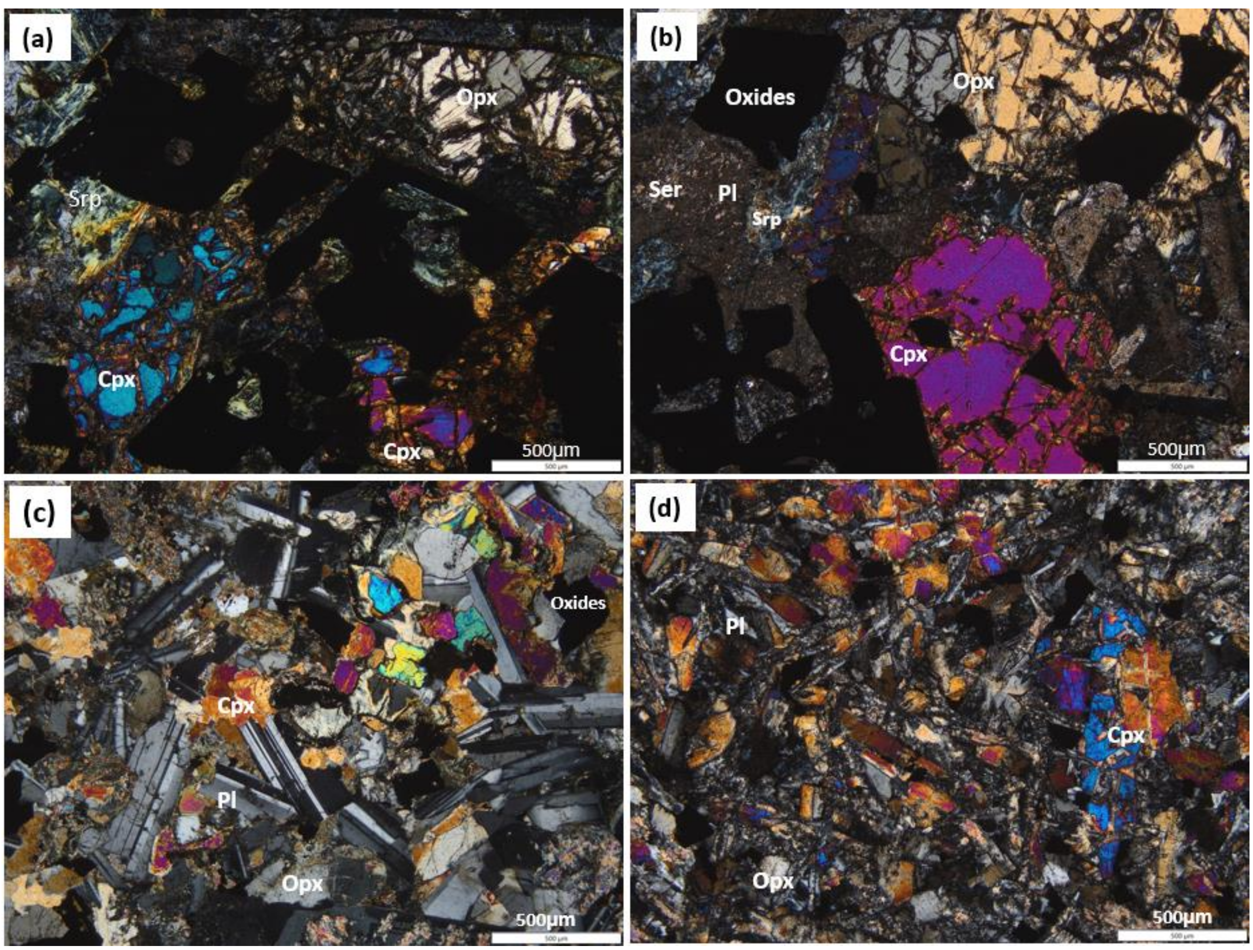

Fig 4.7 Photomicrographs from the 025 showing (a) and (b) Pervasively altered coarse- to medium-grained poikilitic crystals of group I (sample: CAM-021-KY-065 and 093 respectively), (c) and (d) weak to moderately altered subophitic grains of group II (sample: CAM-021-KY-064 and 105 respectively). Where Cpx: clinopyroxene, Opx: orthopyroxene and Pl: plagioclase.

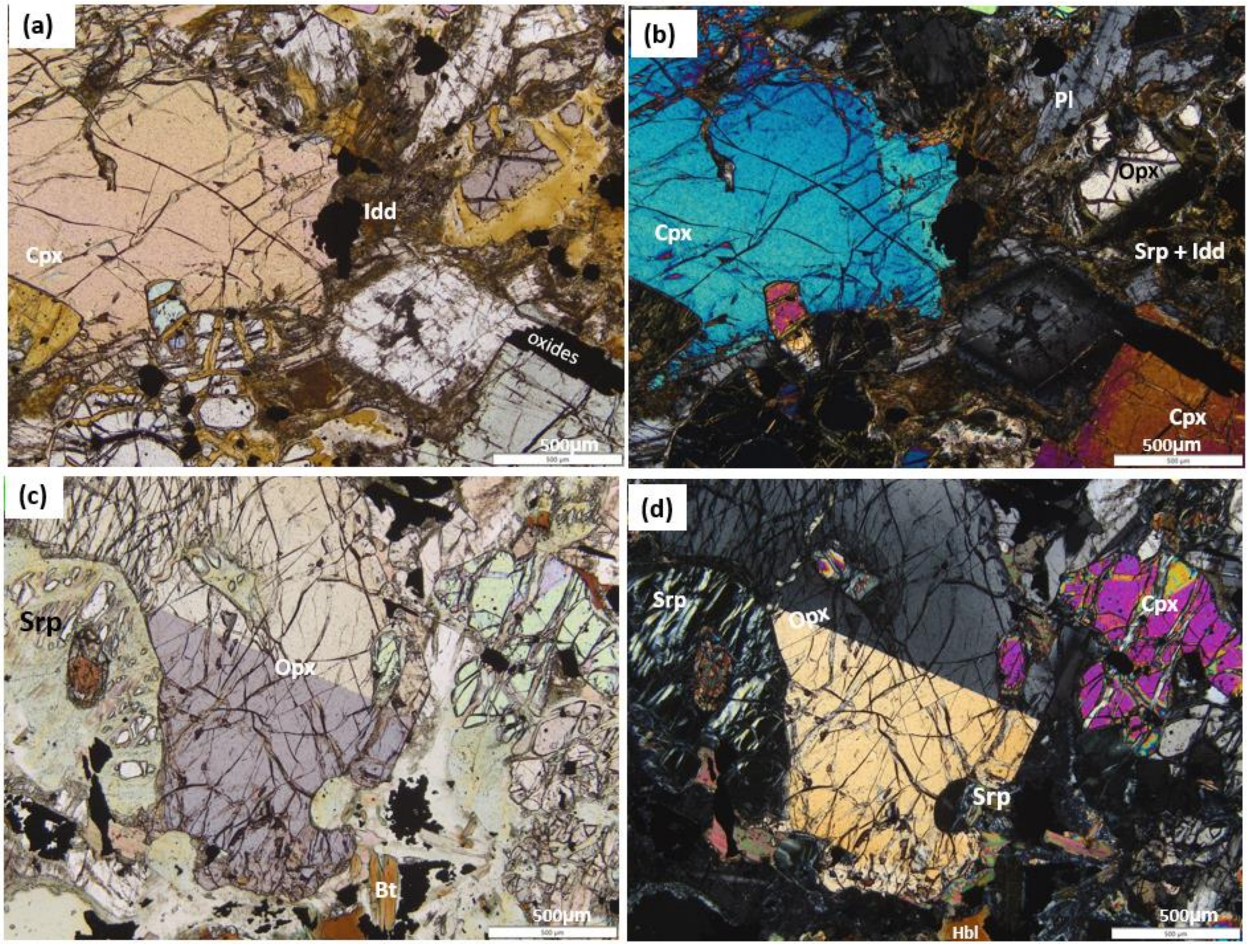

Fig 4.8 (a) Plane-polarized (PPL) and (b) cross-polarized (XP) photomicrographs of strongly altered websterite (sample CAM-021-KY-065), c) Plane-polarized (PPL) and (d) cross-polarized (XP) photomicrographs of moderately altered lherzolite (sample CAM-021-KY-095). Cpx: clinopyroxene, Opx: orthopyroxene, Pl: plagioclase, Hb: hornblende, Ser: sericite, Srp: serpentine and Idd: iddingsite.

Oxide minerals and sulphides are medium-grained in group I and medium-to fine-grained in group II with similar poikilitic texture as the silicate minerals. Later veins crosscut the gabbronorite and websterite rocks of the 025 intrusion, comprise up to 40% concentrically zoned magnetite bands and 30% fine-to medium-grained thin bands of pyrrhotite intergrown with chalcopyrite, cubanite, pyrite, and pentlandite (Fig. 4.9a and b). There are very-fine to fine-grained disseminated blebs of chalcopyrite and sometimes pyrite or cubanite in all of the samples from the 025 intrusion (Fig. 4.9 c and d).

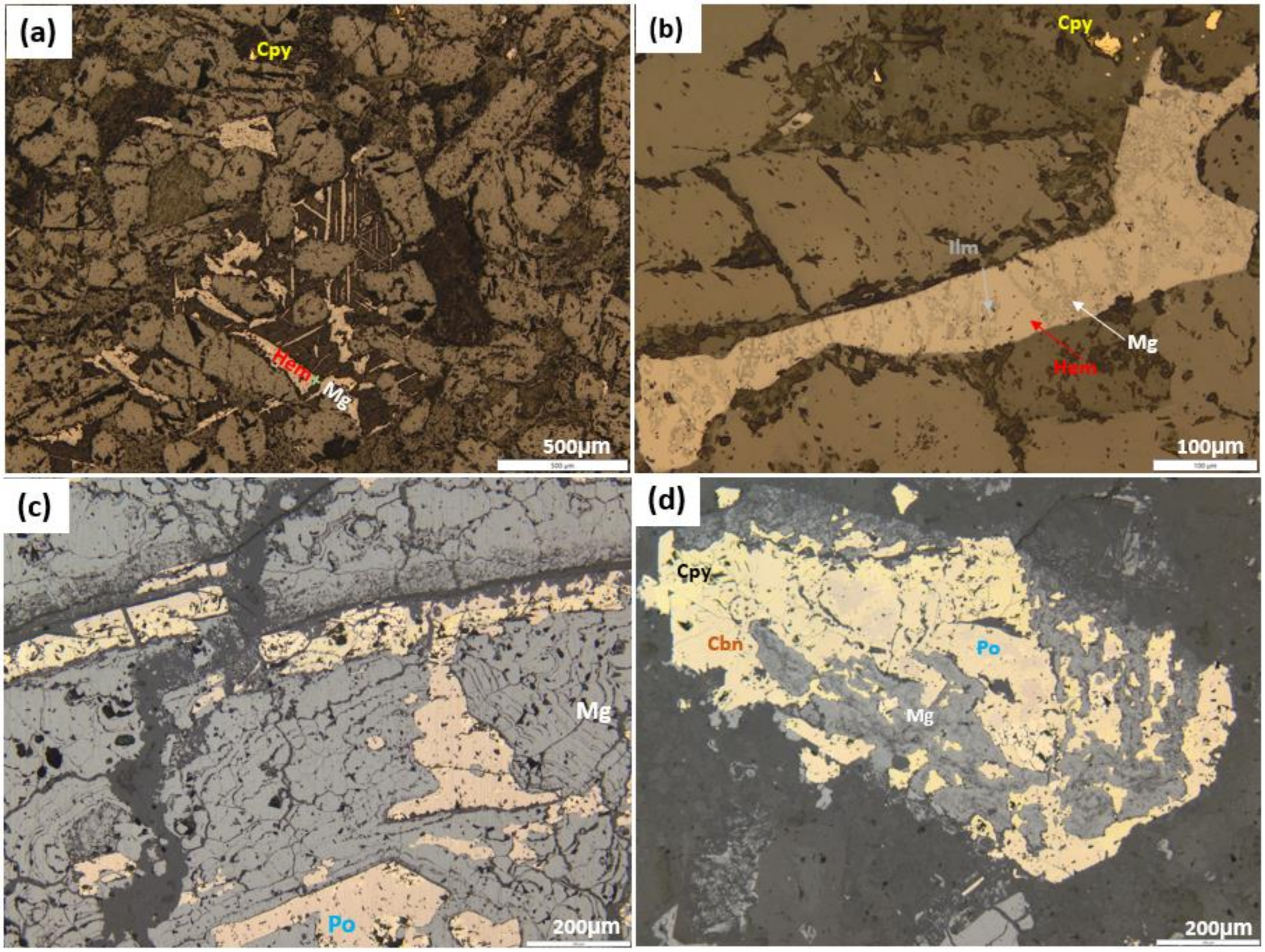

Fig 4.9 Reflected light photomicrographs of (a) Mag with Ilm exsolution, altering to hematite with very-fine to-fine-grained blebs of Cpy, (b) a close-up view showing Mag and Ilm fine-grained relicts in hematite crystal (sample CAM-021-KY-094), c) a vein hosting concentrically zoned Mag crosscuts a websterite, (d) Po, Cpy, Cbn intergrown with Mag in one grain (sample CAM-021-KY-096). Mag: magnetite, Ilm: ilmenite, Hem: hematite, Po: pyrrhotite, Cpy: chalcopyrite, Cbn: cubanite.

4.2.3 Southeast anomaly

The thin gabbroic to peridotitic intrusive units of the SEA crosscut the Quetico rocks, with sharp contacts. The gabbroic portions of the SEA comprise strongly sericitized, medium-to fine-grained plagioclase with strongly serpentinized, medium- to fine-grained pyroxene; plagioclase ranges from 30% in gabbro to about 50% in the hybrid grey gabbro (Fig. 4.10 a and b). The medium-grained peridotite is strongly serpentinized and is classified as websterite with 30-40% clinopyroxene, 20-30% orthopyroxene, and 5% olivine (Fig. 4.10 c and d). All of the SEA samples contain 2-3% biotite that has been partially altered to chlorite; and hornblende is rare. Carbonate alteration is observed in most of the samples, ranging from 3-8%.

Serpentine (4-6%), sericite (5-17%) and iddingsite (1-3%) are also present in all of the samples. Most SEA samples are poikilitic, comprising medium-grained plagioclase surrounding chadacrysts of clinopyroxene and lesser orthopyroxene (Fig. 4.10a, b, c, and d). The SEA (alongside the GI and EWC; described below) is one of the most altered intrusions studied.

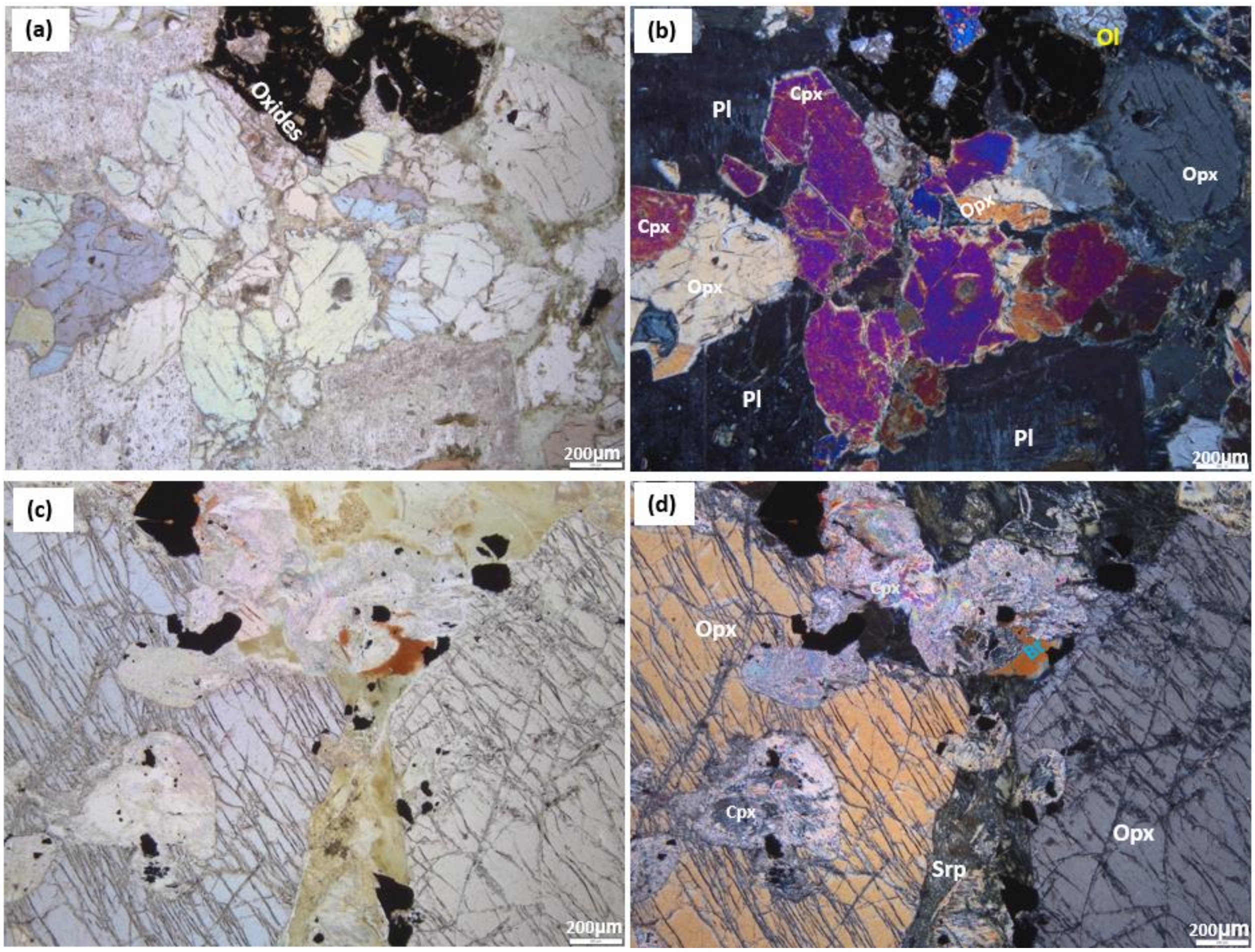

Fig 4.10 (a) Plane polarized and (b) XP photomicrographs showing the medium-to fine-grained anhedral poikilitic gabbronorites of the SEA (from sample: CAM-021-KY-109), (c) and (d) are PPL and XP respectively of a strongly altered medium-grained websterite (sample: CAM-021-KY-110). Cpx: clinopyroxene, Opx: orthopyroxene, Pl: plagioclase, Ol: olivine, Bt: biotite, Ser: sericite and Srp is serpentine.

Oxides are the most abundant opaque minerals in the SEA intrusion with 1-5% content. Magnetite is present as subhedral grains and sometimes multiply zoned, moderately to strongly hematized with ilmenite lamellae and grain boundaries replaced by plagioclase (Fig. 4.11a,b,c, and d). Chalcopyrite (1%) occurs as fine-grained disseminated grains, sometimes as rare medium-grained crystals intergrown with pyrite or disseminated in the oxide grains (Fig. 4.11d).

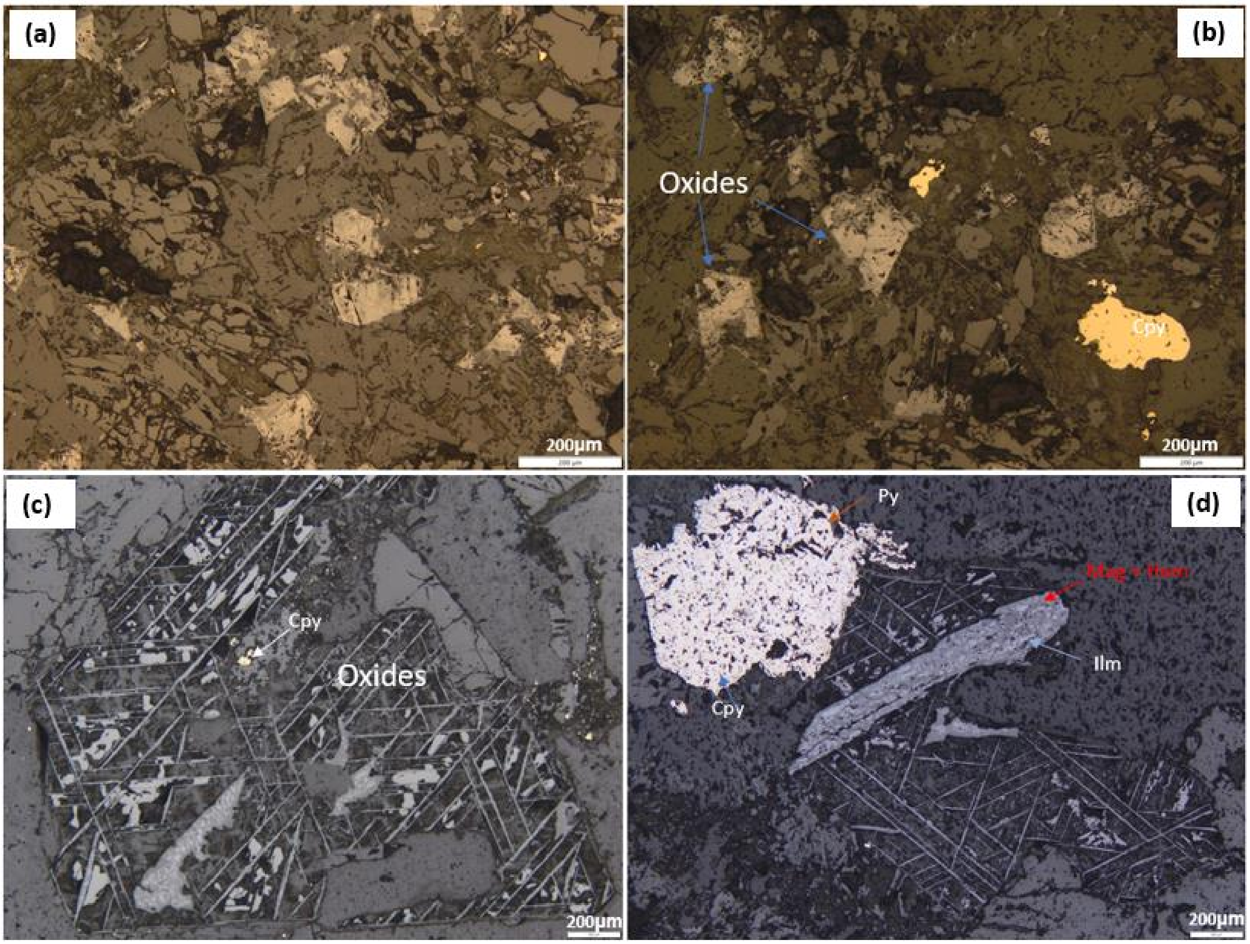

Fig 4.11 Reflected light photomicrographs of (a) Mag, Hem, and Ilm subhedral grains with grain boundaries replaced by Pl and pyroxene, (b) very-fine to fine-grained blebs of Cpy (sample CAM-021-KY-029), c) Zoned oxides (Mag, Hem, and Ilm) with very fine-grained Cpy, (d) strongly hematized Ma, and Py intergrown with Cpy (sample CAM-021-KY-109). Mag: magnetite, Ilm: ilmenite, Hem: hematite, Cpy: chalcopyrite, Pl: plagioclase.

4.2.4 EWC and Greenwich intrusions

The mafic Greenwich and EWC intrusions are located in geographically distinct areas of the TBNIC but are both pervasively altered. Alteration minerals comprises 50-65% sericite, 35-50% serpentine, iddingsite, and carbonates (Fig. 4.12 a, b, c, and d). Serpentine veins crosscut the rocks of the Greenwich intrusion. Two groups of Greenwich were identified in thin sections; one with subophitic texture (Greenwich-1), Fig.4.12 e) and a second group (Greenwich-2)) with a pervasively altered poikilitic texture (Fig. 4.12 f).

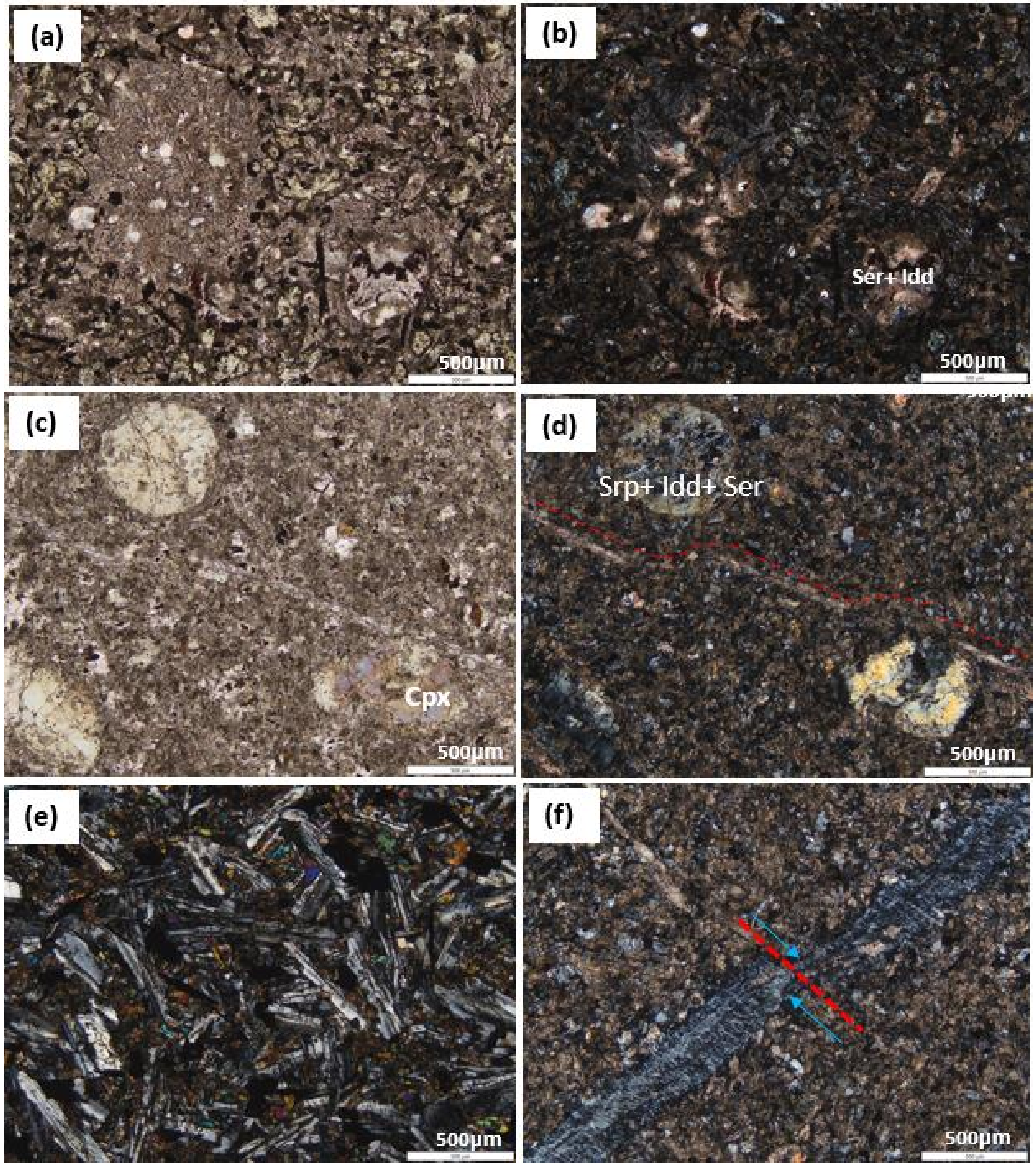

Fig 4.12 (a) PPL and (b) XP photomicrographs from sample CAM-021-KY-036 of EWC with a pervasive sericitization and serpentinization and some relicts of poikilitic texture, (c) and (d) PPL and XP photomicrographs from CAM-021-KY-070 (GI) with pervasively sericitized and serpentinized gabbroic polished thin sections, (e) ophitic texture in GI, (f) serpentine vein (from CAM-021-KY-070 of GI) with brittle deformation as indicated with red line and blue arrows.

Both the Greenwich intrusion and EWC have lower oxide (magnetite, hematite, and ilmenite) and sulphide (mostly chalcopyrite) content than Lone Island and SEA, comprise fine- to very fine-grained anhedral chalcopyrite, pyrite, and pyrrhotite, and fine-grained magnetite blebs with ilmenite oxy-exsolution and hematite alteration (Fig. 4.13 a and b).

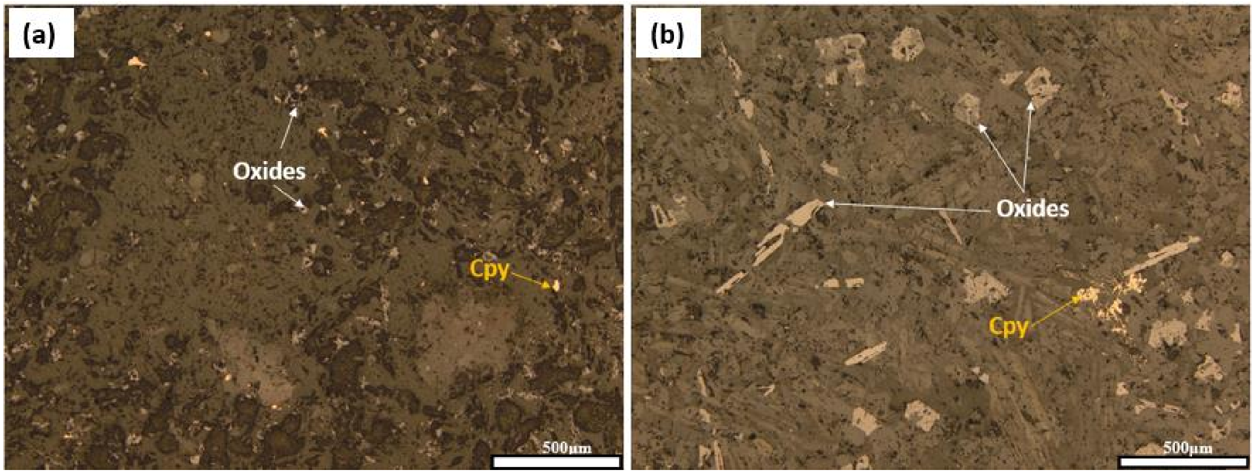

Fig 4.13 Reflected light photomicrographs of (a) fine-grained oxides (Mag, Hem, and Ilm) with very-fine to fine-grained blebs of Cpy (sample CAM-021-KY-036, EWC), (b) fine-grained oxides and fine-to very-fine-grained Cpy (sample CAM-021-KY-074, GI). Mag: magnetite, Ilm: ilmenite, Hem: hematite, Cpy: chalcopyrite.

4.3 Geochemistry

Whole rock major and trace-element data were obtained for 94 samples. A complete dataset of the whole-rock major-element chemistry of the five intrusions is presented in Appendix C. The data have been recalculated to 100% anhydrous compositions to correct for loss on ignition and serpentinization.

The five intrusions largely comprise mafic rocks with SiO_2 ranging between 44.8 to 52.8% (average of 51.0%), 6.24 to 15.7% Fe_2O_3, 3.21 to 18.6% MgO and 0.56 to 3.33% TiO_2. Lesser ultramafic rocks are present with concentrations of 42.8 to 43.9% SiO_2 (average of 43.42%), 15.8 to 20.6% Fe_2O_3, 6.78 to 27.9% MgO and 0.56 to 3.63% TiO_2. On the MgO vs Al_2O_3, NaO_2, CaO, TiO_2, Cr_2O_3 and Ni binary variation diagrams, the Lone Island, EWC, SEA and portion of the 025 and Greenwich intrusions plot in clear fractionation trends, and continued with data from the surrounding Escape and Current intrusions. Whereas portion of the other portions of the 025 and Greenwich intrusions are plotted apart from the first group of intrusions (Fig. 4.14). On the Total Alkali versus Silica (TAS) binary diagram, the mafic samples of the five intrusions plot in the gabbro field, whereas the peridotite samples show lower SiO_2 content and plot in the ultramafic field (Fig. 4.15).

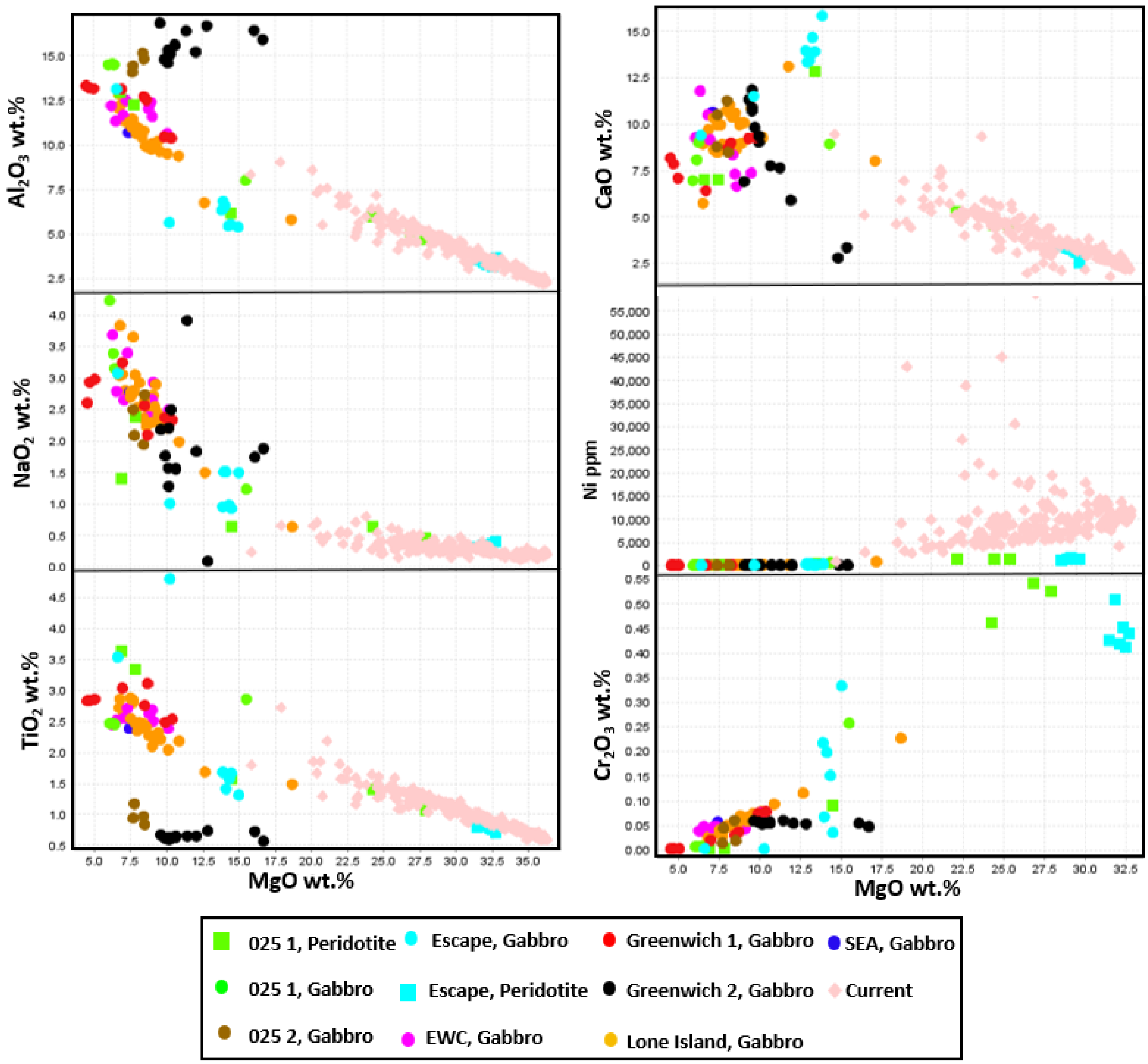

Fig 4.14 Binary variation diagrams of MgO vs selected major elements (Al2O3, NaO2, CaO, TiO2, Cr2O3 and Ni) for the five intrusions, showing the fractionation trends of the Lone Island, EWC, SEA and portion of the 025 and Greenwich intrusions with the surrounding Escape and Current intrusions from the TBN. The data for the Escape intrusion (Connor Caglioti, MSc, 2021), Current (Clean Air Metals, 2021).

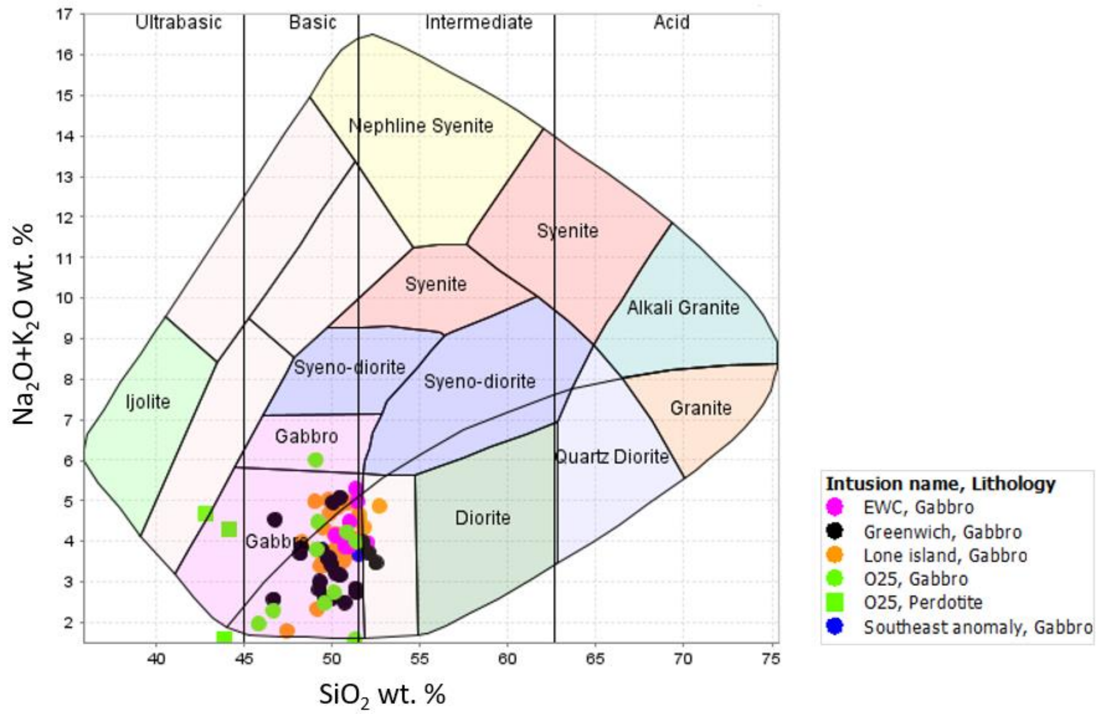

Fig 4.15. Total Alkali Silica diagram for mafic and ultramafic rocks from the TBNIC. Adopted from Cox et al. (1979) and Wilson (1989).

4.3.1 Lone Island Intrusion

No ultramafic rocks were sampled from the Lone Island intrusion. However, the gabbroic rocks have major element concentrations between 47.4 to 52.7% SiO_2, 4.5 to 18.7% MgO, 0.02 to 0.23% Cr_2O_3 with 58.8 to 817.23 ppm Ni and 2.34 to 4.12 La/Sm_n. Most of the gabbroic rocks were gabbronorite with some orthopyroxene gabbro samples. The orthopyroxene gabbro samples are located at the top portion of the Lone Island, starting at 18 m depth and continuing down to 155 m depth (drillhole: LIL-10-01) or 174 m (drillhole: LIL-10-04), they have higher SiO_2 and lower MgO than the lower basal gabbronorite portion (Figs. 4.16 and 4.17). The lower gabbronorite portion start at 155/174 m depth to the bottom of the tested holes, they have lower SiO_2 and higher MgO (Figs. 4.16 and 4.17). The increase in MgO content of the lower ultramafic portion of the LI is associated with an increase in Cr, Ni and Cu abundances and decrease in Fe_2O_3, K_2O, Al_2O_3, however the top gabbroic portion has higher SiO_2,Fe_2O_3, K_2O and Al_2O_3 but lower MgO, Cr, Ni, and Cu (Figs. 4.16 and 4.17). The magnesium number (Mg#) of the LI gabbroic rocks range between 51 to 72.

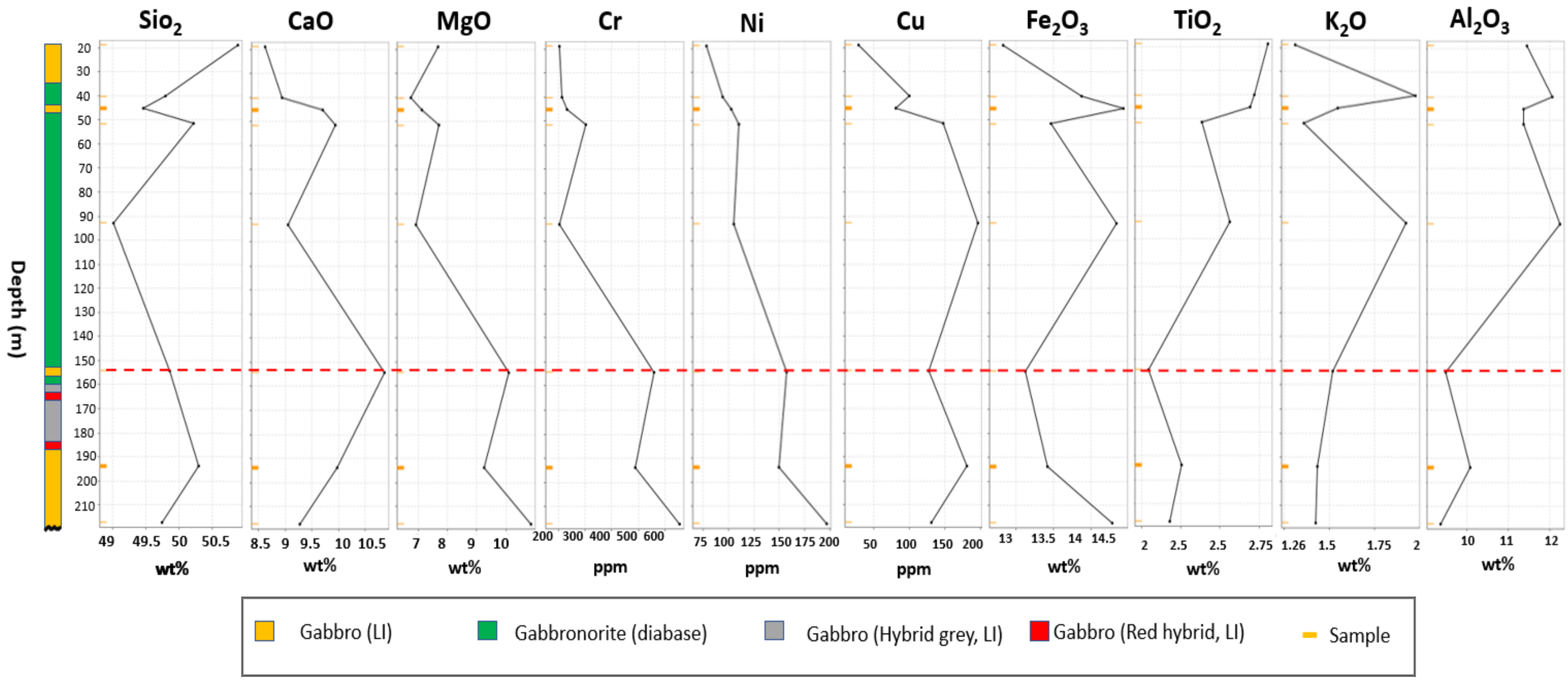

Fig4.16 Downhole plot of hole LIL-10-01 displaying the variation in major element composition of the LI, lower SiO_2 and higher MgO, Cr, Ni and Cu in the base of the LI (from 155m and below) compared to the upper portion (at 18 to 154m depth). The red line separates the lower and upper portions of LI.

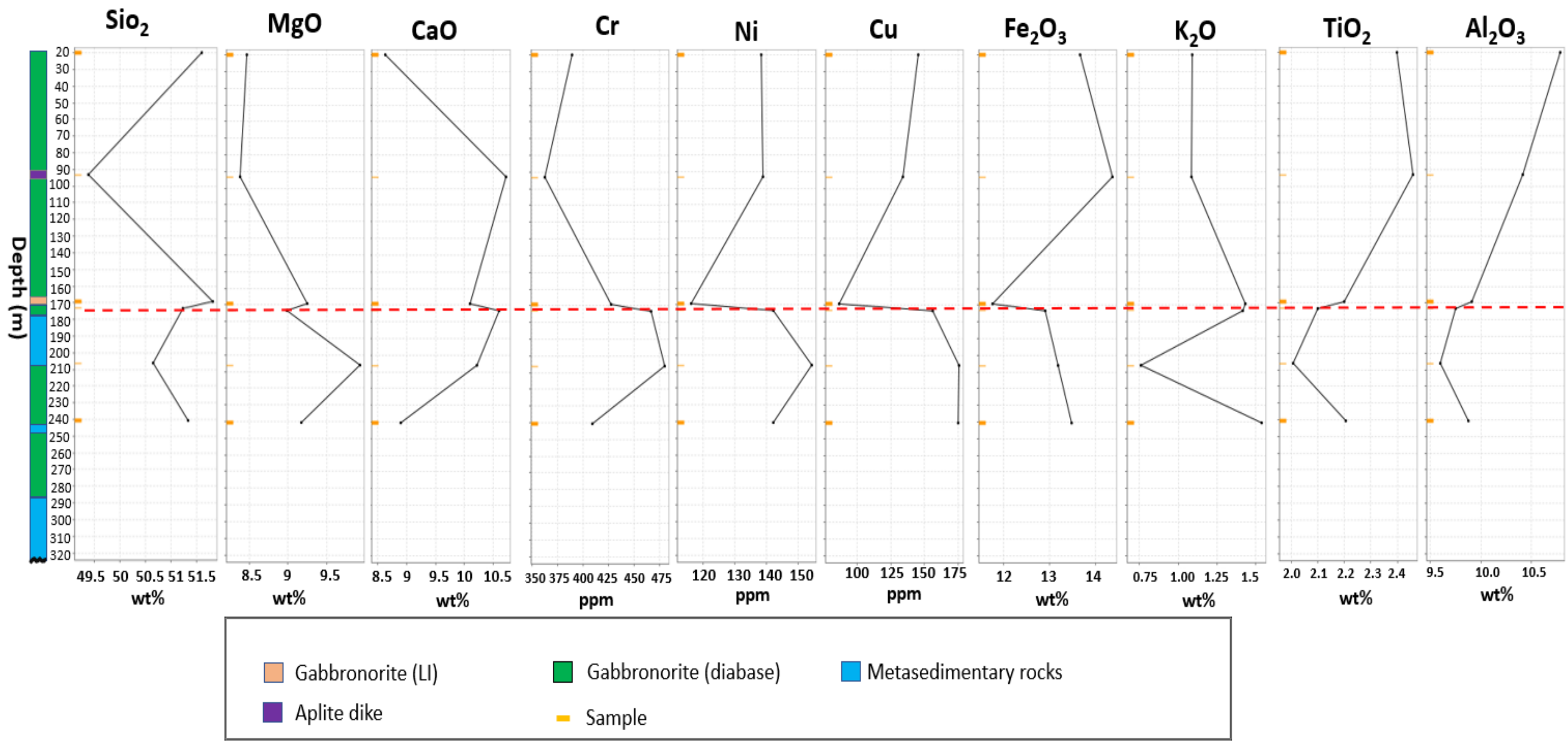

Fig4.17 Downhole plot of hole: LIL-10-04 showing the major element composition variation of the LI, lower SiO_2 and higher MgO, Cr, Ni and Cu at the ultramafic base of the LI (from 155m and below) than the upper portion (at 18 to 176m depth). The red line separates the lower and upper portions of LI.

The orthopyroxene-gabbro samples at the top of the Lone Island have La/Sm$_n$ ratios range between 2.3 to 3.7 and 4.2 to 4.9 Gd/Yb$_n$, whereas the gabbronorite at the lower portion of the Lone Island has ratios range between 2.4 to 4.1 La/Sm$_n$ and 5.3 to 3.9 Gd/Yb$_n$. Primitive mantle normalized diagrams of the Lone Island exhibit heavy rare earth element (HREE) depletion with negative Zr, Nb, Ti and Y anomalies, strong Sc depletion, and enrichment of V (Fig. 4.18). The Lone Island intrusion is enriched in light REE (LREE) and medium REE (MREE) with a steep pattern on primitive mantle normalized diagrams.

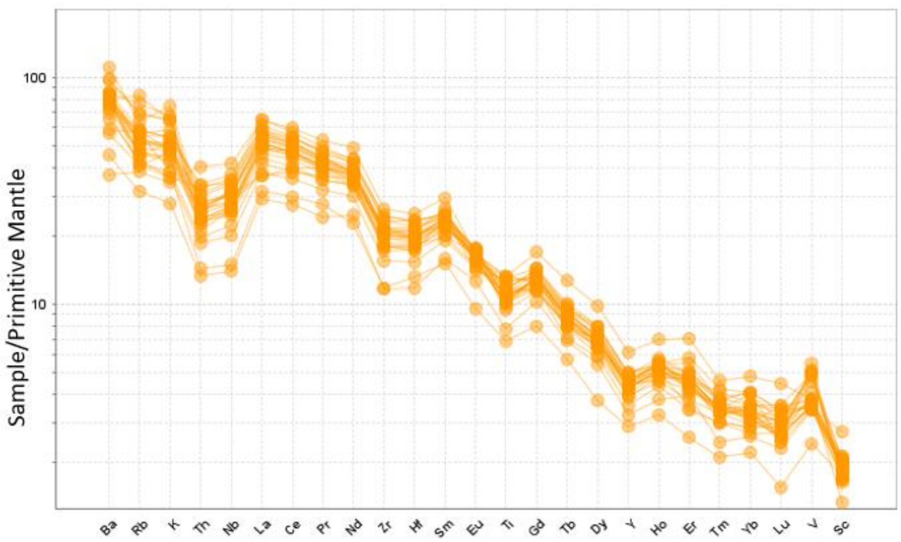

Fig 4.18 Primitive mantle-normalized diagram for the Lone Island intrusion. Normalizing values from Sun and McDonough (1989).

4.3.2 EWC

Due to the very short length of some intervals and some missing core boxes no ultramafic rocks were sampled for the EWC, thus all the samples were gabbroic. Based on the petrographic analysis, all of the gabbroic rocks of the EWC are gabbronorites. These gabbronorites have major element abundances between 50 to 52% SiO_2, 6.25 to 10.1% MgO, and 0.039 to 0.078% Cr_2O_3. The EWC mafic samples were plotted on the Total Alkali Silica diagram (SiO_2 versus K_2O+Na_2O). It shows similarity of composition between the EWC samples, and exhibits alkalic gabbro composition (Fig. 4.19). The EWC gabbroic rocks have magnesium number (Mg#) range between 52.4 to 62.3, which is lower than Lone Island (51.1 to 71.8).

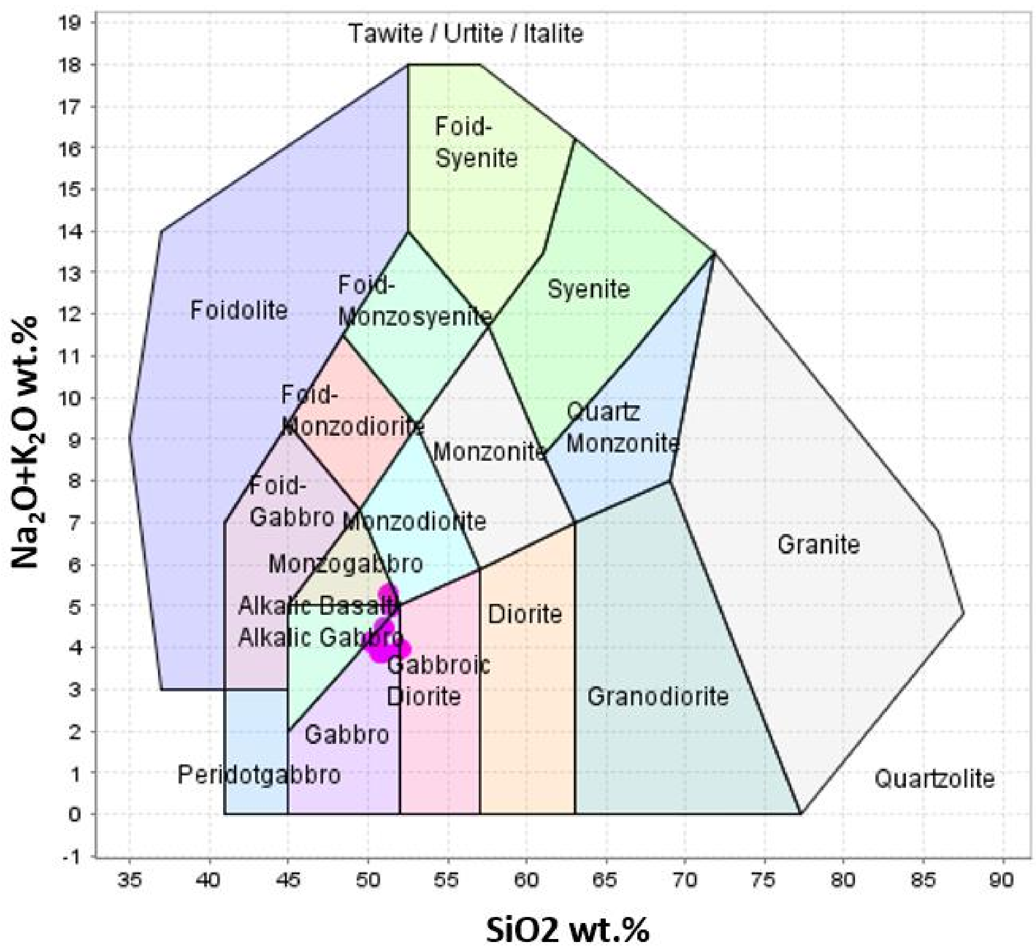

Fig 4.19 Total Alkali Silica diagram for the gabbroic rocks from the EWC (adopted from Cox et al. (1979) and Wilson (1989).

Primitive mantle normalized diagram for the EWC exhibits a similar steep pattern as LI, but the EWC displays slightly higher REE enrichment, depicts steep LREE enrichment (3.22 to 3.87 La/Sm) and HREE depletion (4.58 to 5.23 Gd/Yb) with negative Zr, Nb, Ti and Y anomaly, strong Sc depletion, have positive V anomaly (Fig. 4.20).

Fig 4.20 Primitive mantle-normalized diagram for the EWC. Normalizing values from Sun and McDonough (1989).

4.3.3 Southeast anomaly

The Southeast anomaly comprises peridotitic, gabbroic, and gabbro-dioritic to diorite rocks. All the samples that were tested for whole rock geochemistry were gabbroic and gabbro-dioritic-to-diorite rocks with one peridotite sample. The gabbroic samples have major element concentrations between 51.5 to 52.8% SiO_2, 9.45 to 12.0% Fe_2O_3, 7.4 to 11.9% MgO and 0.054 to 0.132% Cr_2O_3. The gabbroic to gabbroic diorite samples exhibit positive correlations on the MgO versus SiO_2 and Al_2O_3 versus SiO_2 and positive correlations on the CaO versus SiO_2 and Na_2O versus SiO_2 diagrams. The SEA rocks exhibit a higher range of Mg# (55.81 to 72) than the EWC (52.4 to 62.3) and the LI (51.1 to 71.8). To geochemically classify the SEA, Na_2O+K_2O were plotted vs SiO_2 on the Total Alkali Silica diagram (TAS) with the samples plotting at the margin of the gabbro and gabbroic-diorite fields (Fig. 4.21).

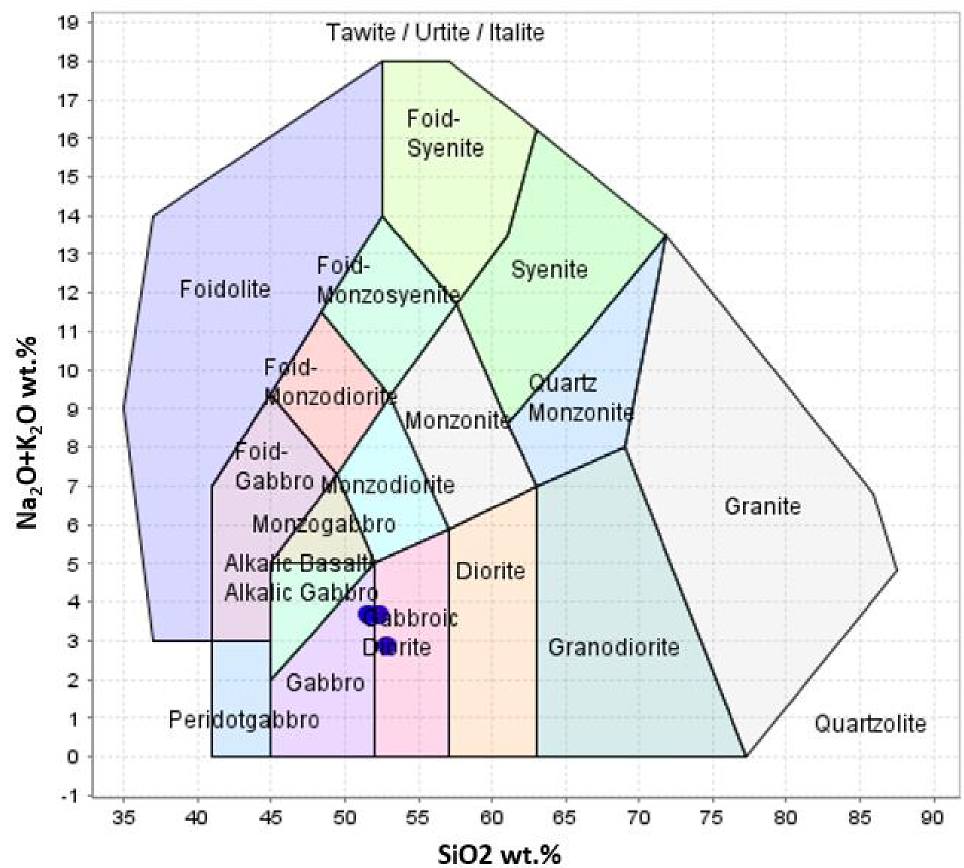

Fig 4.21 Total Alkali Silica diagram for the gabbroic rocks from the SEA depicting gabbro and gabbroic-diorite rocks (adopted from Cox et al. (1979) and Wilson (1989).

Primitive mantle normalized plots of the SEA are relatively similar to the Lone Island and EWC intrusions with LREE enrichment (3.65 to 4.39 La/Sm_n), and HREE depletion (2.3 to 6.4 Gd/Yb_n), but the SEA have strongly negative anomalies of Zr, Nb, Ti and Y compared to the LI and EWC (Fig. 4.22). Most of the SEA samples display higher K, Rb, and Ba abundance than those of the LI and the EWC. The majority of the SEA rocks are depleted in V which is the opposite for the LI and EWC.

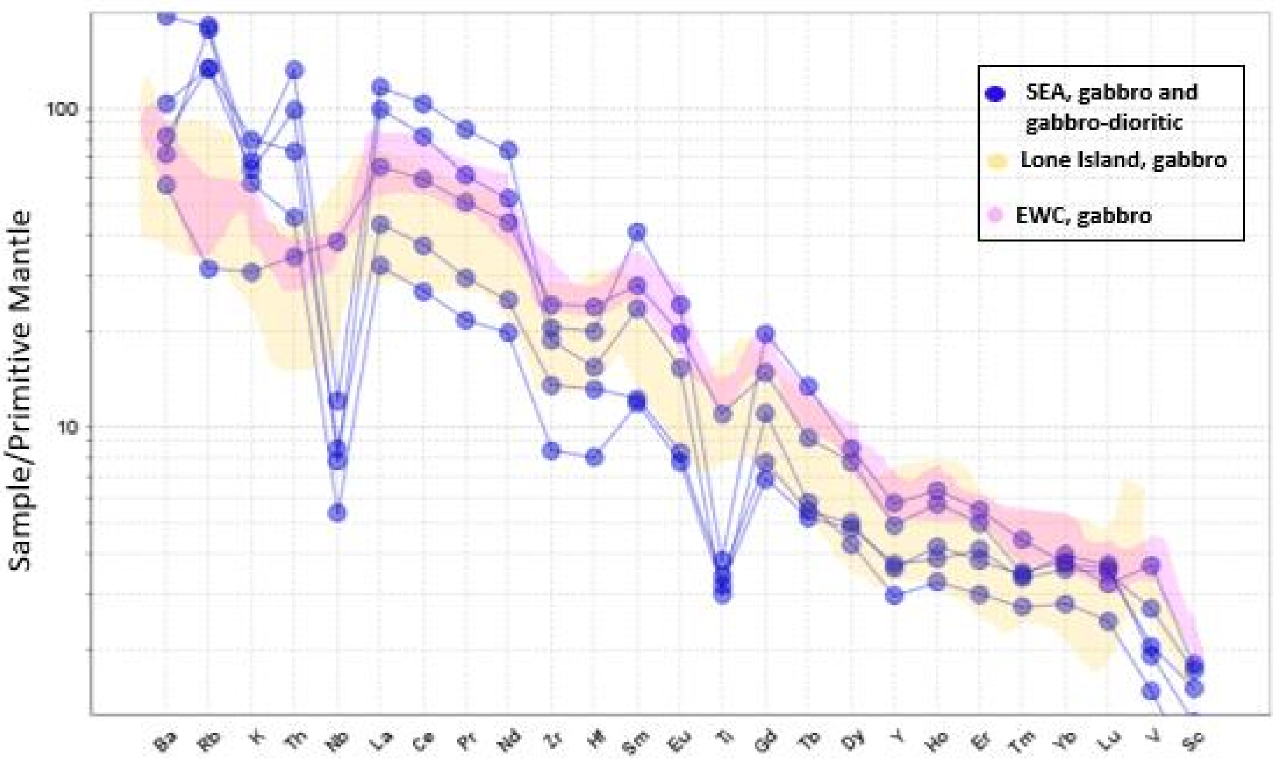

Fig 4.22 Primitive mantle-normalized diagram of the SEA. Normalizing values from Sun and McDonough (1989).

4.3.4 Greenwich Intrusion

The Greenwich intrusion comprises gabbroic rocks with between 46.7 to 52.5% SiO_2, 4.5 to 16.7% MgO, and 0.002 to 0.078% Cr_2O_3. The major element plots of the Greenwich exhibit two distinct groups which can be named Greenwich-1 and Greenwich-2. The Greenwich-1 group comprises eight gabbroic samples with between 48.0 to 52.5% SiO_2 , 4.5 to 10.4% MgO, 0.002 to 0.078% Cr_2O_3, and Mg# between 40.5 to 62.9. Thirteen samples comprise the Greenwich-2 group, are gabbroic rocks with between 46.7 to 51.4% SiO_2 , 9.3 to 16.7% MgO, 0.050 to 0.070% Cr_2O_3, and magnesium numbers between 52.8 to 78.7. Majority of the Greenwich-2 samples plot within the gabbro field, few plot in the alkalic gabbro and the division line between the monzogabbro and alkalic field (Fig. 4.23).

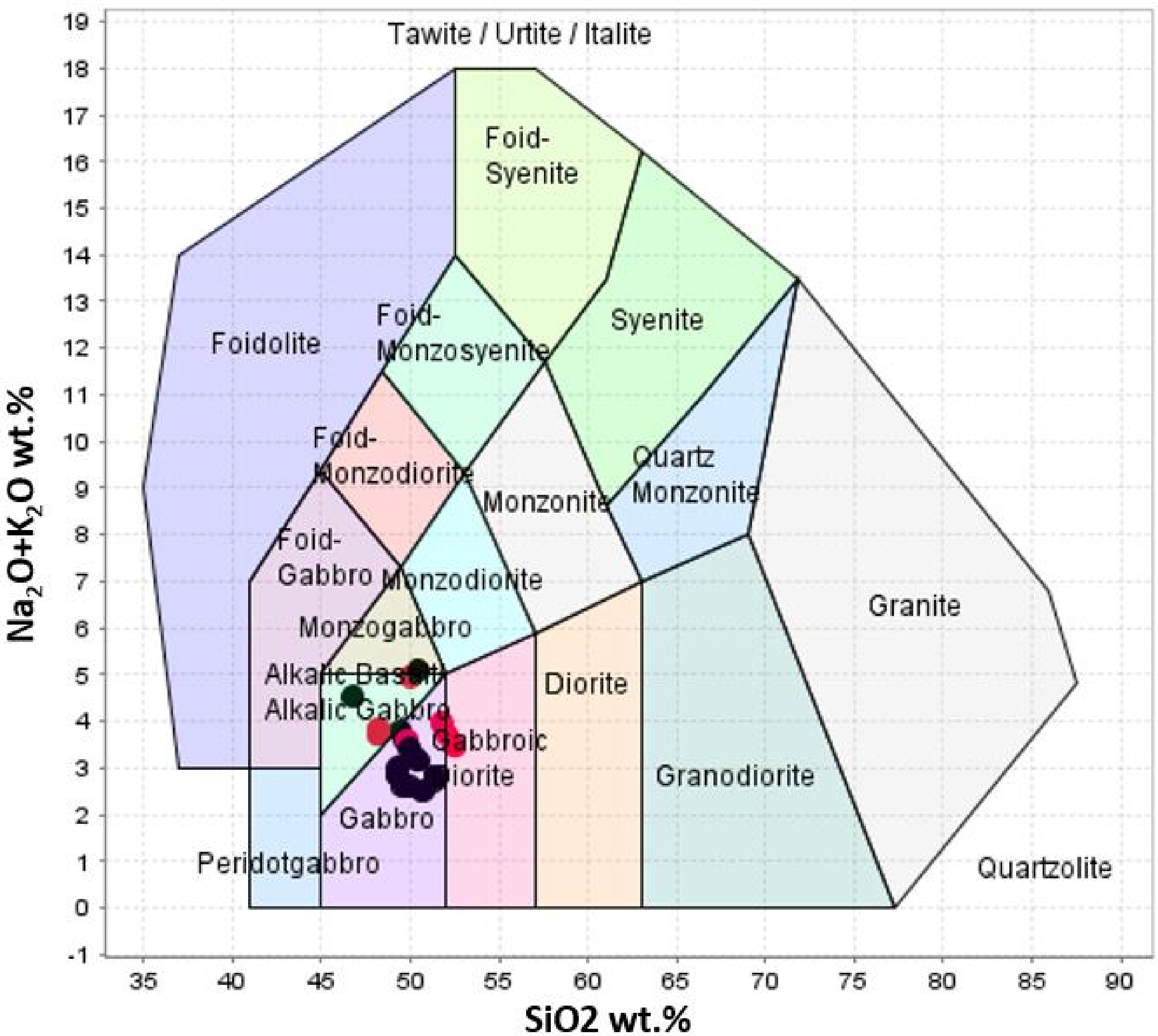

Fig 4.23 Total Alkali Silica diagram for the gabbroic rocks from the Greenwich intrusion, the majority of Greenwich-2 plot in the gabbroic field (black circles), and GI1 gabbros plotted in three fields (red circles). Adopted from Cox et al. (1979) and Wilson (1989).

The difference between the two groups of the Greenwich intrusion is more evident and on the AFM diagram. The Greenwich-1 samples exhibit higher FeO than the Greenwich-2, plotting mostly between the Irvine and Baragar (1971) and the Kuno (1969) lines towards tholeiitic compositions (Fig. 4.24). The Greenwich-2 samples have higher MgO than the Greenwich-1 samples, plotting closer to the calc-alkaline field or on the Irvine and Baragar line (1971). The difference between the Greenwich-1 and 2 is also seen in the MgO versus SiO_2, Fe_2O_3 versus SiO2, TiO_2 versus SiO_2, and Al_2O_3 variation diagrams of the Greenwich intrusion (Fig. 4.25).

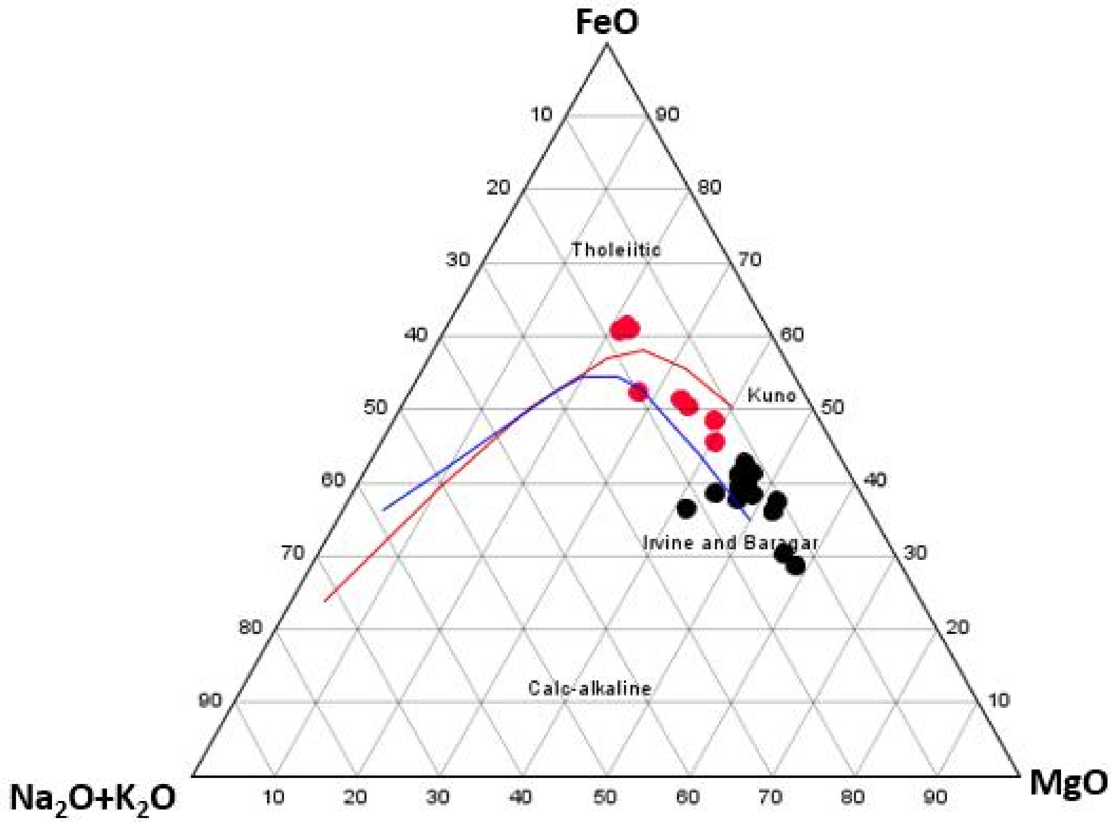

Fig 4.24 AFM diagram shows Greenwich-1 (red circles) with higher FeO and more tholeiitic composition, and the Greenwich-2 (black circles) with higher MgO and closer to the calc-alkaline field. Division lines from Irvine and Baragar (1971) and Kuno (1969).

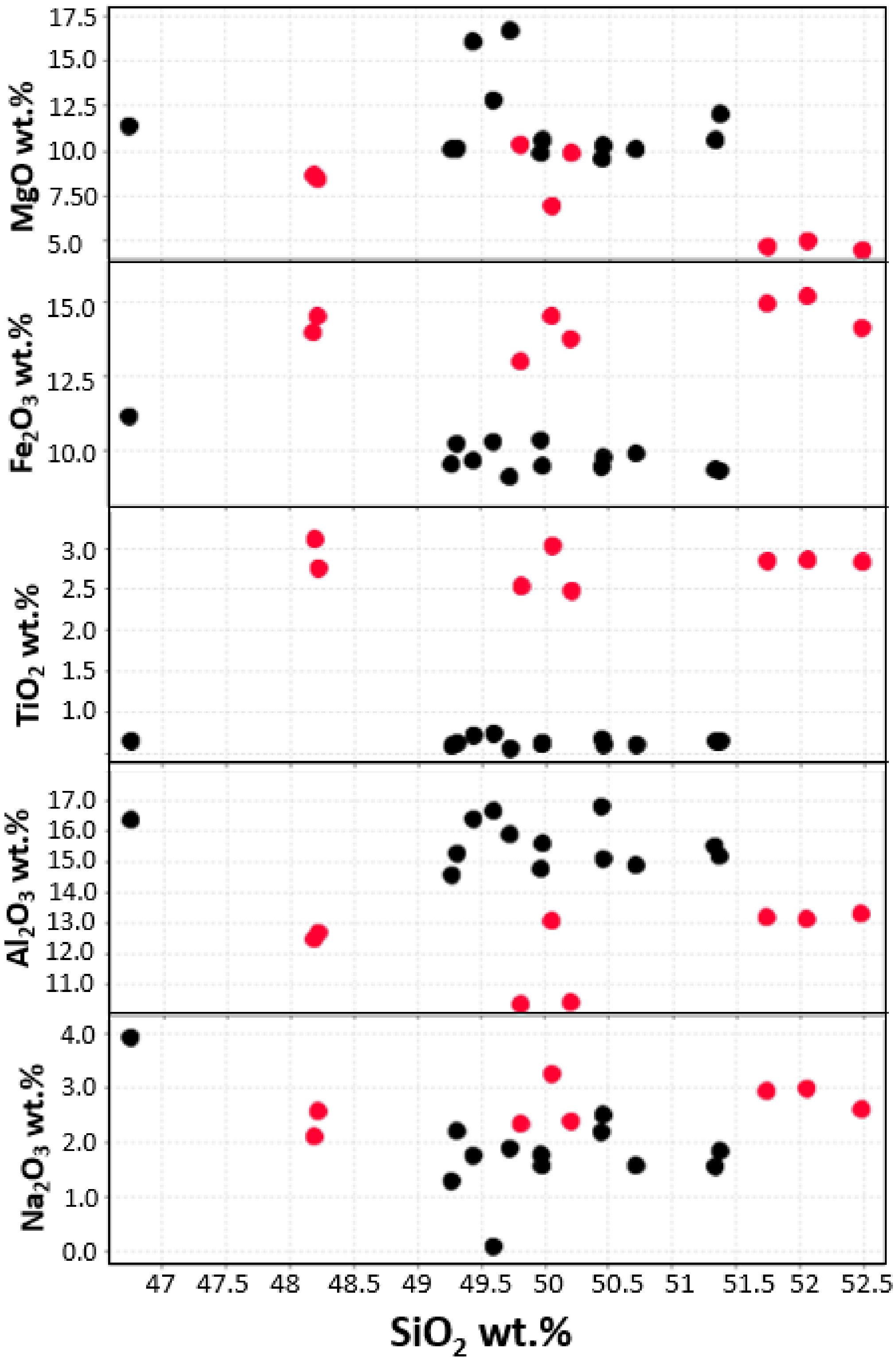

Fig 4.25 Variation diagrams showing the major element compositions of the Greenwich, the positive correlation on the MgO vs SiO_2, Fe2O3 vs SiO_2, and Al_2O_3 vs SiO_2 and a negative correlation on CaO vs SiO_2 and Na_2O SiO_2 diagrams. Greenwich-1: red and Greenwich-2: black.

A primitive mantle normalized diagram for the Greenwich intrusion shows two distinct types (Fig. 4.26). The Greenwich-1 samples have a pattern similar to the LI, SEA, and EWC patterns with steep REE patterns, enriched LREE (2.6 to 3.3 La/Sm_n), slightly enriched MREE, and decreased HREE (2.9 to 5.7 Gd/Yb_n), elevated V, strongly depleted Sc, and enriched K, Rb and Ba (Fig. 4.26). The Greenwich-2 pattern is flatter than Greenwich-1, exhibits less enriched LREE (2.6 to 9 La/Sm_n) and flat HREE (1.5 to 2.4 Gd/Yb_n) higher Sc with an enrichment of K and Rb similar to the LI, SEA, EWC, and the Greenwich-1 but with depleted Ba (Fig. 4.26).

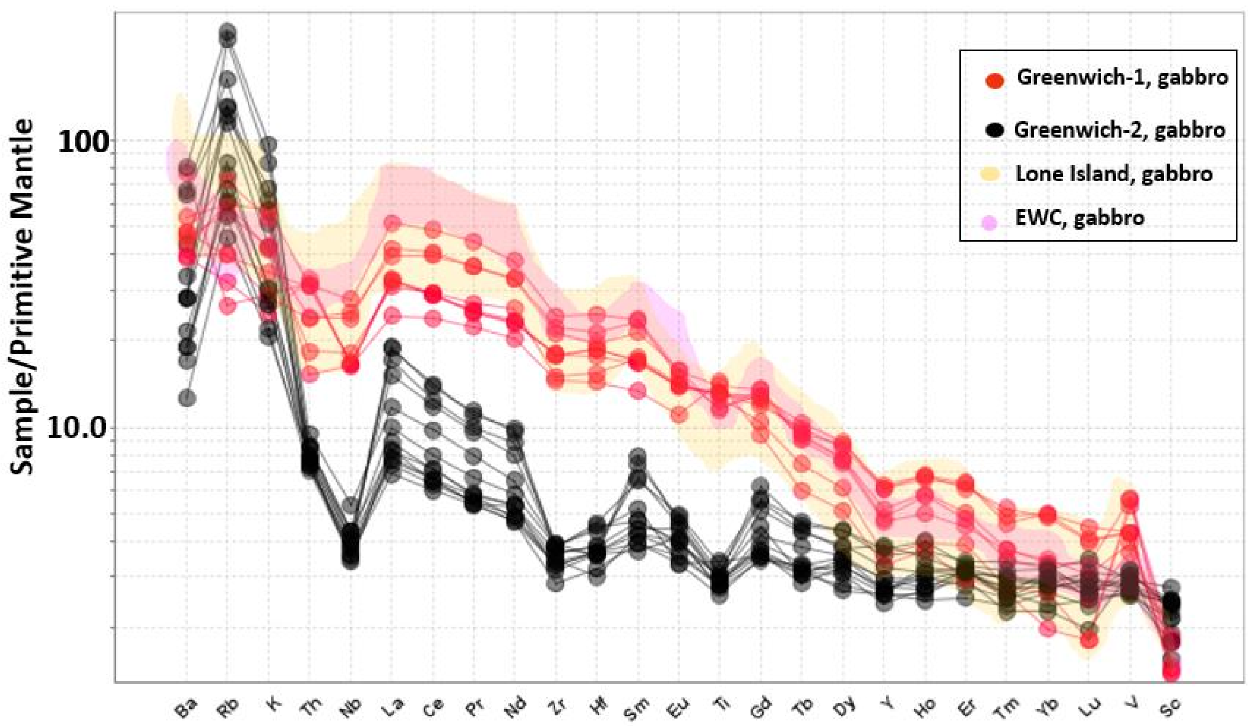

Fig 4.26 Primitive mantle-normalized diagram of the Greenwich-1 (red) and Greenwich-2 (black). Normalizing values from Sun and McDonough (1989).

4.3.5 025 Intrusion

Major element chemistry of the 025 intrusion reveals clear chemical differences between the gabbroic and peridotitic samples. The gabbroic rocks of the 025 intrusion have major element concentrations between 45.8 to 51.4% SiO_2, 6.42 to 15.50% MgO, 0.0021 to 0.25% and Cr_2O_3. The ultramafic rocks of the 025 have major element concentrations of 42.8 to 44.1% SiO_2, 6.9 to 27.9% MgO and 0.002 to 0.050% Cr_2O_3. On the Total Alkali Silica diagram, the gabbroic samples plot in the gabbro field and peridotites in the ultrabasic field (Fig. 4.27).

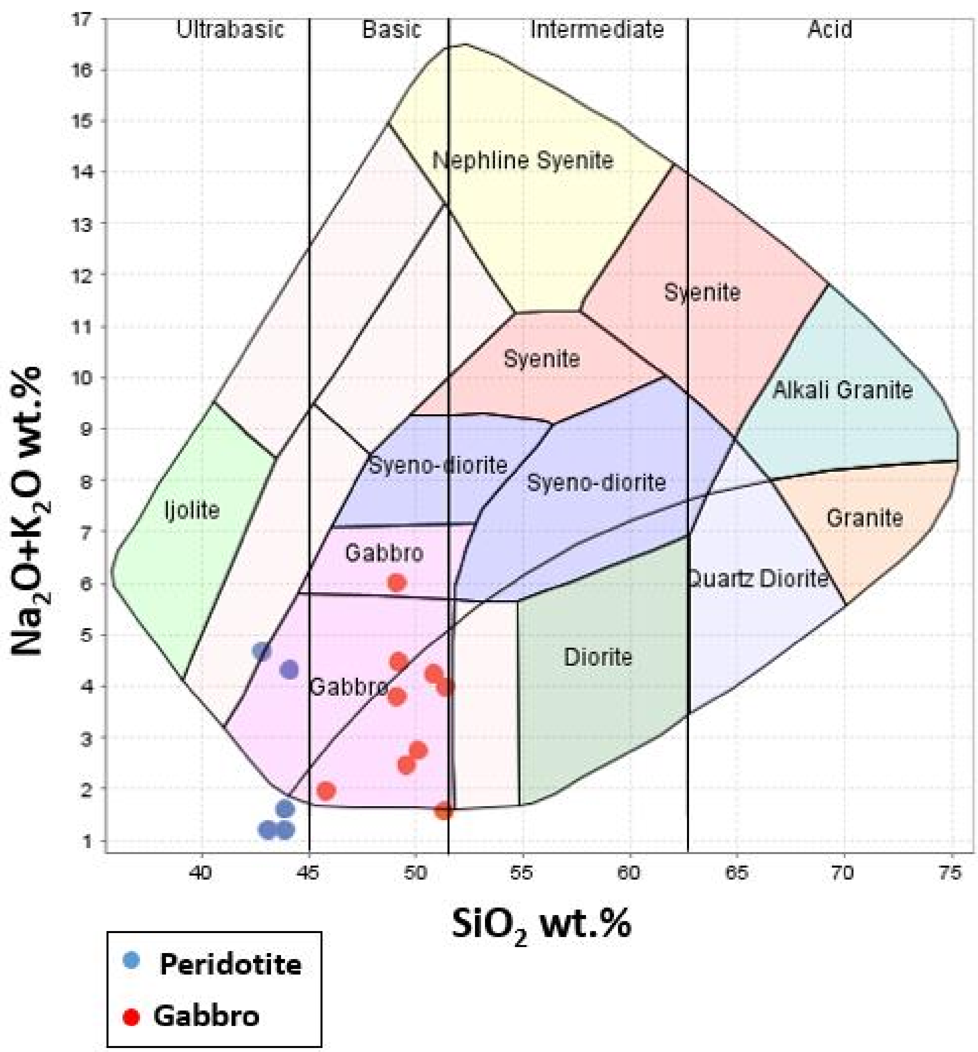

Fig 4.27 Total Alkali Silica diagram for mafic and ultramafic rocks from the 025. Adopted from Cox et al. (1979) and Wilson (1989). Green circles: gabbros and turquoise circles: peridotites.

Variation diagrams of the 025 intrusion show two distinct types of peridotites, one with high MgO, and a second type with a lower MgO content similar to the gabbroic samples (Fig. 4.28). The CaO, Na_2O, and the Al_2O_3 all show higher concentrations in the gabbroic rocks compared to the peridotitic rocks (Fig. 4.28).

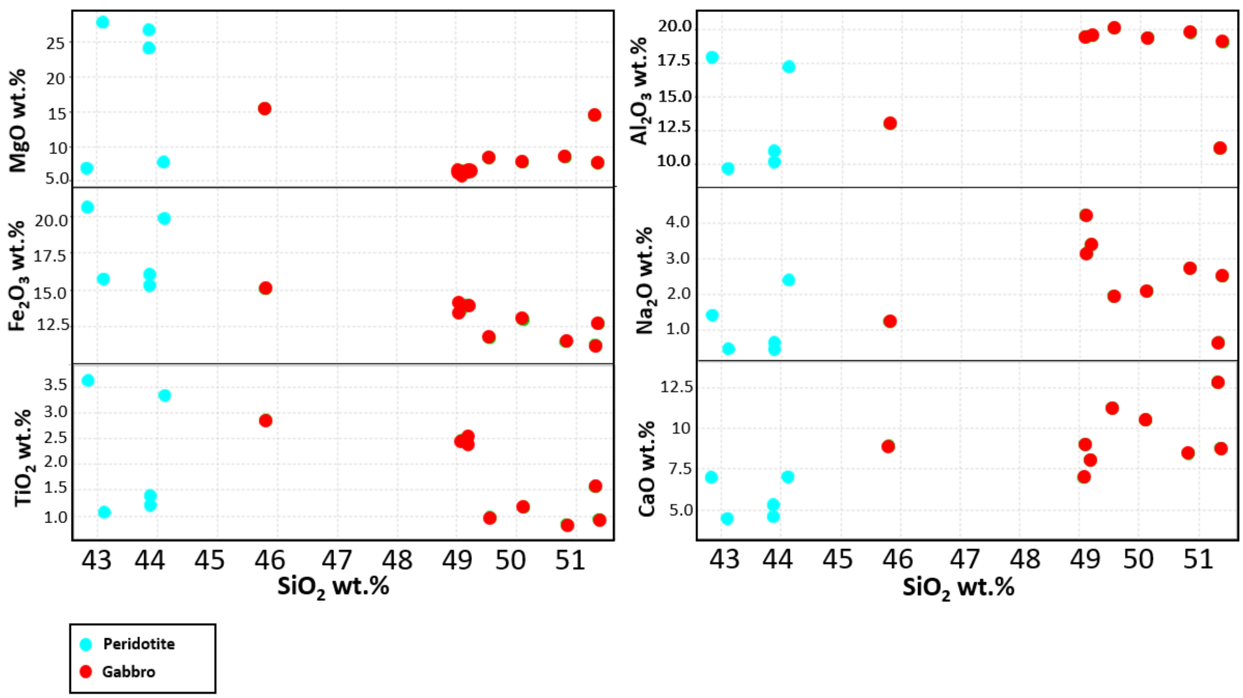

Fig 4.28 Variation diagram showing the major element composition of the 025 intrusion.

Two patterns of REE were displayed for the gabbros and peridotites from the 025 (Fig. 4.29a). The 025-1 has a higher LREE concentrations and Ba, Rb and K enrichment, and lower HREE contents (Fig. 4.29a and b). The gabbros from the 025-1 (green circles) have steep pattern of HREE (3.3 to 4 Gd/Yb) and LREE (2.7 to 3.1 La/Sm). The peridotitic samples from the 025-1 have similar primitive mantle normalized patterns but variable Ti anomalies (Fig. 4.29a). The primitive mantle normalized pattern of the 025-1 is comparable to the Greenwich-1, LI, SEA, and the EWC (Fig. 4.29c). The gabbroic samples from the 025-1 have Mg# between 45.9 to 73, whereas the peridotites from the 025-1 range between 76 to 78. The gabbroic rocks of the 025-2 have Mg# range between 56 to 60.

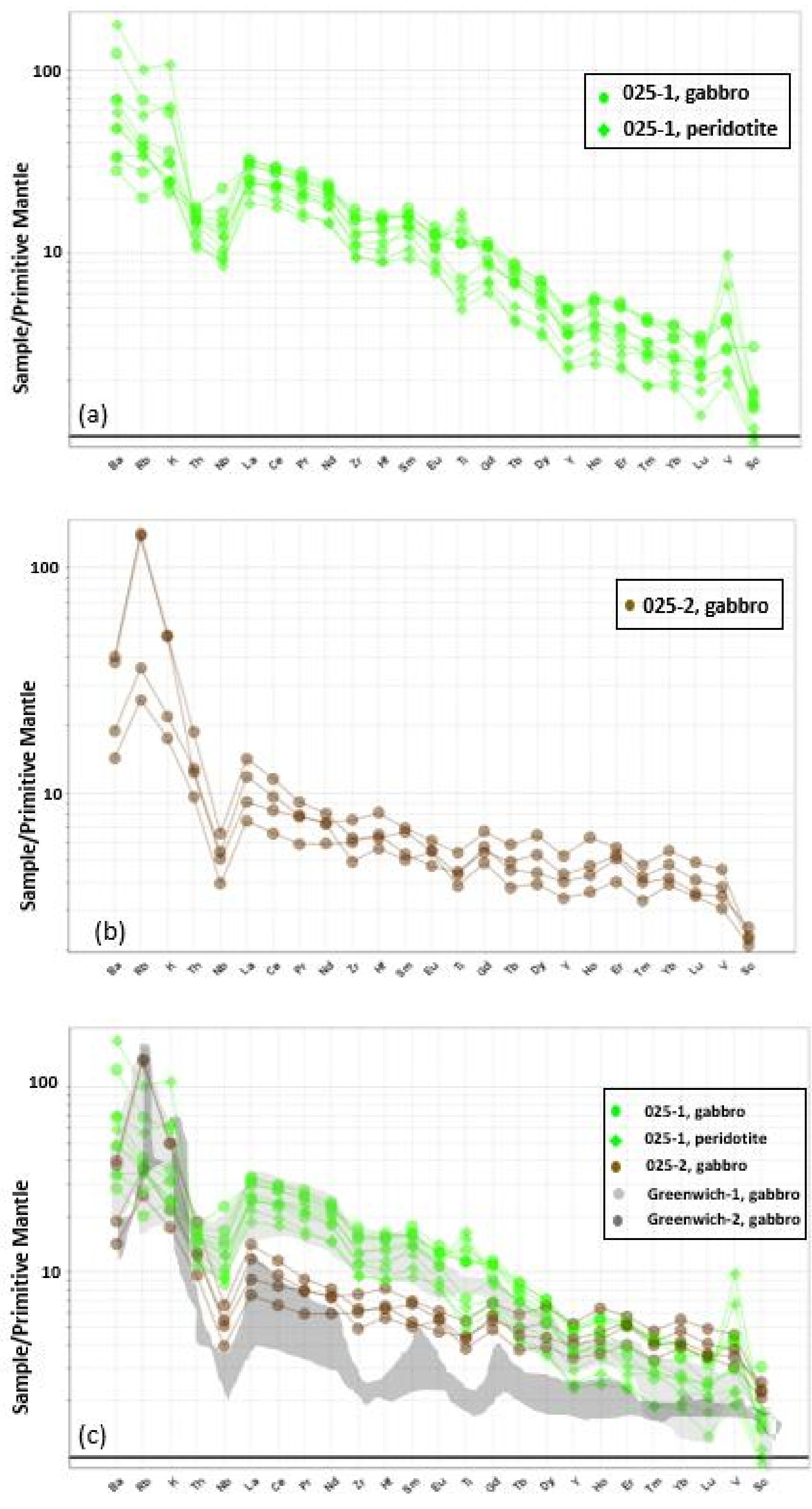

Fig 4.29 Primitive mantle-normalized diagram of (a) the 025-1, (b) the 025-2, (c) comparison between 025-1, 025-2, Greenwich-1, and Greenwich-2. Normalizing values from Sun and McDonough (1989).

4.4 Radiogenic isotopes

4.4.1 Radiogenic isotopes of the five intrusions

Samarium–Nd and Rb–Sr isotopes were determined for 17 samples across the five intrusions (Table 4.1). A full data set of the Sm–Nd and Rb–Sr analysis is presented in Appendix D. Together, the εNd_t values range between -7.49 to +0.14 and Sr_i values range between 0.7030 to 0.7058 (Table 4.1).

Three gabbroic samples from the Lone Island were analyzed, they are characterized by $\varepsilon_{Nd(1107.9)}$ values between -4.4 to -5.3 and Sr_i values range between 0.7000 to 0.7058 (Table 4.1). One sample from the SEA was analyzed with $\varepsilon Nd_{(1107.9)}$ value of -3.45 which is slightly less negative than the values from the Lone Island with a Sr_i value of 0.704023 (Fig. 4.30). Two gabbroic samples from the EWC have smaller $\varepsilon_{Nd(1107.9)}$ values of -4 and Sr_i values of 0.7057 and 0.7040 (Fig. 4.30). Three gabbroic samples from the Greenwich intrusion were analyzed, two samples exhibited the most negative $\varepsilon Nd_{(1105.7)}$ value of -7, and one sample which had $\varepsilon_{Nd(1105.7)}$ of -4 which is similar to the EWC, Lone Island and close to the SEA value. The Greenwich intrusion has the highest Sr_i values among the five intrusions that range between 0.7056 to 0.7159 (Fig. 4.30). Six samples from the 025 (three gabbros and three peridotites) were analyzed for Sm–Nd and Rb–Sr (Table 4.1). One gabbroic sample from the 025-2 has $\varepsilon_{Nd(1105.7)}$ value of +0.14 and 0.7047 Sr_i. Five samples from the 025-1 ranged between -2 to -3 $\varepsilon_{Nd(1105.7)}$ and 0.7030 to 0.7051 Sr_i. The 025-2 εNd_t values were lower than the 025-1 value, but the Sr_i values of the 025-1 similar to the values of the 025-2 (Fig. 4.30).

Table.4.1 Summary of the ε_{Ndt} and Sr_i of the 17 selected samples of the five intrusions.

Sample Id	**Intrusion name**	**Sri**	**$\varepsilon_{Nd(1107.9Ma)}$**
CAM-021-KY-001	Lone island	0.705873	-5.30468
CAM-021-KY-004	Lone island	0.704202	-4.39301
CAM-021-KY-012	Lone island	0.700427	-4.60683
CAM-021-KY-018	Southeast anomaly	0.704023	-3.44607
CAM-021-KY-029	East-west connector	0.705733	-4.35678
CAM-021-KY-036	East-west connector	0.704184	-4.27836
			$\varepsilon_{Nd(1105.7Ma)}$
CAM-021-KY-070	Greenwich intrusion	0.715980	-7.49168
CAM-021-KY-074	Greenwich intrusion	0.705663	-4.34707
CAM-021-KY-092	Greenwich intrusion	0.712935	-7.20414
			$\varepsilon_{Nd(1107.9Ma)}$
CAM-021-KY-064	O25	0.704713	0.136062
CAM-021-KY-065	O25	0.704767	-3.17658
CAM-021-KY-066	O25	0.703758	-3.18351
CAM-021-KY-093	O25	0.704480	-3.43599
CAM-021-KY-094	O25	0.705105	-2.7395
CAM-021-KY-095	O25	0.703093	-2.83873

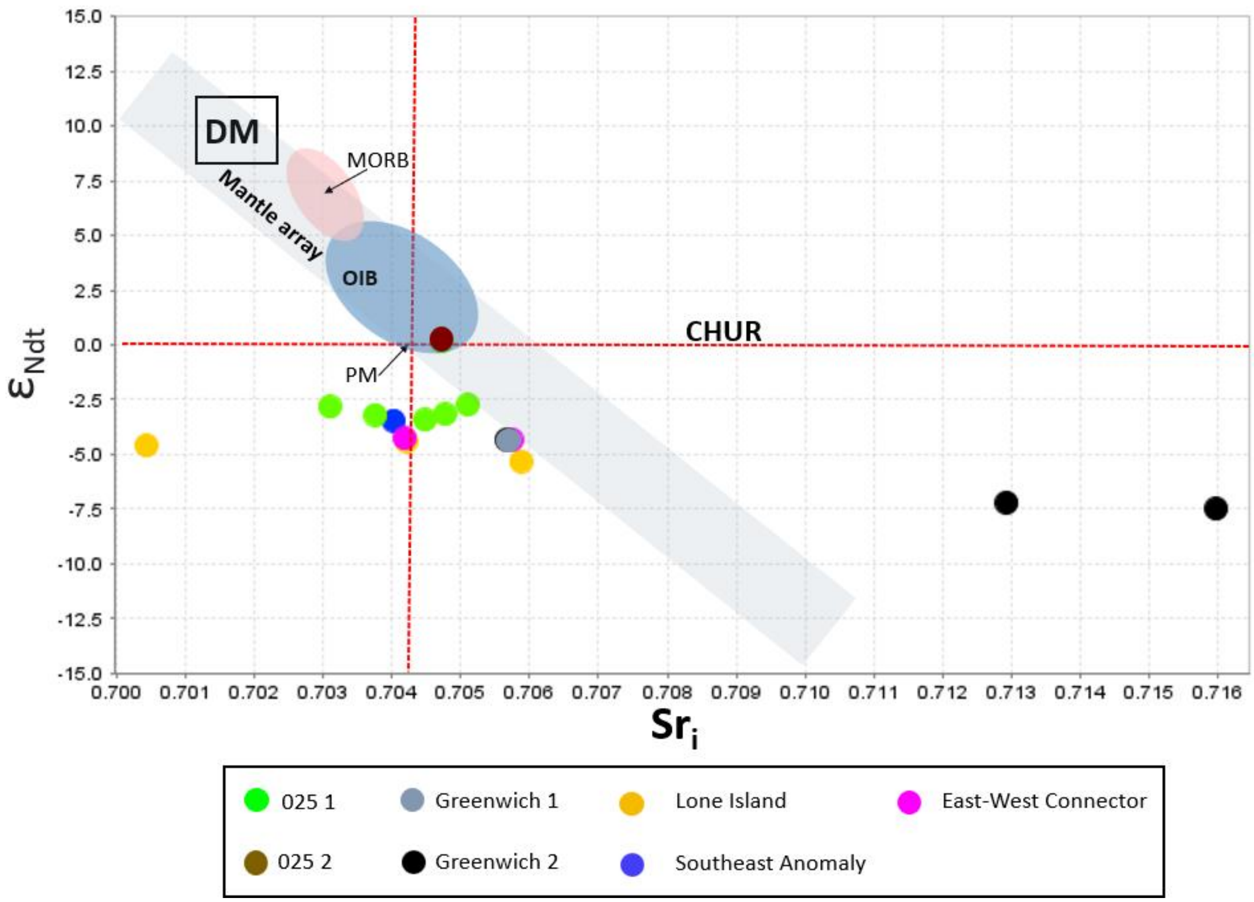

Fig 4.30: Sr_i versus ε_{Ndt} for the Lone Island, EWC, 025, SEA and Greenwich.

4.4.2 Geochemistry and radiogenic isotope results of the country rocks

Field observations and drillcore logging results show that the mafic to ultramafic rocks of the five intrusions intruded into Archean granitoids and metasedimentary rocks of the Quetico Subprovince. To assess the geochemistry of the country rocks and to evaluate their effect and role in the contamination of the five intrusions, whole rock and radiogenic isotope analysis was done for three metasedimentary and ten granitoid samples.

The geochemistry of the country rocks exhibited clear differences from the MCR related intrusions. The country rocks have higher Th concentrations, which effectively elevated the Th/Nb_n ratios as they range between 0.017 to 2.3, whereas it was significantly lower in the five intrusions as the highest Th/Nb_n ratio for the five intrusions was 0.3369. The metasedimentary rocks have Th/Yb_n ratios that range between 3.030 to 23.2, and the granitoids have Th/Yb_n ratios range between 2.75 to 64.2 that are higher than the five intrusions ratios, which range between 1.11 to 6.08 (an average of 1.01).

To estimate the role of the country rocks in the contamination of the five intrusions, one metasedimentary sample and one granitoid sample were analyzed for Sm-Nd and Rb-Sr isotopes. The metasedimentary sample has $\varepsilon_{Nd(1106)}$ -20 and Sr_i 0.7636, and the granitoid sample has ε_{Ndt} -20 and Sr_i 0.7041. The εNd_t values of the two samples are more negative than the εNd_t values of the five intrusions that range between -7.49 to +0.14 and Sr_i values range between 0.7030 to 0.7058. Other publications in the region have examined the country rocks, and samples were also assessed, for example samples from Quetico exhibited ε_{Ndt} of -16 and -23 and Sr_i of 0.7167 and 0.7155, whereas the other samples from the Sibley Group have -5 ε_{Ndt} and 0.7199 to 0.75039 Sr_i (Pan et al., 1999; Cundari, 2012). Thus, the negative ε_{Ndt} and Sr_i values of the country rocks in this study, are similar to published data.

4.5 Geochronology

The U-Pb geochronological results were obtained from precise ID-TIMS dating of zircon and of baddeleyite (ZrO_2) from various intrusions around TBN (Appendix E). The samples were collected from the EWC (CAM-021-KY-061, monzogabbro), 025 (CAM-021-KY-065, monzogabbro), Greenwich (CAM-021-KY-081, monzogabbro), SEA (CAM-021-KY-109, olivine gabbro) and Escape intrusion (18-DL-039, monzogabbro). The first four samples were all collected from drill core, but sample: 18-DL-039 of the Escape intrusion was collected in the summer of 2018 by former University of Toronto PhD candidate Dustin Liikane but was not dated as part of that project.

4.5.1 East-West connector (CAM-021-KY-061)

A monzogabbro "red hybrid classic" was collected from drill hole EWC 10-01 at a depth of 50m. This sample yielded only a sparse amount of zircon with varying quality and morphology (Fig. 4.30a). Only a dozen of these zircons were of acceptable quality for U-Pb geochronology, and are irregular, clear to slightly clouded, lack prismatic forms or facets, ranging in color from completely colorless to pale brown. The EWC also carried pale blue, euhedral, and zoned anatase. Three fractions of zircon were analyzed from this sample (Appendix E; Fig. 4.31a).

The U-Pb isotopic result for fraction Z1, which is a single, clear, colorless, cracked fragment yielded a $^{206}Pb/^{238}U$ age of 1070.5 ± 2.3 Ma and a $^{207}Pb/^{206}Pb$ age of 1076.4 ± 5.2 Ma. The analyses of Z2 and Z3 yield concordant $^{207}Pb/^{206}Pb$ ages of 2699.0 ± 1.8 Ma and 2772.8 ± 1.5 Ma, respectively (Appendix E; Fig. 4.33b), reflecting xenocrystic zircons inherited from the surrounding Archean country rocks (Fig. 4.31c).

To get better geochronology results, a second attempt was made to sample the EWC in Clean Air Metals core yard, but no suitable coarse grained mafic or ultramafic rocks were found in all of the EWC drill cores.

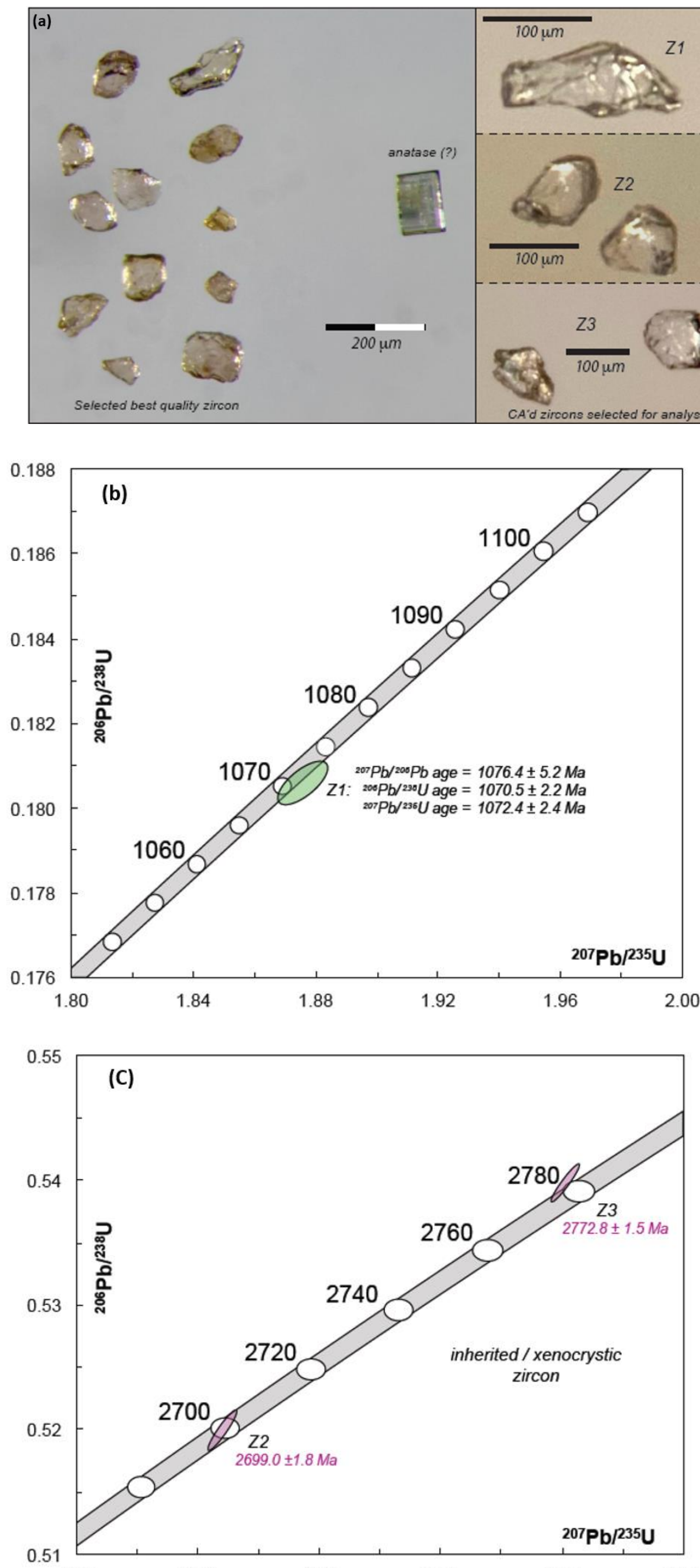

Fig 4.31 (a) An image of the irregular clear to pale brown zircons of CAM-021-KY-061 from the EWC intrusion and the selected Z1, Z2, and Z3, (b) a concordia plot of Z1 with of an age of 1070.5 Ma, (c) a concordia plot of Z2 and Z3 of CAM-021-KY-061 of the EWC with an age of 2699.0 ± 1.8 Ma and 2772.8 ± 1.5 Ma respectively.

4.5.2 Greenwich intrusion (CAM-021-KY-081)

The Greenwich intrusion was sampled from drill hole GL10-08, 35cm of spilt core of a monzogabbroic collected from a depth of 3.6-4.0 meters (Fig. 4.32). No zircon was found during heavy mineral processing for U-Pb geochronology (likely due to silica undersaturation). However, a robust population of fine-grained, fresh blades, blade fragments, and small blocky fragments of baddeleyite were recovered (Fig. 4.33a).

Fig 4.32: A photo of the dated monzogabbro drill core sample from the Greenwich (drill core: GL10-08).

A dozen grains of baddeleyite were washed, spiked and dissolved for U-Pb analysis, and all yielded low Th/U ratios (0.07-0.09), which is typical for fresh baddeleyite with no alteration or late magmatic zircon overgrowths. The measured uranium concentrations are relatively high (750-1200 ppm). Two analyzed fractions of baddeleyite Bd1 and Bd2 fall within the concordia with 0.6% discordant (Fig. 4.33b). Both fractions have nearly identical model $^{207}Pb/^{206}Pb$ ages of 1105.8-1105.7 Ma (MWSD < 0.01, prob. of concordance = 99.8%, n=3; Fig. 4.35b). The average weighted $^{207}Pb/^{206}Pb$ age of the two fractions yielded an age of 1105.7 ± 0.9 Ma (Fig. 4.33b).

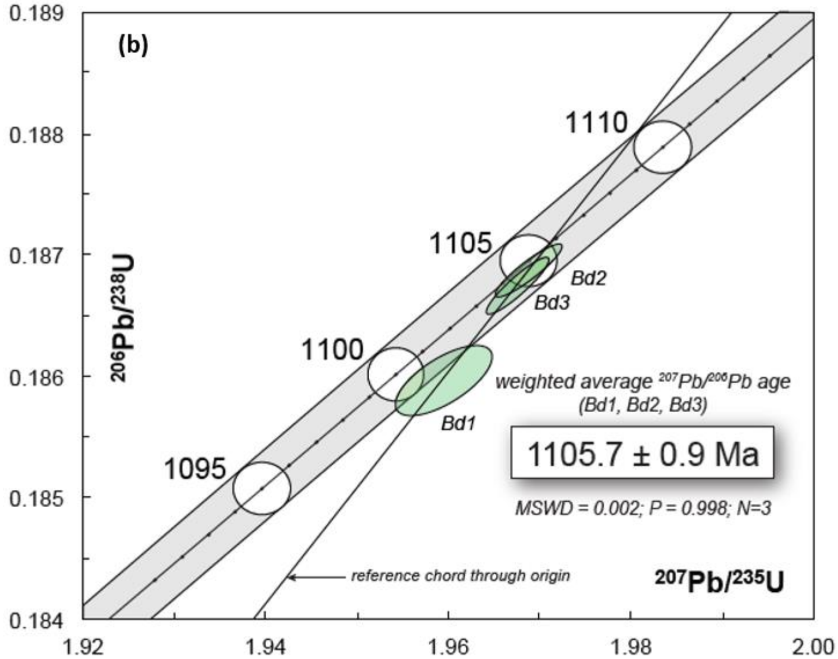

Fig 4.33 (a) Fresh blades, blade fragments, and small blocky fragments of baddeleyite from sample: CAM-021-KY-061 of the GI, (b) a concordia plot of the Bd1, Bd2 and Bd3 yielding an average weighted $^{207}Pb/^{206}Pb$ age of 1105.7 ± 0.9 Ma.

4.5.3 025 intrusion (CAM-021-KY-065)

A peridotitic hand sample was collected from a surface outcrop of the 025 intrusion. Unfortunately, no datable zircon or baddeleyite grains were obtained from this sample, therefore no age was generated for the CAM-021-KY-065 sample from the 025 intrusion.

4.5.4 Southeast Anomaly intrusion (CAM-021-KY-109)

Three coarse-grained core samples were collected from drill hole SEA08-01 including CAM-021-KY-108 (Hr: "hybrid classic red"), CAM-021-KY-109 (MgO: olivine gabbro), and CAM-021-KY-108 (Mgm: melanocratic gabbro). Based on grainsize and degree of alteration sample CAM-021-KY-109 was selected as a first option for U-Pb geochronology, and CAM-021-KY-108 as a second option. Sample CAM-021-KY-109 yielded 30 grains of zircons with poor quality, small sizes, irregular forms, that were highly altered and highly turbid, therefore they could not be dated. The second sample was (CAM-021-KY-108, Hr) may be examined in the future, however the degree of alteration indicates that is not anticipated to be better than that of CAM-021-KY-109.

4.5.5 Escape intrusion (18-DL-039)

A monzogabbro sample was collected in 2018 by a former University of Toronto PhD candidate Dustin Liikane, from Rio Tinto drill core 11-CL-0008 from a depth of 215.5-222.09 meters. Relatively abundant skeletal zircon was recovered from dense heavy liquid separates with considerable sulphide. The recovered zircon is coarse grained, up to 300 microns in size, has common opaque oxide inclusions, and was stained reddish orange with hematite alteration from late magmatic or hydrothermal fluids. A small population of cloudy zircon was recovered, that is characterized by irregular/anhedral forms that could be due to late crystallization (Fig. 4.34a). Rare fine-grained, pale brown baddeleyite were also present but excluded from the analysis due to their low abundance. Four fractions of chemically abraded, elongate and skeletal 3 zircon grains, with hollow axial, central channels were selected (Fig. 4.34a). The uranium concentration of these zircons is high ranging between 450-770 ppm, with relatively high Th/U ratios of 0.72-0.84. This is not uncommon for zircons from melts evolved from differentiated mafic magmas. The model $^{207}Pb/^{206}Pb$ ages calculated for the four fractions lie in a narrow range between 1107.7-1107.4 Ma with a range in discordance from perfectly discordant to 2.7% reverse discordant. Based on the collinearity of the isotopic results of Z1, Z2, Z3 and Z4 (mean square weighted deviation <0.01, fit = 99.9%, n=4). A precise calculated average age model $^{207}Pb/^{206}Pb$ age for this sample was 1107.6 ± 0.9 Ma (Fig. 4.34b).

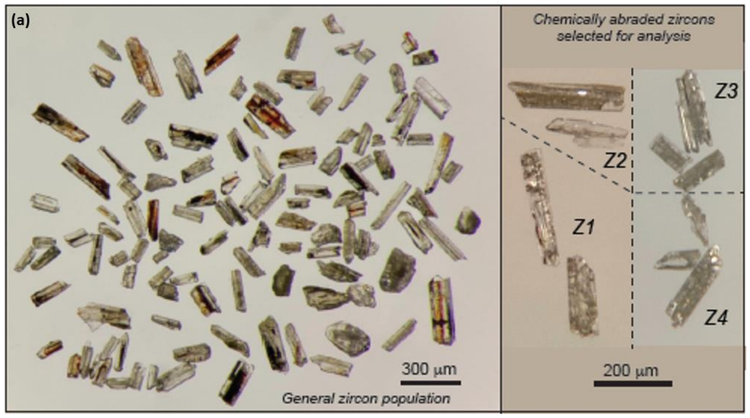

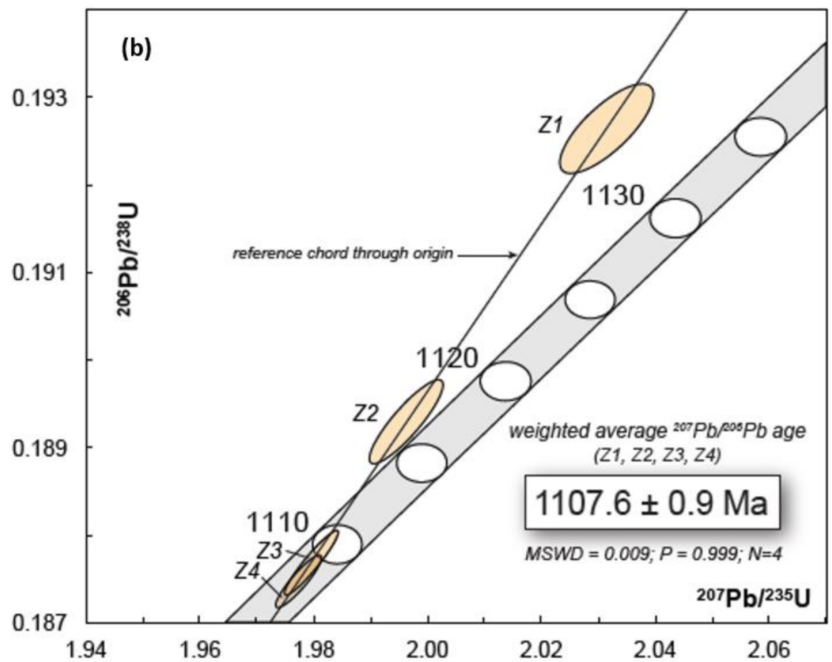

Fig4. 34 Depicts (a) the population of zircons and Z1, Z2, Z3 and Z4 from sample:18-DL-036 from the Escape intrusion, (b) a concordia plot of the same sample with a weighted average $^{207}Pb/^{206}Pb$ age of 1107.6 ± 0.9 Ma.

5 Discussion

5.1 Spatial and temporal emplacement of the five intrusions

The Thunder Bay North intrusions are small, mafic to ultramafic intrusive bodies that were emplaced between (1108 to 1105 Ma). According to Woodruff et al. (2020), within the framework of the MCR stages, this falls within the early stage, ranging between (1109 to 1104 Ma). The 025 and Greenwich are likely satellite intrusions to the Current intrusion, whereas the Lone Island, EWC, and SEA intrusions are closer to the mineralized Current and Steepledge-Escape intrusions of the TBN, and may represent part of the same conduit system. New ages for some of the TBN intrusions have been obtained in this study to better constrain the magmatic evolution of the TBNIC.

Two baddeleyite fractions from the Greenwich Intrusion yielded an average weighted $^{207}Pb/^{206}Pb$ age of 1105 ± 0.9 Ma. These baddeleyite crystals were fresh with no alteration or late magmatic overgrowths, suggesting that the age is reliable. The 1105 ± 0.9 Ma date for the Greenwich intrusion is consistent with the published dates of the other TBN intrusions and other regional MCR intrusions e.g., the Hele intrusion 1106.6 ± 1.5 Ma (Heaman et al., 2007). Metsaranta and Kamo (2021) published an age of 1106.3 ± 2.1 Ma for the Lone Island intrusion, which is similar to the previously published date for the Current intrusion of ca. 1106.6 ± 1.6 Ma (Bleeker et al., 2020).

Despite several attempts to date the EWC intrusion, all geochronological analyses failed to yield reliable dates. Efforts to find suitable coarse-grained samples from drill cores were not successful. Three zircon fractions were identified in the EWC (Z1, Z2, and Z3). Fraction Z1 has a $^{206}Pb/^{238}U$ age of 1070.5 ± 2.3 Ma and a $^{207}Pb/^{206}Pb$ age of 1076.4 ± 5.2 Ma, both of which are significantly younger than the ages of the other TBN intrusions. Fractions Z2 and Z3 also yielded older ages of 2699.0 ± 1.8 Ma and 2772.8 ± 1.5 Ma, respectively. These significantly older ages suggest that Z2 and Z3 fractions are xenocrysts that were inherited from the surrounding Archean country rocks. The EWC, therefore, remains undated, but it is likely to be coeval with the Lone Island or Escape intrusions, as the two intrusions have been interpreted to be physically connected by the EWC (Heggie, 2015).

A single sample from the SEA intrusion contained 30 zircon grains, but they were all of poor quality, being small in size, having irregular forms, and having been affected by alteration to variable degrees. The SEA intrusion could, therefore, not be dated in this study, but it is spatially related to the Current (1106.6 ± 1.6 Ma; Bleeker et al., 2020), Lone Island (1106.3 ± 2.1 Ma; Metsaranta and Kamo, 2021) and Escape intrusions (1107.6 ± 0.9 Ma) and is expected to have a similar age.

A monzogabbro sample from the Escape intrusion yielded a zircon average model age of $^{207}Pb/^{206}Pb$ of 1107.6 ± 0.9 Ma, which is consistent with the age of the Greenwich and Current intrusions, as well as some regional mafic-ultramafic intrusions, such as the 1108 ± 1.0 Ma Thunder intrusion (Trevisan, 2015).

The correlation between the new ages (reported in this study), previously published ages of some of the five intrusions and other TBN intrusions, and ages from other mafic-ultramafic MCR-related intrusions emphasize that the Lone Island, Greenwich, Escape, and Current were emplaced broadly coevally within the Initiation Stage (between 1115 and 1106 Ma) of the MCR (Table).

Table.5.1 Summary of the published new ages dated in this study, previously published, and the undated intrusions of the TBN.

Intrusion Name	Age	Author
Lone Island	1106.3 ± 2.1 Ma	Metsaranta and Kamo (2021)
Current	1106.6 ± 1.6 Ma	Bleeker et al. (2020)
Greenwich	**1105 ± 0.9 Ma**	**Dated in his study**
Escape	**1107.6 ± 0.9 Ma**	**Dated in this study**
025	-	No published age
EWC	-	Not published age
SEA	-	Not published age

5.2 Petrology, geochemistry, and isotopic characteristics

Major-and trace-element compositions of the rocks from the five intrusions exhibit significant variability, with three populations of samples noted. Each of the three identified populations is similar to other mafic-ultramafic intrusions from the MCR region. The Lone Island, EWC, SEA, and portions of Greenwich and 025 (Greenwich-1 and 025-1) have similar major-element compositions. The 025 intrusion can be subdivided into two groups, one group comprising ultramafic samples and a portion of the mafic samples with lower SiO_2 (025-1), and another group (025-2) that is similar to the Greenwich-2 samples. Samples from the Greenwich intrusion also plot in two groups – some samples have low Al_2O_3 and high TiO_2, Fe_2O_3, and P_2O_5, and other samples are similar to the Lone Island, EWC, SEA and 025-1 groups. The Lone Island and EWC intrusions have lower MgO and Al_2O_3, and higher TiO_2 than the Greenwich and the 025 intrusions (Fig. 4.14). The 025-1 and Greenwich-1 have the highest MgO and Fe_2O_3 and the lowest SiO_2 because most of samples are peridotites (Fig. 4.14).

The amount of olivine in mafic-ultramafic magma and its composition (NiO and MgO content) are key indicators for many magmatic process that are essential for magmatic mineralization, for example olivine composition can be used to check for early sulphide segregation from silicate melts in the upper mantle (Maier et al., 1998). The Current and Escape intrusions display a strong positive trend on a MgO vs Ni variation diagram, suggesting a strong role for olivine fractionation (Hollings et al., 2007a; Fig. 4.14d). In contrast, the lower tail of the same trend (Fig. 4.14d) comprises data from the five intrusions with weak positive correlation that indicate less control by olivine fractionation and likely a bigger role for clinopyroxene fractionation. A plot of MgO vs CaO shows a weak negative to no trend for the five intrusions, suggesting little to no olivine fractionation and a greater role for clinopyroxene and plagioclase fractionation (Fig. 4.14b). Consistent with the MgO data, plagioclase fractionation of the five intrusions is also supported by the strong trend displayed in the MgO vs Na_2O_2 diagram, in contrast to the weaker trend that was exhibited by the Current and Escape intrusions (Fig. 4.14c). The MgO vs Al_2O_3 diagram shows a strong continuous trend between the Lone Island, EWC, SEA, 025-1, Greenwich-1 with high Al_2O_3 and lower MgO as most of the samples are gabbronorites and gabbros (Fig. 4.14a). The Escape and Current intrusions follow the same trend as the five intrusions, but they have higher MgO and lower Al_2O_3 (Fig. 4.14a). The decreasing trend of the Al_2O_3 is consistent with fractional crystallization of plagioclase (Hollings et al., 2007a), and the high plagioclase content observed in the five intrusions. Overall, the major element chemistry is consistent with the petrography, as plagioclase and clinopyroxene fractionation was the dominant process in the Lone Island, EWC, SEA, 025-1 and Greenwich-1 intrusions, with limited olivine fractionation.

The five intrusions are enriched in incompatible elements, and characterized by negative Nb, Zr, Hf, Ti, Y, and Sc anomalies with a positive V anomaly (Fig. 5.1). The highest V anomaly was noted in portions of the 025 (025-1) and Greenwich (Greenwich-1), and is consistent with petrography results. For example, the 025-1 and Greenwich-1 intrusions have higher magnetite and ilmenite abundance than the Lone Island, EWC, SEA, 025-2 and Greenwich-2 intrusions. The five intrusions display a strongly negative Sc anomaly, which might be caused by early garnet retention in the lithospheric mantle or clinopyroxene removal from the magma in the pathways (Chassé et al., 2018). When silicate melts get fractionated in the garnet stability zone, Sc is compatible, and thus the garnet will retain about 75% of the Sc (Chassé et al., 2018). The HFSE/HSFE* anomalies for the five intrusions were calculated based on the McCuaig et al. (1994) logarithmic method, with Eu replaced by Gd for Hf/Hf* and Zr/Zr*, and $2*Eu_{cn}/(Sm_{cn}+Gd_{cn})$ was used to calculate Eu/Eu*. The five intrusions exhibit no anomaly to slightly negative Zr-Hf anomalies (a few samples have Zr-Hf positive anomalies) with Zr/Zr* ranging between 0.37 to 1.07 and Hf/Hf* ranging between 0.36 to 1.15. The five intrusions also have strong negative Nb anomalies with Nb/Nb* ranging between 0.90 to 0.05. According to Hollings et al. (2007c) such sharp decrease in Nb abundance are results of crustal contamination. Generally, the five intrusions show slightly positive Eu anomalies with Eu/Eu* ranging between 0.53 to 1.14. Elevated Eu content can be caused by the accumulation of plagioclase and it also reflects reduced magma conditions (Kimata, 1988; Terekhov and Shcherbakova, 2006).

Based on the patterns on primitive mantle normalized diagrams, three sample populations were identified (A, B, and C). As mentioned in the results chapter, populations A and relatively B have similar geochemical characteristics, however, the samples from population C are distinct from the majority of the samples (Fig. 5.1). Populations A and B have MgO contents ranging between 4.46 to 27.9% and LREE enrichment similar to other mafic-ultramafic rocks in the MCR region, which were characterized by Brzozowski et al. (2023) as being similar to ocean island basalts (OIB) or Phanerozoic mantle plume magmatism. Samples from population C include 025-2 and Greenwich-2, which are petrographically different from each other but geochemically similar, and are different from populations A and B. Petrographically, the Greenwich-2 samples contain more plagioclase and higher degrees of alteration, whereas the 025-2 samples have less plagioclase and is more pristine with only minor alteration. Geochemically, the Greenwich-2 and 025-2 have different major element compositions, but have similar REE abundances with flatter primitive mantle normalized patterns than populations A and B (Fig. 5.1).

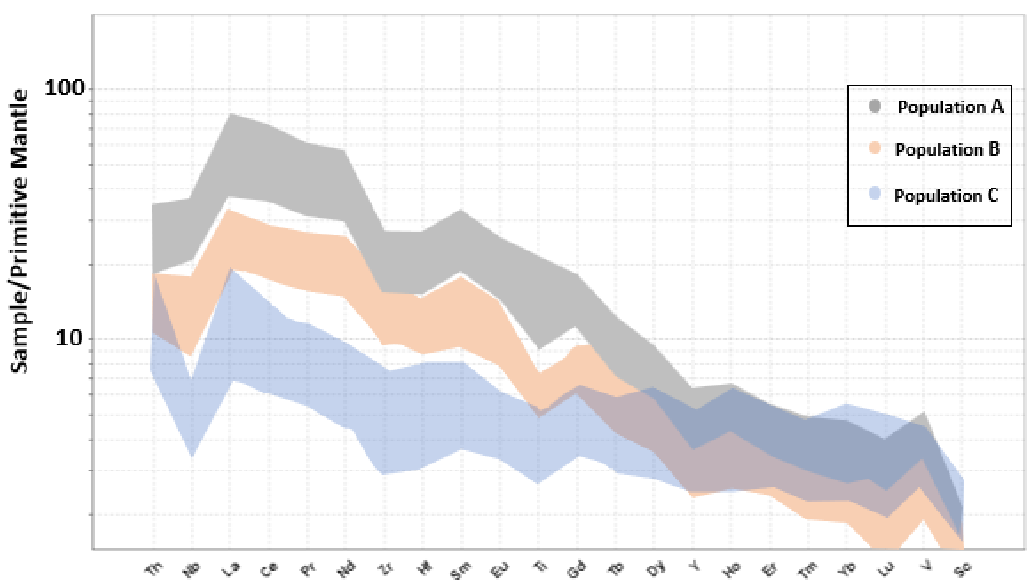

Fig 5.1 Primitive mantle-normalized diagrams of all of the samples from the five intrusions, population A (grey) and B (orange) with steep pattern of MREE and LREE, population C (blue) with flatter patterns compared to population A and B. Normalizing values from Sun and McDonough (1989).

5.2.1 Population A

Population A comprises gabbronoritic to gabbroic lithologies with different degrees of alteration. It includes all the samples from the Lone Island, SEA, EWC, and a few samples from the Greenwich and 025 intrusions. Geochemically, it has the highest LREE abundances of the three populations, with steep patterns on primitive mantle normalized diagrams (Fig. 5.1). The LREE enrichment in some of the MCR related mafic rocks has been interpreted to be result of an interaction with the shallow and hydrated Archean rocks of Superior Province, which are more enriched in LREE (Shirey et al., 1994). This is consistent with the noted LREE enrichment and low Nb and Ti abundance in thirteen samples collected from Archean country rocks in this study. The Archean granitoids showed more elevated LREE abundance with a negative Ti and Sc anomalies compared to the mafic-ultramafic rocks of the five intrusions (Fig. 5.2). Thus, the LREE enrichment in the five intrusions may to have been the result of crustal contamination by the older Archean host rocks.

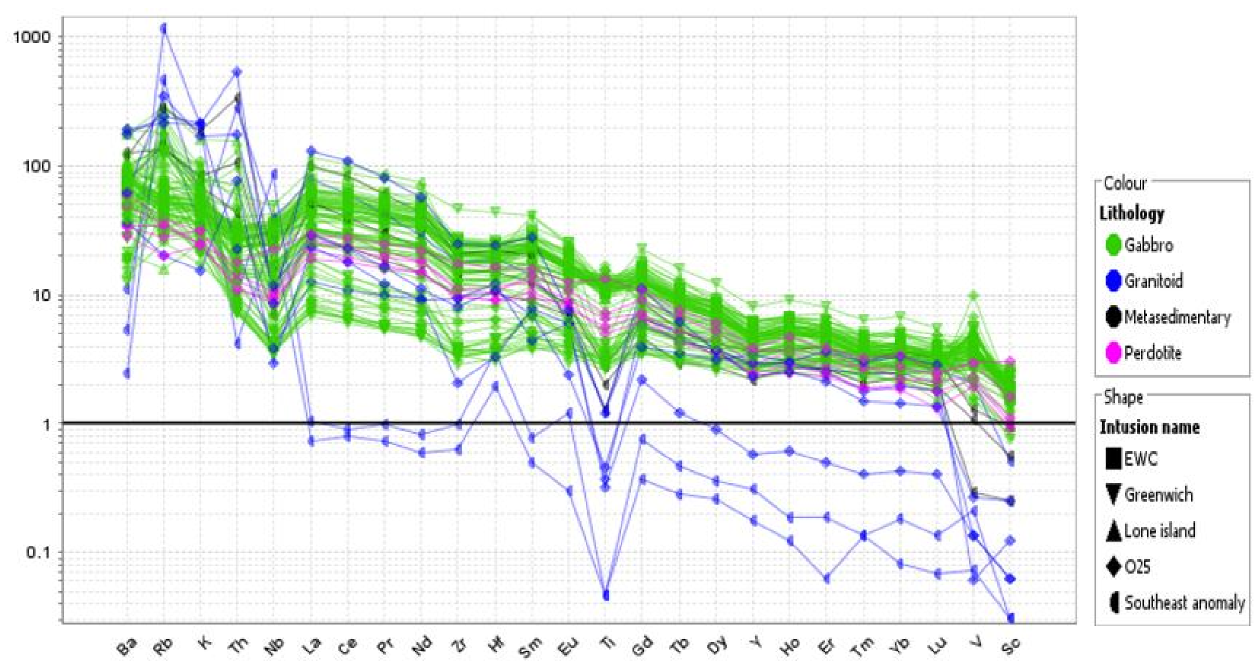

Fig 5.2 Primitive mantle-normalized diagram of thirteen country rock samples (some peridotite and gabbro samples were plotted for correlation reasons), showing MREE and LREE enrichment and Ti and Nb decreases. Normalizing values from Sun and McDonough (1989).

The 1106.3 ± 2.1 Ma (Metsaranta and Kamo, 2021) Lone Island intrusion is part of population A, and it consists of two circular magnetic anomalies. The Lone Island south and Lone Island Lake are petrographically, geochemically, and isotopically similar, consisting of gabbroic lithologies with a minor ultramafic basal portion, which suggests that both Lone Island south and Lone Island Lake are part of the same intrusion with a similar magmatic history. Heggie (2010) defined two magmatic fractionation cycles in the Lone Island intrusion, namely Cycle-1 and Cycle-2, which are interpreted to be the result of multiple magmatic injections (Heggie, 2010; Fig. 2.6). Petrographic results from this study confirmed the presence of Cycle-1 and 2, with the samples of the Lone Island intrusion being divided into an upper gabbroic portion and a lower gabbronorite portion. The upward fractionation that was suggested by Heggie (2010) is consistent with the major element chemistry of the Lone Island intrusion, particularly the SiO_2 content, where the top of the Lone Island intrusion contains higher SiO_2 than the lower gabbronorite rocks (Fig. 4.2 and 4.3). Petrographic analysis shows increasing orthopyroxene modal abundance with depth, with the top portion having gabbroic compositions with 2-3% orthopyroxene, whereas the basal portion comprises gabbronorite rocks with 20-25% orthopyroxene. The increasing abundance of orthopyroxene in the lower portion of the Lone Island intrusion implies a higher temperature and MgO content compared to the upper portion, suggesting a more evolved magma in the upper portion of the Lone Island intrusion. The samples from the Lone Island intrusion are geochemically similar, having similar trace element concentrations with steeply enriched LREE (2.6 to 3.3 La/Sm_n) and fractionated HREE (2.9 to 5.7 Gd/Yb_n). These steep patterns suggest that the magma which formed the Lone Island intrusion was melted from a source with high LREE content. Nicholson and Shirey (1990) suggested that the main volume of MCR related basaltic rocks were generated from an enriched mantle plume with zero ε_{Ndt} and La/Sm_n between 2 to 3. The Lone Island intrusion exhibited La/Sm_n values of 2.6 to 3.3 with $\varepsilon_{Nd(1107.9)}$ values range between -4.4 to -5.3 and Sr_i values range between 0.7000 to 0.7058. The negative $\varepsilon_{Nd(1107.9)}$ values likely resulted from crustal contamination of plume related magmas, whereas the variability in Sr_i can be result of multiple Archean contaminants with various Sr_i signatures (Hollings et al., 2007b), or the result of a heterogenous sedimentary contaminant with lateral and/or vertical variations (Fig. 4.30). Thus, the geochemical and isotopic results imply that the original magma that produced the Lone Island intrusion was produced from an enriched mantle source with zero ε_{Ndt}, and was subjected to a later contamination by crustal Archean granitoids and/or metasedimentary rocks.

The East-West-Connector consists of petrographically and geochemically similar thin mafic intrusive bodies that have been interpreted to be a physical connector between the Lone Island and Escape intrusions. It comprises strongly-to-pervasively-sericitized poikilitic to subophitic gabbronorite. Major and trace element chemistry (e.g., MgO vs major elements, Fig. 4.14, and primitive mantle normalized diagrams, Fig. 4.20) of the EWC exhibit similar compositions to the Lone Island Intrusion, suggesting the same magmatic source for the EWC and Lone Island intrusions. The strong degree of alteration noted in the petrographic analysis of the EWC is consistent with the whole rock results as it has the highest LOI (1.07%) of the five intrusions.

The EWC has an average Th/Nb_n ratio of (0.10) which are typical of mantle values (cutoff = 0.12) suggesting the EWC experienced less crustal contamination than Greenwich-2 and 025-2 that have the highest Th/Nb ratios of the five intrusions, or that the EWC contaminant had low Th/Nb. The strongly negative ε_{Ndt} of the EWC of (-4) indicates that the intrusion assimilated older crust (Hollings et al., 2007b). Similarly, the EWC has Sr_i values that range between (0.7057 to 0.7041). Such a big range of Sr_i values may suggest multiple contaminants (Hollings et al., 2007b, Table. 4.2). This suggests the EWC may have undergone a more complicated contamination history than the other intrusions.

Based on the petrographic analysis of the SEA, the mafic samples from the SEA were all classified as gabbronorite. These gabbronorite samples have major element chemistry similar to the Lone Island and EWC intrusions, but with higher Cr_2O_3 and magnetite and ilmenite, and lower FeO and MgO than most of the other gabbro and gabbronorite samples, except the gabbro from 025-1, suggesting that the SEA magma is more evolved (less primitive) than most of the other five intrusions.

On a primitive mantle normalized diagram, the SEA intrusion exhibits very pronounced Ti, Nb, Zr and Hf depletion. The SEA has a large range of HREE (2.3 to 6.4 Gd/Yb_n), enriched LREE (3.6 to 4.4 La/Sm_n), and strong fractionation from HREE to LREE (La/Yb_n 12). The LREE enrichment could be a result of crustal contamination. This is supported by the negative ε_{Ndt} and Sr_i value, which implies that they may have been through similar crustal contamination conditions to the Lone Island intrusions (Fig. 4.30).

5.2.2 Population B

Population B comprises gabbroic and peridotitic rocks, and consists of a portion of the 025 (025-1) and Greenwich (Greenwich-1) intrusions. Samples from population B have LREE that range between (2.6 to 3.6 La/Sm_n) and MREE abundances, a large range of HREE (2.9 to 5.8 Gd/Yb_n), and higher V concentrations than population A (Fig. 5.1). Petrographic analysis and the major element composition of the gabbronorite rocks from the 025-1 and 025-2 show no clear differences. The gabbronorite rocks from the 025-1 have Mg# ranging between 46 to 73 and Ti/Ti* ranging between 0.21 to 0.91, whereas the 025-2 samples have Mg# ranging between 56 to 60 with Ti/Ti* range between (0.31 to 1.05). The differences between the gabbronorite rocks from 025-1 and 025-2 are shown by different patterns on primitive mantle normalized diagrams, whereas 025-1 is more enriched LREE (Fig. 5.1). The peridotite samples from the 025-1 show variation in their Ti and V abundance, which may reflect slight variations in the magma conditions and/or their degree of fractionation. Overall, two peridotites originated from the same magmatic source with different Ti and V abundances, suggesting slight changes in the Ti and V budget of the magma source.

The Greenwich intrusion is a satellite intrusion, but a portion of it (Greenwich-1) is similar to the other TBN intrusions suggesting a common origin. In contrast, the other portion of it (Greenwich-2) is similar to the 025-2 portion of the 025 intrusion. The Greenwich-1 and 025-1 have similar values of TiO_2, Cr_2O_3, LOI, and similar patterns in primitive mantle normalized diagrams, which suggests that 025-1 and Greenwich-

1 were produced from similar magma source. The trace element differences between the Greenwich subtypes (Greenwhich-1 and 2) suggest different magmatic processes and magma sources, with the higher LREE abundances in Greenwich-1 and less negative ε_{Ndt} (-4) than Greenwich-2 (-7 ε_{Ndt}), which suggest possibly different degrees of crustal contamination. These compositional and crustal contamination differences suggest two different magma sources for Greenwich-1 and 2 (Fig. 4.26).

5.2.3 Populations C

Population C includes segments of the Greenwich (Greenwich-2) and 025 (025-2) intrusions, which are characterized by a flatter REE pattern than populations A and B (Fig. 4.26). These rocks have the lowest LREE abundances of the three populations (Fig. 5.1). The 025-2 samples are similar to Greenwich-2, except that 025-2 have higher HREE and MREE abundances (Fig. 4.29 b). Samples from Greenwich-2 have slightly less steep REE patterns, with HREE ratios ranging between 1.4 to 5.7 Gd/Yb_n, and LREE ratios ranging between 2.6 to 4.4 La/Sm_n. The Greenwich-1 samples have steeper pattern, with HREE ratios ranging between 2.9 to 5.7 Gd/Yb_n, and more fractionated LREE with ratios ranging between 3.3 to 6.2 La/Sm_n. The Sm-Nd and Rb-Sr isotope data for population C are consistent with the whole rock geochemistry results, suggesting involvement of different types and/or degrees of contamination. The Greenwich-2 has more negative ε_{Ndt} values (-7) and higher Sr_i (0.7159 to 0.7129) than Greenwich-1 (-4 ε_{Ndt} and 0.7056 Sri), suggesting a greater degree of contamination.

Clean Air Metals (2023) proposed that the different chemistry of the 025-2 segment of the 025 intrusion indicated it was a mafic Archean intrusive body. Mafic Archean rocks from MCR region are generally more altered and deformed than Proterozoic rocks, which is not the case with the samples from 025-2 from this study, which are similar to the fresher, less altered, and less deformed MCR related intrusive rocks. This study suggests that the geochemical characteristics of 025-2 are more similar to portions of the Nipigon Sills with lower Gd/Yb_n and higher Th/Nb_n ratios, implying a shallower source and more contaminated magma than the other TBN magma (Fig. 4.16). This suggests that 025-2 is MCR related with similar trace element composition as Nipigon sills rather than Archean. The isotopes data show that the 025-2 has a positive ε_{Ndt} value (+0.14), which suggests lower degree of crustal contamination than the other TBN intrusions and Nipigon sills.

5.2.4 The relationship between the five intrusions and the surrounding TBN intrusions

Based on the major-and-trace-element compositions, the Lone Island, SEA, EWC (population A) are geochemically similar, and are comparable to the Current intrusion. The 025-1 and Greenwich-1 of population B are similar and relatively comparable to population A and portions of the Escape intrusion (Escape-1), whereas 025-2 and Greewhich-2 (population C) are similar to each other, but are distinct from the Lone Island, EWC, SEA, 025-1, and Greewnich-1 intrusions (Figs. 5.1 and 5.3).

The three populations have distinct TiO_2 and Mg#, as the gabbros of population C have very low TiO_2 and higher Mg# than most of the gabbros in population A and B (Fig. 5.3). Populations A and B plot on a trend with the Current and Escape intrusions, whereas population C samples lie on a distinct trend connecting 025-2 and Greenwich-2 with lower TiO_2 (Fig. 5.3).

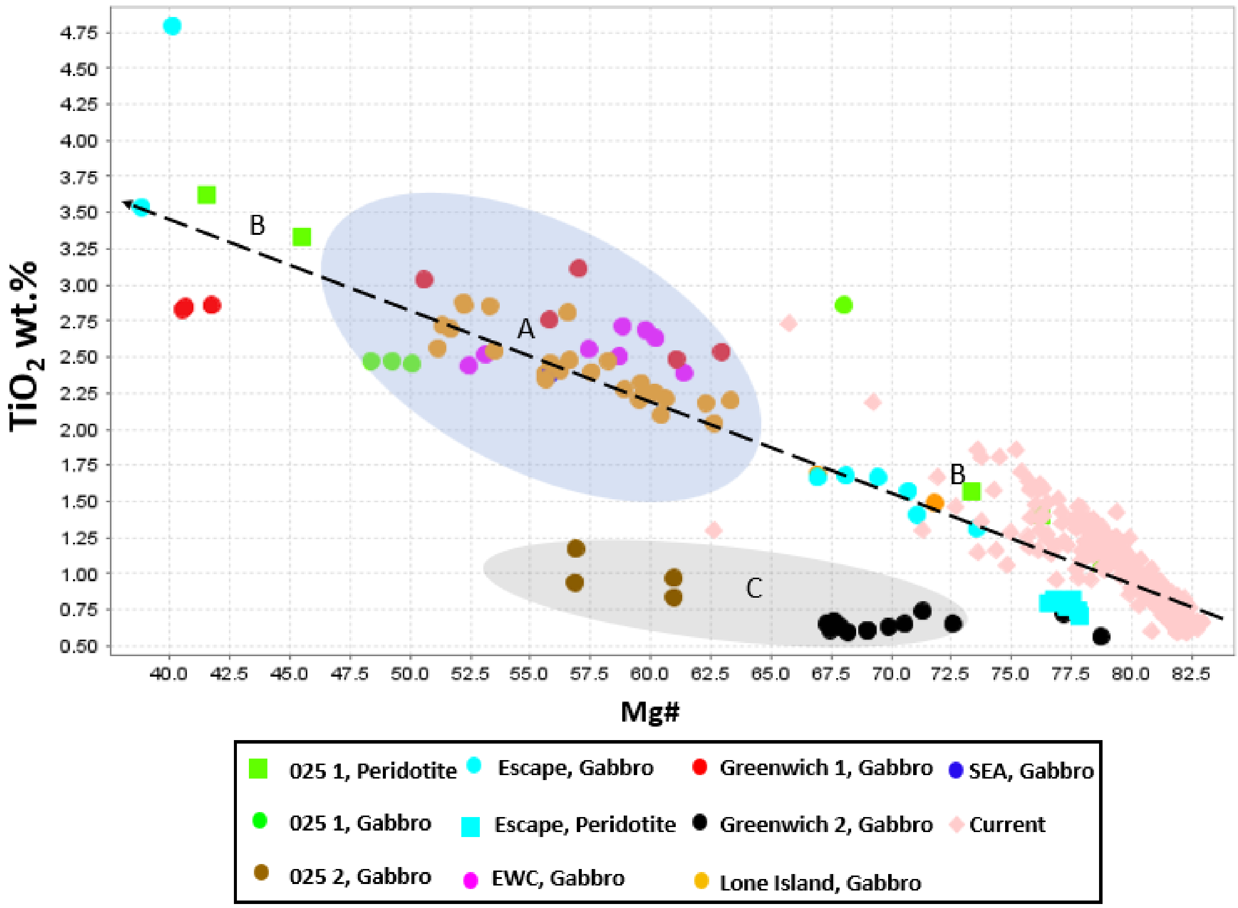

Fig 5.3 Mg# vs TiO_2 diagram showing the variation of Mg# vs TiO_2 and the two different trends displayed by the five intrusions, Current and Escape intrusions. The data for the Escape intrusion (Caglioti, MSc, 2023), Current (Clean Air Metals, 2021).

The Lone Island and EWC have similar trace element composition, with more negative ε_{Ndt} values than the 025-1 and the SEA, whereas Greenwich-2 has the most negative ε_{Ndt} values (Fig. 4. 30). This implies the Lone Island, SEA and EWC underwent higher degrees of crustal contamination compared to the 025-1, and less contamination than the Greenwich-2. Heggie (2010) suggested that the Lone Island intrusion is genetically and geochemically similar to the Current intrusion. The Lone Island, EWC, and SEA intrusions have similar petrography, whole rock compositions, and Rb-Sr and Sm-Nd isotope data. To test the relationship between the intrusions, whole rock data from the Current and Escape were compared with other four intrusions of this study (Fig. 5.4). The Current intrusion had the highest REE abundance among all of the TBN intrusions (Fig. 5.4). The Escape intrusion can be subdivided into two subgroups, one with a distinct REE pattern (the lowest HREE abundance among all the TBN intrusions), and a second segment with similar REE to population B, suggesting the same magmatic source for portions of the Escape intrusion and population B (Fig. 5.4). There is a similarity between the Lone Island and Current intrusions, but the Current samples have flatter HREE and higher abundances of REE than the Lone Island, EWC and SEA intrusions. This suggests that these intrusions originated from a distinct source to the one that produced the Current intrusion (Fig. 5.4).

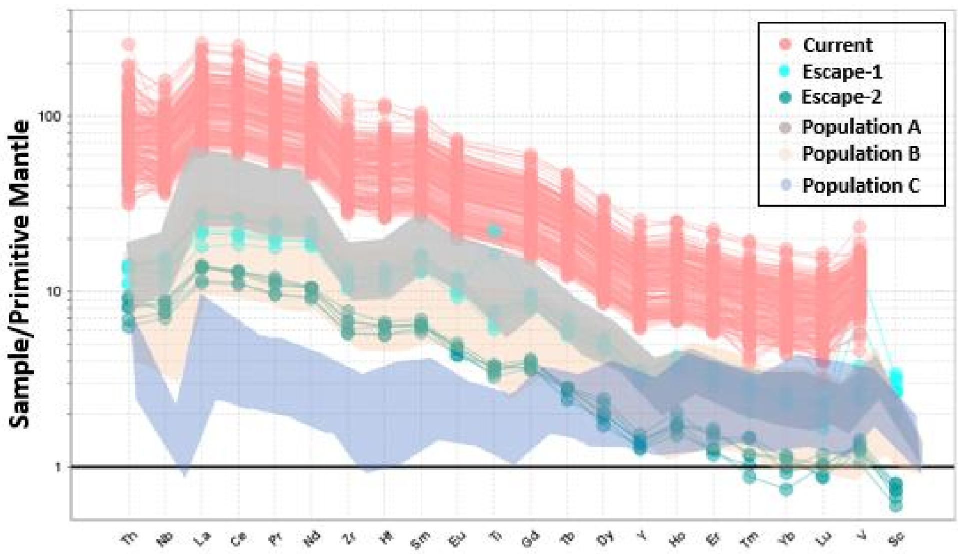

Fig 5.4 Showing a primitive mantle normalized diagram of populations A, B, and C with most of the samples from the Current intrusion plotted within population B. Current intrusion data from Clean Air Metals (2021), Escape intrusion data from Connor Cagliotì thesis (2021). Normalizing values from Sun and McDonough (1989).

The source of the magmatism associated with the MCR has been commonly accepted to have been a mantle plume emplaced at the base of the continental lithosphere (Hollings et al., 2007a). However, many studies have suggested that some of the mafic-ultramafic intrusions of the MCR have variable mantle sources. For example, the intrusive units of the Logan Basin have been interpreted to have been derived from two different sources – an early deep-seated source, with little crustal contamination, and a later shallower source, with a higher degree of crustal contamination (Hollings et al., 2007b; Cundari et al., 2021). Overall, the MCR related intrusive and volcanic rocks have a heterogeneous isotopic signature with at least four different geochemical reservoirs; plume lithospheric mantle, depleted upper mantle, subcontinental lithospheric-mantle, and continental crust (Rooney et al., 2022). Recently, osmium isotopes have been used to demonstrate that the earliest rocks of the MCR were derived from the subcontinental lithospheric mantle (SCLM; Brzozowski et al., 2023). During the early Proterozoic (1100 Ma), mafic magmas that were derived from a depleted mantle source are expected to have ε_{Ndt} values from +5 to +7, and the mafic magma that originated from enriched mantle would have had ε_{Ndt} of +3 to +5 (Nicholson & Shirey, 1990). The negative ε_{NdT} values and LREE enrichment of some of the mafic magmas at ca. 1100 Ma are caused by the interaction with the Archean crust that have ε_{Ndt} down to -17 (Nicholson & Shirey, 1990). This is consistent with the isotope data of this study that support contamination by metasedimentary and granitoid country rocks that have negative ε_{Ndt} values (down to -20). Thus, the differences in LREE content, Sr_i, and ε_{Ndt} in the five intrusions of this study and the other TBN intrusions were likely caused by differences in crustal contamination of plume-derived magmas.

5.3 Magmatic evolution of the five intrusions

The mafic-ultramafic Thunder Bay North Igneous Complex formed during the early stages of the MCR (1109 to 1104 Ma). This study reports two new ages, one for the Greenwich intrusion (1105.7± 0.9 Ma) that is similar but statistically younger than the second age measured for the Escape intrusion (1107.6 ± 0.9 Ma, Fig. 5.5). The Current intrusion yielded an age of 1106.6 ± 1.6 Ma (Bleeker, 2020), which is similar to the age of 1106.3 ± 2.1 Ma for the Lone Island intrusion (Metsaranta & Kamo, 2021). The combined data set provide useful time constraints for understanding the relationship between the five intrusions and the TBNIC within the MCR. The differences in age between the TBN intrusions can be interpreted as multiple stages of magmatic activity that occurred at spaced but broadly coeval times (Fig. 5.5). The SEA, EWC, and a portion of the Lone Island intrusions were all emplaced along the Escape fault and strike E-W. They have similar major and trace element compositions, suggesting they formed at similar or shortly time (Fig. 5.5). In contrast, the Greenwich and 025 intrusion were emplaced further from each other and from the TBN intrusions.

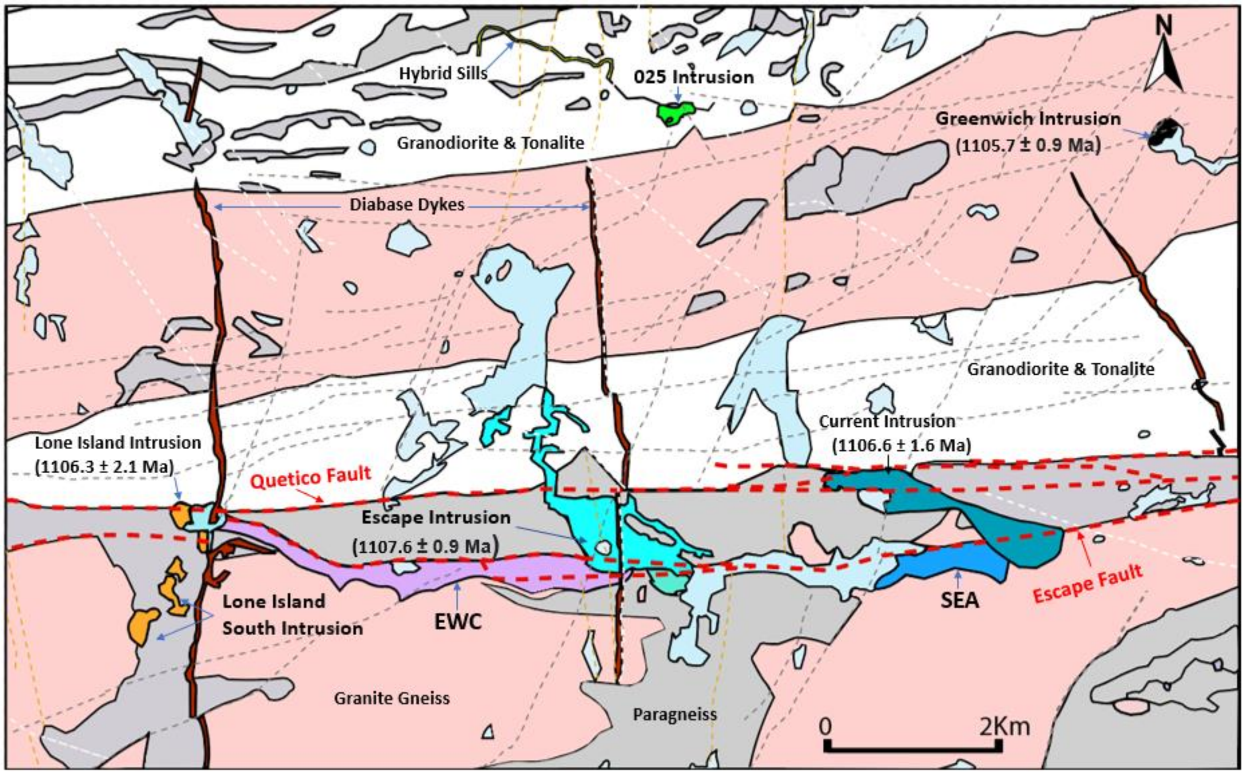

Fig 5.5 A geologic map of the study area showing the TBN intrusions and the new ages from this study, other surrounding intrusions, and the older Archean granitoids and metasedimentary rocks of Quetico Subprovince (modified from Clark, 2020).

Based on the petrography, geochemistry, and isotopic data from the five intrusions, combined with the available data from the Current and Escape intrusions, at least two types of magmas were responsible for forming the TBN intrusions. The first type of magma was a modified mantle plume magma characterized by a LREE enrichment similar to OIB. This magma formed the Lone Island, EWC, SEA, 025-1, Greenwich-1, Escape intrusions, and part of Current intrusion. According to Condie et al. (2003) La/Yb_n can be used to identify OIB magmas, which have La/Yb_n range between 17.3 to 29.2. Population A have La/Yb_n between (14.3 to 24.3) for the Lone Island, and 12.5 to 25.0 for the SEA and between 21.1 to 25.4 for the EWC intrusions. These La/Yb ratios are broadly similar to the OIB ratios (Condie et al., 2003).

The second type of magma has a flat LREE pattern, and includes the 025-2, and Greenwich-2 intrusions (population C). It is geochemically similar to the Nipigon sills-like magmas with lower Gd/Yb_n, higher Th/Nb_n, elevated Sr_i and more negative ε_{Ndt} values than populations A and B. The intrusions of the TBN complex have very closely spaced ages, exhibit different trace element and isotopic characteristics, and are located in a restricted geographic area, suggesting rapid changes in magmatic and contamination conditions. Alternatively, it can indicate for multiple magmatic sources that were actively feeding the TBN system with different magma types in a short time and limited space. The trace element and isotopic data from this study together with the available ages, are more consistent with multiple magma sources account for the isotopic and geochemical differences between population A and B versus population C. In contrast, populations A and B formed from similar magmas with very minimal differences, suggesting temporal changes in the magmatic characteristics of the same source.

O'Neill (2016) proposed a polynomial method for evaluating REE patterns, which allows for the calculation of shape coefficients that can be used to compare and classify different patterns. The method precisely quantifies REE pattern shapes, allowing a larger number of REE to be compared (O'Neill, 2016). The method involves normalizing the REE patterns to chondrite values and using orthogonal polynomials to fit smooth curves. Using this method, the difference between the magmas of the five intrusions can be displayed on the polynomial coefficients' diagrams as lambda values, where λ_1 represents the slope, and λ_2 the curvature of REE patterns (Fig. 5.6). The resulting coefficients can be used to identify the source of magma and to test the validity of petrogenetic hypotheses. Applying this method using the data from the five intrusions shows three groups; the first group includes the Lone Island, EWC and SEA intrusions, and lies close to the second group which includes 025-1 and Greenwich-1, whereas the third group is the 025-2 and Greenwich-2, which showed distinct λ_1 and λ_2 values that are different than Lone Island, EWC, SEA, 025-1 and Greenwich-1 intrusions (Fig. 5.6).

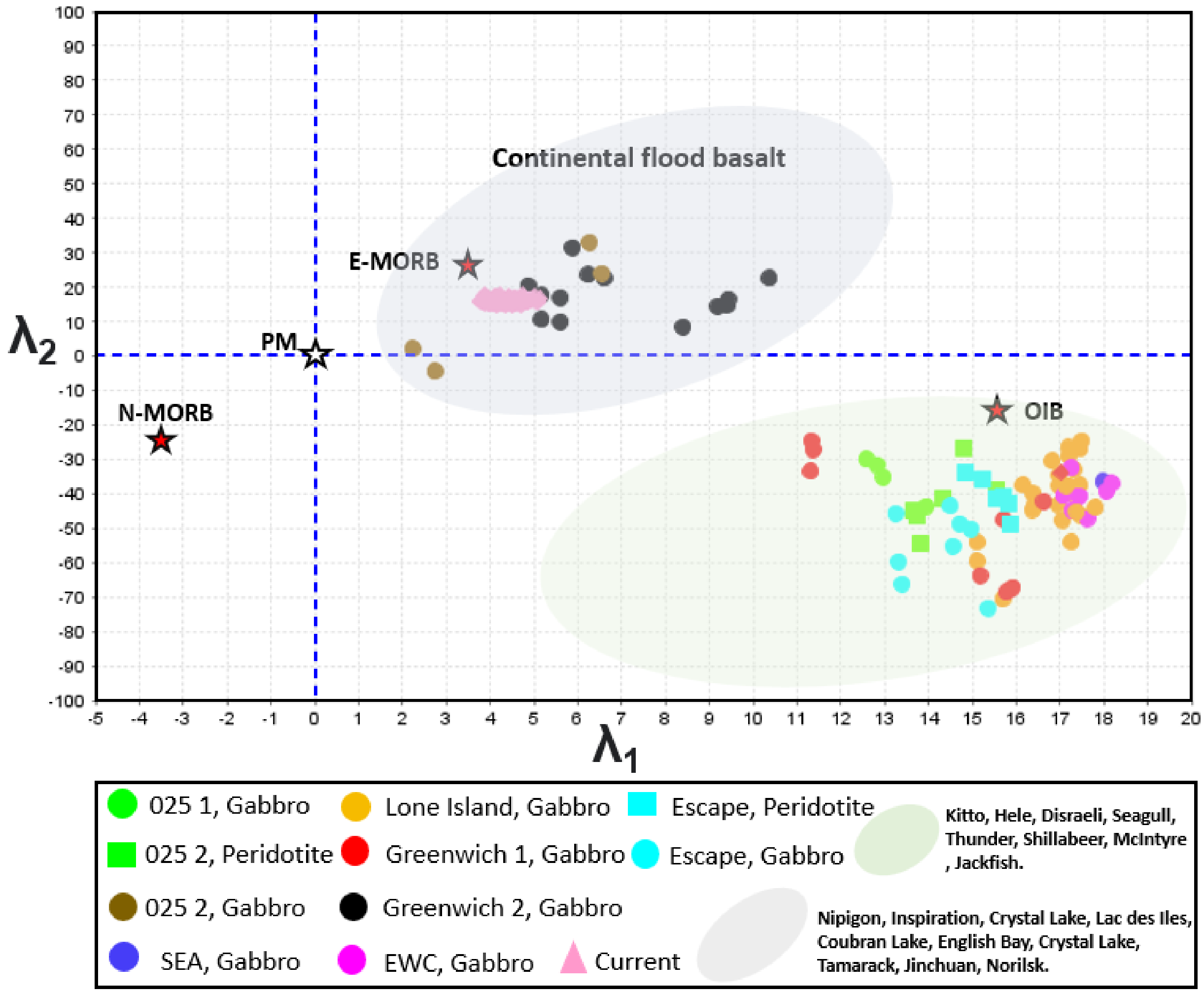

Fig 5.6 A diagram showing lambda1 vs lambda2 (λ_1 vs λ_2) with at least two distinct types of magmas. The data for the Escape intrusion (Caglioti, MSC, 2023), Current (Clean Air Metals, 2021). Field of continental flood basalt (dashed grey) from Barnes et al. (2021).

The Lone Island, EWC, SEA, 025-1 and Greenwich-1 magmas display OIB-like composition with higher λ_1 values, suggesting lower degrees of partial melting (Brzozowski et al., 2023), whereas 025-2 and Greenwich-2 magma is similar to continental flood basalts (CFB) and E-MORB with lower λ_1 values, suggesting higher degrees of partial melting (Brzozowski et al., 2023; Fig. 5.6). The Lone Island, EWC, SEA, 025-1 and Greenwich-1 are similar to the Eva Kitto, Jackfish, Seagull, McIntyre intrusions and relativity close to the Thunder intrusions, whereas 025-2 and Greenwich-2 magma is similar to Nipigon Sills, Inspiration, Crystal Lake, Coubran Lake and Tamarack intrusions (Fig. 5.6). The presence of these two types of magmas in one intrusion or multiple intrusions at such a large regional scale, requires the difference in the magmatic characteristics to be inherited from the source as local changes would likely not be systemically repeated over a regional scale, suggesting multiple magma sources that may have had been active at the same time or over short time. Therefore, we suggest that 025-2 and Greenwich-2 are sills with similar geochemical characteristics to the Nipigon sills, and are from a distinct source that is different from the source that produced the Lone Island, EWC, SEA, 025-1 and Greenwich-1 intrusions.

The primitive mantle normalized La/Sm_n vs La_n can be used to investigate the magmatic process and the composition of the mantle source (Hofmann, 2007). Magmas that exhibit different trends on La/Sm_n vs La_n diagram are interpreted to originate from different parental magmas by different batches of partial melting (Blein et al., 2001). According to Hofmann (2007), strong positive correlation between La/Sm_n vs La_n is due to the fact that lanthanum is much more variable than samarium, and it demonstrates that variations in REE abundance were not controlled by crystal fractionation of the magmas, but rather that it was controlled either by partial melting or changes in the source composition. In contrast, vertical La/Sm_n trends to La_n reflect rapid melting (Mvodo et al., 2022). The Lone Island, EWC, SEA, 025-1, Greenwich-1 samples (population A and B), and the gabbroic samples from the Escape intrusion exhibit steep positive trends, suggesting partial melting was the dominant magmatic process (Fig. 5.7). The Greenwich-2, 025-2 and the peridotites from the Escape intrusion display a vertical trend to the La_n, indicating a lesser degree of partial melting control, and suggest it was affected more by rapid melting events. In contrast, the Current intrusion exhibits a horizontal trend, suggesting a stronger role for fractional crystallization in the Current intrusion (Blein et al., 2001). Therefore, the different magmatic processes that controlled each type of magma may have an important role in controlling the similarities and differences between the TBN intrusions. Thus, it is suggested that populations A and B and the gabbroic rocks of the Escape intrusion represent different batches of magma that were derived from the same parental source, and they are different from population C and the Current intrusion magmas. Hence, three types of magmas were identified within the TBN and they are; population A and B type, population C type (Nipigon sills-like), and the Current intrusion type of magma.

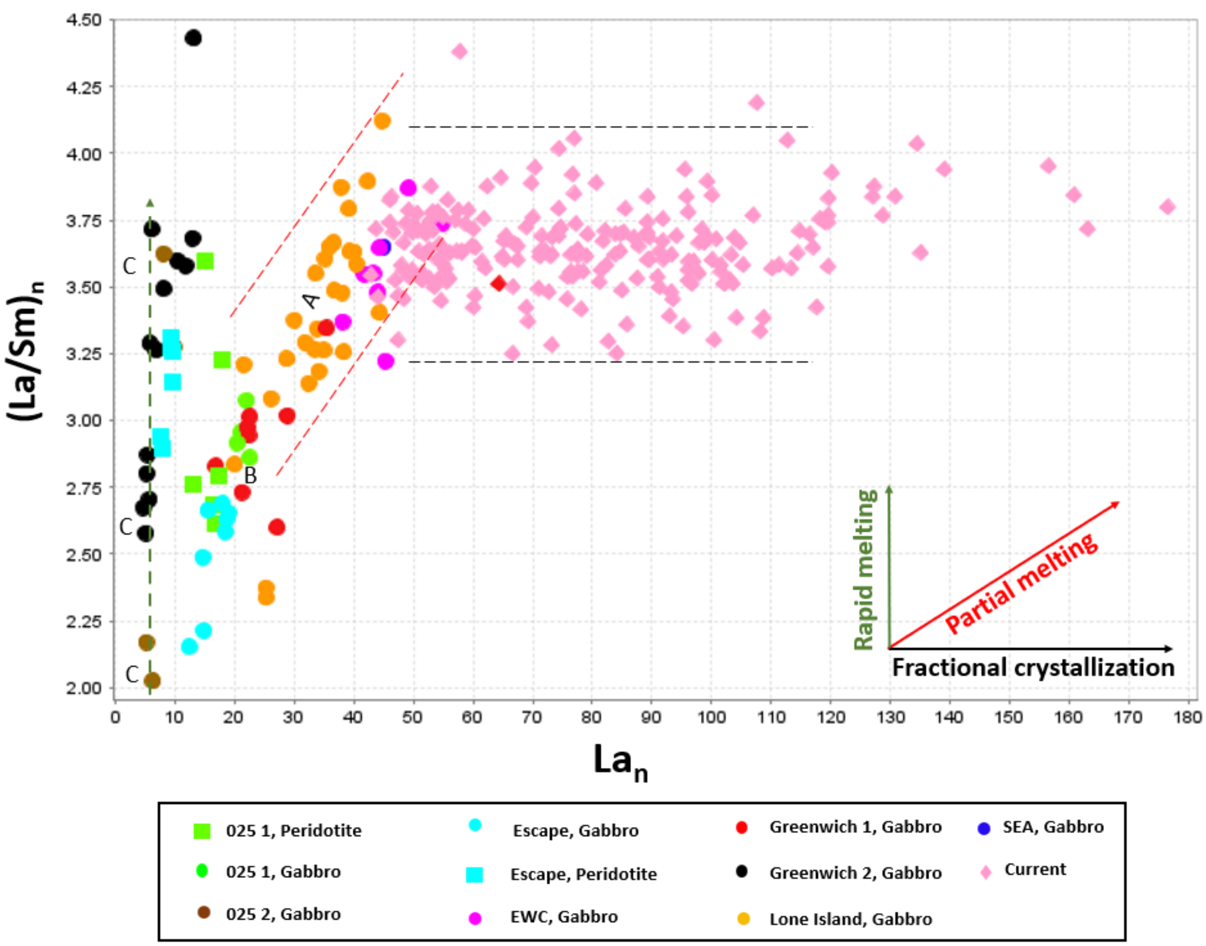

Fig 5.7 La/Sm$_n$ vs La$_n$ diagram showing the three types of magmas in the study area with variability in the effect of partial melting. The data for the Escape intrusion (Caglioti, MSC, 2023), Current (Clean Air Metals, 2021

The Ta/La and Ta/Th ratios are not as affected by changes in the degree of partial melting as Ce/Yb, making them useful tools for detecting changes in the magma source (Shirey et al., 1994). On Figure. 5.8, populations A and B plot in the mantle field with values relatively close to plume values. In contrast, most of the samples from population C plot in the crustal portion of the diagram with Ta/La and Ta/Th that are closer to SCLM and continental crust (Fig. 5.8). The two groups indicate different degrees of contamination as Ta and Th are enriched in the crustal rocks whereas La is enriched in the mantle. The Current intrusion data mainly plots in the mantle field with Ta/La and Ta/Th ratios that are relatively similar to those of population B, with few samples like the Nipigon sills and population C (Fig. 5.8). Population C which has been described by this study were also intruded in/ and around the Current intrusion.

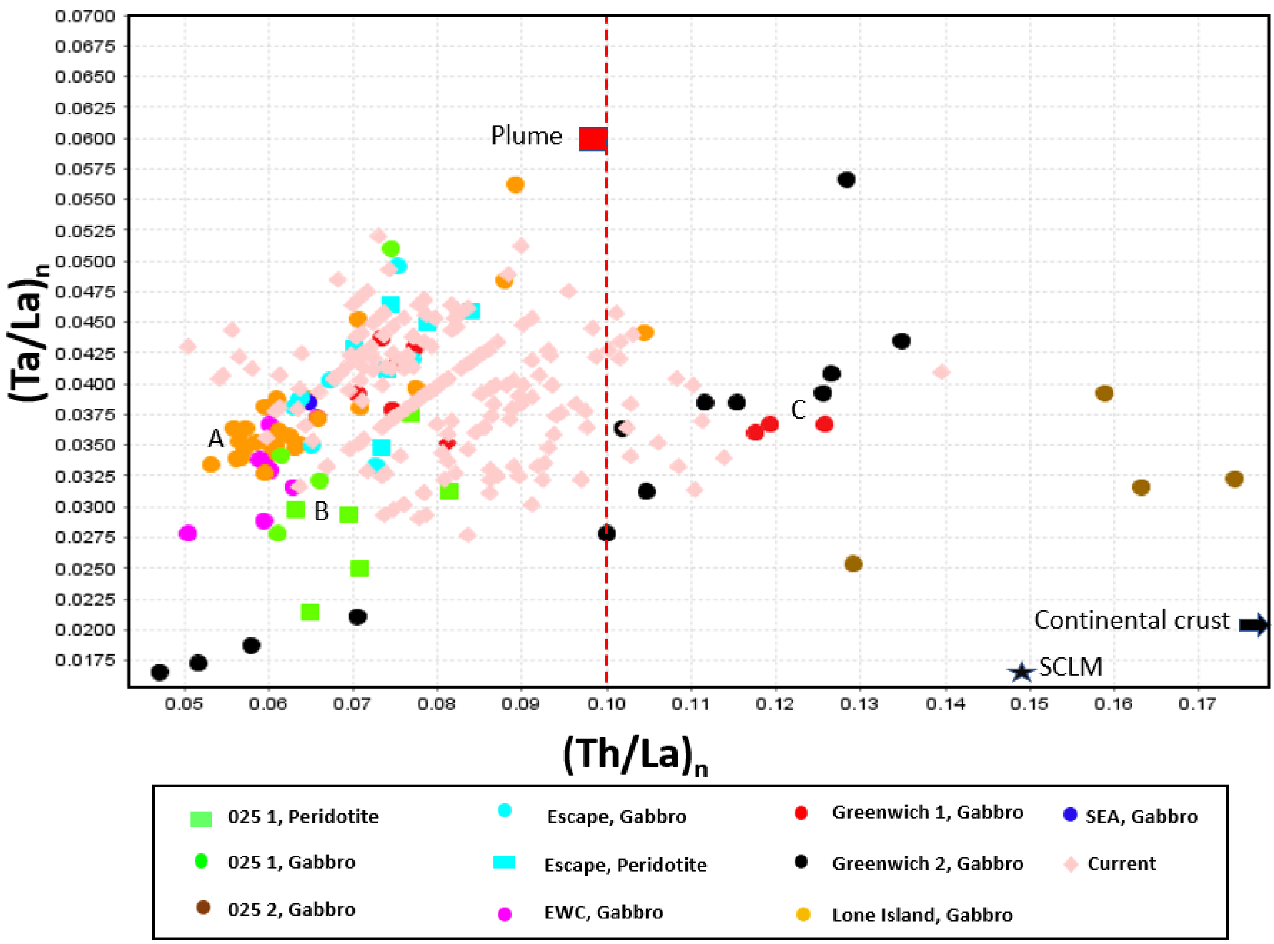

Fig 5.8 Ta/La$_n$ vs Th/La$_n$ diagram showing the two types of magmas in the study area. The data for the Escape intrusion (Caglioti, MSC, 2023), Current (Clean Air Metals, 2021). SCLM (Subcontinental lithospheric mantle).

5.4 Contamination of the five intrusions

Except for one sample from 025 with $\varepsilon_{Nd(t)}$ value of +0.14 and Sr_i of 0.7047, all the samples from the five intrusions have negative $\varepsilon_{Nd(t)}$ values that range between -2.73 to -7.49 with Sr_i values range between 0.7030 to 0.7058, which are indicative of contamination of the melts by older crustal rocks (Hollings et al., 2007b). Trace-element and isotope data from the five intrusions suggest that there are three contamination histories; (1) the Lone Island, SEA, EWC intrusions and 025-1, Greenwich-1 are the least contaminated, and (2-3) the 025-2 and Greewich-2 are the most contaminated but with two different styles of contamination (Fig. 4.30).

Many studies suggested that the MCR magmatism resulted from a mantle plume emplaced at the base of the continental lithosphere (Nicholson and Shirey 1990; Walker et al. 2002; Hollings et al., 2007b). Recent studies suggested that mantle sources of the MCR melts were more enriched in the early stages and became less-enriched to depleted in the later stages (Cundari et al., 2022). Brzozowski et al. (2023) combined osmium isotope data with previously published geochemical and isotope data to described two types of magma sources in the MCR region with two types of contamination. They proposed that the first type includes MCR rocks that are older than 1109 Ma, that were produced from enriched SCLM melts with limited to no Archean crustal contamination, and included; the Eva Kitto, Seagull, and Thunder intrusions and Shillabeer and Jackfish sills (Brzozowski et al., 2023). The second type comprises melts that were produced from depleted magma sources that were contaminated by Archean crustal rocks, such as the Nipigon and McIntyre sills (Brzozowski et al., 2023). This is consistent with the geochemistry and isotope data from the five intrusions, which identified two types of magmas with different styles of contamination; LREE enriched OIB-like magma (population A and B, the Current and Escape intrusions) and less-enriched Nipigon sills-like magma (close to SCLM magmas).

The sedimentary rocks of the Proterozoic Sibley Group and the Archean granitoids and metasedimentary rocks of the Quetico subprovince are potential crustal contaminants for the rocks of the MCR (Hollings et al., 2007b). Field observations and drill core logging show that nearby country rocks are Archean granitoids and metasedimentary rocks. Data from this study showed that the Archean metasedimentary and granitoid samples had more negative $\varepsilon_{Nd(t)}$ -20 than the five intrusions. The two Archean samples also have different Sr_i values with the metasedimentary sample having higher Sr_i 0.7636 than the granitoid sample (0.7041 Sr_i), whereas the five intrusions have Sr_i that range between 0.7030 to 0.7058. The isotopic data from the country rocks of this study are consistent with previously published data. For example, Nicholson & Shirey (1990) estimated Archean crust to have $\varepsilon_{Nd(t)}$ values that range between -12 to -17. Thus, we suggest that the differences in the isotopic characteristics of the five intrusions are caused by the differences in the types and/or the amounts of contaminants.

The LREE enrichment in populations A and B might be caused by crustal contamination or an interaction between the ascending magma and the SCLM. The SCLM functions in many ways as a chemical filter absorbing material from the rising melts and other fluids, which makes it chemically and isotopically different from the surrounding mantle through time (Menzies, 1990; Griffin, 1998). Therefore, the upward migration of magma through the SCLM may cause incompatible-element enrichment (Sun & McDonough, 1989; Nicholson & Shirey, 1990). Thus, it is possible that the LREE enrichment in population A and B intrusions could be due to the magma interaction with SCLM. However, the Archean granitoid sample analyzed in this study shows enriched LREE, strongly negative $\varepsilon_{Nd(t)}$ (-20) values and lower Sr_i (0.7041) that can explain the LREE enrichment in population A and B. Therefore, the Archean granitoid rocks likely contaminated the magma that formed populations A and B. Although the metasedimentary sample analyzed in this study has $\varepsilon_{Nd(t)}$ value of -20, it has an elevated Sr_i (0.7636), which reduces the likelihood of the Archean metasedimentary rocks as a possible contaminant for populations A and B (Figs. 5.8 and 5.10). Population C exhibited two different types of contamination; the gabbros from the Greenwich-2 that have higher MgO than the other intrusions of this study (Fig. 4.14), are less enriched in LREE than populations A and B, but have more negative $\varepsilon_{Nd(t)}$ and higher Sr_i, which is likely due to a contamination by the metasedimentary rocks of the Quetico Basin with their elevated Sr_i and strongly negative $\varepsilon_{Nd(t)}$ (Fig. 4.30). The 025-2 sample from 025-2 has negative Nb anomaly in primitive mantle normalized diagrams, $\varepsilon_{Nd(t)}$ value of (+0.14), and Sr_i (0.7047). Thus, it represents the least contamination among the five intrusions, which is consistent with the geochemical and isotopic results, as the 025-2 samples have less LREE enrichment.

Analysis of some of the trace element data from the five intrusions are inconsistent with portions of the isotopic data. For example, although the relative isotopic similarity between populations A and B is consistent with trace element and isotopic data (Figs. 5.9 and 5.10), samples from Greenwich-2 and 025-2 (population C) exhibit similar in trace element data (Fig. 5.1), but show differences in isotopic data (Fig. 5.9 and Fig. 5.10). This suggests that the contamination affecting Greenwich-2 and 025-2 did not impact the trace element compositions to the same extent as the isotopic composition. Thus, it indicates for two different types of contamination. The samples from Greenwich-2 are $\varepsilon_{Nd(t)}$ comparable to Pillar Lake volcanics and portion of Jackfish and Inspiration, which all have more negative $\varepsilon_{Nd(t)}$ than the average subcontinental lithospheric mantle (SCLM, Fig. 5.10) that suggests a contaminant with a more negative $\varepsilon_{Nd(t)}$ values than SCLM (likely the older Archean rocks). Thus, the differences between populations A and B and portion of population C (025-2) were likely caused by the differences in types and degrees of crustal contamination, which is also likely to be responsible for the LREE enrichment in populations A and B.

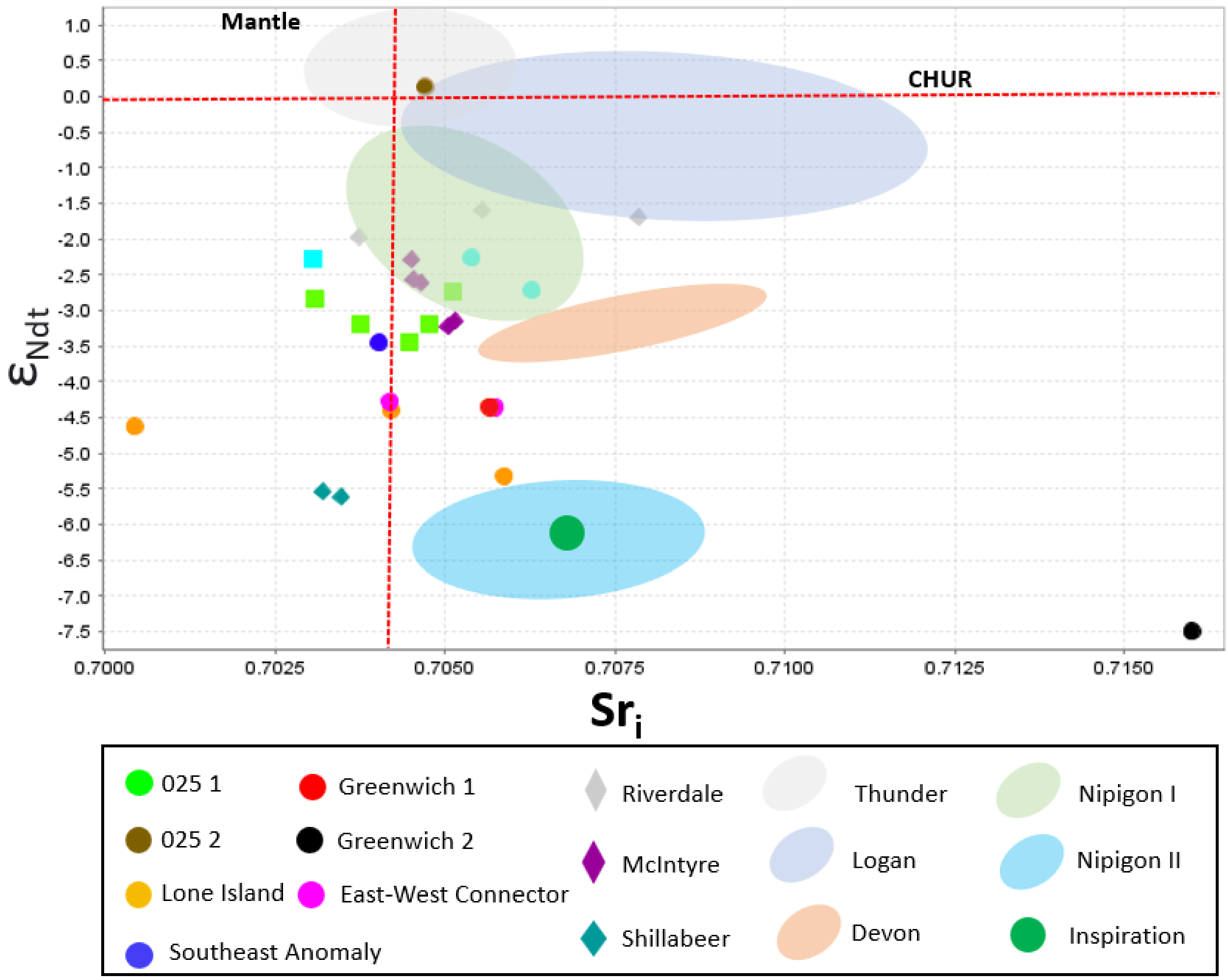

Fig 5.9: Sr_i versus ε_{Ndt} for the Lone Island, EWC, 025, SEA and Greenwich intrusions compared to other MCR related intrusions; Riverdale, McIntyre, Shillabeer, Thunder, Logan, Devon, Nipigon, and Inspiration. The data for the Shillabeer (Hollings et al., 2007a), Riverdale (Hollings et al., 2012),Thunder (Trevisan et al., 2015), Nipigon (Hollings et al., 2007a), McIntyre (Hollings et al., 2007a), Devon (Hollings et al., 2012), Logan (Cundari et al., 2013), and Inspiration (Hollings et al., 2007a).

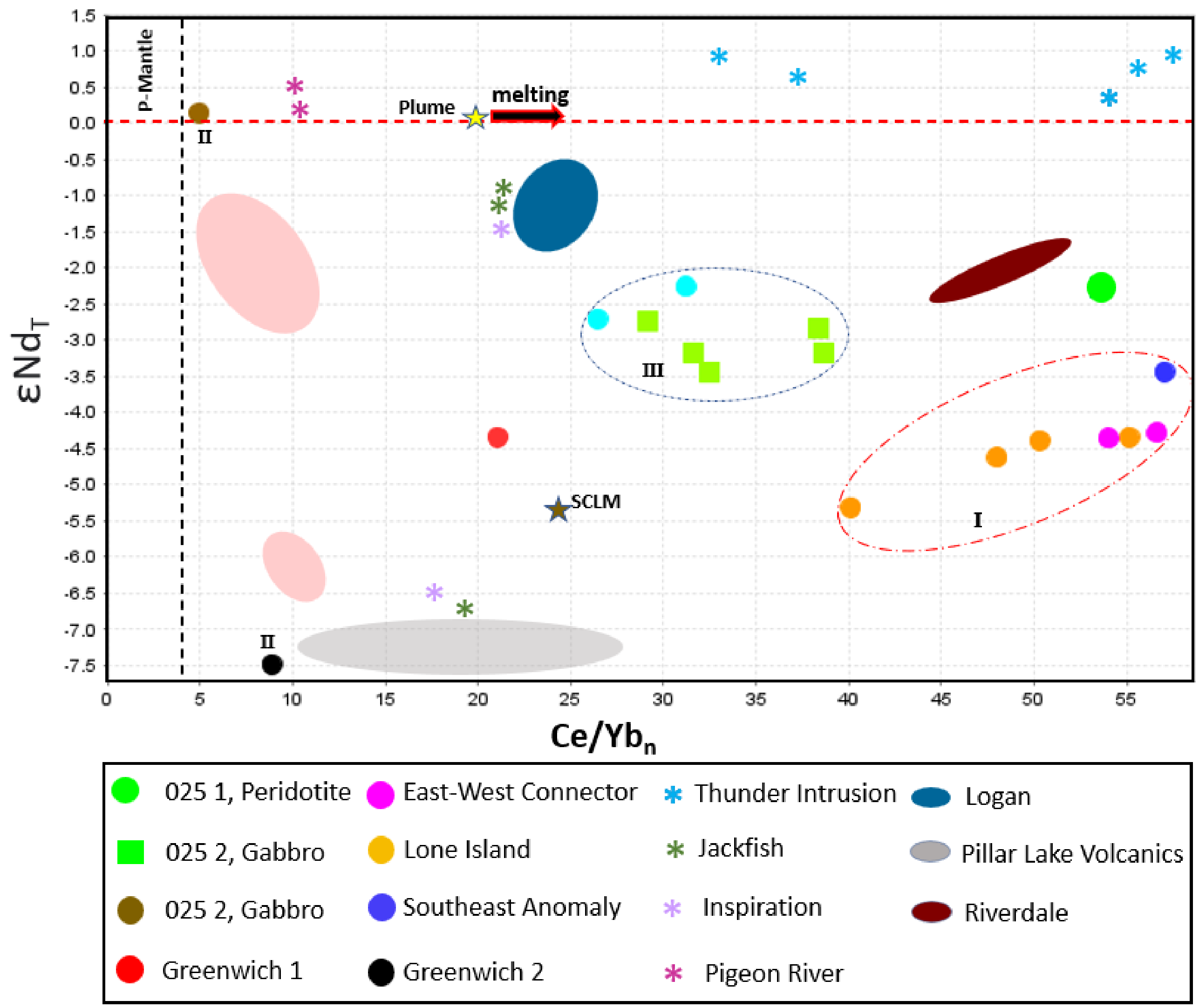

Fig 5.10 A plot of $\varepsilon_{Nd(T)}$ vs Ce/Yb$_n$ shows population A, B, and C among other intrusions and volcanics from the MCR region. The data for the Riverdale (Hollings et al., 2012),Thunder (Trevisan et al., 2015), Jackfish (Hollings et al., 2007a), Pigeon River (Cundari et al., 2013), Logan (Cundari et al., 2013), and Inspiration (Hollings et al., 2007a).

Granitoid and metasedimentary xenoliths were found in different drill cores from the five intrusions (especially Lone Island), suggesting assimilation of country rocks in the five intrusions. To evaluate the amount of assimilated crust in the five intrusions, numerical modeling was attempted. According to Aitcheson and Forrest (1994) bulk contamination calculations can be used to estimate the amount of assimilated crustal rocks in the magma. The following equation of Aitcheson and Forrest (1994) shows the factors used for bulk assimilation calculations in this study:

ε_{Ndt} Mixture = (ε_{Ndt} End member 1 x Proportion of End member 1) + (ε_{Ndt} End member 2 x proportion of End member 2)

Nicholson & Shirey (1990) estimated the enriched 1.1 Ga plume to have had lower Nd isotopic composition than the OIB magmas of today, with enriched mantle that had ε_{Ndt} of +3 to +5, and depleted mantle source to have had ε_{Ndt} from +5 to +7. In this study, we used an average value of $\varepsilon_{Nd(1.1\ Ga)}$ of +6 for the depleted mantle to approximate the mafic to ultramafic magmas from the study area at 1.1 Ga, whereas both the Archean granitoids and metasedimentary rocks from this study have - 20 ε_{Ndt}. The estimated bulk assimilation calculations showed that assimilation of about 24% Archean rocks was required to generate the negative $\varepsilon_{Nd(1.1\ Ga)}$ of the five intrusions. In addition, about 38 to 42% assimilation of Archean rocks in the magma was required to achieve (-3 to -5) $\varepsilon_{Nd(1.1\ Ga)}$ in the Lone Island, EWC, SEA, 025-1. Whereas about 50% Archean rocks were required to achieve the -7 $\varepsilon_{Nd(1.1\ Ga)}$ of the Greenwich-2. These estimated quantities (38 to 50%) of possible assimilated Archean crust are not reasonable, and suggesting that other possible contaminants may be involved. The top unmineralized portions of the Current and Escape intrusions are hematized red hybrid gabbros, have carbonate ocellae, and visible evidence of quartz rich sedimentary rocks that were likely assimilated country rocks (Chaffee, 2015; Caglioti, 2023). Despite the absence of the strong hematization and carbonate ocellae in the Lone Island, EWC, 025, and Greenwich intrusions, it is possible that they were not able to generate higher abundance of mineralization due to assimilation of some quartz-rich country rocks, which were not sampled by this study.

7 Conclusions

The new (1105 ± 0.9 Ma) age for the Greenwich intrusion and (1107.6 ± 0.9 Ma) for the Escape intrusion in conjunction with the previously published dates, better constrain the age of the five intrusions and their relationships with the mineralized 1106.6 ± 1.6 Ma Current (Bleeker et al., 2020) and the 1107.6 ± 0.9 Ma Escape intrusions, as well as the other MCR related intrusions in the region. The 1106.3 ± 1.5 Ma Lone Island (Kamo, 2020) and the 1106.6 ± 1.6 Ma Current (Bleeker et al., 2020) intrusions are within uncertainty of the new 1105 ± 0.9 Ma (dated by this study) age for the Greenwich intrusion, whereas 1107.6 ± 0.9 Ma age for the Escape intrusion is the oldest age among the TBN intrusions and likely represents the initiation of the magmatic activity in the TBN.

The petrography and geochemistry of the five intrusions revealed that they share both similarities and differences. The Lone Island intrusion is mostly medium-grained poikilitic gabbronorite, with lesser amounts of orthopyroxene gabbro and websterite, and it is the least altered among the five intrusions with sericitization of plagioclase and serpentinization of pyroxene. The EWC intrusion comprises highly altered poikilitic gabbronorite rocks with remnants of plagioclase and clinopyroxene and chalcopyrite and pyrrhotite, with lesser amounts of pentlandite. The 025 intrusion comprises gabbronorite and websterite with sulphides and oxides that are similar to those of the Lone Island intrusion, with magnetite being the dominant oxide and lesser ilmenite and hematite and rare blebs of chalcopyrite. The SEA intrusion comprises strongly sericitized gabbroic rocks with some peridotitic rocks. The peridotites are coarser-grained compared to the gabbroic rocks, and are mainly websterite with fine- to medium-grained oxides and sulphides. Two styles of mineralization are common in the five intrusions. The most dominant styles is found in all of the intrusions, it is characterized by fine-to very-fine disseminated magmatic blebs of chalcopyrite, pyrrhotite, pentlandite, and occasional pyrite, along with prevalent oxides (ilmenite, magnetite, and hematite). The second style is less common, consists of late vein-associated chalcopyrite and uncommon ilmenite and magnetite. Except for some elevated mineralization in parts of the Lone Island (154 to 175 m depth) and 025-1 intrusions, no anomalous mineralization was found in this study.

Geochemically, the five intrusions were subdivided into three populations. Populations A and B have similar major element compositions but slightly different trace elements. They are enriched in LREE and are similar to plume related magmas. Population C has different major and trace element compositions with less-enriched LREE but still similar to plume related magmas, and are similar to Nipigon sills. The data suggests two types of magmas were involved in the formation of the TBN intrusions, where one was plume-like magmas giving rise to populations A and B. The second type of magma has a less-enriched LREE pattern and it includes Greenwich-2 and 025-2. The three populations went through different types and degrees of contamination. Population A includes Lone Island, SEA, and EWC intrusions, and population B are Greenwich-1 and 025-1 intrusions. Populations A and B have slightly similar trace element and isotopic compositions. They have negative $\varepsilon_{Nd(t)}$ values ranging between -2 to -5 and low Sr_i ranging between 0.7004 to 0.7058, whereas population C was subjected to two types of contamination; Greenwich-2 that has the highest Sr_i of 0.7129 and 0.7159 and the most negative $\varepsilon_{Nd(t)}$ of -7 among the five intrusions, and 025-2 that has the least degree of contamination with positive $\varepsilon_{Nd(t)}$ of +0.14 and low Sr_i of 0.7047.

The five intrusions share many similarities and differences with TBN intrusions. The Current intrusion and Lone Island, EWC, SEA intrusions have relatively similar REE patterns on primitive mantle normalized diagrams, but Current has higher REE abundance than Lone Island, EWC, SEA intrusions. Using the O'Neill (2016) polynomial method of evaluating REE patterns, the difference between the two types of magmas is clear, with the Current being similar to continental flood basalts with higher degree of partial melting (lower λ_1), whereas Lone Island, SEA, and EWC intrusions are similar to OIB magmas with lower degree of partial melting (higher λ_1). The 025-1, Greenwich-1, and Escape intrusions are relatively similar to Lone Island, SEA, and EWC intrusions, but have different REE patterns and abundances, suggesting different magma batches with slightly different magma characteristics. Clean Air Metals (2023) proposed that portions of the 025 intrusions (025-2) is a mafic Archean rock, but the fresher and less deformed lithology suggest that it is likely Proterozoic, moreover it is geochemically similar to portions of the Nipigon Sills, which suggests that 025-2 is MCR related, and it was likely originated from the same source portions of the Nipigon sills.

The differences between the three types of crustal contamination suggested in this study reflect the differences in magma types and type and quantity of contaminants. All the five intrusions have negative $\varepsilon_{Nd(t)}$ and Sr_i indicative of crustal contamination. The Archean granitoids and metasedimentary rocks of Quetico Basin are possible contaminants that were found in the drill core and outcrops. The granitoids and metasedimentary samples have -20 $\varepsilon_{Nd(t)}$, are enriched in LREE. Based on their strongly negative $\varepsilon_{Nd(t)}$ and low Sr_i, the Archean granitoids are suitable contaminants for the Lone Island, EWC, SEA, 025-1, Greenwich-1, which have lower Sr_i than Greenwich-2. In contrast, the Greenwich-2 was likely contaminated by the Archean metasedimentary rocks that have negative $\varepsilon_{Nd(t)}$ and higher Sr_i than the Archean granitoid rocks. The strong negative Nb anomalies in all of the mafic to ultramafic samples from the five intrusions suggest pervasive contamination by crustal rocks, indicating the enriched LREE in the five intrusions was likely derived from assimilated crust, and it was not caused by OIB magma source.

The magmatic evolution of Thunder Bay North Igneous Complex involved three types of magmas with three distinct contamination histories. The differences in magma types, degrees and types of crustal contamination are likely the main factors that led to the differences in mineralization between the Current and Escape-Steepledge versus the less mineralized intrusions.

References

Aitcheson, S.J. and Forrest, A.H., (1994). Quantification of crustal contamination in open magmatic systems. Journal of Petrology, 35(2), pp.461-488.

Barnes, S. J., A.J. Naldrett, M.P. Gorton. 1985. The origin of the fractionation of platinum-group elements in terrestrial magmas. pp. 303-323.

Barnes, S. J., Cruden, A. R., Arndt, N., & Saumur, B. M. (2016). The mineral system approach applied to magmatic Ni–Cu–PGE sulphide deposits. Ore Geology Reviews, 76, pp. 296–316.

Bleeker, W., Smith, J, et al. 2020. The Midcontinent Rift and its mineral systems: overview and temporal constraints of Ni–Cu–PGE mineralized intrusions. In: Bleeker, W. and Houlé, M.G. (eds) Targeted Geoscience Initiative 5: Advances in the understanding of Canadian Ni-Cu-PGE and Cr ore Systems Examples from the Midcontinent Rift, the Circum-Superior Belt, the Archean Superior Province, and Cordilleran Alaskan-Type Intrusions. Geological Survey of Canada, Open File 8722, 7–35

Blein, O., Lapierre, H. and Schweickert, R.A., (2001). A Permian island-arc with a continental basement: the Black dyke formation (Nevada), North American Cordillera. Chemical Geology, 175 (3-4), pp.543-566.

Brzozowski, M. J., Hollings, P., Zhu, J.-J., & Creaser, R. A. (2023). Osmium isotopes record a complex magmatic history during the early stages of formation of the North American Midcontinent Rift implications for rift initiation. Lithos, pp. 436-437.

Chaffee, M.R. (2015). Petrographic and geochemical study of the hybrid rock unit associated with the Current Lake Intrusion. Unpublished MSc. Thesis, University of Minnesota. pp. 1-139.

Chassé, M., Griffin, W. L., Alard, O., O'Reilly, S. Y., & Calas, G. (2018). Insights into the mantle geochemistry of scandium from a meta-analysis of Garnet Data. Lithos, 310-311, pp. 409–421.

Clark J. Garry, 2020. Technical Report on the Thunder Bay North and Escape Lake Properties, Northern Ontario. Technical Report by Clark Exploration Consulting (Thunder Bay, Ontario). Prepared for Regency Goldcorp. pp. 1-62.

Condie, K.C., (1999). Mafic crustal xenoliths and the origin of the lower continental crust. Lithos, 46(1), pp.95-101.

Cousens, B. L. (1996). Magmatic evolution of Quaternary mafic magmas at Long Valley Caldera and the Devils Postpile, California: Effects of crustal contamination on lithospheric mantle-derived magmas. Journal of Geophysical Research: Solid Earth, 101(B12), pp. 27673-27689.

Cumming, V. M., Poulton, S. W., Rooney, A. D., & Selby, D. (2013). Anoxia in the terrestrial environment during the late Mesoproterozoic. Geology, 41(5), pp. 583–586.

Cundari, R. (2013). Geology and geochemistry of midcontinent rift-related igneous rocks. MSc Thesis, Lakehead University. pp. 1-142.

Cundari, R.M., Carl, C.F.J., Hollings, P. and Smyk, M.C. (2013). New and compiled whole-rock geochemical and isotope data of Midcontinent Rift-related rocks, Thunder Bay area: Ontario Geological Survey, Miscellaneous Release Data 308. pp. 1-9.

Cundari, R., Hollings, P., Smyk, M. and Carl, C., (2022). The geochemical evolution of the Logan Igneous Suite, Ontario, Canada: new insights from the Logan Basin and implications for the genesis of the Mesoproterozoic Midcontinent Rift System, pp.1-23.

Ding, X., Ripley, E. M., Shirey, S. B., & Li, C. (2012). Os, Nd, O and S isotope constraints on country rock contamination in the conduit-related eagle Cu–Ni–(PGE) deposit, Midcontinent Rift System, Upper Michigan. Geochimica Et Cosmochimica Acta, 89, pp. 10–30.

Davis, D. W., Pezzutto, F., & Ojakangas, R. W. (1990). The age and provenance of metasedimentary rocks in the Quetico Subprovince, Ontario, from single zircon analyses: implications for Archean

sedimentation and tectonics in the Superior Province. Earth and Planetary Science Letters, 99(3), pp. 195–205.
D'Angelo, Mike. (2016). Geochemistry, petrography and mineral chemistry of the Guichon Creek and Nicola batholiths, south-central British Columbia." Unpublished MSc. thesis, Lakehead University, Thunder Bay, Ontario.
Eckstrand, O. R., & Hulbert, L. J. (2007). Magmatic nickel-copper-platinum group element deposits. Mineral deposits of Canada: a synthesis of major deposit types, district metallogeny, the evolution of geological provinces, and exploration methods: geological association of Canada, mineral deposits division, Special Publication, 5, pp. 205-222.
Evans-Lamswood, D. M. (2000). Physical controls associated with the distribution of sulfides in the Voisey's bay Ni-Cu-co deposit, Labrador. Economic Geology, 95(4), pp. 749–769.
Fralick, P., Davis, D. W., & Kissin, S. A. (2002). The age of the gunflint formation, Ontario, Canada: Single Zircon U–Pb age determinations from reworked volcanic ash. Canadian Journal of Earth Sciences, 39(7), pp. 1085–1091.
Franklin, J. M., McIlwaine, W. H., Poulsen, K. H., & Wanless, R. K. (1980). Stratigraphy and depositional setting of the Sibley Group, Thunder Bay District, Ontario, Canada. Canadian Journal of Earth Sciences, 17(5), pp. 633–651.
Gerstenberger, H. and Haase, G., (1997). A highly effective emitter substance for mass spectrometric Pb isotope ratio determinations. Chemical Geology 136, pp. 309-312.
Godel, B. M., Barnes, S. J., & Barnes, S.-J. (2013). Deposition mechanisms of magmatic sulphide liquids: Evidence from high-resolution X-ray computed tomography and trace element chemistry of komatiite-hosted disseminated sulphides. Journal of Petrology, 54(7), pp. 1455–1481.
Goodgame, V.R., (2010). Initial lithogeochemical study of the Current Lake Intrusive Complex, Ontario, Canada: Taloumba, Inc. Magma Metals (Canada) Limited internal report. pp. 1-85.
Griffin, W. L. (1999). The composition and origin of sub-continental lithospheric mantle. Mantle Petrology: Field Observations and High Pressure Experimentation, A Tribute to Francis R.(Joe) Boyd, pp. 13-45.
Hart, T.R. and MacDonald, C.A. (2007). Proterozoic and Archean Geology of the Nipigon Embayment: implications for emplacement of the Mesoproterozoic Nipigon diabase sills and mafic-ultramafic intrusions. Canadian Journal of Earth Sciences 44: pp. 1021-1040.
Hart, T., Richardson, A., MacDonald, C. A., & Hollings, P. (2007). Geochemistry of the Mesoproterozoic intrusive rocks of the Nipigon embayment, Northwestern Ontario: Evaluating the earliest phases of Rift Development. Canadian Journal of Earth Sciences, 44(8), pp. 1087–1110.
Heggie, G.J., (2005), Whole rock geochemistry, mineral chemistry, petrology, and Pt, Pd mineralization of the Seagull intrusion, Northwestern Ontario: Unpublished M.Sc. Thesis, Thunder Bay, ON, Lakehead University. pp. 1-156.
Heggie, G.J, (2010a), Interpretation of the LIL and EWC drilling, Part2. Geochemistry and petrology, Lone Island Lake, and East-West Connector Projects. Thunder Bay Mining Division, Northwestern Ontario. Internal report to Magma Metals (Canada) LTD. pp. 1-20.
Heggie, G.J, (2010b), SEA10-06 Mafic Intrusives, lithogeochemistry. Thunder Bay Mining Division, Northwestern Ontario. Internal report to Magma Metals (Canada) LTD. pp. 1-16.
Heggie, G.J and Hughes. W, (2011), 2011 Drill Results and Interpretations, Part1. Southeast Anomaly Area, Thunder Bay, ON. pp. 1-7.
Heggie, G.J. and MacTavish. A., (2015), North Current Chonolith Field Trip, Thunder Bay, ON. pp. 1-28.
Heaman, L.M., Easton, M., Hart, T.R., Hollings, P., MacDonald, C.A., Smyk, M., 2007, Further refinement to the timing of Mesoproterozoic magmatism, Lake Nipigon Region, Ontario: Canadian Journal of Earth Sciences, v. 44, pp. 1055–1086.

Hinze, W. J., & Chandler, V. W. (2020). Reviewing the configuration and extent of the Midcontinent Rift System. Precambrian Research, pp. 1-18.

Holwell, D. A., & McDonald, I. (2010). A review of the behaviour of platinum group elements within natural magmatic sulfide ore systems. Platinum Metals Review, 54(1), pp. 26–36.

Hollings, P., Hart, T., Richardson, A. and MacDonald, C.A., (2007a). Geochemistry of the mid-Proterozoic intrusive rocks of the Nipigon Embayement, northwestern Ontario. Canadian Journal of Earth Sciences 44, pp. 1087-1110.

Hollings, P., Richardson, A., Creaser, R. and Franklin, J., (2007b). Radiogenic isotope characteristics of the mid-Proterozoic intrusive rocks of the Nipigon Embayement, northwestern Ontario. Canadian Journal of Earth Science 44, pp. 1111-1129.

Hollings, P., Fralick., P. and Cousens, B., (2007c). Early history of the Midcontinent Rift inferred from geochemistry and sedimentology of the Mesoproterozoic Osler Group, northwestern Ontario. Canadian Journal of Earth Sciences 44,pp. 389-412.

Hollings, P., Fralick, P., Kissin, S., (2004). Geochemistry and geodynamic implications of the Mesoproterozoic English Bay Granite-Rhyolite complex, northwester Ontario Canada. Canadian Journal of Earth Sciences 41, pp. 1329-1338.

Hochstaedter, A., Gill, J., Peters, R., Broughton, P., Holden, P., & Taylor, B. (2001). Across-arc geochemical trends in the Izu-bonin arc: Contributions from the subducting slab. Geochemistry, Geophysics, Geosystems, 2(7), pp. 1-45.

Hofmann, A. W. (2007). Sampling mantle heterogeneity through oceanic basalts: Isotopes and trace elements. Treatise on Geochemistry, pp. 1–44.

Iwano, H., Danhara, T., Yuguchi, T., Hirata, T., & Ogasawara, M. (2019). Duluth Complex Apatites: Age reference material for LA–ICP–ms-based fission-track dating. Terra Nova, 31(3), 247–256.

Jaffey, A.H., Flynn, K.F., Glendenin, L.E., Bentley, W.C. and Essling, A.M., (1971). Precision measurement of half-lives and specific activities of 235U and 238U. Physical Review 4, pp. 1889-1906.

Khedr, M. Z., Takazawa, E., Arai, S., Stern, R. J., Morishita, T., & El-Awady, A. (2022). Styles of Fe–Ti–V ore deposits in the Neoproterozoic layered mafic-ultramafic intrusions, southeastern desert of Egypt: Evidence for fractional crystallization of V-rich melts. Journal of African Earth Sciences, pp. 1-4.

Kimata, M., (1988). The crystal structure of non-stoichiometric Eu-anorthite: an explanation of the Eu-positive anomaly. Mineralogical Magazine, 52(365), pp.257-265.

Kissin, S. A., Heggie, G. J., & Somarin, A. K. (2006). Sulfide Saturation Mechanisms in Gabbroic Intrusions in the Nipigon Embayment: Lake Nipigon Region Geoscience Initiative. Ontario Geological Survey.

Laarman, J.E., (2007). Geochemistry and PGE mineralization of the Kitto intrusion: A product of Mesoproterozoic plume magmatism through fault bounded Archean crust, east Nipigon Embayment, northern Ontario. M.Sc. thesis, Lakehead University, Thunder Bay, ON. 276 p.

Le Vaillant, M., Barnes, S. J., Fiorentini, M. L., Santaguida, F., & Törmänen, T. (2016). Effects of hydrous alteration on the distribution of base metals and platinum group elements within the Kevitsa Magmatic Nickel Sulphide Deposit. Ore Geology Reviews, 72, pp. 128–148.

Lesher, C.M., Burnham, O.M., Keays, R.R., Barnes, S.J. and Hulbert, L., (2001). Trace-element geochemistry and petrogenesis of barren and ore-associated komatiites. The Canadian Mineralogist, 39(2), pp.673-696.

Liu, W., Migdisov, A., & Williams-Jones, A. (2012). The stability of aqueous nickel(ii) chloride complexes in hydrothermal solutions: Results of UV–visible spectroscopic experiments. Geochimica Et Cosmochimica Acta, 94, pp. 276–290.

Ludwig, K.R., (2009). User's manual for Isoplot 3.71 a geochronological toolkit for Excel. Berkeley Geochronological Center Special Publication, 72(4), pp. 1-56.

Maier, W.D., Barnes, S.J. and De Waal, S.A., (1998). Exploration for magmatic Ni-Cu-PGE sulphide deposits: A review of recent advances in the use of geochemical tools, and their application to some South African ores. South African Journal of Geology, 101(3), pp.237-253.

Maier, W. D. (2005). Platinum-group element (PGE) deposits and occurrences: Mineralization styles, genetic concepts, and exploration criteria. Journal of African Earth Sciences, 41(3), pp. 165–191.

Makkonen, H.V., Mäkinen, J. and Kontoniemi, O., (2008). Geochemical discrimination between barren and mineralized intrusions in the Svecofennian (1.9 Ga) Kotalahti Nickel Belt, Finland. Ore Geology Reviews, 33(1), pp.101-114.

Mattinson, J., (2005). Zircon U-Pb chemical abrasion (CA-TIMS) method: Combined annealing and multi-step partial dissolution analysis for improved precision and accuracy of zircon ages. Chemical Geology 220, pp. 47-66.

Metsaranta, R. T. (2006). Sedimentology and geochemistry of the Mesoproterozoic pass lake and Rossport formations, Sibley Group. Unpublished MSc. Thesis, Lakehead University).pp. 1-216.

Metsaranta, R. T. and M.A. Hamilton, (2020). A precise U/Pb age for a North-trending Mafic Dike from the Western Flank of the Marathon Swarm, East Bay Area, Northern Ontario. pp. 1-9.

Metsaranta, R.T. and Kamo, S.L. (2021). A uranium–lead baddeleyite age for the Midcontinent Rift–related Lone Island Lake intrusion, northwestern Ontario; in Summary of Field Work and Other Activities, 2021, Ontario Geological Survey, Open File Report 6380, p.12-1 to 12-8.

Miller, J.D., Jr., Green, J.C., Severson, M.J., Chandler, V.W., Hauck, S.A., Peterson, D.M., and Wahl, T.E., (2002), Geology and mineral potential of the Duluth Complex and related rocks of northeastern Minnesota: Minnesota Geological Survey Report of Investigations 58, 207, pp. 21-31.

Miller, J. D., Nicholson, S. W., Easton, R. M., Ripley, E. M., & Feinberg, J. M. (2013). Geology and mineral deposits of the 1.1 Ga Midcontinent Rift in the Lake Superior region—An overview. Field guide to the copper-nickel-platinum group element deposits of the Lake Superior Region. Edited by Miller, J. Precambrian Research Center Guidebook, 13(01), pp. 1-49.

Morey, G. B., & Green, J. C. (1982). 3: Status of the Keweenawan as a stratigraphic unit in the Lake Superior Region. Geological Society of America Memoirs. pp. 15–26.

Mungall, J. E. (2002). Kinetic controls on the partitioning of trace elements between silicate and sulfide liquids. Journal of Petrology, 43(5), pp. 749–768.

Mungall, J.E., (2014). 13.8 Geochemistry of Magmatic Ore Deposits. In practice, 1, pp.195-218.

Mvodo, H., Ganno, S., Kouankap Nono, G. D., Fossi, D. H., Nga Essomba, P. E., Nzepang Tankwa, M., & Nzenti, J. P. (2022). Petrogenesis, LA-ICP-MS Zircon U-Pb geochronology and geodynamic implications of the Kribi Metavolcanic Rocks, Nyong Group, Congo Craton. Acta Geochimica, 41(3), pp. 470–495.

Naldrett, A. J. (2004). Magmatic sulfide deposits: geology, geochemistry, and exploration. Springer Science & Business Media. pp. 1-232.

Naldrett, A. J. (1997). Key factors in the genesis of Noril'sk, Sudbury, Jinchuan, Voisey's Bay and other world-class Ni-Cu-PGE deposits: Implications for exploration. Australian Journal of Earth Sciences, pp. 283-315.

Nicholson, S.W., & Shirey, S.B., (1990). Midcontinent rift volcanism in the Lake Superior region: Sr, Nd, and Pb isotopic evidence for a mantle plume origin. Journal of Geophysical Research: Solid Earth, 95(B7), pp.10851-10868.

Ojakangas, R. W., Morey, G. B., & Green, J. C. (2001). The Mesoproterozoic Midcontinent Rift System, Lake Superior region, USA. Sedimentary Geology, 141-142, pp. 421–442.

O'Brien, S. (2018). Petrology of the Crystal Lake Gabbro and the Mount Mollie Dyke, Midcontinent Rift, Northwest Ontario, Thunder Bay, Ontario]: Lakehead University, 364p.

Pearce, J. A. (2008). Geochemical fingerprinting of Oceanic Basalts with applications to ophiolite classification and the search for Archean oceanic crust. Lithos, 100(1-4), pp. 14–48.

Paces, J. B., & Miller, J. D. (1993). Precise U-PB ages of Duluth Complex and related mafic intrusions, northeastern Minnesota: Geochronological Insights to physical, petrogenetic, paleomagnetic, and tectonomagmatic processes associated with the 1.1 ga midcontinent rift system. Journal of Geophysical Research: Solid Earth, 98(B8), pp. 13997–14013.

Percival, J. A., & Williams, H. R. (1989). Late Archean Quetico accretionary complex, Superior Province, Canada. Geology, 17(1), pp. 23-25.

Percival, J., Sanborn-Barrie, M., Skulski, T., Stott, G., Helmstaedt, H. and White, D. (2006) Tectonic evolution of the western Superior Province from NATMAP and Lithoprobe studies. Canadian Journal of Earth Sciences 43, pp. 1085-1117.

Percival, J., (2007). Geology & Metallogeny of the Superior Province, Canada. In Goodfellow, w., ed., Mineral Deposits of Canada: A Synthesis of Major Deposit Types, District Metallogeny, the Evolution of Geological Provinces, and Exploration Methods: Geological Association of Canada, Mineral Deposits Division, Special Publication No. 5, pp. 903-928.

Poulton, S. W., Fralick, P. W., & Canfield, D. E. (2004). The transition to a sulphidic ocean ∼ 1.84 billion years ago. Nature, 431(7005), pp. 173–177.

Puchalski, R., 2010. The petrography and geochemistry of the Riverdale sill. H.B.Sc. thesis, Lakehead University, Thunder Bay, ON. pp. 1-65.

Ripley, E. M., Dong, S., Li, C., & Wasylenki, L. E. (2015). Cu isotope variations between conduit and sheet-style Ni–Cu–PGE sulfide mineralization in the Midcontinent Rift System, North America. Chemical Geology, pp. 414, 59-68.

Ripley, E. M. (2014). Ni-cu-PGE mineralization in the Partridge River, South Kawishiwi, and Eagle Intrusions: A review of contrasting styles of sulfide-rich occurrences in the Midcontinent Rift System. Economic Geology, 109(2), pp. 309–324.

Ripley, E. M., & Li, C. (2011). A review of Conduit-related Ni-cu-(PGE) sulfide mineralization at the Voisey's Bay Deposit, Labrador, and the Eagle Deposit, Northern Michigan. Magmatic Ni-Cu and PGE Deposits Geology, Geochemistry, and Genesis. pp. 181-197.

Rogala, B., Fralick, P. W., Heaman, L. M., & Metsaranta, R. (2007). Lithostratigraphy and chemostratigraphy of the Mesoproterozoic Sibley Group, Northwestern Ontario, Canada. Canadian Journal of Earth Sciences, 44(8), pp. 1131–1149.

Rooney, T. O., Konter, J. G., Finlayson, V. A., LaVigne, A., Brown, E. L., Stein, C. A., Stein, S., & Moucha, R. (2022). Constraining the isotopic endmembers contributing to 1.1 ga keweenawan large Igneous Province magmatism. Contributions to Mineralogy and Petrology, 177(4), pp. (1-49).

Samalens, N., Barnes, S.-J., & Sawyer, E. W. (2017). The role of black shales as a source of sulfur and semimetals in magmatic nickel-copper deposits: Example from the Partridge River Intrusion, Duluth Complex, Minnesota, USA. Ore Geology Reviews, 81, pp. 173–187.

Scoates. R.F.J. & Heggie, G.J, (2011), Dynamic textures, fabrics and lithogeochemistry, TBN, Ontario. Internal report to Magma Metals (Canada) LTD. pp. 1-27.

Setterfield, T., and Gilman, T., (2009), Report on 2008 Exploration by Mega Uranium LTD. On the Greenwich Lake property, Greenwich Lake area, NTS map sheet 52A/15, Northwestern, Ontario.

Shirey, S. B., klewin, K. W., Berg, J. H., & Carlson, R. W. (1994). Temporal changes in the sources of flood basalts: Isotopic and trace element evidence from the 1100 ma old keweenawan Mamainse point formation, Ontario, Canada. Geochimica Et Cosmochimica Acta, 58(20), pp. 4475–4490.

Song, X.-Y., Keays, R. R., Xiao, L., Qi, H.-W., & Ihlenfeld, C. (2009). Platinum-group element geochemistry of the continental flood basalts in the Central Emeisihan Large Igneous Province, SW China. Chemical Geology, 262(3-4), pp. 246–261.

Song, X., Wang, Y., & Chen, L. (2011). Magmatic Ni-Cu-PGE deposits in magma plumbing systems: Features, formation, and exploration. Geoscience Frontiers, 2(3), pp. 375–384.

Stott, G., Corkery, M., Percival, J., Simard, M. and Goutier, J. (2010). A revised terrane subdivision of the Superior Province. Ontario Geological Survey, Open File Report 6260. pp. 20-21.

Stacey, J.S. and Kramers, J.D., (1975). Approximation of terrestrial lead isotope evolution by a two-stage model. Earth and Planetary Science Letters 26, pp. 207-221.

Sun, S.-s., & McDonough, W. F. (1989). Chemical and isotopic systematics of oceanic basalts: Implications for mantle composition and Processes. Geological Society, London, Special Publications, 42(1), pp. 313–345.

Swanson-Hysell, N. L., Hoaglund, S. A., Crowley, J. L., Schmitz, M. D., Zhang, Y., & Miller, J. D. (2020). Rapid emplacement of massive Duluth Complex intrusions within the North American Midcontinent Rift. Geology, 49(2), pp. 185–189.

Tanaka, T., Togashi, S., Kamioka, H., Amakawa, H., Kagami, H., Hamamoto, T., ... & Dragusanu, C. (2000). JNdi-1: a neodymium isotopic reference in consistency with LaJolla neodymium. Chemical Geology, 168(3-4), pp. 279-281.

Terekhov, E.N. & Shcherbakova, T.F., (2006). Genesis of positive Eu anomalies in acid rocks from the Eastern Baltic Shield. Geochemistry International, 44, pp.439-455.

Thomas, D.G., Melnyk, J., Gormely, L., Searston, S., Kulia, G. 2009: Magma Metals Limited, Thunder Bay North Polymetallic Project Ontario, Canada, NI 43-101 Technical Report on Preliminary Assessment, pp. 1-127.

Todt, W., Cliff, R.A., Hanser,A., Hofmann, A.W., (1996), Evaluation of a 202Pb – 205Pb Double Spike for High - Precision Lead Isotope Analysis, Earth Processes: Reading the Isotopic Code Geophysical Monograph 95, the American Geophysical Union. 95, pp. 429-437.

Trevisan, B. E. (2015). The petrology, mineralization, and regional context of the Thunder mafic to ultramafic intrusion, Midcontinent Rift, Thunder Bay, Ontario (Master dissertation). pp.

Walker, J.A., Gmitro, T.T. and Berg, J.H., (2002). Chemostratigraphy of the Neoproterozoic Alona Bay lavas, Ontario. Canadian Journal of Earth Sciences, 39(7), pp.1127-1142.

Wang, S., Kuzmich, B., Hollings, P., Zhou, T., & Wang, F. (2020). Petrogenesis of the Dog Lake Granite Chain, Quetico Basin , Superior Province, Canada: Implications for Neoarchean crustal growth. Precambrian Research. pp. 346, 105828.

Williams, H.R., Stott, G.M., Heather, K.B., Muir, T.L. and Sage, R.P. (1991). Wawa Subprovince. In: Geology of Ontario, Ontario Geological Survey, Special Volume 4, Part I. pp. 485-539.

Williams, H.R., 1990. Quetico Subprovince. In: Geology of Ontario, Ontario Geological Survey, Special Volume 4, Part I. pp. 383-409.

Winter, B. L., & Knauth, L. P. (1992). Stable isotope geochemistry of early Proterozoic carbonate concretions in the Animikie Group of the Lake Superior region: Evidence for anaerobic bacterial processes. Precambrian Research, 54(2-4), pp. 131–151.

Wood, B. J., Wade, J., & Kilburn, M. R. (2008). Core formation and the oxidation state of the earth: Additional constraints from Nb, V and CR partitioning. Geochimica Et Cosmochimica Acta, 72(5), pp. 1415–1426.

York, D., 1969. Least-squares fitting of a straight line with correlated errors. Earth and Planetary Science Letters 5, pp. 320-324.

Zhou, M. E. I.-F. U., Robinson, P. A. U. L. T., Lesher, C. M. I. C. H. A. E. L., KEAYS, R. E. I. D. R., Zhang, C. H. E. N. G.-J. I. A. N. G., & Malpas, J. O. H. N. (2005). Geochemistry, petrogenesis and metallogenies of the Panzhihua gabbroic layered intrusion and associated Fe–Ti–v oxide deposits, Sichuan Province, SW China. Journal of Petrology, 46(11), pp. 2253–2280.

Appendix A

Sample descriptions

Abbreviations:

WR: Whole rock analysis

T.S: Polished thin section

G: Geochronology sample.

Sample ID	Intrusion Name	Hole ID	From (m)	To (m)	Lithology	Analysis type
CAM-021-KY-001	Lone Island	LIL 08-01	18.75	19.05	Gabbro	W.R + T.S
CAM-021-KY-002	Lone Island	LIL 08-01	22.49	22.63	Gabbro	W.R + T.S
CAM-021-KY-003	Lone Island	LIL 08-01	40	40.31	Gabbro	W.R + T.S
CAM-021-KY-004	Lone Island	LIL 08-01	45	45.36	Gabbro	W.R + T.S
CAM-021-KY-005	Lone Island	LIL 08-01	51.4	51.75	Gabbro	W.R + T.S
CAM-021-KY-006	Lone Island	LIL 08-01	60.10	60.60	Gabbro	W.R + T.S+G
CAM-021-KY-007	Lone Island	LIL 08-01	92.63	93	Gabbro	W.R + T.S
CAM-021-KY-008	Lone Island	LIL 08-01	153.9	154.43	Gabbro	W.R + T.S
CAM-021-KY-009	Lone Island	LIL 08-01	193.73	194.01	Gabbro	W.R + T.S
CAM-021-KY-010	Lone Island	LIL 08-01	217.12	217.33	Gabbro	W.R + T.S
CAM-021-KY-011	Lone Island	LIL 08-02	62.87	63.86	Gabbro	W.R + T.S
CAM-021-KY-012	Lone Island	LIL 08-02	63.36	63.86	Gabbro	W.R + T.S
CAM-021-KY-013	Lone Island	LIL 08-02	66.9	67.47	Intrusive breccia	W.R + T.S
CAM-021-KY-014	Lone Island	LIL 08-03	202	202.4	Granitoid	W.R + T.S
CAM-021-KY-015	Lone Island	LIL 08-03	172.22	172.65	Granitoid	W.R + T.S
CAM-021-KY-016	Lone Island	LIL 08-03	153.51	153.85	Gabbro	W.R + T.S
CAM-021-KY-038	Lone Island	LIL 08-03	10.9	11.5	Gabbro	W.R + T.S
CAM-021-KY-039	Lone Island	LIL 08-03	15.18	15.6	Gabbro	W.R + T.S
CAM-021-KY-040	Lone Island	LIL 08-03	15	15.18	Gabbro	W.R + T.S
CAM-021-KY-041	Lone Island	LIL 08-03	14.7	15.13	Gabbro	G
CAM-021-KY-042	Lone Island	LIL 08-03	83.4	83.7	Gabbro	W.R + T.S
CAM-021-KY-043	Lone Island	LIL 08-03	221.49	222	Gabbro	W.R + T.S
CAM-021-KY-044	Lone Island	LIL 08-04	19.72	20	Gabbro	W.R + T.S
CAM-021-KY-045	Lone Island	LIL 08-04	93	93.5	Gabbro	W.R + T.S
CAM-021-KY-046	Lone Island	LIL 08-04	169	169.3	Gabbro	W.R + T.S
CAM-021-KY-047	Lone Island	LIL 08-04	172.85	173.85	Gabbro	W.R + T.S
CAM-021-KY-048	Lone Island	LIL 08-04	206.2	206.5	Gabbro	W.R + T.S
CAM-021-KY-049	Lone Island	LIL 08-04	240.5	240.86	Gabbro	W.R + T.S
CAM-021-KY-050	Lone Island	LIL 08-04	321.2	321.4	Gabbro	W.R + T.S
CAM-021-KY-051	Lone Island	LIL 08-05	87.77	88.27	Gabbro	W.R + T.S
CAM-021-KY-052	Lone Island	LIL 08-05	133.4	133.78	Gabbro	W.R + T.S
CAM-021-KY-053	Lone Island	LIL 08-05	382.29	382.63	Gabbro	W.R + T.S
CAM-021-KY-054	Lone Island	LIL 08-07	78	78.7	Gabbro	W.R + T.S
CAM-021-KY-055	Lone Island	LIL 08-07	141	141.8	Gabbro	T.S + G
CAM-021-KY-056	Lone Island	LIL 08-07	150	150.51	Gabbro	W.R + T.S
CAM-021-KY-057	Lone Island	LIL 08-07	201	201.33	Gabbro	W.R + T.S
CAM-021-KY-058	Lone Island	LIL 08-07	360.9	360.96	Gabbro	T.S
CAM-021-KY-059	Lone Island	LIL 08-03	79.1	79.78	Gabbro	T.S + G
CAM-021-KY-060	Lone Island	LIL 08-05	138	138.67	Gabbro	T.S + G
CAM-021-KY-018	SEA	SEA 08-02	265.23	265.85	Sedimentary	WR
CAM-021-KY-019	SEA	SEA 08-02	176.87	177	Granitoid	WR
CAM-021-KY-020	SEA	SEA 08-02	189	189.27	Mafic	WR + T.S

Sample ID	Intrusion Name	Hole ID	From (m)	To (m)	Lithology	Analysis type
CAM-021-KY-022	SEA	SEA 08-02	195.13	195.28	Granitoid	WR
CAM-021-KY-023A	SEA	SEA 08-02	200.05	200.43	Mafic	WR + T.S
CAM-021-KY-023B	SEA	SEA 08-02	2001	2001.1	Mafic	WR + T.S
CAM-021-KY-024	SEA	SEA 08-05	144.58	144.8	Sedimentary	WR
CAM-021-KY-025	SEA	SEA 08-05	149.55	150	Mafic	WR
CAM-021-KY-026	SEA	SEA 08-05	147.65	175.05	Mafic	WR + T.S
CAM-021-KY-027	SEA	SEA 08-06	247.67	248	Sedimentary	WR + T.S
CAM-021-KY-028	SEA	SEA 08-06	556	556.46	Mafic	WR + T.S
CAM-021-KY-108	SEA	SEA 08-01	684.8	685.4	Gabbro	T.S + G
CAM-021-KY-109	SEA	SEA 08-01	878.4	879	Gabbro	T.S + G
CAM-021-KY-110	SEA	SEA 08-01	880	880.8	Gabbro	T.S + G
CAM-021-KY-029	EWC	EWC 10-02	71.34	71.52	Gabbro	WR + T.S
CAM-021-KY-030	EWC	EWC 10-02	73.20	73.6	Gabbro	WR + T.S
CAM-021-KY-031	EWC	EWC 10-04	114	114.34	Gabbro	WR + T.S
CAM-021-KY-032	EWC	EWC 10-04	114.59	144.99	Gabbro	WR + T.S
CAM-021-KY-033	EWC	EWC 10-04	115.35	115.75	Gabbro	WR + T.S
CAM-021-KY-035	EWC	EWC 10-06	149.55	150	Mafic	WR + T.S
CAM-021-KY-036	EWC	EWC 10-06	154.9	155.31	Mafic	WR + T.S
CAM-021-KY-037	EWC	EWC 10-07	19.4	19.71	Mafic	WR + T.S
CAM-021-KY-061	EWC	EWC 10-01	50	50.5	Gabbro	T.S + G
CAM-021-KY-069	Greenwich	GL11-02	175.15	175.82	Mafic	WR + T.S
CAM-021-KY-070	Greenwich	GL11-02	175.4	175.9	Gabbro	WR + T.S
CAM-021-KY-071	Greenwich	GL11-02	134	134.5	Gabbro	WR + T.S
CAM-021-KY-072	Greenwich	GL11-03	67.26	68	Mafic	WR + T.S
CAM-021-KY-073	Greenwich	GL11-03	71.1	71.4	Mafic	WR + T.S
CAM-021-KY-074	Greenwich	GL10-04	2	2.5	Mafic	WR + T.S
CAM-021-KY-075	Greenwich	GL10-04	203.35	203.7	Mafic	WR + T.S
CAM-021-KY-076	Greenwich	GL10-04	237.7	237.8	Mafic	WR + T.S
CAM-021-KY-077	Greenwich	GL10-05	125	125.5	Gabbro	WR + T.S
CAM-021-KY-078	Greenwich	GL10-05	128.57	129	Gabbro	WR + T.S
CAM-021-KY-79	Greenwich	GL10-07	123	123.5	Mafic	WR + T.S
CAM-021-KY-080	Greenwich	GL10-08	1	1.5	Gabbro	WR + T.S
CAM-021-KY-081	Greenwich	GL10-08	3.6	4	Gabbro	WR + T.S
CAM-021-KY-082	Greenwich	GL10-08	119	119.53	Gabbro	WR + T.S
CAM-021-KY-083	Greenwich	GL10-08	119.55	120	Gabbro	WR + T.S
CAM-021-KY-084	Greenwich	GL10-08	143.85	144.13	Gabbro	WR + T.S
CAM-021-KY-085	Greenwich	GL10-08	145	145.5	Gabbro	WR + T.S
CAM-021-KY-086	Greenwich	GL10-02	37.6	38.2	Gabbro	WR + T.S
CAM-021-KY-087	Greenwich	GL10-03	34	34.55	Mafic	WR + T.S
CAM-021-KY-088	Greenwich	GL10-03	49.15	50.45	Mafic	WR + T.S
CAM-021-KY-089	Greenwich	GL10-03	124.7	125	Mafic	WR + T.S
CAM-021-KY-090	Greenwich	GL10-03	178.5	179	Gabbro	WR + T.S
CAM-021-KY-091	Greenwich	GL10-03	179.6	180	Mafic	WR + T.S
CAM-021-KY-092	Greenwich	GL10-03	193.5	194	Mafic	WR + T.S

Sample ID	Intrusion Name	Hole ID	From (m)	To (m)	Lithology	Analysis type
CAM-021-KY-093	025	115TB0001	0.5	1.04	Gabbro	WR + T.S
CAM-021-KY-094	025	115TB0001	9	9.56	Peridotite	WR + T.S
CAM-021-KY-095	025	115TB0001	27	27.7	Peridotite	WR + T.S
CAM-021-KY-096	025	115TB0001	40.14	40.36	Peridotite	T.S
CAM-021-KY-097	025	115TB0001	188.46	188.9	Mafic	WR + T.S
CAM-021-KY-098	025	115TB0001	201	201.55	Granitoid	WR + T.S
CAM-021-KY-099	025	115TB0003	9	9.65	Peridotite	WR + T.S
CAM-021-KY-100	025	115TB0003	86.54	87	Granitoid	WR + T.S
CAM-021-KY-101	025	115TB0003	90	90.41	Granitoid	WR + T.S
CAM-021-KY-102	025	115TB0003	109	109.41	Granitoid	WR + T.S
CAM-021-KY-103	025	115TB0003	116	116.41	Granitoid	WR + T.S
CAM-021-KY-104	025	115TB0003	114.51	114.73	Granitoid	T.S
CAM-021-KY-105	025	115TB0003	141	141.72	Mafic	WR + T.S
CAM-021-KY-106	025	115TB0003	207	207.6	Mafic	WR + T.S
CAM-021-KY-107	025	115TB0003	213	213.68	Peridotite	WR + T.S

Sample ID	Intrusion Name	Hole ID	UTM (N)	16U (E)	Lithology	Analysis type
CAM-021-KY-062	025	Surface	5407690	0354986	Gabbro	WR + T.S
CAM-021-KY-063	025	Surface	5407647	0355024	Gabbro	WR + T.S
CAM-021-KY-064	025	Surface	5407459	0354997	Gabbro	WR+T.S+G
CAM-021-KY-065	025	Surface	5407105	0355789	Peridotite	WR + T.S
CAM-021-KY-066	025	Surface	5407053	0355735	Gabbro	WR + T.S
CAM-021-KY-067	025	Surface	5407500	0355976	Gabbro	WR + T.S
CAM-021-KY-068	025	Surface	5407176	0356381	Gabbro	WR + T.S

Appendix B

Petrographic descriptions

Lone Island Intrusion

Sample ID	Depth (m)	Grainsize	Modal percent of mineral						Alteration					Other minerals	Opaque minerals	Texture	Clean Air Metals code	IUGS Name
			Plagioclase	Amphibole	Clinopyroxen	Orthopyroxe	Olivine	Biotite	Sericite	Chlorite	Carbonates	Hematite	Serpentine					
CAM-021-KY-001	18.75	c	45	2	12	3	1	1	24	2	0	5	1	1	5	Subophitic	Mg	**Orthopyroxene gabbro**
Description	Strongly sericitized, subophitic, coarse-grained Pl with medium-to coarse-grained Cpx, Opx, Bt, rare Ol, and moderately hematized, subhedral, medium-to fine-grained Mag, Ilm lamellae, and rare fine-grained of Cpy with very-fine-grained inclusions of Sp and Cct.																	
CAM-021-KY-002	22.94	c	45	4	16	1	1	2	20	1	4	0	1	1	4	Subophitic	Md	**Orthopyroxene gabbro**
Description	Strongly sericitized, subophitic, coarse-grained Pl intergrew with Cpx. A fine-grained, anhedral xenolith was found in this thin section, comprises Pl, Cpx, and some Qz, Py, and Cpy.																	
CAM-021-KY-003	40	c	50	3	10	2	1	2	20	2	2	1	0	0	9	Ophitic	Mgm	**Orthopyroxene gabbro**
Description	Moderately sericitized, ophitic, medium-to fine-grained plagioclase with Cpx, Opx , Bt, Chl, Cpx, and strongly hematized, medium-grained Mag with Ilm exsolution and fine-grained blebs of Cpy.																	
CAM-021-KY-004	45	c	50	2	15	3	1	4	10	1	7	2	0	1	8	Subophitic	Md	**Orthopyroxene gabbro**
Description	Weakly sericitized, coarse-grained, subophitic, plagioclase with medium-to fine-grained Cpx, Opx and Bio altering to Chl, and fine-grained subhedral Po with fine-to very-fine Cpy blebs.																	
CAM-021-KY-005	51.4	c	50	2	15	3	3	1	15	1	2	1	0	1	6	Subophitic	Md	**Orthopyroxene gabbro**
Description	Strongly sericitized, subophitic, coarse-grained plagioclase intergrew with Opx, and fine-to medium-grained Cpx. Po is present as an anhedral, fine-grains with rare very-fine-grained Cpy blebs. The thin section is crosscut by a fine-grained-mafic-vein.																	
CAM-021-KY-007	92.63	m	60	0	12	4	1	1	15	1	0	1	1	0	4	Subophitic	Md	**Orthopyroxene gabbro**
Description	Strongly sericitized, subophitic, medium-grained plagioclase with medium-to fine-grained Cpx and Opx . Anhedral, fine-grained-Po with rare very fine-grained Cpy blebs are present.																	

Sample ID	Depth (m)	Grainsize	Modal percent of mineral						Alteration					Other minerals	Opaque minerals	Texture	Clean Air Metals code	IUGS Name
			Plagioclase	Amphibole	Clinopyroxene	Orthopyroxene	Olivine	Biotite	Sericite	Chlorite	Carbonates	Hematite	Serpentine					
CAM-021-KY-008	153.9	F	50	0	30	4	0	4	6	2	0	2	0	0	2	Subophitic + poikilitic	M	**Orthopyroxene gabbro**
Description	Moderately saussuritized, subophitic, medium-grained Pl with medium-to fine-grained Cpx and some Opx, and anhedral, fine-grained-Po with rare very fine-grained Cpy blebs.																	
CAM-021-KY-009	193.7	M	50	0	30	4	0	4	6	2	0	2	0	0	2	Subophitic + poikilitic	M	**Orthopyroxene gabbro**
Description	Moderately sericitized and saussuritized, subophitic, medium-grained Pl with medium-to fine-grained Cpx and some Opx . Anhedral, fine-grained-Po with rare very fine-grained Cpy blebs are present.																	
CAM-021-KY-010	217.1	M	55	2	16	2	16	2	2	1	2	1	0	0	>1	Subophitic	Hr	**Orthopyroxene gabbro**
Description	Strongly hematized, subophitic, coarse-grained Pl with medium-grained Cpx and Opx, and Mag altered to hematite.																	
CAM-021-KY-011	62.87	C	5	1	16	1	16	1	20	10	3	10	15	0	0	Poikilitic	Upd	**Wehrlite**
Description	Strongly serpentinized, chloritized, and sericitized poikilitic coarse to medium olivine and pyroxene grains.																	
CAM-021-KY-012	63.36	C	30	1	20	5	0	5	12	10	0	3	10	0	2	Poikilitic	Mg	**Orthopyroxene gabbro**
Description	Strongly serpentinized, chloritized, and sericitized poikilitic, subhedral-to euhedral, coarse-to medium Cpx with Opx, Bt, and strongly sericitized and serpentinized, anhedral, interstitial, coarse-to very-coarse-grained plagioclase. Biotite mostly grows at the rims of Cpx and Opx. Opx intergrown with Cpx. Fine subhedral grains of Mg with very-to fine rare anhedral Po, Py and very rare Cpy.																	
CAM-021-KY-013	66.9	M	55	1	6	1	6	1	1	12	5	1	3	0	10	Lineation	Zib	**Gneiss**
Description	Moderately altered medium grained of plagioclase with lineation and grainsize reduction with sulphide veins.																	
CAM-021-KY-014	202	C	60	1	15	3	1	2	3	7	0	2	5	0	3	Poikilitic	Mg	**Orthopyroxene gabbro**
Description	Weakly sericitized, interstitial, coarse-grained Pl with oikocrysts of weakly serpentinized fine-to medium-grained Cpx and Opx and weakly chloritized biotite. A vein of sulphides injected in the silicates with euhedral Py intergrew with Cpy. Py grain boundaries are replaced by silicate minerals, and some coarser grains of Py are overgrown on a Cpy groundmass.																	

Sample ID	Depth (m)	Grainsize	Modal percent of mineral						Alteration					Other minerals	Opaque minerals	Texture	Clean Air Metals code	IUGS Name
			Plagioclase	Amphibole	Clinopyroxene	Orthopyroxene	Olivine	Biotite	Sericite	Chlorite	Carbonates	Hematite	Serpentine					
CAM-021-KY-015	172.2	C	42	0	10	25	0	2	15	0	0	1	1	1	3	Poikilitic	Mg	**Gabbronorite**
Description	Moderately sericitized, poikilitic, subhedral-to anhedral, coarse-grained Pl with oikocrysts of weakly serpentinized fine-to medium grained Cpx and Opx and weakly chloritized biotite, and fine-to medium-grained, anhedral Po with very fine-grained Cpy.																	
CAM-021-KY-016	153.5	M	40	0	20	17	0	2	15	1	0	0	1	1	3	Poikilitic	Mg	**Gabbronorite**
Description	Moderately sericitized, poikilitic, subhedral-to anhedral, coarse-grained Pl with oikocrysts of weakly serpentinized fine-to medium grained Cpx and Opx with weakly chloritized biotite, and fine-to medium-grained, anhedral Po and Mag with very-fine-grained Cpy.																	
CAM-021-KY-038	10.9	M	47	0	25	10	0	2	10	0	0	0	1	1	4	Subophitic	Md	**Gabbronorite**
Description	Weakly sericitized, poikilitic, coarse-grained Pl crystals with oikocrysts of weakly serpentinized fine-to medium grained Cpx and Opx with weakly chloritized biotite, and fine-to medium-grained, anhedral Po and Mag with very fine-grained Cpy blebs.																	
CAM-021-KY-039	15.18	M	47	0	25	10	0	2	10	0	0	0	1	1	4	Subophitic	Md	**Gabbronorite**
Description	Weakly sericitized, poikilitic, coarse-grained Pl crystals with oikocrysts of weakly serpentinized fine-to medium grained Cpx and Opx and weakly chloritized biotite, and fine-to medium-grained, anhedral Po and Mag with very fine-grained Cpy blebs.																	
CAM-021-KY-040	15	M	47	0	25	9	0	2	10	1	0	2	1	1	2	Subophitic	Md	**Gabbronorite**
Description	Weakly sericitized, poikilitic, coarse-grained Pl with oikocrysts of weakly serpentinized fine-to medium grained Cpx and Opx, and weakly chloritized biotite, and fine-to medium-grained, anhedral Po and Mag with very fine-grained Cpy blebs.																	
CAM-021-KY-041	14.7	M	35	0	15	7	0	10	10	2	0	1	1	1	3	Subophitic+ poikilitic	Md	**Gabbronorite**
Description	Weakly sericitized, poikilitic, coarse-grained Pl crystals with oikocrysts of weakly serpentinized fine-to medium grained Cpx and Opx, and weakly chloritized biotite, and fine-to medium-grained, anhedral Po and Mag with very fine-grained Cpy blebs.																	
CAM-021-KY-042	83.4	M	35	0	15	7	0	10	10	2	0	1	1	1	3	Subophitic+ poikilitic	Md	**Gabbronorite**
Description	Weakly sericitized, poikilitic, coarse-to coarse-grained Pl with oikocrysts of weakly serpentinized, fine-to medium grained Cpx and Opx, weakly chloritized biotite, and fine-to medium-grained, anhedral Po and Mag with very fine-grained Cpy blebs.																	

Sample ID	Depth (m)	Grainsize	Modal percent of mineral						Alteration					Other minerals	Opaque minerals	Texture	Clean Air Metals code	IUGS Name
			Plagioclase	Amphibole	Clinopyroxene	Orthopyroxene	Olivine	Biotite	Sericite	Chlorite	Carbonates	Hematite	Serpentine					
CAM-021-KY-043	221.5	m	30	0	10	4	0	3	40	3	0	1	5	1	3	Poikilitic	Mg	**Gabbronorite**
Description	Strongly sericitized, medium-grained, poikilitic Pl with moderately sericitized and serpentinized medium-to fine-grained Cpx and Opx, and anhedral, medium-to fine-grained-Po and Mag with Ilm exsolution lamellae, and rare very fine-grained Cpy blebs.																	
CAM-021-KY-044	19.72	m	40	1	10	3	0	1	27	1	0	1	10	1	5	Subophitic+ poikilitic	Md	**Gabbronorite**
Description	Strongly sericitized, medium-grained, subophitic poikilitic Pl with moderately sericitized and serpentinized medium-to fine-grained Cpx and Opx, and anhedral, medium-to fine-grained-Po and Mag with rare very fine-grained Cpy and some Cpx is altered to Hbl.																	
CAM-021-KY-045	93	m	55	1	10	5	0	5	14	1	0	1	5	1	5	Subophitic+ poikilitic	Md	**Gabbronorite**
Description	Strongly sericitized, medium-grained, subophitic-to poikilitic Pl with moderately sericitized and serpentinized medium-to fine-grained Cpx and Opx, and anhedral, medium-to fine-grained-Po and Mag with rare very fine-grained Cpy and some Cpx is altered to Hbl.																	
CAM-021-KY-046	169	m	30	2	15	4	0	1	35	1	0	1	5	1	4	Poikilitic	M	**Orthopyroxene gabbro**
Description	Pervasively sericitized, medium-grained, subophitic-to poikilitic Pl with moderately sericitized and serpentinized medium-to fine-grained Cpx and Opx, and anhedral, medium-to fine-grained Po and Mag with rare very fine-grained Cpy.																	
CAM-021-KY-047	172.9	c	30	1	10	4	0	6	20	1	0	1	5	1	4	Subophitic+ poikilitic	Md	**Gabbronorite**
Description	Moderately sericitized, medium-grained, subophitic-to poikilitic Pl with moderately sericitized and serpentinized medium-to fine-grained Cpx and Opx, and anhedral, medium-to fine-grained Po and Mag with rare very fine-grained Cpy.																	
CAM-021-KY-048	206.2	m	10	1	10	4	0	6	43	1	0	1	5	3	4	Poikilitic	Md	**Gabbronorite**
Description	Strongly sericitized, medium-grained, subophitic-to poikilitic Pl with moderately sericitized and serpentinized medium-to fine-grained Cpx and Opx, and anhedral, medium-to fine-grained Po and Mag with rare very fine-grained Cpy.																	
CAM-021-KY-049	240.5	m	10	1	10	4	0	6	43	1	0	1	5	3	4	Poikilitic	Md	**Gabbronorite**
Description	Strongly sericitized, medium-grained, subophitic-to poikilitic Pl with moderately sericitized and serpentinized medium-to fine-grained Cpx and Opx, and anhedral, medium-to fine-grained Po and Mag with rare very fine-grained Cpy.																	

Sample ID	Depth (m)	Grainsize	Modal percent of mineral						Alteration					Other minerals	Opaque minerals	Texture	Clean Air Metals code	IUGS Name
			Plagioclase	Amphibole	Clinopyroxene	Orthopyroxene	Olivine	Biotite	Sericite	Chlorite	Carbonates	Hematite	Serpentine					
CAM-021-KY-051	87.77	m	60	0	10	15	0	2	2	2	0	1	1	4	3	Poikilitic+ interstitial	Mg	**Gabbronorite**
Description	Strongly sericitized, interstitial, anhedral, medium-to coarse-grained Pl, and weakly sericitized and serpentinized, anhedral, fine-grained Opx and lesser Cpx with fine grained Po and hematized Mag.																	
CAM-021-KY-052	133.4	m	40	1	15	15	0	10	5	2	0	2	5	0	5	Poikilitic	Mg	**Gabbronorite**
Description	Weakly sericitized, interstitial, coarse-grained Pl crystals, and oikocrysts of weakly serpentinized fine-to medium-grained Cpx and Opx with weakly chloritized Bt and medium-grained, subhedral Mag altered to Hem and intergrown with Po.																	
CAM-021-KY-053	382.29	m	25	0	35	30	0	1	5	0	0	0	1	0	3	Poikilitic	Mg	**Gabbronorite**
Description	Weakly sericitized, interstitial, medium-grained, anhedral-to subhedral plagioclase with fine to medium poikilitic weakly serpentinized anhedral Cpx and Opx and some Bt, and fine-grained, anhedral Po with very-fine-grained Cpy.																	
CAM-021-KY-054	78	m	30	1	20	10	1	1	24	2	0	1.5	4.5	2	3	Poikilitic	Mg	**Gabbronorite**
Description	Pervasively serpentinized and sericitized, subhedral, medium-grained Cpx and Opx with chloritized Bt, and pervasively sericitized coarse-to very coarse-grained, interstitial, anhedral Pl, and strongly hematized Mag with Ilm exsolution lamellae.																	
CAM-021-KY-055	141	c	5	1	28	3	2	3	40	1	0	10	1	1	5	Poikilitic+ interstitial	Mg	**Gabbronorite**
Description	Pervasively sericitized, coarse-to very-coarse-grained, subhedral prismatic plagioclase crystals with weakly sericitized, poikilitic coarse-grained, anhedral Cpx and some Opx. Strongly hematized, coarse-grained, anhedral-to subhedral Mag intergrown with Po.																	
CAM-021-KY-056	150	c	5	1	15	25	1	10	35	1	0	3.5	1	0	5	Poikilitic+ interstitial	Mg	**Gabbronorite**
Description	Pervasively sericitized, coarse-to very-coarse-grained, subhedral prismatic plagioclase crystals with weakly sericitized, poikilitic coarse-grained, anhedral Cpx and some Opx with strongly hematized, coarse-grained, anhedral-to subhedral Mag intergrown with Po.																	

Sample ID	Depth (m)	Grainsize	Modal percent of mineral						Alteration					Other minerals	Opaque minerals	Texture	Clean Air Metals code	IUGS Name
			Plagioclase	Amphibole	Clinopyroxene	Orthopyroxene	Olivine	Biotite	Sericite	Chlorite	Carbonates	Hematite	Serpentine					
CAM-021-KY-057	201	m	50	2	25	5	1	2	1	2	0	7	1	1	3	Subophitic+ poikilitic	Mg	**Orthopyroxene gabbro**
Description	Weakly sericitized, interstitial, prismatic, subhedral, medium grained Pl and weakly serpentinized, poikilitic, fine-to medium-grained, anhedral Cpx and rare Opx with strongly hematized, medium-grained, subhedral Mag intergrown with Po and rare Cpy.																	
CAM-021-KY-058	360.96	m	25	3	15	10	0	5	20	1	0	1	15	3	2	Poikilitic	Mg	**Gabbronorite**
Description	Pervasively serpentinized, poikilitic, coarse-to medium grained, anhedral Opx and Cpx with good abundance of biotite enclosed by strongly sericitized, coarse-to very coarse grained, anhedral interstitial Pl with fine-grained oxides and fine-grained Cpy.																	
CAM-021-KY-059	79.78	m	15	3	15	10	0	5	28	2	0	1	15	3	3	Subophitic+ poikilitic	Mg	**Gabbronorite**
Description	Pervasively serpentinized, subophitic, coarse-to medium grained, anhedral Opx and Cpx with good abundance of biotite enclosed by strongly sericitized, poikilitic, anhedral, interstitial, coarse-to very coarse grained Pl with fine-grained oxides and fine grained Cpy.																	
CAM-021-KY-060	138	m	10	3	7	15	0	5	40	1	0	4	15	3	2	Poikilitic	Hr	**Gabbronorite**
Description	Pervasively-to completely serpentinized, poikilitic, coarse-to medium grained, anhedral Opx and Cpx with good abundance of biotite enclosed by pervasively-to completely sericitized, coarse-to very coarse grained, anhedral interstitial plagioclase with fine grained oxides with and fine-grained Cpy.																	

SEA

Sample ID	Depth (m)	Grainsize	Modal percent of mineral						Alteration					Other minerals	Opaque minerals	Texture	Clean Air Metals code	IUGS Name
			Plagioclase	Amphibole	Clinopyroxene	Orthopyroxene	Olivine	Biotite	Sericite	Chlorite	Carbonates	Hematite	Serpentine					
CAM-021-KY-018	160	m	34	3	22	3	1	2	10	5	8	2	5	4	1	Ophitic	Md	**Orthopyroxene gabbro**
Description	Pervasively sericitized and serpentinized, fine-to medium grained Cpx and Opx filling the angular spaces between strongly sericitized, ophitic, medium-grained Pl laths, moderately chloritized Bt, and strongly hematized Mag with fine-grained Cpy blebs.																	
CAM-021-KY-023b	201	m	35	3	22	3	0	2	10	5	8	2	5	4	1	Ophitic	M	**Orthopyroxene gabbro**
Description	Pervasively sericitized and serpentinized, fine-to medium grained Cpx and Opx filling angular spaces between strongly sericitized, ophitic, medium-grained plagioclase laths, moderately chloritized Bt, and strongly hematized Mag with fine-grained Cpy blebs.																	
CAM-021-KY-108	684.8	m	60	0	20	1	0	2	5	3	1	2	4	1	1	Poikilitic	Hr	**Orthopyroxene gabbro**
Description	Pervasively sericitized, Poikilitic, medium-to coarse-grained, subhedral-to euhedral Pl oikocrysts with strongly serpentinized medium-to fine-grained Cpx, and moderately hematized, subhedral, medium-to fine Mag with Ilm inclusions and fine-grained Cpy.																	
CAM-021-KY-109	878.4	m	30	1	10	20	0	3	17	1	3	2	6	5	2	Poikilitic	Mgo	**Gabbronorite**
Description	Moderately sericitized, interstitial, medium-grained Pl and moderately serpentinized, subhedral oikocrysts of Cpx and Opx, and moderately hematized, subhedral, medium-to fine-grained Mag with Ilm inclusions, and fine-to medium blebs of Pn and rare Cpy.																	
CAM-021-KY-110	880	m	0	0	40	30	4	3	8	3	3	2	4	1	2	Poikilitic	Mgm	**Websterite**
Description	Pervasive serpentinized and sericitized, coarse-to very-coarse interstitial Cpx and Opx replacing strongly serpentinized and sericitized, medium-to coarse grained, anhedral oikocrysts of Cpx and coarse to very-coarse-grained Opx with fine-to medium-grained Mag and rare fine-grained Cpy.																	

The East-West Connector

Sample ID	Depth (m)	Grainsize	Modal percent of mineral						Alteration					Other minerals	Opaque minerals	Texture	Clean Air Metals code	IUGS Name
			Plagioclase	Amphibole	Clinopyroxene	Orthopyroxene	Olivine	Biotite	Sericite	Chlorite	Carbonates	Hematite	Serpentine					
CAM-021-KY-029	71.34	m	30	0	10	17	0	6	15	5	3	3.5	6	3	1.5	Subophitic	M	**Gabbronorite**
Description	Strongly serpentinized, anhedral, medium-grained Opx intergrown with strongly sericitized, medium-grained Pl, and very-fine-grained oxides and Cpy.																	
CAM-021-KY-030	73.2	f	18	1	6	3	0	1	50	5	3	1	6	3	3	Subophitic	M	**Gabbronorite**
Description	Strongly serpentinized, anhedral, medium-grained Opx intergrown with strongly sericitized, medium-grained Pl, and very-fine-grained oxides and Cpy.																	
CAM-021-KY-031	114	m	18	1	5	3	0	1	50	5	4	1	6	3	2	Subophitic	M	**Gabbronorite**
Description	Strongly serpentinized, anhedral, medium-grained Opx intergrown with strongly sericitized, medium-grained Pl. Opaque minerals are very-fine-grained oxides and Cpy with medium-to fine-grained Cbn intergrown with Cpy.																	
CAM-021-KY-032	114.6	f	10	1	5	3	0	1	60	5	3	1	6	4	2	Poikilitic+ Subophitic	M	**Gabbronorite**
Description	Pervasively sericitized, medium-grained Pl with pervasively serpentinized, poikilitic, anhedral, medium-grained Opx intergrown. Opaque minerals are very-fine-grained oxides and Cpy with medium-to fine-grained Cbn intergrown with Cpy.																	
CAM-021-KY-033	115.4	f	10	1	5	3	0	1	60	5	3	1	6	4	2	Poikilitic+ Subophitic	M	**Gabbronorite**
Description	Pervasively sericitized, medium-grained Pl with pervasively serpentinized, poikilitic, anhedral, medium-grained Opx intergrown, and very-fine-grained oxides and Cpy.																	
CAM-021-KY-034	120.7	f	10	1	5	3	0	1	60	5	3	1	6	4	2	Poikilitic+ Subophitic	M	**Gabbronorite**
Description	Pervasively sericitized, medium-grained Pl with pervasively serpentinized, poikilitic, anhedral, medium-grained Opx intergrown, and very-fine-grained oxides and Cpy.																	
CAM-021-KY-035	149.6	f	8	1	5	3	0	1	55	10	3	1	6	4	2	Poikilitic+ Subophitic	M	**Gabbronorite**
Description	Pervasively sericitized, medium-grained Pl with pervasively serpentinized, poikilitic, anhedral, medium-grained Opx intergrown, and very-fine-grained oxides, Cbn and Cpy.																	

The Greenwich intrusion

Sample ID	Depth (m)	Grainsize	Modal percent of mineral						Alteration					Other minerals	Opaque minerals	Texture	Clean Air Metals code	IUGS Name
			Plagioclase	Amphibole	Clinopyroxene	Orthopyroxene	Olivine	Biotite	Sericite	Chlorite	Carbonates	Hematite	Serpentine					
CAM-021-KY-069	175.2	m	8	0	7	7	0	2	30	2	10	1	30	1	1	Intergranular	M	**Gabbro**
Description	Pervasively serpentinized, anhedral to prismatic laths of medium grained Opx, carbonates and serpentinized Cpx with pervasively sericitized Pl, and rare Mag and fine-grained Cpy.																	
CAM-021-KY-070	175.4	f	5	0	4	1	0	1	35	0	10	0	40	3	1	Poikilitic	Mg	**Gabbro**
Description	Pervasively sericitized and serpentinized, poikilitic Cpx and Pl crystals with very fine-grained disseminated Cpy. Later veins of fine-to medium-grained carbonates, Ser, and Srp cross cut all the primary minerals.																	
CAM-021-KY-071	134	m	15	3	10	6	0	2	25	1	3	0	20	4	1	Ophitic	Mg	**Gabbro**
Description	Strongly sericitized Cpx and Opx enclosed by ophitic Pl laths with very fine-grained disseminated Cpy. A group of veins with 250µm width, zoned and comprise fine-to medium-grained carbonates layer and Srp layer with Ser.																	
CAM-021-KY-072	67.26	m	2	0	3	1	0	0	30	0	1	1	1	60	1	Ophitic	M	**Gabbro**
Description	Pervasively sericitized, prismatic, ophitic laths of Cpx and Opx enclosing a very-fine-grained groundmass with disseminated fine-to very-fine-grained Cpy and oxides.																	
CAM-021-KY-073	71.1	m	7	0	3	1	0	0	15	0	1	1	1	70	1	Ophitic	M	**Gabbro**
Description	Pervasively sericitized, prismatic, ophitic laths of Cpx and Opx enclosing a very-fine-grained groundmass with disseminated fine-to very-fine-grained Cpy and oxides. The sample is crosscut by a medium-grained, subhedral quartz-carbonate vein with rare subhedral Cbn.																	
CAM-021-KY-074	2	M	68	1	10	5	0	3	2	0	0	4	1	1	5	Subophitic	M	**Gabbronorite**
Description	Weakly sericitized, fine-grained Cpx and Opx enclosed by medium-grained, subophitic laths of Pl with medium-to fine-grained Mag and very-fine-grained disseminated Cpy.																	
CAM-021-KY-075	203.4	M	65	1	13	5	0	3	2	0	0	4	1	1	5	Subophitic	M	**Gabbronorite**
Description	Weakly sericitized, fine-grained Cpx and Opx enclosed by medium-grained, subophitic laths of Pl with fine-grained Mag and very-fine-grained disseminated Cpy.																	

Sample ID	Depth (m)	Grainsize	Modal percent of mineral						Alteration					Other minerals	Opaque minerals	Texture	Clean Air Metals code	IUGS Name
			Plagioclase	Amphibole	Clinopyroxene	Orthopyroxene	Olivine	Biotite	Sericite	Chlorite	Carbonates	Hematite	Serpentine					
CAM-021-KY-077	125	m	20	1	13	5	0	3	40	0	0	1	15	1	1	Subophitic	Zmf	**Gabbronorite**
Description	Strongly sericitized, anhedral, medium-to fine-grained Pl with pervasively sericitized, fine-grained Cpx with fine-grained Mag and Cpy.																	
CAM-021-KY-078	128.6	c	1	0	1	4	0	1	65	2	5	2	14	2	3	Poikilitic	Mg	**Gabbronorite**
Description	Pervasively sericitized, serpentinized, and carbonatized, subhedral, coarse-grained Cpx and Opx with some moderately chloritized, medium-grained Bt and with disseminated fine-grained Cpy and oxides. The sample is crosscut by a medium-grained, subhedral quartz-carbonate veins.																	
CAM-021-KY-079	123	M	65	1	14	5	0	3	2	0	0	5	1	1	3	Ophitic	M	**Gabbronorite**
Description	Weakly sericitized, fine-grained Cpx and Opx enclosed by medium-grained, subophitic laths of Pl with medium-to fine-grained Mag and very-fine-grained disseminated Cpy.																	
CAM-021-KY-080	1	c	10	0	10	30	1	1	22	2	1	5	7	1	10	Poikilitic	Mg	**Gabbronorite**
Description	Pervasively sericitized, serpentinized, and carbonatized, subhedral, poikilitic, coarse-grained Cpx and Opx with strongly sericitized, subhedral, coarse-grained Pl disseminated, and strongly hematized, medium-grained Mag intergrew with Po, and has Ilm exsolution lamellae and fine-grained Cpy and Cbn blebs.																	
CAM-021-KY-081	3.6	c	10	0	10	30	1	1	27	2	1	5	5	1	7	Poikilitic	Mg	**Gabbronorite**
Description	Pervasively sericitized, serpentinized, and carbonatized, subhedral, poikilitic, coarse-grained Cpx and Opx with strongly sericitized, subhedral, coarse-grained Pl disseminated, and strongly hematized, medium-grained Mag with Po, has Ilm lamellae and fine-grained Cpy and Cbn blebs.																	
CAM-021-KY-082	119	c	10	0	10	30	1	1	27	2	1	5	5	1	7	Poikilitic	Mg	**Gabbronorite**
Description	Perversely sericitized, subhedral-to anhedral, coarse-grained Pl with weakly sericitized and serpentinized, subhedral, poikilitic, coarse-grained Cpx and Opx, and strongly hematized, medium-grained Mag intergrew with Po, and has Ilm lamellae, and fine-grained Cpy and Cbn blebs.																	
CAM-021-KY-083	119.6	c	10	0	14	30	1	1	20	2	1	5	5	1	10	Poikilitic	Mg	**Gabbronorite**
Description	Perversely sericitized, subhedral, coarse-to medium-grained Pl with weakly sericitized and serpentinized, subhedral, poikilitic, coarse-grained Cpx and Opx, and strongly hematized, medium-grained Mag intergrew with Po, and has Ilm lamellae, and fine-grained disseminated Cpy and Cbn.																	

Sample ID	Depth (m)	Grainsize	Modal percent of mineral						Alteration					Other minerals	Opaque minerals	Texture	Clean Air Metals code	IUGS Name
			Plagioclase	Amphibole	Clinopyroxene	Orthopyroxene	Olivine	Biotite	Sericite	Chlorite	Carbonates	Hematite	Serpentine					
CAM-021-KY-084	143.9	c	10	0	14	30	1	1	20	2	1	5	5	1	10	Poikilitic	Mg	**Gabbronorite**
Description	Strongly sericitized, subhedral, coarse-grained Pl with weakly sericitized and serpentinized, subhedral, poikilitic, coarse-grained Cpx and Opx, and moderately hematized, medium-grained Mag intergrew with Po, and has Ilm lamellae, and fine-grained disseminated Cpy and Cbn.																	
CAM-021-KY-085	145	c	10	0	29	15	1	1	20	2	1	5	5	1	10	Poikilitic	Mg	**Gabbronorite**
Description	Strongly sericitized, subhedral, coarse-grained Pl with weakly sericitized and serpentinized, subhedral, poikilitic, coarse-grained Cpx and Opx, and moderately hematized, medium-grained Mag intergrew with Po, and has Ilm lamellae, and fine-grained disseminated Cpy and rare Cbn.																	
CAM-021-KY-086	37.6	f	5	3	1	0	0	0	25	1	1	1	60	1	1	Ophitic	Mg	**Gabbronorite**
Description	Strongly sericitized, prismatic, ophitic, fine-grained laths of Pl on a very-fine-grained sericitic groundmass and moderately-sericitized, anhedral, fine-grained Cpx and Opx with disseminated very-fine-grained Cpy and oxides.																	
CAM-021-KY-087	34	v.f	3	3	3	1	0	0	25	1	1	1	60	1	1	Ophitic	M	**Gabbronorite**
Description	Completely sericitized, prismatic, ophitic, fine-grained laths of Pl on a very-fine-grained sericitic groundmass and moderately-sericitized, anhedral, fine-grained Cpx and Opx with disseminated very-fine-grained Cpy and oxides.																	
CAM-021-KY-088	49.15	f	5	3	1	0	0	0	25	1	1	1	60	1	1	Ophitic	Mg	**Gabbronorite**
Description	Strongly sericitized, prismatic, ophitic, fine-grained laths of Pl on a very-fine-grained sericitic groundmass and moderately-sericitized, anhedral, fine-grained Cpx and Opx with disseminated very-fine-grained Cpy and oxides.																	
CAM-021-KY-089	124.7	f	3	3	3	1	0	0	25	1	1	1	60	1	1	Ophitic	M	**Gabbronorite**
Description	Completely sericitized, prismatic, ophitic, fine-grained laths of Pl on a very-fine-grained sericitic groundmass and moderately-sericitized, anhedral, fine-grained Cpx and Opx with disseminated very-fine-grained Cpy and oxides.																	
CAM-021-KY-090	178.5	c	10	0	29	15	1	1	20	2	1	5	5	1	10	Subophitic	Mg	**Gabbronorite**
Description	Strongly sericitized, subhedral, coarse-grained Pl with weakly sericitized and serpentinized, subhedral, poikilitic, coarse-grained Cpx and Opx, and moderately hematized, medium-grained Mag intergrew with Po, and has Ilm lamellae, and fine-grained disseminated Cpy.																	

Sample ID	Depth (m)	Grainsize	Modal percent of mineral						Alteration					Other minerals	Opaque minerals	Texture	Clean Air Metals code	IUGS Name
			Plagioclase	Amphibole	Clinopyroxene	Orthopyroxene	Olivine	Biotite	Sericite	Chlorite	Carbonates	Hematite	Serpentine					
CAM-021-KY-091	179.6	f	3	3	3	1	0	0	25	1	1	1	60	1	1	Ophitic	M	**Gabbronorite**
Description	Moderately sericitized, prismatic, ophitic, fine-grained laths of Pl on a very-fine-grained sericitic groundmass and moderately-sericitized, anhedral, fine-grained Cpx and Opx with disseminated very-fine-grained Cpy and oxides.																	
CAM-021-KY-092	193.5	m	65	1	14	5	0	3	2	0	0	5	1	1	3	Ophitic	M	**Gabbronorite**
Description	Weakly sericitized, fine-grained Cpx and Opx enclosed by medium-grained, subophitic laths of Pl with medium-to fine-grained Mag and very-fine-grained disseminated Cpy.																	

025 surface samples

Sample ID	Grainsize	Modal percent of mineral						Alteration					Other minerals	Opaque minerals	Texture	Clean Air Metals code	IUGS Name
		Plagioclase	Amphibole	Clinopyroxene	Orthopyroxene	Olivine	Biotite	Sericite	Chlorite	Carbonates	Hematite	Serpentine					
CAM-021-KY-062	m	50	0	9	10	0	0	10	0	0	9	5	1	6	Subophitic+ poikilitic	Hg	**Gabbronorite**
Description	Weakly-to moderately-sericitized, subhedral, intergranular Pl intergrown with-fine-to medium-grained Cpx and Opx and oikocrysts, and fine-grained Mag with Ilm exsolution lamellae, altered to hematite with fine-grained Cpy and some Py.																
CAM-021-KY-063	m	50	0	5	8	0	0	13	0	3	7	8	1	5	Subophitic+ poikilitic	Hg	**Gabbronorite**
Description	Weakly sericitized, intergranular, subhedral Pl intergrown with fine-to medium-grained Cpx and Opx, and completely serpentinized oikocrysts of Ol. Fine anhedral crystals of Hem altered from Mag, have exsolution of Ilm and relics of Mag with rare fine-grained Py and fine-grained Cpy.																
CAM-021-KY-064	m	50	0	25	9	0	0	5	3	0	3	2	2	1	Poikilitic	Hg	**Gabbronorite**
Description	Weakly sericitized, subhedral plagioclase host crystals with weakly serpentinized, poikilitic, medium-to coarse grained Cpx and Opx, and moderately sericitized Cpx and Opx filling the intergranular gaps between the subhedral crystals pf Pl. Plagioclase is intergrown with opx and biotite is altered to chlorite. Strongly hematized, anhedral, fine-grained Mag with Ilm exsolution lamellae and relics of Mag with rare fine-to medium-grained Py and very-fine-grained Cpy.																
CAM-021-KY-065	m	30	4	10	5	0	1	16	2	0	1	15	2	14	Poikilitic	Mg	**Gabbronorite**
Description	Strongly sericitized, very-coarse-anhedral plagioclase hosting strongly-to moderately serpentinized, poikilitic Cpx and Opx. Strongly hematized, subhedral-to anhedral, medium-grained Mag and Po with Pn exsolution lamellae and rare fine-grained Cpy, Ilm, and Hem.																
CAM-021-KY-066	c	12	8	45	20	0	1	1	1	1	0.5	5	1	4.5	Poikilitic	Upd	**Websterite**
Description	Strongly serpentinized, poikilitic, very-coarse-to coarse-grained Cpx and Opx, and weakly sericitized, anhedral, medium-grained Pl. Opx is intergrown with plagioclase, and altered to Hbl "grain boundaries". Fine-to medium, anhedral Pn with Po and rare Hem, Ilm, Cpy, and Mag.																
CAM-021-KY-067	m	53	1	13	12	0	7	5	1	0	3	4	0	1	Subophitic	Mg	**Gabbronorite**
Description	Weakly sericitized, intergranular plagioclase with medium grained anhedral Cpx and Opx. Fine-grained, hematized Mag with Cpy blebs.																
CAM-021-KY-068	F	62	1	17	8	0	0	5	1	0	4	2	1	1	Ophitic	Hg	**Gabbronorite**
Description	Weakly sericitized, intergranular, fine-grained Pl with fine-grained Cpx and Opx, and moderately hematized Mag with rare blebs of Cpy.																

025 drillhole samples

Sample ID	Depth (m)	Grainsize	Modal percent of mineral						Alteration					Other minerals	Opaque minerals	Texture	Clean Air Metals code	IUGS Name
			Plagioclase	Amphibole	Clinopyroxene	Orthopyroxene	Olivine	Biotite	Sericite	Chlorite	Carbonates	Hematite	Serpentine					
CAM-021-KY-093	0.5	c	20	0	25	10	0	1	20	1	0	1	10	1	11	poikilitic	Mg	**Gabbronorite**
Description	Pervasively sericitized, anhedral, very-coarse-to coarse Pl hosting strongly-to moderately serpentinized, poikilitic, coarse-grained Cpx and Opx with subhedral, medium-to coarse grained Po with Pn exsolution and rare fine-grained anhedral Hem, Cpy, Ilm, and Mag.																	
CAM-021-KY-094	9	m	5	2	45	33	0	1	3	0	0	3.5	4	2	1.5	Equigranular	Upd	**Websterite**
Description	Weakly serpentinized, subhedral, medium-grained Cpx and Opx with weakly sericitized, anhedral, medium-grained Pl. Orthopyroxene is intergrown with plagioclase and sometimes altered to Hbl “in the grain boundaries”. Strongly hematized, anhedral, medium-grained Mag with Ilm exsolution lamellae and fine-grained blebs of Cpy.																	
CAM-021-KY-095	27	c	3	2	60	10	0	6	1	1	1	1	12	1	2	poikilitic	Upd	**Websterite**
Description	Moderately serpentinized, poikilitic, anhedral, medium-grained Cpx and Opx with fine grained Mag and blebs of Cpy.																	
CAM-021-KY-096	40.14	m	1	0	29	20	0	5	15	1	0	1	15	1	12	poikilitic	Upd	**Websterite**
Description	Strongly sericitized, anhedral, medium-grained Cpx hosting strongly to moderately serpentinized, poikilitic, anhedral, medium-grained Cpx and Opx. Opaque minerals are also poikilitic, concentrated in a crosscutting vein. The vein has concentrically-zoned Mag bands with medium grained elongated Py with pentlandite exsolved and Cpy intergrown.																	
CAM-021-KY-097	188.5	f	10	1	10	20	0	2	30	0	1	4	15	1	6	poikilitic	M	**Gabbronorite**
Description	Completely serpentinized, fine-to medium-grained olivine with moderately sericitized, poikilitic Opx and Cpx crystals on pervasively sericitized, fine-grained chadacrysts of Pl. a vein rich in Cpy is cutting the thin section with iddingsite alteration. Fine grained oxides and fine grained Cpy are mainly concentrated in the vein.																	
CAM-021-KY-099	9	m	0	0	30	40	0	10	7	1	0	>1	10	1	>1	poikilitic	Upd	**Websterite**
Description	Strongly serpentinized, anhedral, medium-grained Opx with moderately serpentinized and sericitized, poikilitic, anhedral, medium- grained Cpx and anhedral, medium-to fine grained biotite with rare fine-grained, anhedral Po and very-fine-grained Cpy.																	

Sample ID	Depth (m)	Grainsize	Modal percent of mineral						Alteration					Other minerals	Opaque minerals	Texture	Clean Air Metals code	IUGS Name
			Plagioclase	Amphibole	Clinopyroxene	Orthopyroxene	Olivine	Biotite	Sericite	Chlorite	Carbonates	Hematite	Serpentine					
CAM-021-KY-105	141	m	0	0	60	5	0	1	9	0	0	3	20	0	2	Poikilitic	M	**Websterite**
Description	Moderately serpentinized, medium-grained Cpx and some Opx, and strongly hematized, anhedral, fine-grained Mag with Ilm exsolution lamella, and fine-grained anhedral Cpy and rare Py.																	
CAM-021-KY-106	207	f	40	1	20	20	0	0	10	0	0	2.5	5	0	1.5	Ophitic	M	**Gabbronorite**
Description	Moderately sericitized, fine-grained laths of Pl with fine grained laths of Cpx and Opx, and anhedral fine-grained hematite with Mag relicts and Ilm exsolution and fine-grained blebs of Cpy and rare Py.																	
CAM-021-KY-107	213	m	10	0	30	40	0	2	8	0	0	3.5	5	0	1.5	Poikilitic	Upd	**Websterite**
Description	Moderately sericitized and serpentinized, anhedral, fine-to medium grained chadocrysts and medium grained oikocryst of Opx and Cpx with moderately sericitized, fine-grained, interstitial laths of Pl, and fine grained anhedral Mag with very fine grained blebs of Cpy, Po and rare Py.																	

Appendix C

Whole rock data

SAMPLE	CAM-021-KY-001	CAM-021-KY-003	CAM-021-KY-004	CAM-021-KY-005	CAM-021-KY-007	CAM-021-KY-008
SiO_2	50.2	49.1	48.7	49.9	48.2	49.3
Al_2O_3	11.3	11.9	11.2	11.3	12.05	9.39
Fe_2O_3	12.8	13.85	14.4	13.45	14.3	13.1
CaO	8.5	8.82	9.56	9.88	8.9	10.75
MgO	7.57	6.64	7	7.65	6.8	9.97
Na_2O	3.6	3	2.76	2.79	3.01	2.18
K_2O	1.29	1.95	1.52	1.35	1.89	1.5
Cr_2O_3	0.028	0.029	0.032	0.042	0.028	0.077
TiO_2	2.77	2.68	2.65	2.37	2.52	2.02
MnO	0.13	0.15	0.16	0.16	0.16	0.19
P_2O_5	0.34	0.31	0.3	0.3	0.3	0.27
SrO	0.07	0.1	0.1	0.1	0.1	0.07
BaO	0.05	0.07	0.06	0.06	0.07	0.06
LOI	1.54	1.07	0.88	1.08	1.36	1.9
Total	100.19	99.67	99.32	100.43	99.69	100.78
C	0.03	0.03	0.04	0.04	0.03	0.03
S	0.03	0.03	0.02	0.02	0.02	0.02
Ba	500	679	580	536	667	542
Ce	69.8	84.8	82.5	80	75.8	77.2
Cr	200	210	230	300	200	550
Cs	0.46	0.54	0.62	0.71	0.94	0.71
Dy	5.52	4.72	4.86	4.65	4.33	5
Er	2.35	2.04	2.2	2.1	1.65	2.23
Eu	2.31	2.6	2.62	2.7	2.8	2.79
Ga	20.4	21.9	20.4	20.1	21.7	17.6
Gd	8.41	7.84	7.77	7.4	6.86	6.63
Ge	<5	<5	<5	<5	<5	<5
Hf	6.1	6.1	5.9	5.6	5.4	5.4
Ho	0.93	0.81	0.88	0.88	0.82	0.76
La	24.9	36.2	33.6	33	31.4	32.9
Lu	0.26	0.22	0.18	0.2	0.21	0.19
Nb	21.6	19.6	19.6	18.8	17.9	18.1
Nd	48.7	50	47.1	45.9	44.2	46.5
Pr	10.9	11.5	10.95	10.65	10.3	10.75
Rb	29.4	42.9	32.9	28.9	43.9	31.7
Sm	10.65	9.87	10.05	10.1	9.54	9.26
Sn	1	1	2	2	2	2
Sr	618	884	922	890	897	606
Ta	1.4	1.3	1.2	1.2	1.1	1.1
Tb	1.05	0.86	0.93	0.91	0.84	0.85
Th	2.22	2.22	2.1	1.89	1.91	1.75
Tm	0.28	0.25	0.26	0.24	0.22	0.25
U	0.95	0.79	0.77	0.72	0.61	0.53
V	400	415	445	369	409	289
W	1	<1	<1	<1	1	<1
Y	22.1	19.6	20.1	18.9	18	19.4
Yb	1.74	1.65	1.64	1.59	1.4	1.54
Zr	240	231	218	207	196	199
As	0.6	1.1	1	0.6	0.3	0.8
Bi	0.08	0.12	0.12	0.06	0.07	0.08
Hg	<0.005	<0.005	<0.005	<0.005	<0.005	<0.005
In	0.012	0.009	0.011	0.01	0.018	0.016
Re	0.001	<0.001	<0.001	0.001	<0.001	0.001
Sb	<0.05	<0.05	<0.05	<0.05	<0.05	<0.05
Se	<0.2	0.3	0.2	0.2	0.2	0.3
Te	<0.01	0.01	<0.01	0.01	<0.01	0.01
Tl	0.02	0.02	0.03	0.02	0.04	0.07
Ag	<0.5	<0.5	<0.5	<0.5	<0.5	<0.5
Cd	<0.5	<0.5	<0.5	<0.5	<0.5	<0.5
Co	35	50	58	50	57	64
Cu	28	99	80	146	194	125
Li	50	30	20	20	30	30
Mo	2	2	1	1	1	1
Ni	77	93	102	109	104	154
Pb	5	6	6	4	5	9
Sc	26	27	28	29	27	34
Zn	55	102	120	78	132	120

SAMPLE	CAM-021-KY-009	CAM-021-KY-010	CAM-021-KY-012	CAM-021-KY-013	CAM-021-KY-014	CAM-021-KY-015
SiO_2	49.9	49	45.9	57.8	48.9	49.1
Al_2O_3	10	9.23	5.63	17.4	9.36	9.76
Fe_2O_3	13.4	14.25	15.6	7.28	13.3	13.05
CaO	9.9	9.13	7.74	0.97	9.78	8.38
MgO	9.19	10.7	18.05	4.26	9.3	8.76
Na_2O	2.46	1.96	0.62	2.16	2.2	2.63
K_2O	1.42	1.4	1.12	4.68	1.46	2.17
Cr_2O_3	0.067	0.092	0.22	0.024	0.072	0.061
TiO_2	2.24	2.15	1.44	0.61	2.15	2.15
MnO	0.19	0.18	0.18	0.09	0.2	0.2
P_2O_5	0.3	0.29	0.2	0.15	0.27	0.3
SrO	0.08	0.07	0.02	0.04	0.07	0.02
BaO	0.06	0.06	0.04	0.13	0.06	0.08
LOI	1.55	2.46	4.23	3.85	1.81	2.36
Total	100.76	100.97	100.99	99.44	98.93	99.02
C	0.03	0.03	0.03	0.04	0.03	0.03
S	0.02	0.08	0.34	0.17	0.02	0.03
Ba	540	564	395	1195	561	753
Ce	91	81.1	50.4	77	86.6	88.8
Cr	480	640	1580	170	510	430
Cs	0.72	0.55	2.49	11.1	0.65	0.44
Dy	5.24	4.72	2.65	3.71	4.99	4.9
Er	2.2	1.98	1.19	1.96	1.99	2.12
Eu	2.89	2.56	1.54	1.8	2.76	2.55
Ga	19.5	17.7	11.2	24	18.3	18
Gd	7.46	7.06	4.56	4.67	7.61	7.59
Ge	<5	<5	<5	<5	<5	<5
Hf	6.6	5.2	3.9	4.6	6	6.3
Ho	0.86	0.74	0.51	0.65	0.83	0.86
La	38.7	34.1	20.6	35.6	36.1	37.3
Lu	0.25	0.2	0.11	0.27	0.22	0.23
Nb	23.7	22.2	10.2	8.8	22.5	21
Nd	50.1	47.6	29.5	35.5	50.6	50.9
Pr	12.05	11.05	7.29	9.05	11.6	11.9
Rb	30.4	25.2	35	177	32.7	39.6
Sm	10.65	10.45	6.42	6.84	10.35	11.45
Sn	2	1	1	2	2	2
Sr	763	619	188.5	324	640	247
Ta	1.5	1.3	0.7	0.7	1.4	1.3
Tb	0.97	0.91	0.59	0.68	0.94	0.93
Th	2.5	2.03	1.17	12.8	2.2	2.25
Tm	0.25	0.25	0.15	0.27	0.24	0.24
U	0.71	0.69	0.43	3.41	0.67	0.71
V	308	278	190	131	296	295
W	1	<1	<1	2	1	<1
Y	20.8	19.8	12.6	19	20.2	20.7
Yb	1.73	1.68	1.05	1.71	1.63	1.65
Zr	239	197	126	152	222	234
As	0.6	0.7	1	0.2	0.6	0.3
Bi	0.11	0.09	0.83	0.7	0.11	0.13
Hg	<0.005	<0.005	<0.005	<0.005	<0.005	<0.005
In	0.019	0.023	0.03	0.06	0.019	0.016
Re	0.001	<0.001	0.001	0.001	0.001	<0.001
Sb	<0.05	<0.05	<0.05	<0.05	<0.05	<0.05
Se	0.2	<0.2	1.9	0.3	0.2	0.2
Te	0.01	0.01	0.19	0.05	0.01	0.01
Tl	0.09	0.03	0.08	0.39	0.08	0.06
Ag	<0.5	<0.5	1.4	<0.5	<0.5	<0.5
Cd	<0.5	<0.5	<0.5	<0.5	<0.5	<0.5
Co	63	70	159	24	61	58
Cu	178	128	2170	233	161	163
Li	20	30	80	200	30	40
Mo	1	1	1	2	1	1
Ni	147	192	783	103	147	131
Pb	13	19	59	41	13	10
Sc	32	31	27	15	32	30
Zn	142	91	116	135	155	156

SAMPLE	CAM-021-KY-016	CAM-021-KY-017	CAM-021-KY-018	CAM-021-KY-019	CAM-021-KY-020	CAM-021-KY-022
SiO_2	49.4	73.6	47.6	74	67.2	77.8
Al_2O_3	9.66	14.2	9.89	15.25	14.5	14.3
Fe_2O_3	13.2	2.32	11.9	0.53	4.56	0.7
CaO	10.15	0.78	9.85	0.15	1.44	0.23
MgO	8.59	0.72	6.83	0.08	3.51	0.16
Na_2O	2.41	3.2	2.56	3.91	4.24	5.08
K_2O	1.62	5.74	0.85	6.27	1.01	1.69
Cr_2O_3	0.068	0.003	0.053	0.002	0.013	0.003
TiO_2	2.23	0.28	2.2	0.01	0.26	0.01
MnO	0.19	0.02	0.18	0.01	0.04	0.05
P_2O_5	0.31	0.15	0.33	0.17	0.47	0.22
SrO	0.08	0.02	0.08	<0.01	0.01	<0.01
BaO	0.06	0.09	0.04	<0.01	0.01	<0.01
LOI	1.66	0.76	7.38	0.52	3.03	0.91
Total	99.63	101.88	99.74	100.9	100.29	101.15
C	0.03	0.03	1.24	0.02	0.16	0.03
S	0.02	<0.01	0.27	0.03	0.03	0.05
Ba	581	837	370	37.2	74.8	17
Ce	87.6	148	98.1	1.4	105	1.6
Cr	470	20	380	10	90	20
Cs	0.69	6.93	1.84	14.6	6.58	7.62
Dy	5.48	2.8	5.28	0.19	2.38	0.26
Er	2.23	1.23	2.22	0.03	1.25	0.09
Eu	2.88	0.97	3.06	0.05	1.1	0.2
Ga	18.5	20.8	19.1	28.1	22.7	38.4
Gd	7.64	5.26	8.16	0.22	3.92	0.45
Ge	<5	<5	<5	<5	<5	<5
Hf	6.4	6.7	6.8	0.6	5.7	1.1
Ho	0.86	0.49	0.87	0.02	0.44	0.03
La	37.4	68.8	41.6	0.5	52.8	0.7
Lu	0.22	0.15	0.22	<0.01	0.19	0.01
Nb	21.1	12.1	25.1	20	26.6	61.7
Nd	51.9	58.2	54.9	0.8	38.2	1.1
Pr	11.7	16.75	12.9	0.2	11.4	0.27
Rb	34.9	176	18.4	744	123.5	292
Sm	10.75	8.85	11.4	0.22	6.12	0.34
Sn	2	3	2	8	6	17
Sr	714	176	693	15.5	125.5	23.8
Ta	1.3	1	1.6	3.7	11	20.3
Tb	1.01	0.57	0.92	0.03	0.51	0.05
Th	2.36	28.3	2.69	0.35	23.2	0.8
Tm	0.25	0.18	0.24	0.01	0.17	0.01
U	0.73	3.35	0.76	1.5	3.27	4.15
V	299	24	279	6	163	17
W	1	1	1	1	2	46
Y	20.6	12.5	20.7	0.8	12.7	1.4
Yb	1.94	1.22	1.72	0.04	1.18	0.09
Zr	235	234	250	7	192	11
As	0.7	0.6	0.2	0.1	0.3	0.3
Bi	0.08	0.18	0.04	4.57	1.73	4.53
Hg	<0.005	<0.005	0.007	<0.005	<0.005	<0.005
In	0.019	0.012	0.046	<0.005	0.008	0.005
Re	<0.001	<0.001	0.002	<0.001	0.029	<0.001
Sb	<0.05	<0.05	<0.05	<0.05	<0.05	<0.05
Se	0.3	<0.2	0.4	<0.2	<0.2	<0.2
Te	0.01	<0.01	0.02	0.05	0.03	0.04
Tl	0.07	0.22	0.06	0.15	0.11	0.11
Ag	<0.5	<0.5	<0.5	<0.5	<0.5	<0.5
Cd	<0.5	<0.5	<0.5	<0.5	<0.5	<0.5
Co	61	3	53	<1	8	<1
Cu	170	4	178	12	29	48
Li	20	40	100	20	170	20
Mo	1	3	1	1	23	1
Ni	143	8	112	3	83	4
Pb	8	28	10	12	5	7
Sc	33	4	27	<1	8	<1
Zn	130	38	65	8	29	49

SAMPLE	CAM-021-KY-023A	CAM-021-KY-023B	CAM-021-KY-024	CAM-021-KY-025	CAM-021-KY-026	CAM-021-KY-027
SiO_2	60.7	60.3	66.1	51.9	50.5	63.1
Al_2O_3	18.8	20	17.1	12.2	11.85	16.45
Fe_2O_3	7.41	7.92	4.24	9.44	11.4	6.53
CaO	1.52	1.6	2.81	8.89	6.43	1.98
MgO	3.14	3.19	2.09	11	11.4	2.81
Na_2O	2.42	2.56	3.49	1.63	1.08	3.46
K_2O	2.33	2.45	2.09	2.04	1.67	2.47
Cr_2O_3	0.021	0.022	0.014	0.054	0.126	0.023
TiO_2	0.72	0.76	0.43	0.82	0.66	0.58
MnO	0.08	0.08	0.08	0.16	0.31	0.06
P_2O_5	0.18	0.17	0.16	0.83	0.14	0.14
SrO	0.04	0.04	0.06	0.15	0.03	0.04
BaO	0.08	0.08	0.05	0.14	0.05	0.09
LOI	1.48	1.47	1.42	2.36	3.46	2.38
Total	98.92	100.64	100.13	101.61	99.11	100.11
C	0.03	0.03	0.05	0.09	0.21	0.19
S	0.1	0.11	0.21	0.24	0.4	0.11
Ba	711	685	526	1325	481	857
Ce	64.6	64.8	41.2	178.5	45.4	69.6
Cr	150	160	100	370	930	160
Cs	8.96	9.07	19.5	12.95	19.65	5.86
Dy	3.63	3.38	2.01	6.15	3.42	3
Er	1.8	1.69	1.27	2.58	1.91	1.83
Eu	1.38	1.39	1.16	3.97	1.26	1.36
Ga	26.2	26.6	23.6	16.6	17.7	19.4
Gd	4.54	3.89	2.75	11.4	3.95	3.86
Ge	<5	<5	<5	<5	<5	<5
Hf	4	3.8	3.1	6	2.4	4.5
Ho	0.68	0.65	0.44	1.01	0.61	0.6
La	29.2	28.9	19.8	77.9	21.2	34.7
Lu	0.27	0.25	0.14	0.26	0.25	0.23
Nb	6	6.4	4.9	8.4	3.7	7.7
Nd	33.3	32.7	20.3	97.6	25.8	31.2
Pr	7.97	7.66	5.08	23.1	5.76	8.05
Rb	83.6	88.4	90.8	112.5	107.5	83.1
Sm	5.35	5.17	3.8	17.75	5.08	5.5
Sn	2	1	1	3	16	2
Sr	306	321	480	1260	206	324
Ta	0.5	0.5	0.4	0.4	0.3	0.6
Tb	0.58	0.63	0.31	1.41	0.54	0.55
Th	6.1	5.91	3.68	10.9	3.71	8.83
Tm	0.25	0.27	0.15	0.32	0.24	0.22
U	1.51	1.56	1.08	3.47	1.04	2.66
V	155	163	86	164	213	103
W	1	1	1	1	1	2
Y	16.1	15.8	9.7	25.6	16.3	16.2
Yb	1.93	1.79	1.09	1.79	1.7	1.74
Zr	149	150	108	223	91	162
As	15.9	15.4	0.5	0.7	27	54.8
Bi	0.19	0.17	0.22	0.1	0.62	0.32
Hg	<0.005	<0.005	<0.005	<0.005	<0.005	<0.005
In	0.044	0.044	0.024	0.016	0.025	0.027
Re	0.001	0.001	0.001	<0.001	0.001	0.001
Sb	<0.05	<0.05	<0.05	<0.05	<0.05	<0.05
Se	0.2	0.2	0.3	0.2	0.6	<0.2
Te	0.03	0.04	0.05	0.01	0.06	0.04
Tl	0.4	0.42	0.35	0.7	0.71	0.41
Ag	<0.5	<0.5	<0.5	<0.5	<0.5	<0.5
Cd	<0.5	<0.5	<0.5	<0.5	0.5	<0.5
Co	27	28	16	44	53	21
Cu	38	41	53	122	202	33
Li	180	180	270	240	210	60
Mo	2	3	1	<1	1	1
Ni	102	100	50	176	380	71
Pb	11	14	17	26	11	21
Sc	19	20	9	24	27	15
Zn	96	96	62	115	111	72

SAMPLE	CAM-021-KY-028	CAM-021-KY-029	CAM-021-KY-030	CAM-021-KY-031	CAM-021-KY-032	CAM-021-KY-033
SiO_2	54.9	48.2	48	45.9	45.7	46.9
Al_2O_3	16.55	10.05	10.9	11.15	11.2	11.15
Fe_2O_3	6.76	13.2	13.2	9.98	12	11.4
CaO	5.91	6.97	6.27	8.15	6.61	8.47
MgO	6.5	9.53	8.52	6.48	8.11	5.71
Na_2O	3.41	2.35	2.76	3.03	2.4	3.37
K_2O	1.88	1.32	1.46	1.42	1.3	1.47
Cr_2O_3	0.029	0.073	0.041	0.043	0.042	0.036
TiO_2	0.63	2.26	2.36	2.42	2.43	2.23
MnO	0.09	0.16	0.15	0.21	0.17	0.17
P_2O_5	0.39	0.32	0.36	0.36	0.38	0.35
SrO	0.15	0.05	0.06	0.04	0.05	0.07
BaO	0.06	0.06	0.06	0.04	0.04	0.06
LOI	1.04	4.43	4.68	8.83	8.19	8.14
Total	98.3	98.97	98.82	98.05	98.62	99.53
C	0.04	0.17	0.23	1.42	0.93	1.24
S	0.1	0.14	0.14	0.42	0.4	0.15
Ba	565	573	555	391	404	592
Ce	143	87.5	99	95.7	118.5	106.5
Cr	200	520	290	310	320	260
Cs	7.76	0.39	0.38	0.65	0.79	0.74
Dy	3.11	5.48	6.02	5.75	6.4	5.67
Er	1.42	2.27	2.44	2.49	2.49	2.23
Eu	2.54	2.9	3.37	3.51	3.92	3.27
Ga	19.1	19.4	20.2	17.8	20.6	18.9
Gd	6.49	8.28	8.94	8.98	9.91	9.22
Ge	<5	<5	<5	<5	<5	<5
Hf	4.7	6.4	7.3	7.1	7.5	7
Ho	0.53	0.8	0.91	0.96	1.01	0.89
La	67.3	36.4	41.2	40.3	50.3	45.1
Lu	0.18	0.22	0.24	0.24	0.25	0.24
Nb	5.5	20.2	21.5	22.4	23.6	20.4
Nd	69.6	53.5	58.9	57.6	70.6	62.9
Pr	16.8	11.8	13.35	12.95	15.65	14.05
Rb	83	29.7	35	29.2	27.2	32.6
Sm	10.3	10.8	11.6	11.05	13.45	11.65
Sn	1	2	2	2	2	2
Sr	1240	363	446	327	420	514
Ta	0.3	1.2	1.3	1.5	1.4	1.3
Tb	0.62	0.97	1.06	1.11	1.21	1.01
Th	8.26	2.19	2.59	2.65	2.54	2.68
Tm	0.2	0.26	0.26	0.29	0.33	0.27
U	2.33	0.77	0.71	1.31	0.96	0.9
V	120	278	289	295	306	277
W	1	1	1	1	1	1
Y	13.3	21.3	23.4	25.9	26.6	22.2
Yb	1.36	1.62	1.95	1.9	2.11	1.78
Zr	207	247	268	274	288	263
As	>250	1.7	1.1	0.8	0.7	0.3
Bi	0.1	0.19	0.1	0.14	0.13	0.08
Hg	<0.005	0.005	0.006	0.034	0.013	0.007
In	0.01	0.033	0.04	0.053	0.065	0.057
Re	<0.001	0.002	0.001	0.001	0.002	0.001
Sb	0.19	0.09	0.05	0.08	0.06	<0.05
Se	0.2	0.3	0.4	0.5	0.6	0.5
Te	0.05	0.03	0.02	0.04	0.03	0.03
Tl	0.56	0.16	0.11	0.08	0.12	0.03
Ag	<0.5	<0.5	<0.5	<0.5	<0.5	<0.5
Cd	<0.5	<0.5	<0.5	<0.5	<0.5	<0.5
Co	30	57	53	55	57	45
Cu	40	168	154	188	237	148
Li	50	60	60	70	90	50
Mo	<1	1	1	1	1	1
Ni	157	169	100	98	103	82
Pb	26	5	5	7	10	4
Sc	13	29	29	28	29	26
Zn	91	101	86	64	81	59

SAMPLE	CAM-021-KY-035	CAM-021-KY-036	CAM-021-KY-037	CAM-021-KY-038	CAM-021-KY-039	CAM-021-KY-043
SiO_2	49.3	46.2	45.9	49	47.8	48.8
Al_2O_3	11.05	10.45	10.9	10.9	11.15	9.92
Fe_2O_3	10.9	11.7	11.55	14	14.95	13.65
CaO	9.96	10.85	7.55	8.42	10.25	8.73
MgO	6.68	6.02	7.94	7.32	7.42	9.15
Na_2O	2.51	2.57	2.16	2.71	2.67	2.35
K_2O	1.25	1.25	1.36	1.99	1.27	1.71
Cr_2O_3	0.043	0.044	0.045	0.039	0.04	0.067
TiO_2	2.42	2.32	2.38	2.48	2.85	2.26
MnO	0.16	0.18	0.25	0.17	0.2	0.19
P_2O_5	0.36	0.37	0.37	0.31	0.27	0.33
SrO	0.09	0.09	0.03	0.08	0.12	0.08
BaO	0.05	0.05	0.05	0.06	0.06	0.06
LOI	7.19	7.6	8.58	1.66	1.41	1.99
Total	101.96	99.69	99.07	99.14	100.46	99.29
C	1.21	1.39	0.98	0.04	0.02	0.03
S	0.2	0.17	0.4	0.03	0.01	0.03
Ba	497	482	440	583	533	552
Ce	96.1	91.7	101.5	89.5	70.6	95.3
Cr	290	280	320	280	260	450
Cs	0.67	0.75	0.35	0.57	0.82	0.43
Dy	5.47	5.23	5.83	4.97	4.65	5.24
Er	2.28	2.25	2.37	2.26	2.22	2.17
Eu	3.37	3.02	3.07	2.92	2.77	2.89
Ga	19.1	18.1	19.3	18.3	19.1	17.5
Gd	8.64	8.48	8.98	7.98	7.29	7.55
Ge	<5	<5	<5	<5	<5	<5
Hf	6.9	6.5	7.1	6	5.5	6.7
Ho	0.93	0.89	0.96	0.81	0.78	0.8
La	40.9	38.5	41.4	38.5	29.6	41.5
Lu	0.27	0.2	0.27	0.19	0.22	0.24
Nb	21.7	21	23.3	22.4	17.3	24.2
Nd	57.8	56.1	60.9	53.6	45.2	55.7
Pr	12.95	12.3	13.6	11.95	9.64	12.45
Rb	18.3	18.8	28.8	47.9	28.5	35.1
Sm	11.75	10.85	12.85	10.15	8.77	10.65
Sn	2	2	2	2	2	2
Sr	778	750	244	675	982	589
Ta	1.5	1.3	1.4	1.4	1.1	1.5
Tb	0.97	1	1.09	1	0.85	0.96
Th	2.46	2.29	2.44	2.15	1.95	2.54
Tm	0.29	0.28	0.26	0.24	0.22	0.3
U	0.82	0.73	0.76	0.63	0.58	0.97
V	281	269	293	328	398	281
W	<1	1	3	1	1	<1
Y	22.9	20.7	22.9	20.1	17.5	21.1
Yb	1.77	1.62	1.93	1.65	1.37	1.76
Zr	275	256	272	235	197	256
As	0.6	0.3	1.1	1	0.3	0.8
Bi	0.04	0.04	0.15	0.11	0.08	0.09
Hg	<0.005	0.006	0.041	<0.005	<0.005	<0.005
In	0.046	0.047	0.051	0.021	0.014	0.021
Re	0.002	0.001	0.002	0.001	<0.001	<0.001
Sb	<0.05	<0.05	0.06	0.05	<0.05	<0.05
Se	0.3	0.3	0.4	0.2	0.2	0.2
Te	0.03	0.02	0.03	0.01	0.01	0.01
Tl	0.07	0.06	0.19	0.05	0.06	0.05
Ag	<0.5	<0.5	0.9	<0.5	<0.5	<0.5
Cd	<0.5	<0.5	<0.5	<0.5	<0.5	<0.5
Co	47	48	55	60	60	60
Cu	173	172	235	242	210	210
Li	60	60	70	30	20	30
Mo	1	1	1	1	1	1
Ni	96	97	111	106	106	141
Pb	10	9	23	7	8	10
Sc	27	27	29	28	29	30
Zn	94	85	133	128	172	119

SAMPLE	CAM-021-KY-044	CAM-021-KY-045	CAM-021-KY-046	CAM-021-KY-047	CAM-021-KY-048	CAM-021-KY-049
SiO_2	51.2	48.6	51.6	51	49.5	50.3
Al_2O_3	10.7	10.25	9.87	9.71	9.38	9.68
Fe_2O_3	13.65	14.35	11.75	12.9	13.15	13.45
CaO	8.56	10.55	10.05	10.55	9.98	8.72
MgO	8.4	8.24	9.21	8.95	9.71	8.99
Na_2O	2.61	2.32	2.89	2.29	2.71	2.49
K_2O	1.08	1.07	1.43	1.41	0.74	1.51
Cr_2O_3	0.055	0.05	0.06	0.064	0.067	0.058
TiO_2	2.38	2.42	2.19	2.09	1.96	2.16
MnO	0.15	0.18	0.17	0.17	0.19	0.2
P_2O_5	0.32	0.21	0.25	0.29	0.26	0.29
SrO	0.07	0.1	0.06	0.08	0.07	0.07
BaO	0.04	0.05	0.05	0.05	0.01	0.06
LOI	2.44	0.65	1.9	1.49	2.18	2.29
Total	101.66	99.04	101.48	101.04	99.91	100.27
C	0.04	0.02	0.03	0.03	0.03	0.05
S	0.04	0.01	0.01	0.02	0.03	0.02
Ba	387	453	503	522	141.5	571
Ce	99.2	63	66.2	81	78.4	85.2
Cr	380	360	420	460	470	400
Cs	1.14	1.06	0.56	0.64	0.11	0.5
Dy	5.72	4.27	5.19	5.18	5.38	4.98
Er	2.57	1.62	2.31	1.94	2.38	2.26
Eu	2.53	2.4	2.56	2.68	2.65	2.63
Ga	19.8	17.6	16.9	17.8	17.2	16.3
Gd	7.99	6.85	7.87	7.86	7.57	6.74
Ge	<5	<5	<5	<5	<5	<5
Hf	7	4.7	6	5.9	7.4	6.4
Ho	0.87	0.71	0.89	0.91	0.81	0.81
La	43.7	25.9	24.8	33.6	31.7	37
Lu	0.24	0.2	0.19	0.19	0.22	0.22
Nb	24.7	14.2	20	18	21.3	20.9
Nd	57.4	40.2	47.2	50.3	50.3	50.9
Pr	13.3	8.72	9.9	11.1	10.95	11.55
Rb	25.4	27.3	36	34.2	9.9	28.2
Sm	10.6	8.4	10.45	10.55	10.1	9.55
Sn	2	1	1	2	2	1
Sr	577	873	470	707	549	525
Ta	1.5	0.9	1.2	1.1	1.4	1.3
Tb	1.03	0.76	0.98	0.94	0.87	0.86
Th	2.67	1.57	2.18	2	3.31	2.35
Tm	0.27	0.22	0.27	0.26	0.26	0.27
U	0.98	0.49	0.9	0.66	1.03	0.76
V	287	404	284	292	267	273
W	1	<1	1	1	1	1
Y	22.2	16.2	20.5	19.9	20.3	18.8
Yb	1.97	1.32	1.52	1.5	1.82	1.59
Zr	270	172	227	223	285	225
As	1.2	0.2	1.8	0.6	1.2	0.3
Bi	0.14	0.06	0.11	0.07	0.06	0.11
Hg	<0.005	<0.005	<0.005	<0.005	<0.005	<0.005
In	0.018	0.009	0.008	0.011	<0.005	0.01
Re	0.001	<0.001	<0.001	0.001	<0.001	<0.001
Sb	<0.05	<0.05	<0.05	<0.05	<0.05	<0.05
Se	0.2	0.2	<0.2	<0.2	<0.2	0.3
Te	<0.01	0.01	<0.01	<0.01	<0.01	0.01
Tl	0.04	0.07	0.02	0.04	<0.02	0.04
Ag	<0.5	<0.5	<0.5	<0.5	<0.5	<0.5
Cd	<0.5	<0.5	<0.5	<0.5	<0.5	0.7
Co	49	65	50	60	51	58
Cu	142	133	85	154	172	171
Li	40	20	40	20	30	30
Mo	2	1	1	1	1	1
Ni	135	138	114	140	151	139
Pb	11	5	10	12	4	19
Sc	28	33	32	34	32	31
Zn	69	134	61	149	82	215

SAMPLE	CAM-021-KY-050	CAM-021-KY-051	CAM-021-KY-052	CAM-021-KY-053	CAM-021-KY-054	CAM-021-KY-056	CAM-021-KY-057
SiO_2	61.6	50.5	50.4	48.4	50.8	49	48.2
Al_2O_3	17.55	10.9	10.7	6.65	12.4	10.8	9.71
Fe_2O_3	6.23	12.9	12.5	13.55	13.1	14.5	14.35
CaO	1.05	8.35	8.71	12.9	5.55	8.34	10.75
MgO	3.42	7.65	7.92	12.45	6.51	7.52	8.38
Na_2O	2.93	2.99	2.86	1.48	3.7	2.7	2.18
K_2O	2.86	1.6	1.59	0.82	1	1.92	1.13
Cr_2O_3	0.022	0.044	0.047	0.114	0.016	0.037	0.052
TiO_2	0.61	2.43	2.42	1.66	2.76	2.8	2.35
MnO	0.05	0.18	0.19	0.21	0.12	0.17	0.18
P_2O_5	0.17	0.35	0.31	0.16	0.39	0.29	0.24
SrO	0.03	0.09	0.09	0.06	0.06	0.08	0.09
BaO	0.07	0.06	0.06	0.03	0.03	0.06	0.05
LOI	2.97	1.46	1.58	0.78	3.05	1.4	1.11
Total	99.56	99.5	99.38	99.26	99.49	99.62	98.77
C	0.02	0.04	0.04	0.03	0.07	0.02	0.03
S	0.12	0.04	0.04	0.04	0.08	0.03	0.02
Ba	631	527	595	315	251	546	482
Ce	48.7	95.1	93.6	48.1	103	81	68
Cr	180	300	320	780	110	260	350
Cs	5.67	0.39	0.68	1.05	0.47	0.49	0.79
Dy	2.41	5.75	5.77	3.97	7	5.07	4.74
Er	1.49	2.74	2.38	1.89	3.28	2.09	1.79
Eu	1.17	2.78	2.79	2.1	2.72	2.58	2.43
Ga	22.4	18.5	17.9	12.5	21.2	20	18.6
Gd	3.29	8.36	8.44	6.04	9.81	7.3	6.83
Ge	<5	<5	<5	<5	<5	<5	<5
Hf	3.4	7.1	7.1	3.6	7.5	5.7	5.3
Ho	0.5	0.89	0.87	0.62	1.11	0.83	0.74
La	22.3	39.8	39.4	19.8	42.9	34.7	28.4
Lu	0.2	0.18	0.25	0.17	0.32	0.23	0.19
Nb	5.3	26.2	24.1	9.9	28.9	18.9	15.7
Nd	23.6	58	56	33.2	64	50.5	44.8
Pr	5.94	12.95	12.7	6.61	14.15	10.9	9.61
Rb	92.6	36.9	36.8	19.8	23.6	52	26.2
Sm	4.33	11.1	10.85	6.98	12.6	9.62	8.79
Sn	1	2	2	1	2	1	1
Sr	257	642	640	462	471	653	739
Ta	0.4	1.8	1.5	0.7	1.7	1.2	1
Tb	0.47	1	1.07	0.74	1.33	0.88	0.85
Th	4.41	2.81	2.79	1.12	3.32	1.98	1.66
Tm	0.21	0.31	0.28	0.18	0.33	0.24	0.24
U	1.35	1.05	1.13	0.39	1.61	0.68	0.6
V	121	276	283	279	303	388	396
W	1	1	1	<1	<1	<1	1
Y	11.4	22.1	21.8	14.6	27	18.9	17.7
Yb	1.6	1.96	1.96	1.28	2.3	1.43	1.63
Zr	132	267	256	130	284	218	190
As	5.4	0.6	1.3	0.3	0.7	1	1
Bi	0.11	0.1	0.09	0.06	0.08	0.08	0.06
Hg	<0.005	<0.005	<0.005	<0.005	0.006	<0.005	<0.005
In	0.016	0.022	0.018	0.01	0.025	0.016	0.014
Re	0.001	0.001	0.001	<0.001	0.001	0.001	<0.001
Sb	<0.05	<0.05	<0.05	<0.05	<0.05	<0.05	<0.05
Se	0.2	0.2	<0.2	<0.2	<0.2	0.2	<0.2
Te	0.03	0.01	<0.01	0.01	0.01	0.01	0.01
Tl	0.27	0.04	0.06	0.11	0.02	0.04	0.05
Ag	<0.5	<0.5	<0.5	<0.5	<0.5	<0.5	<0.5
Cd	<0.5	<0.5	<0.5	<0.5	<0.5	<0.5	<0.5
Co	24	50	51	77	23	60	66
Cu	58	156	127	145	88	172	100
Li	80	30	40	20	50	30	20
Mo	1	1	1	1	1	1	1
Ni	92	108	106	217	57	98	130
Pb	8	5	7	6	4	4	6
Sc	15	27	27	44	21	30	33
Zn	32	101	116	122	54	100	118

SAMPLE	CAM-021-KY-062	CAM-021-KY-063	CAM-021-KY-064	CAM-021-KY-065	CAM-021-KY-066	CAM-021-KY-067
SiO_2	48	46.9	49.1	41	42	50.4
Al_2O_3	14.2	13.85	15	12.4	5.71	14.5
Fe_2O_3	13.95	13.55	11.75	20.4	15.95	13
CaO	7.88	6.66	11.15	6.7	5.07	10.55
MgO	6.15	5.77	8.33	6.58	23.2	7.79
Na_2O	3.31	4.04	1.93	1.35	0.62	2.1
K_2O	1.06	1.71	0.52	3.13	0.92	0.66
Cr_2O_3	0.008	0.007	0.06	<0.002	0.443	0.045
TiO_2	2.41	2.36	0.96	3.47	1.34	1.18
MnO	0.18	0.22	0.18	0.3	0.25	0.23
P_2O_5	0.34	0.35	0.09	0.2	0.15	0.1
SrO	0.06	0.06	0.01	0.06	0.04	0.01
BaO	0.05	0.09	0.01	0.13	0.04	0.01
LOI	2.54	3.82	0.79	3.73	4.96	0.89
Total	100.14	99.39	99.88	99.45	100.69	101.47
C	0.09	0.32	0.04	0.05	0.11	0.03
S	0.2	0.21	0.01	0.19	0.26	0.01
Ba	469	836	98.7	1210	396	130.5
Ce	48.2	50.8	11.6	40.5	40.6	14.7
Cr	50	50	400	<10	3110	310
Cs	1.35	0.39	0.68	0.32	1.76	0.82
Dy	4.7	4.95	3.88	4	3.11	4.73
Er	2.36	2.39	2.52	1.81	1.28	2.72
Eu	2.07	2.25	0.79	1.81	1.44	1.02
Ga	24.5	23.8	18.1	23	11.3	19.9
Gd	6.35	6.63	3.22	5.12	4.02	3.98
Ge	<5	<5	<5	<5	<5	<5
Hf	4.7	4.5	2	4.1	3.4	2.5
Ho	0.87	0.9	0.77	0.65	0.54	1.03
La	20.5	21.6	5.1	16	17	6.2
Lu	0.23	0.24	0.3	0.15	0.15	0.36
Nb	9.7	10.3	2.8	8.4	7.2	3.6
Nd	29.7	31.2	8	27	23.6	9.9
Pr	6.82	7.39	1.62	6.11	5.58	2.14
Rb	25.8	42.1	16.3	62.3	23.2	22.6
Sm	6.93	7.55	2.35	6.12	5.27	3.06
Sn	2	2	1	2	1	1
Sr	608	591	144.5	502	329	158.5
Ta	0.7	0.6	0.2	0.6	0.5	0.2
Tb	0.85	0.91	0.53	0.72	0.53	0.63
Th	1.26	1.32	0.81	1.23	1.18	1.08
Tm	0.32	0.3	0.31	0.23	0.2	0.35
U	0.33	0.32	0.21	0.32	0.32	0.29
V	342	330	309	779	180	370
W	<1	<1	<1	<1	<1	1
Y	21.2	21.9	19.6	15.9	12.8	23.6
Yb	1.94	1.9	2.35	1.28	1.05	2.7
Zr	166	174	67	135	120	84
As	0.5	0.2	0.5	0.3	1.1	0.3
Bi	0.02	0.02	0.04	0.07	0.15	0.04
Hg	<0.005	<0.005	<0.005	0.006	<0.005	<0.005
In	0.034	0.027	0.013	0.061	0.03	0.015
Re	0.001	0.002	<0.001	0.001	0.003	0.001
Sb	<0.05	<0.05	<0.05	<0.05	0.05	<0.05
Se	0.4	0.2	<0.2	0.4	1.4	<0.2
Te	<0.01	0.01	0.01	0.03	0.09	0.01
Tl	0.04	0.03	0.05	0.03	0.3	0.07
Ag	<0.5	<0.5	<0.5	<0.5	0.5	<0.5
Cd	<0.5	<0.5	0.5	1.2	0.8	<0.5
Co	58	52	50	92	142	46
Cu	75	120	164	212	408	200
Li	40	50	20	40	30	20
Mo	<1	<1	<1	<1	1	<1
Ni	97	89	160	97	1420	130
Pb	4	8	2	18	29	<2
Sc	23	22	36	28	17	37
Zn	112	139	86	538	197	144

SAMPLE	CAM-021-KY-068	CAM-021-KY-069	CAM-021-KY-070	CAM-021-KY-071	CAM-021-KY-072	CAM-021-KY-073
SiO_2	48.8	44.3	48.9	50	44.7	41.7
Al_2O_3	14.4	14.9	14.8	14.7	13.25	17.1
Fe_2O_3	14	10.15	9.28	9.85	9.42	16.4
CaO	8.96	5.27	8.59	10.75	10.75	2.51
MgO	6.38	11.45	10.1	9.97	9.18	8.32
Na_2O	3.13	0.08	1.48	1.55	1.16	0.34
K_2O	0.65	2.24	1.22	0.91	1.4	1.96
Cr_2O_3	0.009	0.048	0.052	0.053	0.05	0.062
TiO_2	2.44	0.66	0.62	0.6	0.54	0.75
MnO	0.17	0.16	0.15	0.16	0.21	0.12
P_2O_5	0.34	0.04	0.04	0.04	0.04	0.06
SrO	0.07	<0.01	0.01	0.01	0.01	0.01
BaO	0.04	0.02	0.02	0.01	0.02	0.01
LOI	0.9	10.65	6.64	2.8	9.9	8.25
Total	100.29	99.97	101.9	101.4	100.63	97.59
C	0.07	1.18	0.62	0.2	1.87	0.55
S	0.03	0.04	0.15	0.09	0.08	0.01
Ba	333	175.5	219	115.5	178	96.7
Ce	51.7	15.5	11.9	11.3	11.3	49.5
Cr	60	330	360	370	340	420
Cs	2.65	3.69	4.51	2.08	4.83	3.11
Dy	5.18	2.02	2.28	2.24	2.32	1.7
Er	2.57	1.26	1.4	1.41	1.21	1.01
Eu	2.13	0.5	0.63	0.6	0.62	0.45
Ga	25.1	14.4	14.6	14.5	12.8	18.6
Gd	6.49	1.89	2.07	2.27	1.85	2.19
Ge	<5	<5	<5	<5	<5	<5
Hf	4.6	1.2	1.1	1.1	1	1.3
Ho	0.89	0.4	0.5	0.5	0.44	0.37
La	21.8	7.2	5.3	5.1	5.5	25.6
Lu	0.26	0.13	0.18	0.21	0.2	0.12
Nb	11.9	3.4	2.9	2.8	2.3	3.3
Nd	30.9	7.9	6.8	6.4	6.5	17.3
Pr	7.2	1.95	1.48	1.55	1.46	5.28
Rb	24.1	127	68.2	46.7	74.1	117.5
Sm	7.09	2.06	1.96	1.82	1.48	2.84
Sn	2	1	1	1	1	<1
Sr	678	37.8	150.5	156	132	29.9
Ta	0.7	0.2	0.3	0.2	0.2	0.2
Tb	0.92	0.3	0.32	0.35	0.32	0.31
Th	1.44	0.72	0.68	0.64	0.56	0.76
Tm	0.31	0.15	0.21	0.2	0.17	0.16
U	0.26	0.75	0.16	0.14	0.1	1.37
V	361	230	234	228	205	270
W	<1	1	<1	<1	<1	1
Y	22.1	9.9	11.5	11.7	11.2	9.3
Yb	1.7	1	1.34	1.33	1.21	0.96
Zr	170	39	38	36	32	43
As	0.5	0.2	0.5	0.1	0.5	0.2
Bi	0.02	0.04	0.02	0.03	0.02	0.09
Hg	<0.005	<0.005	<0.005	<0.005	0.007	<0.005
In	0.026	0.039	0.033	0.012	0.03	0.025
Re	<0.001	0.001	0.001	0.001	0.001	<0.001
Sb	<0.05	<0.05	<0.05	<0.05	<0.05	<0.05
Se	0.2	0.3	0.3	0.2	0.2	<0.2
Te	<0.01	0.02	0.01	0.01	0.02	0.01
Tl	0.17	0.1	0.29	0.12	0.16	0.08
Ag	<0.5	<0.5	<0.5	<0.5	<0.5	<0.5
Cd	0.8	<0.5	<0.5	<0.5	<0.5	<0.5
Co	53	41	47	50	45	35
Cu	89	4	109	118	110	1
Li	20	170	90	30	100	190
Mo	1	<1	<1	<1	<1	<1
Ni	111	105	113	121	115	124
Pb	4	4	8	<2	3	<2
Sc	24	33	36	34	36	39
Zn	116	63	34	46	35	76

SAMPLE	CAM-021-KY-074	CAM-021-KY-075	CAM-021-KY-076	CAM-021-KY-077	CAM-021-KY-078	CAM-021-KY-079
SiO_2	51.3	50.8	61.7	45	45	51.2
Al_2O_3	13.1	12.9	13.95	14.95	14.4	12.95
Fe_2O_3	14.9	14.05	11.5	9.54	8.99	15.15
CaO	7.79	7.92	0.62	2.54	3.03	6.98
MgO	4.64	4.35	4.56	14.65	15.1	4.93
Na_2O	2.91	2.52	2.4	1.59	1.7	2.93
K_2O	1.03	0.84	1.51	1.86	1.55	0.73
Cr_2O_3	0.003	0.002	0.02	0.05	0.043	0.003
TiO_2	2.82	2.74	0.52	0.66	0.51	2.81
MnO	0.17	0.19	0.09	0.1	0.1	0.19
P_2O_5	0.42	0.39	0.11	0.05	0.03	0.42
SrO	0.04	0.04	<0.01	0.01	0.01	0.04
BaO	0.03	0.06	0.03	0.03	0.04	0.03
LOI	0.59	3.02	3.8	8.58	9.23	1.3
Total	99.74	99.82	100.81	99.61	99.73	99.66
C	0.04	0.35	0.12	0.42	0.53	0.04
S	0.04	0.25	0.09	0.05	0.05	0.09
Ba	331	522	277	278	423	268
Ce	51.2	50.3	94.1	19.1	10.4	50.3
Cr	20	20	140	350	300	20
Cs	0.88	1.12	1.46	4.02	2.18	1.16
Dy	6.17	6.21	1.92	2.93	1.89	6.43
Er	3.02	2.98	0.94	1.49	1.11	2.89
Eu	2.3	2.28	0.75	0.76	0.51	2.31
Ga	26.4	25.1	25.9	14.5	12.4	25.8
Gd	7.04	7.13	3.6	3.06	1.9	7.48
Ge	<5	<5	<5	<5	<5	<5
Hf	5.7	5.6	4.1	1.3	0.9	5.4
Ho	1.08	1.08	0.31	0.56	0.37	1.09
La	22.2	21.8	42.9	9.5	5.2	21.8
Lu	0.3	0.32	0.13	0.18	0.16	0.29
Nb	11.8	11.5	6.3	2.8	2.2	11.6
Nd	30.7	30.8	35.3	9.9	5.8	31.1
Pr	6.92	6.81	10.8	2.42	1.36	6.81
Rb	25.1	16.3	58.3	70.4	93.9	20.1
Sm	7.54	7.23	6.3	2.64	1.58	7.33
Sn	2	2	2	1	<1	2
Sr	362	375	36.8	83.3	123.5	348
Ta	0.8	0.8	0.5	0.2	0.2	0.8
Tb	1.06	0.99	0.41	0.46	0.3	1.1
Th	2.61	2.6	7.79	0.67	0.6	2.74
Tm	0.36	0.33	0.09	0.23	0.16	0.38
U	0.75	0.6	2.48	0.16	0.09	0.63
V	348	341	99	240	203	346
W	1	<1	1	<1	<1	1
Y	27.6	27.6	8	14.8	10.7	27.3
Yb	2.43	2.38	0.68	1.49	1.19	2.36
Zr	199	192	145	39	29	198
As	0.7	0.9	0.3	<0.1	0.1	0.5
Bi	0.03	0.03	0.02	0.02	0.01	0.03
Hg	<0.005	0.005	<0.005	<0.005	<0.005	<0.005
In	0.027	0.053	0.034	0.053	0.039	0.039
Re	0.001	0.001	0.001	0.002	<0.001	0.001
Sb	<0.05	<0.05	<0.05	<0.05	<0.05	<0.05
Se	<0.2	<0.2	<0.2	<0.2	0.4	0.2
Te	<0.01	<0.01	0.01	0.02	0.01	0.01
Tl	0.08	0.09	0.04	0.06	0.05	0.13
Ag	<0.5	<0.5	<0.5	<0.5	<0.5	<0.5
Cd	1	0.7	<0.5	<0.5	<0.5	0.9
Co	51	53	20	44	45	49
Cu	57	53	6	83	107	54
Li	20	20	100	230	180	30
Mo	1	1	1	<1	<1	1
Ni	54	53	63	115	102	54
Pb	5	10	<2	2	3	7
Sc	23	22	12	23	28	22
Zn	144	123	47	56	53	137

SAMPLE	CAM-021-KY-080	CAM-021-KY-081	CAM-021-KY-082	CAM-021-KY-083	CAM-021-KY-084	CAM-021-KY-085
SiO_2	48.5	56.5	47.2	46.6	49.5	47.9
Al_2O_3	12.7	13	12.45	12.1	10.3	9.98
Fe_2O_3	14.45	10.55	14.45	13.9	13.7	12.9
CaO	6.21	3.83	8.53	8.69	9.11	8.95
MgO	6.72	4.17	8.28	8.37	9.76	9.96
Na_2O	3.14	4.29	2.51	2.03	2.34	2.25
K_2O	1.67	2.33	1.26	1.55	0.84	1.2
Cr_2O_3	0.02	0.002	0.03	0.036	0.074	0.075
TiO_2	2.94	2.08	2.7	3.01	2.45	2.44
MnO	0.16	0.11	0.16	0.16	0.17	0.16
P_2O_5	0.32	0.67	0.23	0.17	0.27	0.28
SrO	0.03	0.03	0.06	0.05	0.06	0.05
BaO	0.04	0.04	0.03	0.04	0.03	0.03
LOI	2.98	2.57	2.87	2.99	2.35	2.5
Total	99.88	100.17	100.76	99.7	100.95	98.68
C	0.05	0.09	0.04	0.04	0.06	0.05
S	0.03	0.04	0.03	0.03	0.02	0.05
Ba	366	369	311	323	269	285
Ce	83.7	153.5	50.7	41.1	70.5	68.4
Cr	140	10	210	270	580	550
Cs	0.43	0.3	0.64	0.63	0.9	1.03
Dy	5.52	8.88	4.38	3.66	5.38	5.54
Er	2.34	3.82	1.82	1.38	2.12	2.24
Eu	2.56	4.19	2.31	1.8	2.59	2.44
Ga	22.4	20.8	20.1	20	20.5	18.8
Gd	7.87	13.25	6.04	5.43	7.82	7.49
Ge	<5	<5	<5	<5	<5	<5
Hf	7.4	13.3	4.6	4.3	5.9	6.4
Ho	0.93	1.46	0.63	0.59	0.8	0.92
La	34.3	62.4	20.6	16.3	28.1	26.4
Lu	0.24	0.39	0.13	0.13	0.22	0.18
Nb	19.3	34.4	12.5	11.3	16.6	17.4
Nd	50	86.9	34.1	26.7	43.3	43.7
Pr	11.85	21.1	7.23	6	9.77	9.77
Rb	36.6	45	34.2	44.6	24.9	37.3
Sm	10.25	17.75	7.54	5.76	9.31	10.15
Sn	3	2	1	1	2	2
Sr	248	248	570	342	508	379
Ta	1.3	2.2	0.9	0.7	1.1	1.1
Tb	1	1.68	0.78	0.63	0.95	0.97
Th	2.56	5.05	1.51	1.26	1.98	1.99
Tm	0.27	0.46	0.2	0.19	0.27	0.25
U	0.84	1.25	0.5	0.42	0.67	0.76
V	446	160	421	445	317	291
W	1	<1	1	<1	<1	<1
Y	22.8	36.2	16	14.5	20.8	21.3
Yb	1.6	3.21	1.26	0.95	1.66	1.53
Zr	264	510	163	158	232	243
As	0.7	0.7	0.7	0.5	0.6	1.1
Bi	0.04	0.06	0.03	0.02	0.04	0.13
Hg	<0.005	<0.005	<0.005	<0.005	<0.005	<0.005
In	0.038	0.04	0.023	0.019	0.014	0.02
Re	0.001	0.003	0.001	<0.001	0.001	0.001
Sb	<0.05	<0.05	<0.05	<0.05	<0.05	<0.05
Se	<0.2	0.3	<0.2	0.2	0.2	0.2
Te	0.02	0.01	0.01	0.01	<0.01	0.01
Tl	0.03	0.03	0.03	0.03	0.02	0.02
Ag	<0.5	<0.5	<0.5	<0.5	<0.5	<0.5
Cd	0.7	<0.5	0.7	0.9	0.8	0.5
Co	47	27	60	62	54	52
Cu	144	192	129	110	131	190
Li	30	20	40	50	50	60
Mo	1	1	1	<1	1	1
Ni	94	26	121	139	187	179
Pb	6	13	5	4	5	4
Sc	23	12	28	29	29	28
Zn	112	69	92	92	119	97

SAMPLE	CAM-021-KY-086	CAM-021-KY-087	CAM-021-KY-088	CAM-021-KY-089	CAM-021-KY-090	CAM-021-KY-091
SiO_2	47.1	46.5	46.7	42.2	47.4	47.9
Al_2O_3	13.95	15.5	14.6	14.8	14.7	14.35
Fe_2O_3	9.2	9.32	9.39	11	10.15	9.68
CaO	7.02	6.38	8.76	7	10.3	9.33
MgO	11.05	8.84	9.9	10.3	9.74	9.79
Na_2O	1.68	2.01	1.46	3.53	2.12	2.37
K_2O	0.83	2.68	1.73	0.56	0.77	0.63
Cr_2O_3	0.05	0.055	0.053	0.055	0.054	0.052
TiO_2	0.6	0.62	0.59	0.59	0.61	0.58
MnO	0.12	0.15	0.14	0.16	0.19	0.17
P_2O_5	0.05	0.06	0.06	0.06	0.06	0.05
SrO	0.02	0.01	0.01	0.01	0.02	0.03
BaO	0.02	0.06	0.05	0.01	0.02	0.01
LOI	6.42	9.17	7.83	10.3	3.12	3.46
Total	98.11	101.36	101.27	100.58	99.25	98.4
C	0.43	1.13	1	1.39	0.11	0.09
S	0.08	0.17	0.16	0.15	0.1	0.08
Ba	183	509	415	79	128.5	128
Ce	13.2	19.9	22.6	22.4	10.8	11.2
Cr	380	420	400	420	370	400
Cs	1.51	2.96	3.16	1.05	1.69	2.16
Dy	2.36	2.54	2.63	2.89	2.31	2.51
Er	1.41	1.36	1.43	1.43	1.47	1.46
Eu	0.62	0.74	0.71	0.7	0.72	0.65
Ga	16.2	16.9	16.3	19.4	15.8	15.2
Gd	2.51	3	2.81	3.32	2.12	2.4
Ge	<5	<5	<5	<5	<5	<5
Hf	1.3	1	1.1	1	1.1	0.9
Ho	0.45	0.52	0.47	0.59	0.43	0.44
La	6.4	10.7	12.1	11.6	4.9	5.2
Lu	0.19	0.21	0.19	0.23	0.18	0.21
Nb	2.7	2.8	2.5	2.5	2.6	2.4
Nd	7.4	10.9	12	12	6.4	6.9
Pr	1.72	2.51	2.9	2.71	1.47	1.44
Rb	49.6	137.5	76.7	26	41.4	33.1
Sm	1.96	2.99	2.73	3.15	1.9	1.81
Sn	<1	<1	<1	1	<1	<1
Sr	142	109	127	97	208	235
Ta	0.2	0.2	0.2	0.2	0.2	0.2
Tb	0.31	0.43	0.43	0.44	0.3	0.4
Th	0.67	0.62	0.57	0.6	0.62	0.58
Tm	0.18	0.2	0.2	0.21	0.19	0.18
U	0.27	0.24	0.37	0.4	0.14	0.13
V	204	226	216	216	209	213
W	<1	1	<1	1	<1	<1
Y	12.6	16	13.7	15.4	12.2	12.9
Yb	1.45	1.27	1.27	1.42	1.14	1.42
Zr	40	40	37	38	37	37
As	0.1	0.7	0.2	0.3	0.1	0.2
Bi	0.02	0.05	0.03	0.17	0.01	0.02
Hg	0.005	0.009	<0.005	<0.005	<0.005	<0.005
In	0.032	0.051	0.045	0.067	0.012	0.015
Re	0.001	0.001	<0.001	0.001	0.001	0.001
Sb	<0.05	<0.05	<0.05	<0.05	<0.05	<0.05
Se	0.3	0.2	0.3	0.5	0.3	0.2
Te	0.01	0.02	0.01	0.03	0.01	0.01
Tl	0.04	0.15	0.06	0.04	0.06	0.06
Ag	<0.5	<0.5	<0.5	<0.5	<0.5	<0.5
Cd	<0.5	<0.5	<0.5	<0.5	<0.5	<0.5
Co	48	46	48	49	50	48
Cu	142	19	20	119	114	115
Li	100	130	100	130	40	50
Mo	<1	<1	<1	<1	<1	<1
Ni	116	130	123	125	122	120
Pb	5	4	3	3	2	3
Sc	27	37	37	40	38	38
Zn	69	66	57	70	63	63

SAMPLE	CAM-021-KY-092	CAM-021-KY-093	CAM-021-KY-094	CAM-021-KY-095	CAM-021-KY-097	CAM-021-KY-098
SiO_2	49	42.2	49.8	40.5	44	69.3
Al_2O_3	14.5	11.7	5.97	4.4	7.94	16.15
Fe_2O_3	10.3	19.65	11.25	15.6	14.6	1.45
CaO	11.1	6.73	12.45	4.2	7.64	1.16
MgO	9.7	7.45	14.05	26.2	14.4	0.5
Na_2O	1.73	2.29	0.62	0.43	1.12	3.91
K_2O	0.81	1.84	0.91	0.71	1.04	6.56
Cr_2O_3	0.056	0.003	0.087	0.494	0.236	<0.002
TiO_2	0.6	3.19	1.52	1.01	2.81	0.08
MnO	0.18	0.3	0.22	0.24	0.2	0.02
P_2O_5	0.05	0.19	0.14	0.12	0.3	0.26
SrO	0.02	0.06	0.01	0.03	0.02	0.09
BaO	0.02	0.06	0.02	0.03	0.04	0.13
LOI	2.05	3.13	3.3	6.96	5.27	1
Total	100.12	98.79	100.35	100.92	99.62	100.61
C	0.07	0.05	0.05	0.06	0.08	0.11
S	0.09	0.31	0.16	0.04	0.16	0.04
Ba	148	482	227	318	339	1230
Ce	10.4	40	38.5	32.6	68.1	19.2
Cr	390	<10	660	3930	1890	10
Cs	1.19	0.45	0.24	1.32	0.85	4.04
Dy	1.95	3.91	3.72	2.57	5.97	2.75
Er	1.46	1.45	1.63	1.04	2.66	1.19
Eu	0.58	1.74	1.74	1.32	2.66	1
Ga	15.3	22.6	13.3	9.9	19.1	22.4
Gd	2.09	4.92	5.3	3.4	8.59	3.41
Ge	<5	<5	<5	<5	<5	<5
Hf	1.1	3.9	3.1	2.6	6.6	1
Ho	0.42	0.64	0.6	0.38	1.02	0.48
La	4.6	16	16.8	14	27.6	8.6
Lu	0.19	0.18	0.17	0.09	0.24	0.13
Nb	2.5	8.6	6.6	5.7	22.1	2.7
Nd	6.2	26	23.8	18.4	42.1	12.5
Pr	1.44	5.71	5.28	4.34	9.46	2.71
Rb	38.1	35.2	17.1	20.8	25.6	153.5
Sm	1.72	5.96	6.02	3.89	10.55	3.48
Sn	1	2	1	1	2	<1
Sr	148.5	422	114.5	223	121	705
Ta	0.2	0.5	0.5	0.3	1.4	0.4
Tb	0.34	0.73	0.71	0.44	1.11	0.48
Th	0.62	1.3	1.06	0.91	2.03	1.9
Tm	0.2	0.21	0.19	0.13	0.31	0.13
U	0.12	0.3	0.48	0.36	0.64	2.86
V	207	534	241	147	304	11
W	<1	<1	1	<1	1	<1
Y	11.7	16	16	10	24.2	13.3
Yb	1.43	1.23	1.32	0.85	1.69	0.94
Zr	36	141	118	100	266	23
As	0.5	0.2	1.4	1.2	0.4	0.1
Bi	0.02	0.03	0.1	0.15	0.04	0.08
Hg	<0.005	<0.005	<0.005	<0.005	<0.005	<0.005
In	0.008	0.049	0.024	0.032	0.04	0.005
Re	<0.001	0.001	0.005	0.001	0.001	<0.001
Sb	0.17	0.05	0.05	0.06	<0.05	<0.05
Se	0.2	0.6	0.6	0.2	0.2	<0.2
Te	0.02	0.02	0.19	0.07	0.02	0.01
Tl	0.06	0.02	0.02	0.25	0.04	0.03
Ag	<0.5	<0.5	0.8	0.5	<0.5	<0.5
Cd	<0.5	1	0.5	0.7	0.9	<0.5
Co	50	93	62	134	71	1
Cu	114	131	750	354	141	4
Li	30	30	30	20	90	10
Mo	<1	1	2	1	1	<1
Ni	127	82	294	1460	577	3
Pb	2	14	13	15	8	27
Sc	34	27	48	14	28	1
Zn	67	303	132	183	399	10

SAMPLE	CAM-021-KY-099	CAM-021-KY-100	CAM-021-KY-101	CAM-021-KY-102	CAM-021-KY-103	CAM-021-KY-105	CAM-021-KY-106	CAM-021-KY-107
SiO_2	41.2	78.1	60.7	72.1	75.9	50.9	48.7	42.6
Al_2O_3	4.86	12.7	14.15	14.3	13.5	13.95	14.2	7.46
Fe_2O_3	15.15	1.12	8.27	2.23	1.22	12.7	11.45	14.9
CaO	4.29	2.53	3.58	0.92	0.71	8.7	8.13	8.3
MgO	25.2	0.36	3.86	0.79	0.27	7.6	8.12	14.4
Na_2O	0.42	4.51	3.14	2.9	3.61	2.48	2.62	1.15
K_2O	0.71	0.46	1.76	6.38	5.2	1.48	1.44	0.68
Cr_2O_3	0.508	0.003	0.026	0.002	<0.002	0.014	0.018	0.24
TiO_2	1.14	0.07	0.69	0.26	0.1	0.93	0.8	2.66
MnO	0.25	0.02	0.15	0.03	0.02	0.18	0.19	0.26
P_2O_5	0.14	0.03	0.1	0.16	0.02	0.09	0.08	0.28
SrO	0.02	0.05	0.04	0.05	0.01	0.03	0.03	0.04
BaO	0.02	0.03	0.07	0.14	0.05	0.03	0.03	0.03
LOI	7.68	0.67	1.56	0.72	0.77	2.26	2.37	3.96
Total	101.59	100.65	98.1	100.98	101.38	101.34	98.18	96.96
C	0.07	0.09	0.16	0.06	0.1	0.04	0.05	0.09
S	0.03	0.02	0.37	0.01	0.01	0.12	0.11	0.13
Ba	220	251	650	1325	428	260	274	190.5
Ce	29.4	31.8	36.9	192.5	40.5	20	16.6	47.4
Cr	4010	20	190	10	10	100	140	1420
Cs	1.53	0.37	2.32	1.3	6.59	1.54	1.75	1.29
Dy	2.41	0.66	3.1	2.69	2.31	3.18	2.82	4.24
Er	1.08	0.24	1.63	1.02	1.73	2.39	1.88	1.79
Eu	1.23	1	1.04	1.26	0.4	0.91	0.9	2.02
Ga	11.1	18.9	20.3	19.3	20.9	18.9	17.2	13.6
Gd	3.78	1.3	3.31	6.51	2.31	3.35	2.84	6.19
Ge	<5	<5	<5	<5	<5	<5	<5	<5
Hf	2.6	3.7	3.5	7.5	3.3	1.9	1.7	4.8
Ho	0.43	0.1	0.56	0.41	0.49	0.69	0.58	0.74
La	12	16.1	17.5	89.8	19.6	9.5	7.9	19.6
Lu	0.12	0.03	0.23	0.1	0.21	0.26	0.25	0.18
Nb	6.1	2.1	4.9	6.1	8.3	4.6	3.8	15.5
Nd	18.8	12.1	17.8	76.6	15.1	10.7	9.6	28.3
Pr	4.03	3.31	4.32	22	4.55	2.45	2.14	6.58
Rb	20.1	12.7	59.8	137.5	221	86.4	87.4	12.3
Sm	4.35	1.94	3.8	12.2	3.05	2.9	2.18	6.72
Sn	1	<1	1	<1	2	1	1	1
Sr	178	435	309	399	103.5	275	242	256
Ta	0.3	0.1	0.4	0.3	0.9	0.3	0.2	1
Tb	0.42	0.13	0.46	0.66	0.38	0.48	0.4	0.78
Th	0.85	6.53	3.88	45	14.75	1.55	1.02	1.46
Tm	0.13	0.03	0.27	0.11	0.22	0.29	0.24	0.23
U	0.28	3.79	1.1	1.33	5.97	0.27	0.19	0.52
V	168	11	180	22	5	278	245	232
W	1	<1	1	<1	1	<1	1	<1
Y	10.4	2.6	14.9	10.4	15.6	17.9	15.1	16.9
Yb	0.9	0.21	1.75	0.7	1.63	2.01	1.88	1.61
Zr	99	103	121	277	89	69	54	187
As	0.7	0.3	<0.1	0.2	0.3	<0.1	<0.1	0.3
Bi	0.1	0.01	0.11	0.02	0.27	0.02	0.03	0.04
Hg	<0.005	<0.005	<0.005	<0.005	<0.005	<0.005	<0.005	<0.005
In	0.029	<0.005	0.032	0.01	0.006	0.007	0.011	0.027
Re	0.002	<0.001	0.001	<0.001	<0.001	0.001	0.001	0.002
Sb	<0.05	<0.05	<0.05	<0.05	<0.05	<0.05	<0.05	<0.05
Se	0.2	<0.2	0.2	<0.2	<0.2	0.2	0.2	<0.2
Te	0.03	<0.01	0.03	<0.01	<0.01	0.02	0.01	0.02
Tl	0.13	0.05	0.47	0.13	0.04	0.08	0.06	0.05
Ag	<0.5	<0.5	<0.5	<0.5	<0.5	<0.5	<0.5	<0.5
Cd	0.6	<0.5	<0.5	<0.5	<0.5	<0.5	<0.5	<0.5
Co	124	2	33	3	1	51	48	82
Cu	168	3	56	2	2	105	96	174
Li	20	10	40	10	10	40	40	80
Mo	1	3	1	5	1	<1	1	1
Ni	1340	7	97	6	<1	62	78	649
Pb	21	20	9	32	17	3	5	8
Sc	15	1	23	4	2	40	33	25
Zn	149	15	119	27	12	72	76	246

Appendix D

Radiogenic isotope data

Sample	CAM-021-KY-001	CAM-021-KY-004	CAM-021-KY-012
AGE	1106.3	1106.3	1106.3
Sample Wt. (g)	0.03034	0.03055	0.05014
Spike Wt. (g)	0.0506	0.05085	0.05264
$^{146/144}$Nd	0.7219	0.7219	0.7219
$^{148/144}$Nd	0.46081038	0.462733489	0.464728859
$^{143/144}$Nd	0.512279381	0.512259201	0.512264721
$^{147/149}$Sm	0.37183043	0.35098434	0.3523202
$^{152/149}$Sm	0.66353885	0.62633857	0.62872245
Sm (ppm)	10.3	9.47	6.00
Nd (ppm)	48.7	48.2	30.1
Eps $_{Nd\ (CHUR)1106.3}$	-5.32	-4.41	-4.62
$^{87Sr/86}$Sr (current)	0.70805	0.70583	0.71455
$^{87Sr/86}$Sr initial	0.46081	0.46273	0.45791
Eps $_{Sr}$	5365.50	5253.70	5604.37

Sample	CAM-021-KY-017	CAM-021-KY-018	CAM-021-KY-028	CAM-021-KY-029	CAM-021-KY-036
AGE	1107.9	1107.9	1107.9	1107.9	1107.9
Sample Wt. (g)	0.0304	0.03007	0.03025	0.03045	0.03052
Spike Wt. (g)	0.06113	0.06135	0.07476	0.05855	0.06325
$^{146/144}$Nd	0.7219	0.7219	0.7219	0.7219	0.7219
$^{148/144}$Nd	0.469122776	0.489592898	0.457917622	0.473034683	0.486144492
$^{143/144}$Nd	0.511266855	0.512332751	0.511248033	0.512287236	0.512295906
$^{147/149}$Sm	0.29158947	0.31796868	0.2980918	0.34221493	0.32432065
$^{152/149}$Sm	0.52034725	0.56742147	0.53195078	0.61068939	0.57875669
Sm (ppm)	8.77	10.0	11.1	10.5	10.5
Nd (ppm)	56.6	52.7	73.2	53.2	54.3
Eps $_{Nd\ (CHUR)1107.9}$	-20.5	-3.45	-20.2	-4.36	-4.28
$^{87Sr/86}$Sr (current)	0.80999	0.70523	0.70880	0.70948	0.70533
$^{87Sr/86}$Sr initial	0.46912	0.48959	0.45791	0.47303	0.48614
Eps $_{Sr}$	7266.22	4404.56	5478.79	4998.65	4508.82

Sample	CAM-021-KY-070	CAM-021-KY-074	CAM-021-KY-092	CAM-021-KY-064	CAM-021-KY-065
AGE	1107.9	1107.9	1107.9	1107.9	1107.9
Sample Wt. (g)	0.14023	0.05012	0.15046	0.13064	0.05067
Spike Wt. (g)	0.03435	0.05362	0.03192	0.03519	0.04862
$^{146/144}$Nd	0.7219	0.7219	0.7219	0.7219	0.7219
$^{148/144}$Nd	0.453312151	0.461532232	0.418123897	0.445050328	0.469308924
$^{143/144}$Nd	0.512348576	0.512445597	0.512308266	0.512936613	0.512462981
$^{147/149}$Sm	0.42810782	0.39996647	0.4781681	0.48420945	0.37753807
$^{152/149}$Sm	0.76396697	0.71374817	0.85330054	0.86408145	0.67372423
Sm (ppm)	1.90	7.43	1.99	2.58	6.09
Nd (ppm)	7.41	31.1	7.69	8.48	26.9
Eps $_{\text{Nd (CHUR)1107.9}}$	-7.49	-4.35	-7.20	0.14	-3.18
$^{87Sr/86}$Sr (current)	0.73684	0.70883	0.72469	0.70986	0.71046
$^{87Sr/86}$Sr initial	0.45331	0.46153	0.41812	0.44505	0.46930
Eps $_{\text{Sr}}$	6254.60	5358.40	7332.08	5950.28	5138.56

Sample	CAM-021-KY-066	CAM-021-KY-093	CAM-021-KY-094	CAM-021-KY-095
AGE	1107.9	1107.9	1107.9	1107.9
Sample Wt. (g)	0.05027	0.05067	0.05023	0.05015
Spike Wt. (g)	0.04256	0.04613	0.04203	0.03374
$^{146/144}$Nd	0.7219	0.7219	0.7219	0.7219
$^{148/144}$Nd	0.468722612	0.434856047	0.457413388	0.481234502
$^{143/144}$Nd	0.512397531	0.512374151	0.512476867	0.512422794
$^{147/149}$Sm	0.36201122	0.41561503	0.39418162	0.34529427
$^{152/149}$Sm	0.64601627	0.74167333	0.70342498	0.61618453
Sm (ppm)	5.04	6.73	5.68	3.73
Nd (ppm)	23.8	30.1	24.8	17.9
Eps $_{\text{Nd (CHUR)1107.9}}$	-3.18	-3.44	-2.74	-2.84
$^{87Sr/86}$Sr (current)	0.70699	0.70831	0.71198	0.70735
$^{87Sr/86}$Sr initial	0.46872	0.43485	0.45741	0.48123
Eps $_{\text{Sr}}$	5083.41	6288.40	5565.56	4698.78

Appendix E

Geochronological isotope data

Fraction	Description	U (ppm)	Th/U	Pb^T (pg)	Pb_C (pg)	$^{206}Pb/^{204}Pb$	$^{207}Pb/^{235}U$	± 2σ	$^{206}Pb/^{238}U$	± 2σ	$^{207}Pb/^{206}Pb$	± 2σ	Ages (Ma) $^{207}Pb/^{235}U$	± 2σ	$^{206}Pb/^{238}U$	± 2σ	$^{207}Pb/^{206}Pb$	± 2σ	Disc. (%)
18-DL-039; Monzogabbro, Escape Lake intrusion																			
Z1	2 cls, clr-sl. cldy skel frags	459	0.838	149.64	2.15	3913	2.03108	0.00673	0.192605	0.000413	0.076482	0.000166	1126.0	2.3	1135.5	2.2	1107.7	4.3	-2.7
Z2	2 cls, clr-sl. cldy skel frags	485	0.806	104.22	0.72	8241	1.99583	0.00534	0.189291	0.000389	0.076470	0.000100	1114.1	1.8	1117.5	2.1	1107.4	2.6	-1.0
Z3*	3 cls, cldy skel frags	765	0.812	163.17	0.40	23240	1.97916	0.00386	0.187689	0.000301	0.076479	0.000053	1108.4	1.3	1108.8	1.6	1107.6	1.4	-0.1
Z4*	3 cls, cldy skel frags	773	0.724	161.39	0.66	14140	1.97693	0.00337	0.187483	0.000245	0.076476	0.000059	1107.7	1.1	1107.7	1.3	1107.6	1.5	0.0
CAM-021-KY-061; Monzogabbro, EWC intrusion																			
Z1	1 clr, cls, flat, crkd frag	146	0.990	31.15	0.47	3632	1.87540	0.00668	0.180639	0.000412	0.075297	0.000194	1072.4	2.4	1070.5	2.2	1076.4	5.2	0.6
Z2	2 sm, clr pr frags, few facets	222	0.541	66.25	0.94	3953	13.27362	0.03935	0.520134	0.001306	0.185086	0.000205	2699.3	2.8	2699.7	5.5	2699.0	1.8	0.0
Z3	2 irr. clr, cls frags	171	0.479	52.75	0.51	5812	14.40912	0.03894	0.539857	0.001238	0.193579	0.000178	2777.0	2.6	2782.8	5.2	2772.8	1.5	-0.4
CAM-021-KY-081; Monzogabbro, Greenwich intrusion																			
Bd1	12 brn blades & blocky frags	747	0.071	104.83	3.81	1895	1.95931	0.00437	0.185978	0.000234	0.076408	0.000126	1101.6	1.5	1099.5	1.3	1105.8	3.3	0.6
Bd2	12 brn blades & blocky frags	1177	0.086	166.73	1.78	6391	1.96859	0.00301	0.186869	0.000178	0.076404	0.000059	1104.8	1.0	1104.4	1.0	1105.7	1.5	0.1
Bd3	10 brn blades & blocky frags	958	0.084	146.48	1.80	5757	1.96738	0.00283	0.186750	0.000190	0.076405	0.000050	1104.4	1.0	1103.7	1.0	1105.7	1.3	0.2

Notes:

- All analyzed zircon fractions represent best optical quality (crack-, inclusion-, core-free), fresh (least altered) grains. Zircons were chemically abraded.
- Abbreviations: Z- zircon; Bd – baddeleyite; cls - colorless; brn - medium brown; clr - clear, cldy – cloudy; sl. cldy - slightly cloudy; crkd - cracked; frag(s) - fragment(s); pr-prism/prismatic; irr – irregular/anhedral; sm – smaller, skel – skeletal.
- *Fraction spiked with ET535 ^{205}Pb-^{233}U-^{235}U isotopic tracer; remaining fractions spiked with JSGL ^{205}Pb-^{235}U tracer.
- Pb^T is total amount (in picograms) of Pb.
- Pb_C is total measured common Pb (in picograms) assuming the isotopic composition of laboratory blank: 206/204 - 18.49±0.4%; 207/204 - 15.59±0.4%; 208/204 - 39.36±0.4%.
- Pb/U atomic ratios are corrected for spike, fractionation, blank, and, where necessary, initial common Pb; $^{206Pb/204}Pb$ is corrected for spike and fractionation.
- Th/U is model value calculated from radiogenic $^{208}Pb/^{206}Pb$ ratio and $^{207}Pb/^{206}Pb$ age, assuming concordance.
- Disc. (%) - per cent discordance for the given $^{207}Pb/^{206}Pb$ age.
- Uranium decay constants are from Jaffey et al. (1971).